THÈSE

En vue de l'obtention du

DOCTORAT DE L'UNIVERSITÉ DE TOULOUSE

Délivré par :

Institut National Polytechnique de Toulouse (Toulouse INP)

Discipline ou spécialité :

Génie Electrique

Présentée et soutenue par :

Mme ANDREA AL HADDAD

le vendredi 21 octobre 2022

Titre :

Méthodes de modélisation de dégradation d'objets du génie électrique en vue du prognostic de la durée de vie.

Ecole doctorale :

Génie Electrique, Electronique, Télécommunications (GEETS)

Unité de recherche :

Laboratoire Plasma et Conversion d'Energie (LAPLACE)

Directeur(s) de Thèse :

M. PASCAL MAUSSION

M. ANTOINE PICOT

Rapporteurs :

M. AZZEDINE BOUDRIOUA, UNIVERSITE PARIS 13

M. CLAUDE DELPHA, CENTRALESUPELEC GIF SUR YVETTE

Membre(s) du jury :

MME MARIE-CÉCILE PERA, UNIVERSITE DE FRANCHE COMTE, Président

M. ANTOINE PICOT, TOULOUSE INP, Membre

M. GEORGES ZISSIS, UNIVERSITE TOULOUSE 3, Membre

M. LAURENT CANALE, UNIVERSITE TOULOUSE 3, Invité(e)

M. PASCAL DUPUIS, UNIVERSITE TOULOUSE 3, Invité(e)

M. PASCAL MAUSSION, TOULOUSE INP, Membre

Acknowledgements

First of all, I would like to express my deepest gratitude to the members of the jury, Pr Marie-Cécile Pera, Mr. Claude Delpha and Pr. Azzedine Boudrioua for having accepted this role and for their insightful comments and questions.

I am extremely grateful to my thesis director, Pr. Pascal Maussion, for his trust and support. He gave me the necessary autonomy to improve myself, supported me when I needed it and defended me when it was necessary. I also thank M. Antoine Picot, my co-supervisor, for his participation and engagement in the thesis and my teaching service.

I could not have undertaken this journey without Mr. Pascal Dupuis who I can name as my godfather. He was present during all my thesis, not only to help me technically but also to support me psychologically. It was not possible to continue this thesis without all the wisdom that you transferred to me, so I am deeply indebted to you. Thanks should also go to Pr. Georges Zissis, for all the opportunities he gave me, and to Mr. Laurent Canale, for his contribution to the OLED bench. I also thank all the technical support I got from the mechanical and electrical technical services at the LAPLACE UPS site.

I thank my LAPLACE colleagues with whom I had the pleasure to work, on the course of four years, and who became friends and more. I'd like to acknowledge the emotional support I received from my Lebanese friends and the Toulouse society, as well as my best friends Maria and Maria.

Last but not least, I thank my parents, Nabih and Georgette, who traveled halfway around the world to attend my defense, and to whom I dedicate this thesis. I thank my brothers and their wifes, Jamil and Yara, Georges and Roshan and my sister Tania, for always believing in me and treating me like the princess I am.

I thank my partner, Davin Guedon, for being the soulmate who understood me, loved me and shared his life with me.

Finally, I thank my God, for he is good, for his mercy endures forever.

Résumé

La fiabilité des composants électriques est une problématique étudiée pour améliorer la qualité des produits, et pour planifier la maintenance en cas de défaillance. La fiabilité est mesurée en étudiant les causes de défaillance et le temps moyen jusqu'à la défaillance. Une des méthodes appliquées dans ce domaine est l'étude du vieillissement des composants, car la défaillance se produit souvent après une dégradation.

L'objectif de cette thèse est de modéliser la dégradation des composants en génie électrique, afin d'estimer leur durée de vie. Plus spécifiquement, cette thèse étudiera les sources de lumière blanche organiques à grande surface (OLEDs). Ces sources offrent plusieurs avantages dans le monde de l'éclairage grâce à leur finesse, leur faible consommation d'énergie et leur capacité à s'adapter à de larges domaines d'application. Les seconds composants étudiés sont des isolants électriques appliqués à des paires de fils de cuivre torsadés, qui sont couramment utilisés dans les machines électriques à basse tension. Tout d'abord, les mécanismes de dégradation et de défaillance des différents composants électriques, y compris les OLED et les isolants, sont étudiés. Ceci est fait pour identifier les contraintes opérationnelles afin de les inclure dans le modèle de vieillissement.

Après avoir identifié les principales causes du vieillissement, des modèles physiques généraux sont étudiés pour quantifier les effets des contraintes opérationnelles. Des modèles empiriques sont également présentés lorsque la physique de la dégradation est inconnue ou difficile à modéliser.

Ensuite, des méthodes d'estimation des paramètres de ces modèles sont présentées, telles que la régression multilinéaire et non-linéaire, ainsi que des méthodes stochastiques. D'autres méthodes basées sur l'intelligence artificielle et le diagnostic en ligne sont également présentées, mais elles ne seront pas étudiées dans cette thèse.

Ces méthodes sont appliquées aux données de dégradation des LEDs organiques et des isolateurs de paires torsadées. Pour cela, des bancs de vieillissement accéléré et multifactoriel sont conçus sur la base de plans d'expériences factoriels et de méthodes de surface de réponse, afin d'optimiser le coût des expériences. Ensuite, un protocole de mesure est décrit, afin d'optimiser le temps d'inspection et de collecter des données périodiques.

Enfin, les méthodes d'estimation traitent des modèles de dégradation déterministes sans contrainte basés sur les données mesurées. Le meilleur modèle empirique de la trajectoire de dégradation est alors choisi en fonction de critères de sélection de modèles.

Dans un second temps, les paramètres des trajectoires de dégradation sont modélisés en fonction des contraintes opérationnelles. Les paramètres des facteurs de vieillissement et de leurs interactions sont estimés par régression multilinéaire et selon différents ensembles d'apprentissage. La significativité des paramètres est évaluée par des méthodes statistiques si possible. Enfin, la durée de vie des expériences dans les ensembles de validation est prédite sur la base des paramètres estimés par les différents ensembles d'apprentissage. L'ensemble d'apprentissage qui présente le meilleur taux de prédiction de la durée de vie est considéré comme le meilleur.

Abstract

Reliability of electrical components is an issue studied to improve the quality of products, and to plan maintenance in case of failure. Reliability is measured by studying the causes of failure and the mean time to failure. One of the methods applied in this field is the study of component aging, because failure often occurs after degradation.

The objective of this thesis is to model the degradation of components in electrical engineering, in order to estimate their lifetime. More specifically, this thesis will study large area organic white light sources (OLEDs). These sources offer several advantages in the world of lighting thanks to their thinness, their low energy consumption and their ability to adapt to a wide range of applications. The second components studied are electrical insulators applied to pairs of twisted copper wires, which are commonly used in low voltage electrical machines.

First, the degradation and failure mechanisms of the various electrical components, including OLEDs and insulators, are studied. This is done to identify the operational stresses for including them in the aging model.

After identifying the main causes of aging, general physical models are studied to quantify the effects of operational stresses. Empirical models are also presented when the physics of degradation is unknown or difficult to model.

Next, methods for estimating the parameters of these models are presented, such as multilinear and nonlinear regression, as well as stochastic methods. Other methods based on artificial intelligence and online diagnosis are also presented, but they will not be studied in this thesis.

These methods are applied to degradation data of organic LEDs and twisted pair insulators. For this purpose, accelerated and multifactor aging test benches are designed based on factorial experimental designs and response surface methods, in order to optimize the cost of the experiments. Then, a measurement protocol is described, in order to optimize the inspection time and to collect periodic data.

Finally, estimation methods tackle unconstrained deterministic degradation models based on the measured data. The best empirical model of the degradation trajectory is then chosen based on model selection criteria.

In a second step, the parameters of the degradation trajectories are modeled based on operational constraints. The parameters of the aging factors and their interactions are estimated by multilinear regression and according to different learning sets. The significance of the parameters is evaluated by statistical methods if possible. Finally, the lifetime of the experiments in the validation sets is predicted based on the parameters estimated by the different learning sets. The training set with the best lifetime prediction rate is considered the best.

Résumé de la thèse en français

Chapitre 1: L'état de l'art, motivation de l'étude de la dégradation

Le premier chapitre présente les notions de fiabilité en général, et plus particulièrement celles liées à la défaillance. Les modes de défaillance sont ensuite classés en fonction de leurs causes et de leurs conséquences. Ainsi, le mode de défaillance progressif basé sur le vieillissement des composants est choisi pour être étudié dans cette thèse. Ce choix est basé sur le fait que la défaillance survient souvent après une dégradation.

L'étude du vieillissement peut se faire selon plusieurs stratégies telles que l'approche expérimentale, les approches basées sur des modèles, le savoir-faire des experts, ou les approches basées sur des données. Cette thèse étudie l'approche par modèles pour comprendre l'évolution de la dégradation en fonction des conditions de fonctionnement.

Afin de modéliser la dégradation, les conditions de vieillissement de divers composants du génie électrique et leurs mécanismes de dégradation sont étudiées. Les catégories de différents composants comprennent les métaux, les semi-conducteurs et les micro-électroniques, les systèmes de stockage d'énergie et les diélectriques. Les mécanismes de vieillissement communs à toutes ces catégories sont la fatigue, l'usure, la corrosion, la modification des paramètres électriques, etc.

En particulier, deux composants électriques sont étudiés dans cette thèse ; les premiers composants sont les sources de lumière blanche organiques à grande surface (OLEDs). Ces sources offrent plusieurs avantages dans le monde de l'éclairage grâce à leur finesse, leur faible consommation d'énergie et leur capacité à s'adapter à de larges domaines d'application. Les seconds composants étudiés sont des isolants électriques appliqués à des fils de cuivre, qui sont couramment utilisés dans les machines électriques à basse tension. Les facteurs de vieillissement communs à ces deux composants sont les facteurs électriques et thermiques.

La modélisation de la dégradation nécessite également des données concrètes, pour lesquelles des essais de vieillissement doivent être réalisés. Parmi ces tests, il y a le vieillissement normal et le vieillissement accéléré. De plus, les tests peuvent appliquer des méthodes de mesure destructives ou non destructives. Dans cette thèse, seules les méthodes de vieillissement accélérées et non-destructives (ce qui est original) seront testées pour la modélisation.

Enfin, les méthodes de prétraitement, d'analyse et de post-traitement des données sont présentées pour être appliquées dans les chapitres suivants.

Chapitre 2 : Synthèse des modèles de dégradation dans la littérature

Le deuxième chapitre se concentre sur les modèles de dégradation présents dans la littérature. Les modèles de dégradation des composants électriques peuvent être divisés en deux catégories: les modèles basés sur la physique de dégradation et les modèles empiriques basés sur les données.

Les modèles basés sur la physique de la dégradation incluent un ou plusieurs des facteurs les plus

influents, ainsi que des paramètres liés aux mécanismes de dégradation de chaque composant. Le modèle d'Arrhenius, par exemple, modélise le taux de dégradation en fonction de la température et de l'énergie d'activation de la réaction chimique à l'origine de la dégradation. D'autres modèles physiques sont le modèle d'Eyring qui modélise le taux de dégradation en fonction de la température et d'un autre facteur tel que la charge mécanique, la densité de courant ou l'humidité.

Ces modèles ne modélisent que le taux de dégradation et ne définissent pas la trajectoire de dégradation en fonction du temps. De plus, ces modèles incluent des paramètres physiques qui nécessitent une connaissance approfondie des mécanismes de dégradation. Par ailleurs, les modèles empiriques sont des modèles qui définissent des trajectoires générales que suit un indicateur de vieillissement en fonction du temps de vieillissement. Par exemple, un indicateur peut avoir une dégradation linéaire, exponentielle ou inversement proportionnelle au temps de vieillissement. Ces modèles empiriques présentent des méthodes générales qui peuvent être appliquées à n'importe quel produit électrique, mais ils n'incluent aucun facteur de vieillissement.

Concernant les OLEDs, les modèles de dégradation existants dans la littérature sont des modèles semi-empiriques, qui sont un mélange des deux méthodes présentées ci-dessus. Le modèle empirique de base pour ces composants est le "Stretched Exponential Decay", dont les paramètres sont modélisés avec un seul facteur au maximum (courant ou température). L'indicateur de vieillissement utilisé dans la modélisation est souvent la luminance des OLEDs. Quant aux isolants, la majorité des modèles de la littérature se limitent à la modélisation de la durée de vie. Les modèles utilisés sont également des modèles semi-empiriques exponentiels ou de type "puissance", où les facteurs les plus modélisés sont la température, la tension et le champ électrique. Seul le modèle de Simoni modélise de manière exponentielle le taux de dégradation en fonction de la contrainte thermique et électrique. Ce taux de dégradation n'est pas indiqué et peut être un indicateur d'un vieillissement quelconque. En revanche, les modèles présentés ci-dessus nécessitent l'estimation de leurs paramètres. Cette estimation se fait par des méthodes déterministes ou stochastiques. La méthode déterministe la plus couramment utilisée est la régression, qu'elle soit linéaire, non linéaire ou multidimensionnelle. La régression peut inclure des algorithmes d'estimation robustes ou pondérés. En outre, elle permet d'estimer l'intervalle de confiance de la trajectoire de dégradation.

D'autres méthodes d'estimation sont basées sur des processus stochastiques, où pour les mêmes conditions de vieillissement, il existe plusieurs trajectoires de dégradation. Ces méthodes sont utilisées lorsqu'il y a une grande source de danger, et ne seront pas détaillées dans cette thèse.

Enfin, il existe dans la littérature des méthodes de prédiction de l'évolution du vieillissement basées sur l'intelligence artificielle. Ces méthodes sont basées sur un grand nombre de données et utilisent en entrée les conditions de vieillissement pour prédire en sortie les indicateurs de dégradation. Ces méthodes sont très efficaces pour la prédiction mais elles nécessitent une grande taille de données et ne sont pas basées sur un modèle de dégradation, ce qui est l'objectif de cette thèse. Pour ces raisons, elles ne seront pas étudiées dans la suite.

Chapitre 3 : Conception d'expériences, applications aux LEDs organiques et isolants des paires de fils de cuivre torsadées

Précédemment, des modèles empiriques et physiques sont présentés, qui nécessitent des données pour estimer leurs paramètres. Ces données sont obtenues par des expériences menées au laboratoire. Les expériences sont planifiées en 5 étapes : établir l'objectif de l'expérience, développer une stratégie, créer un plan, mettre en œuvre le plan, puis observer et analyser les résultats.

Les objectifs de ces expériences sont de surveiller la dégradation des composants tout au long du processus de vieillissement et de prédire avec précision la durée de vie des composants sous différentes

contraintes.

La stratégie de l'expérience est basée sur la méthode des plans d'expériences. En effet, les modèles présentés dans le chapitre précédent n'incluent pas plusieurs facteurs, ni n'estiment l'interaction entre les facteurs. Les paramètres des modèles semi-empiriques de dégradation peuvent également être modélisés en fonction des contraintes opérationnelles, afin de les inclure.

Le plan d'expériences permet d'avoir des données multifactorielles, car il permet de réaliser des expériences sous plusieurs contraintes en même temps. Le plan d'expériences factoriel par exemple, permet de placer les expériences orthogonalement dans un plan dont les axes sont les contraintes opérationnelles dont les effets sont à quantifier. Cette méthode permet d'optimiser le nombre d'expériences à choisir, si la relation entre les contraintes opérationnelles et le résultat (taux de dégradation par exemple) est linéaire.

Dans le cas où la relation entre les contraintes opérationnelles et le résultat est du second ordre ou plus, la stratégie des expériences à réaliser peut être basée sur la méthode des surfaces de réponse. Les autres méthodes de plans d'expériences existantes dans la littérature sont les plans optimaux (les plans factoriels en font partie) et la méthode "un facteur à la fois" (OFAT).

Après avoir défini la stratégie d'expérimentation, l'étape suivante consiste à créer un plan. Dans ce plan, il faut définir le nombre de composants à mettre dans chaque expérience, le nombre d'inspections à effectuer pendant le processus de vieillissement, et le temps maximum avant d'arrêter l'expérience si aucune défaillance ne se produit.

La quatrième étape consiste à mettre en œuvre le plan créé. Pour cela, deux bancs d'essai sont utilisés, l'un pour les LED organiques et l'autre pour les isolateurs des paires de fils de cuivre torsadées.

Le banc de vieillissement des LED organiques se compose de trois fours thermiques reliés à des sources de courant continu pour appliquer des contraintes à la fois thermiques et électriques. Les sources de courant alimentent les OLED de manière continue ou cyclique par l'intermédiaire d'un dispositif électronique. Ainsi, trois facteurs de vieillissement sont testés à des niveaux plus élevés que leurs valeurs nominales pour un vieillissement accéléré : la température, le courant et le cyclage électrique.

La campagne d'essais teste un plan expérimental basé sur différents plans factoriels et surfaces de réponse. Pendant la campagne, les caractéristiques des OLEDs sont mesurées périodiquement. Ces caractéristiques comprennent des mesures optiques comme la luminance et des mesures électriques comme l'impédance. D'autres mesures sont également effectuées avant le début de la campagne pour bien la planifier, comme les mesures de la réponse transitoire de la température, du courant et de la tension. Des photos à faible courant sont également prises avant le début de la campagne pour détecter les OLED défectueuses.

D'autre part, le banc de vieillissement des isolants consiste à fabriquer les paires torsadées (contrairement aux OLEDs qui sont des produits industriels). Les paires sont ensuite placées dans des fours électriques sous une tension inférieure à la tension d'inception des décharges partielles (PDIV). En plus des contraintes thermiques et électriques, les paires sont testées à deux niveaux de haute fréquence.

La campagne d'essais teste plusieurs plans expérimentaux factoriels et fractionnaires. La PDIV

de ces paires est ensuite mesurée périodiquement pendant la campagne, jusqu'à la défaillance des paires ou l'arrêt de l'expérience.

Chapitre 4 : Méthodes de modélisation de la dégradation sans contraintes avec application aux OLED et aux isolateurs de machines

Dans ce chapitre, la dégradation de la luminance des LEDs organiques et l'évolution de la PDIV des isolateurs de paires torsadées sont modélisées. Cette modélisation n'inclut pas de contraintes de vieillissement, mais se concentre sur le choix approprié de modèles semi-empiriques pour les trajectoires de dégradation.

Pour bien choisir les modèles et estimer leurs paramètres, un prétraitement des données est effectué afin de les classer en différents groupes. Les expériences sont ensuite classées selon plusieurs critères, tels que le nombre d'échantillons affectés à cette expérience, ou si les intervalles de temps de vieillissement entre chaque mesure sont uniformes ou non, etc. En plus de ces critères, la présence de temps de défaillance avec les données de dégradation est un critère de classification lié uniquement aux isolateurs car il est possible que les isolants aient une rupture causée par des décharges partielles.

Après avoir nettoyé les données, la dégradation de la luminance des OLEDs est ensuite modélisée de façon déterministe en suivant une trajectoire linéaire ou en suivant le modèle "Stretched Exponential Decay". Plusieurs méthodes d'estimation sont appliquées pour estimer les paramètres de ces modèles. Ces méthodes comprennent la régression linéaire de base, la régression linéaire robuste pour éliminer toutes les valeurs aberrantes, la régression linéaire pondérée pour représenter équitablement tous les échantillons d'une même expérience. Enfin, dans le même but de représenter équitablement tous les échantillons d'une expérience, la dégradation de la luminance de chaque spécimen d'OLED est modélisée séparément, puis la moyenne des paramètres de chaque échantillon est considérée pour l'ensemble de l'expérience.

Le modèle exponentiel est modélisé par une régression non linéaire, qui nécessite la définition d'algorithmes récursifs, de paramètres de départ et de limites de paramètres. La régression non linéaire a également le choix d'être robuste ou pondérée.

Pour choisir le meilleur modèle pour chaque expérience, et la meilleure estimation de ses paramètres, des critères de sélection de modèle sont utilisés, tels que le coefficient de détermination R^2, et le critère d'information d'Akaike AIC. Enfin, la méthode de modélisation qui a été la meilleure par expérience le plus de fois est choisie comme la meilleure pour représenter la dégradation générale de la luminance des OLEDs.

D'autre part, l'évolution de la PDIV des isolants est modélisée selon deux modèles empiriques exponentiels et de puissance. Les méthodes d'estimation sont basées sur la régression non linéaire, ou il y a la possibilité d'être robuste pour éliminer les valeurs aberrantes. Cependant, l'algorithme le plus important est l'estimation pondérée qui est utilisée pour augmenter le poids de toutes les données mesurées avant l'échec d'un échantillon de l'expérience. De même, le meilleur modèle est choisi en fonction des critères présentés ci-dessus.

Chapitre 5 : Méthodes de modélisation de la dégradation sans contraintes avec application aux OLED et aux isolateurs de machines

Dans ce chapitre, l'influence des contraintes de vieillissement sur la dégradation de la luminance des LEDs organiques et l'évolution de la PDIV des isolateurs à paires torsadées sont quantifiées. Pour les LEDs organiques, trois facteurs sont modélisés, la température, le courant et le mode de cyclage

électrique. Pour les isolants, les facteurs sont la température, la tension et la fréquence. Ainsi, les contraintes étudiées dans cette thèse sont uniquement les contraintes thermiques et électriques.

Les paramètres des trajectoires de dégradation sont modélisés en fonction des facteurs de contrainte, afin de quantifier leur influence sur la vitesse de dégradation. Pour ce faire, nous vérifions d'abord que tous les paramètres identifiés ne suivent pas une loi de distribution normale grâce à des tests statistiques. Cela permet de montrer que les contraintes ont une influence non aléatoire sur la variation des paramètres.

Dans une deuxième étape, la relation entre les paramètres et chaque contrainte est identifiée séparément des autres facteurs. Ceci est fait en considérant toutes les expériences qui partagent le même niveau de stress de ce facteur étudié. Notez que cette étude utilise les paramètres de dégradation linéaire de la luminance des OLEDs comme exemple, mais elle peut être appliquée pour tous les autres modèles également. Ainsi, il a été possible de déterminer que le courant a une relation quadratique avec la pente de dégradation par exemple. N'ayant que trois niveaux de température testés, il n'a pas été possible de bien modéliser sa relation avec les paramètres. Pour cela, nous avons eu recours à des modèles physiques qui indiquent que la température a une relation inversement proportionnelle avec le taux de dégradation.

Ensuite, un modèle général qui incorpore non seulement des facteurs quantitatifs mais aussi des facteurs qualitatifs comme le cyclage, en plus des interactions entre les facteurs, est étudié. Les relations entre les paramètres et les facteurs sont estimées par une régression multilinéaire en utilisant différents ensembles d'apprentissage. Une transformation des facteurs est effectuée afin de présenter correctement la relation quadratique entre le courant et le taux de dégradation par exemple. Les ensembles d'apprentissage comprennent des plans factoriels complets et fractionnaires et des surfaces de réponse. Les effets estimés des facteurs sont ensuite comparés entre eux pour chaque ensemble d'apprentissage, afin d'identifier les effets les plus significatifs. La significativité des effets est également mesurée par un test d'analyse de la variance si possible.

Cependant, le critère de sélection le plus important de l'ensemble d'entraînement est la prédiction de la pente de dégradation des expériences qui font partie des ensembles de validation. La pente de dégradation prédite est utilisée pour prédire la durée de vie de l'OLED, lorsque le niveau de luminance chute à 70% de sa valeur initiale. Ainsi, si la durée de vie prédite est incluse dans l'intervalle de confiance de la durée de vie réelle estimée/mesurée de l'expérience, la prédiction est acceptée. De plus, l'erreur de prédiction relative entre la durée de vie mesurée et prédite est calculée afin de choisir le modèle d'apprentissage qui a l'erreur de prédiction la plus faible et les durées de vie prédites les plus acceptées.

Enfin, afin d'avoir un modèle plus généralisé, des données d'autres types d'OLEDs (provenant de thèses précédentes) sont incorporées dans l'étude pour confirmer l'estimation des facteurs. Finalement, l'influence des facteurs sur le taux de dégradation de la PDIV des isolants est également étudiée en suivant la même procédure que celle utilisée pour les OLEDs.

List of publications

Journal papers

Farah Salameh, Andrea Al Haddad, Antoine Picot, Laurent Canale, Georges Zissis, Marie Chabert, and Pascal Maussion. Modeling the luminance degradation of oleds using design of experiments. *IEEE Transactions on Industry Applications*, 55(6):6548–6558, 2019

Andrea Al Haddad, Antoine Picot, Laurent Canale, Pascal Dupuis, Georges Zissis, and Pascal Maussion. Prediction of oled luminance using impedance measurements. *IEEE Transactions on Industry Applications*, 58(1):996–1004, 2022

Conference papers

Andrea al Haddad, Antoine Picot, Laurent Canale, Georges Zissis, and Pascal Maussion. Parametric degradation model of oled using design of experiments (doe). In *2019 IEEE 12th International Symposium on Diagnostics for Electrical Machines, Power Electronics and Drives (SDEMPED)*, pages 432–438, 2019

Andrea Al Haddad, Laurent Canale, Antoine Picot, Georges Zissis, Pascal Maussion, and Pascal Dupuis. Degradation of the luminance and impedance evolution analysis of an oled under thermal and electrical stress. In *IECON 2019 - 45th Annual Conference of the IEEE Industrial Electronics Society*, volume 1, pages 4260–4267, 2019

Oussama Ben Abdellah, Andrea Al Haddad, Mustapha El Halaoui, Pascal Dupuis, Laurent Canale, Adel Asselman, and Georges Zissis. Colorimetric characterizations of large area white oleds under thermal and electrical stress using tm-30-18 method. In *2020 Fifth Junior Conference on Lighting (Lighting)*, pages 1–6, 2020

Andrea Al Haddad, Antoine Picot, Laurent Canale, Georges Zissis, Pascal Maussion, and Pascal Dupuis. Oled luminance prediction using impedance measurements. In *2020 IEEE Industry Applications Society Annual Meeting*, pages 1–6, 2020

Andrea Al Haddad, Antoine Picot, Laurent Canale, Pascal Dupuis, Georges Zissis, and Pascal Maussion. Modeling oled luminance decay under thermal, constant and cyclic electrical stress. In *2021 IEEE Industry Applications Society Annual Meeting (IAS)*, pages 1–6, 2021

Acronyms

OLED	Organic Light Emitting Diodes
PDIV	Partial Discharge Inception Voltage
MTTF	Mean Time To Failure
FMEA	Failure Modes and Effects Analysis
ELT	Experiential Learning Theory
MOSFET	Metal Oxide Semiconductor Field Effect Transistor
P/E	Program/Erase
SEM	Scanning Electron Microscope
PEM	Proton Exchange Membrane
UV	Ultra-Violet
PWM	Pulse-Width Modulation
TEAM	Thermal, Electrical, Ambient and Mechanical ALT
Accelerated Life Testing	
ADT	Accelerated Degradation Testing
R^2	R-squared
ANOVA	Analysis of variance
AIC	Akaike Information Criterion
CV curve	Current-Voltage curve
SLR	Simple Linear Regression
MLR	Multi Linear Regression
OLS	Ordinary Least square
CI	Confidence Interval
SSD	Sample Size Determination
MRA	Meta Regression Analysis
NN	Neural Network
SVM	Support Vector Machine
OFAT	One Factor A Time

RSM	Response surface methodology
CCC	Central Composite Circumscribed
CCF	Central Composite faced
CCI	Central Composite Index
AC	Alternating Current
HV	High Voltage
OLR	Ordinary Linear Regression
WLR	Weighted Linear Regression
RLR	Robust Linear Regression
WRLR	Weighted Robust Linear Regression
SED	Stretched Exponential decay
LED	Logarithmic Exponential decay
QQ-plot	Quantile-Quantile plot
AD test	Anderson Darling test
L70	70 % Lifespan
RMSE	Root Mean Square of error
CR	Current Ration
A	Area

General introduction

Nowadays, the industrial market faces many challenges such as competition between companies, meeting the requirements of safety standards and greener production, as well as meeting customer expectations. Specifically, the industry includes electrical systems almost everywhere in the modern world, from power generation, to transportation, telecommunications and logistics. Since electrical systems could take their share in the failures of industrial components, there is a need to manufacture highly reliable and safe electrical products with improved quality. Given the industrial competition, companies need to develop fast manufacturing processes, which include reliability assessment. In fact, the study of the reliability of a product consists mainly in evaluating its life span and the causes of its failure. However, destructive failure studies are very costly because most of the failed components cannot be repaired. Moreover, for highly reliable components, it may take several years before a failure is observed, which is not possible due to production time constraints.

In this manner, another reliability assessment is possible, based on the study of the behavioral degradation of components. This is possible because most failures often occur after a degradation. The study of degradation is therefore about understanding the mechanisms at the origin of degradation and identifying a threshold below which an aged component has a high probability of failure. This field is very broad and addresses different challenges such as and finding some indicators able to predict the failure and modeling the degradation of this indicator as a function of the reaction causing the failure.

This method requires a thorough understanding of the failure mechanisms, which is not always possible, especially considering that the failure mechanisms are sometimes intertwined. Degradation can also be measured using real-time monitoring or predicted using artificial intelligence methods. However, these techniques do not really identify a general method that can be generalized for the particular component, which can be very costly especially if the product is still being conceptualized. Other methods are based on stochastic modeling of degradation, which is mainly applied if degradation is caused by unidentified random processes. This is not the case for the study of product reliability, especially when degradation experiments are performed in a controlled context.

Finally, deterministic approaches based on the identification of degradation trajectories of electrical components can help to assess reliability. These approaches consists of empirical degradation models that are simple to use, which are developed in this PhD thesis, with the following objectives:

- Modeling degradation paths of electrical components as a function of time
- Identifying a limit below which the degradation path reaches a failure stage
- Predicting accurately the uncertainty of this threshold
- Modeling of degradation trajectories of electrical components with different stress constraints that are common to all electrical systems
- Aging of electrical components under constant and dynamic constraints

- Studying the effect of the interaction of these constraints on the degradation rate of electrical components
- Identifying a good criterion for model selection, in order to evaluate the effectiveness of the models
- Verifying of the modeling approach using different types of electrical components
- Defining of a non-accelerated degradation procedure so as not to modify the degradation mechanisms under normal operating conditions

Keeping in mind these objectives, the PhD thesis is structured as follows:

The first chapter will present the notions of reliability in general, and more particularly those related to failure. The progressive failure mode based on component aging is chosen to be studied in this thesis. More particularly, this thesis will study the model-based approach to understand the evolution of degradation as a function of operating conditions.

In order to model degradation, the aging conditions of various electrical engineering components and their degradation mechanisms will be studied. In particular, two electrical components will be studied in this thesis; the first components are large area organic white light sources (OLEDs). These sources offer several advantages in the world of lighting due to their thinness, low power consumption and their ability to adapt to large application areas. The second components studied are electrical insulators applied to enamelled copper wires, which are commonly used in low voltage electrical machines. The aging factors common to these two components are electrical and thermal factors.

Finally, degradation modeling requires defining the test methods applied, as well as data analysis, which will be presented in this chapter.

The second chapter will focus on the degradation models present in the literature. Degradation models for electrical components can be divided into two categories: degradation physics-based models and empirical data-based models.

A survey of the present physics-based and empirical degradation models found in literature will be presented, and the main degradation models used for OLEDs and insulators will be listed.

On the other hand, these models require the estimation of their parameters. Therefore, several estimation methods and their application to electrical components will be presented. In particular, deterministic methods based on regression analysis will be detailed.

Considering that empirical and physical models require data to estimate their parameters, these data are obtained through experiments conducted in the laboratory. The steps for planning an experiments will be listed in the third chapter including defining the objectives of each experiment and the strategy used. A focus on the design of experiments methodology will be made, to optimally perform multi-factorial experiments.

The experimental campaigns will be detailed for two electrical components, one for organic LEDs and one for twisted pairs of enamelled copper. These campaign will include aging the components under thermal and electrical, constant and cyclic, stress factors.

In the fourth chapter, the luminance degradation of organic LEDs and the PDIV evolution of twisted pair insulators will be modeled. This modeling will not include aging constraints, but shall focus on the appropriate choice of semi-empirical models for the degradation trajectories.

Based on several model selection criteria, the modeling method that is best per experiment the most times will be chosen as the best one to represent the overall luminance degradation of OLEDs and the Partial Discharge Inception Voltage (PDIV) evolution of the twisted pairs of enamelled copper wires.

In the last chapter, the influence of aging stresses on the luminance degradation of organic LEDs and the evolution of the PDIV of twisted pair of insulators will be quantified. For organic LEDs, three stress factors will be modeled, temperature, current and electrical cycling mode. For insulators, the factors will be temperature, voltage and frequency. Thus, the constraints studied in this thesis will be only thermal and electrical stresses factors.

The parameters of the degradation trajectories will be modeled as a function of the stress factors, in order to quantify their influence on the degradation rate. For this purpose, several training sets will be used, where the estimated effects of the stress factors are compared to each other to identify the most significant effects. The best model is selected based on its efficiency to predict either the decay evolution or the lifetime of experiments that are not part of the training set.

The last part of this thesis will present some conclusions with the key outcomes of this PhD study and some perspectives for future work.

Contents

List of Figures

List of Tables

Chapter 1

State of the art: Motivation of studying degradation

Contents

1.1 Introduction

A product must go through several stages, from design to manufacturing, as shown in Figure 1.1. During this process, it is important to test the performance of the product and verify that there are no defects that would lead the product to failure. This is where the study of what is called "reliability", or the study of the immunity of the system to failures [173], comes in, especially from a statistical point of view. Product reliability tests are performed throughout the process, when the product is designed, manufactured and marketed. The International Electrotechnical Commission (IEC) has defined reliability as the ability of a component to perform its appropriate functions under certain conditions for a specified time [103]. In fact, reliability is related to quality, because when a product is highly reliable, it indicates that it is of high quality, reliability being an important factor in today's quality criteria.

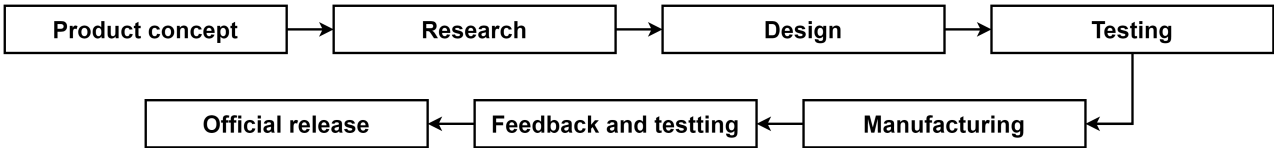

Figure 1.1: Steps of industrial production according to [41]

In engineering, the reliability of a component must take into account all stages of its life. The decisions made at each step of the production process, illustrated by Fig. 1.1, will affect the performance of the product and therefore its reliability. Indeed, two steps of this procedure, the prototype test and the post manufacturing test, directly require a reliability study. However, other steps can add more variability to reliability studies, as the quality of materials used in manufacturing, the manufacturing process, transportation, and the installation process can differ from one product to another, thus changing its reliability. Hazardous incidents encountered in production constitute the "initial" variability that the reliability study must take into account. However, it is the operating and maintenance conditions that differ from one customer to another. Thus, an overall reliability estimate takes into account the customer's environment and usage profile, i.e. the operating conditions of the product.

The operating conditions can lead to a degradation of the product, system or asset under study. However, a degradation is not always related to reliability, because only the degradation that affects the required function of the system is influential. When a degradation is minor, such as a change in appearance, for example, it is not related to reliability. On the other hand, some degradations may lead to system failure, which is directly related to the reliability and maintainability of the system (terms that will be explained later). In this context, the degradation that would lead to a failure plays an important role in the study of reliability. It is therefore important to study the failure modes, and to understand which failure is induced by the system degradation.

In what follows, the concepts of reliability and degradation are introduced, as well as the failure modes and effects analysis that would lead to reliability studies. On this basis, the study of degradation, one of the failure modes, is selected, where its advantages and disadvantages, as well as the objectives sought by degradation modeling, are listed.

The second part studies the approaches that can be adopted to learn about the degradation. The strategies chosen in this thesis are the experimental and model-based approaches, which require a thorough understanding of the degradation mechanisms. Thus, part three presents several examples of degradation in electrical engineering, such as the degradation of metals, semiconductors, and dielectrics. In particular, the degradation mechanisms of organic light-emitting diodes and wire

insulation are studied in depth.

Finally, one of the strategies chosen is the experimental approach, therefore degradation testing methods are presented. The second strategy is degradation modeling, which requires data collection. Thus, some concepts concerning data analysis are introduced.

1.2 Reliability study

1.2.1 Basic concepts of reliability

The basic concepts related to reliability, such as quality, availability, maintainability ... are:

Reliability is *the ability of an item to perform a required function, under given environmental and operational conditions and for a stated period of time* [103]

The item may be a component, a subsystem, or a complete system designed to perform one or more required functions. To provide a service, the item may have one or a combination of required functions. The reliability of an electrical system, according to the North American Electric Reliability Council (NERC), has two aspects: adequacy and safety. Adequacy is the ability of the electric system to meet overall electricity demand and customer energy needs at all times, taking into account scheduled and reasonably expected outages of system elements. Security is the ability of the electrical system to withstand sudden disturbances such as electrical shorts or unanticipated losses of system elements [179].

Quality *"The totality of features and characteristics of a product or service that bear on its ability to satisfy stated or implied needs"* (according to ISO 8402 [102]). Quality is defined as the conformity of a product to specifications. While quality refers to the conformity of the product to its specifications at the time of manufacture, reliability refers to its ability to continue to meet its specifications throughout its useful life. Reliability is therefore an *extension of quality in the temporal domain.*

Availability *The ability of a component to perform its required function at a given time or for a given period of time*[179]. When a system is not repairable, availability is equivalent to reliability.

Maintainability *The ability of an item, under given conditions of use, to be maintained or restored to a condition in which it can perform its required functions, when maintenance is performed under given conditions and using prescribed procedures and resources*[179]. This concept is valid only for repairable systems.

Other concepts Concepts like safety, security and dependability are also related to reliability. Safety is defined as *the level of acceptable risk*, and security as *dependability with respect to prevention of deliberate hostile actions*[179]. Dependability is defined here as availability performance and its influencing factors: reliability performance, maintainability performance and maintenance support performance.

Reliability, depending on the case study, is measured in different ways:

1. Mean time to failure MTTF
2. Number of failures per time unit (failure rate)
3. Survival probability, or the probability that the system won't fail in a time interval $(0, t]$

4. Availability at time t, or the probability that the item is able to function at time t

Most of the methods listed above include failure studies to measure reliability. In this context, the definition of failure is *"the termination of the ability of an item to perform a required function"* [97]. A failure occurs when the required function of the system cannot be performed, or has a performance that does not meet the requirements. Figure 1.2 shows an example presented in [179], if a component with a certain strength is subjected to a certain type of load, a failure will occur as soon as the load is greater than the strength. The study of the reliability of systems or components then includes the

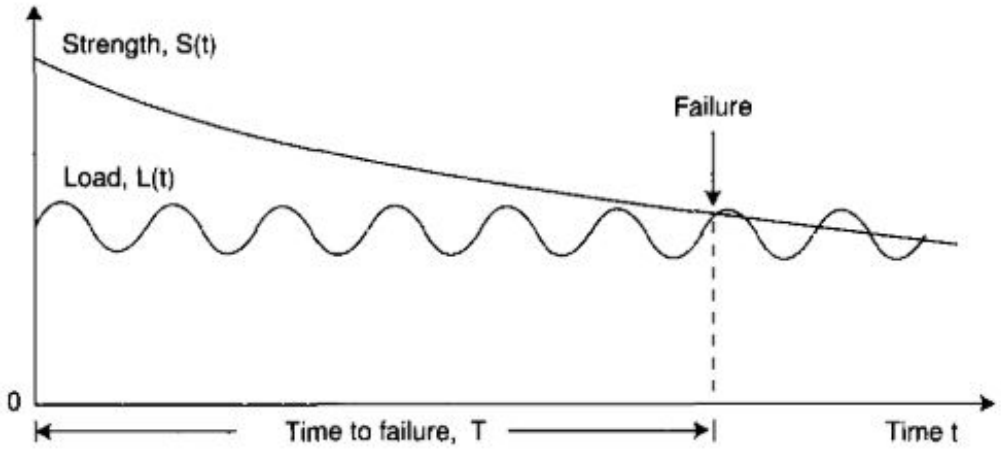

Figure 1.2: Possible realization of the load and the strength of an item leading to a its failure (according to [179])

study of failures and it is therefore important to know all the causes and possible modes of failure, it is a full-fledged study called FMEA, but will be presented briefly in what follows.

1.2.2 Failure Modes and Analysis Effect

Understanding failure modes is very important for improving product reliability, because when potential failure modes and their impact are identified, appropriate corrective actions and plans can be implemented. For instance, if excessive temperature causes a lamp to burn out prematurely, it would be best to modify the design of the lamp to allow for better heat dissipation, or to add an additional cooling process, *etc.*

FMEA, or Failure Modes and Effects Analysis, is a common process analysis tool used to identify all possible failures in a design, manufacturing or assembly process, or product or service [3]. This study is applied in many cases, like

- When a product is being designed or redesigned
- When the application conditions of an existing product change
- Before developing control plans for a new or modified process
- When improvement goals are planned for an existing product
- When failure analysis is performed on an existing product
- Periodically throughout the life of the product

In this thesis, the FMEA study is required for the last two points mentioned above: FMEA studies are performed periodically throughout the life of the product and when analyzing the failures of an existing product. Failure modes, however, differ from the cause of failure, as the former means how the component or system failed, and the latter refers to the circumstances during design, manufacture or use that led to a failure.

Failure can be caused by natural aging, the "primary" failure occurring under nominal system operating conditions. Besides natural aging, it can be caused by external reasons like excessive environmental stress, or by neighboring components like additional thermal, mechanical, electrical, chemical or radioactive shock; the failure is then classified as secondary failure. Finally, transient failure can be caused by an inappropriate control signal or by noise [90].

Many examples of natural and forced degradation, caused by conditions of use, neglect, inadequate skill levels, or poor documentation can be found in [32]. When considering the degradation of engine oil quality in a car, for example, it may be natural due to the internal workings of the engine. The engine has a natural abrasion of its moving parts that would infuse particles into the oil over time, making the oil less effective. Forced oil degradation, on the other hand, occurs when the wrong type or amount of oil is used, which deteriorates the quality of the oil more quickly. Another example of forced degradation due to operating conditions is a refrigerator placed near an oven. In this case, the refrigerator will have to work harder to perform its function than a fridge placed in a cool area, i.e. use more energy to maintain the same temperature level.

Besides natural aging, system failure can be caused by inadequate design relative to the function of the system, or by system weakness when stressed within the nominal range of the function. It can also be caused by a manufacturing error, by a misuse of the system that causes stresses above the standards, by a mishandling of the system or finally by aging because the probability of occurrence increases with time [179].

Concerning failure modes, according to Blache and Shrivastava, there are two types of failures, intermittent and extended failure [29]. An intermittent failure occurs for a very short period of time, after which the system immediately returns to its dull operating norm. Some opinions doubt that this mode should be considered a failure because the defective case is immediately repaired. The second failure mode is called extended failure, or the failure that was not immediately addressed. Extended failure is complete when the system cannot be repaired, it completely ceases to perform its function. If the system does not perform its function, but not completely, due to redundancy for example, the extended failure is partial.

Independently, a failure is said to be "sudden" when its probability is random, or in other words, the failure was not expected, and it could not be predicted by monitoring the system or by measuring the age of the asset. On the other hand, when the failure can be predicted by some condition monitoring indicators, it is called "gradual" or "soft" failure, as opposed to "hard" failure when it is sudden. Failure is called catastrophic when it combines a sudden and complete failure, and is considered degradation when it is partial and gradual. Fig. 1.3, taken from [29], shows the classification of failure modes based on what has been explained above. Keeping in mind all the failure modes presented earlier, the thesis will elaborate on degradation failure in what follows.

Note that the second term of the FMEA is the analysis of the effects caused by the failure modes presented above. This analysis is part of the risk management study, along with failure analysis and reliability estimation. Nevertheless, this thesis focuses only on degradation analysis, and not on risk management or failure analysis to take precautions in operation for example. Therefore, the effects

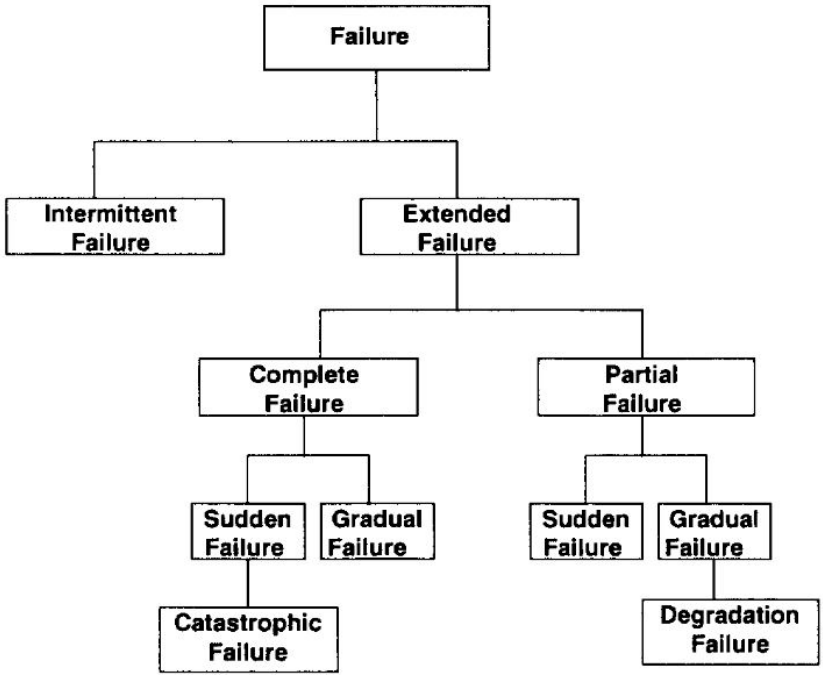

Figure 1.3: Failure modes(from [29])

of failure modes on the system will not be further developed.

As stated earlier, the thesis will focus on the gradual degradation that leads to eventual failure. This study is part of the reliability degradation analysis, or the analysis of the occurrences. This means that degradation occurs before any failure, and therefore provides more data and information about the performance of the component than the time of failure. The data collection could lead to maintenance scheduling, prediction of remaining life of the system, and reliability assessment.

Reliability degradation analysis consists of two types of studies, according to Vesley and Samanta [219]: analysis of the time trends of degradation and analysis of the effect of maintenance on the performance of components. Time trend analysis of degradation involves applying statistical techniques to determine and evaluate the rate at which degradation is progressing and the increase in severity. The effect analysis of maintenance on component performance, on the other hand, is performed when corrective maintenance has been performed after a component has degraded to prevent failure. The concept is to compare the degradation data of two components, one with a maintenance procedure and the other without, to analyze the effect of maintenance on the performance of the component. On the other hand, maintenance is not only performed to extend the overall life of a system, but also to prevent catastrophic failures. In this case, there is usually no data collected for an aged component without maintenance, and this data must be simulated, not measured. This is the case with nuclear power plants, where it is not possible for the component to fail, as this would cause a catastrophic failure of the system.

Additionally, maintenance based on performance data must take into account three criteria: economic, structural and stochastic [213]. For example, maintenance of a system has an *"economic dependency"*, if there is a difference between the maintenance cost of several components and the sum of their individual maintenance costs. There is also a *"stochastic dependency"*, where the condition of one component can affect the condition of other components or their failure rate, e.g. a pump can fail due to contact oxidation and bearing wear.

In this thesis, the degradation of individual components that are not part of a system is studied. Therefore, if the performance of the component deteriorates, it will not cause a catastrophic failure of the system. Hence, no maintenance is required, as the components will be aged to a certain state of failure, whether it is degradation below a certain threshold or destructive failure . . . Moreover, only single components are studied, thus, any dependency between subsystems is not considered here.

In the following, reliability analysis based on the time trends of degradation only is studied thoroughly.

1.2.3 Reliability assessment based on performance data

Reliability is required for complex systems and high-precision products, such as nuclear systems, aerospace systems, underwater cables, and laser devices. Assessing reliability using traditional life tests that record only failure times is not possible for these systems because they are designed to operate for a long period of time without failure. Furthermore, in some cases, systems must not reach a state of failure as this would have catastrophic consequences. To overcome these difficulties, degradation testing is performed, where reliability is assessed based on performance data. However this method has some limitations, that are discussed in the following;

Degradation testing is an important method for assessing the reliability of complex systems and highly reliable products. These systems are designed to operate without failure for many years and the failure process cannot be accelerated unless a new failure mode is introduced. Nevertheless, most of the failure mechanisms can be attributed to underlying degradation processes (e.g., wear, stress corrosion, impact, cracking, fatigue fatigue, etc) for which models may exist.

The effectiveness of a degradation, however, depends heavily on the adequacy of the model to describe the process. For example, components can fail suddenly due to random events, such as thermal and mechanical shocks that result in intense increases in stress [144]. If such events occur in addition to the degradation process, they must be taken into account, typically using a Poisson process for example [137].

On the other hand, since performance data are primarily used to study products that are highly reliable and less likely to fail, there is a tendency to use accelerated degradation to assess lifetime. In this case, very severe degradation can alter degradation performance, and it would cause extreme damage and traumatic failure that would not necessarily occur under natural aging conditions [230].

In other circumstances, where a failure could actually occur, performance data would increase the accuracy of failure detection. Because failure detection depends on many factors and measurements can be noisy, following a degradation path that would lead to eventual failure would reduce the uncertainty surrounding the time of failure. However, this method is not as optimal as simply measuring failure, because performance data must be collected frequently, which requires a lot of effort and time.

Nevertheless, degradation modeling based on performance data, has many objectives that can overcome the limitations presented above.

1.2.4 Objectives of degradation modeling

According to Samanta *et al.* [185], degradation modeling has the following objectives:

- To quantify and characterize the dynamics of degradation.
- To model and quantify the effects of aging on degradation characteristics.

- To model and quantify the failure frequency of components and the effects of aging on this frequency.

- To use component degradation modeling and degradation characteristics to plan component operational activities and to avoid degradation.

- To estimate the frequency of failure of the component from the dynamics of the component and its degradation characteristics.

- To develop a reliability model for component aging using degradation and failure information as input for reliability and aging risk studies.

These objectives fall into different categories such as risk management, prognostic health management and reliability assessment. This thesis will focus on the first two objectives of degradation modeling, namely to quantify the dynamics of degradation and the effects of aging on it. However, the first step in modeling degradation is to select an approach to study degradation and achieve these goals, in addition to understanding the dynamics of degradation, identifying the causes of degradation and what is affected by it. In addition, the approach chosen will determine whether it is useful to study degradation or whether a failure study is more appropriate.

1.3 Degradation learning strategies

There are four groups of approaches that are used for prognosticating degradation models: Experience-based approaches, model-based approaches, knowledge-based approaches, and data-based approaches [84].

Experienced-based approaches Experiential Learning Theory (ELT) is *"the process whereby knowledge is created through the transformation of experience"* [123]. It consists of a four-part cycle beginning with concrete experience, followed by reflective observation, then abstract conceptualization, and finally active experimentation; this method is used widely in education [20, 163]. In fault prognostics, this is the well-known traditional approach to modeling reliability based on the distribution of event records for a population of identical elements. The most widely used distribution is the Weibull distribution represented by the bathtub curve (Fig 1.4), and it is primarily used to describe the three stages of failure: Early failure, represented by a decreasing Weibull rate, random failures, represented by a constant rate, and wear-out failures represented by an increasing failure rate [120].

Experience-based approaches are implemented when failure data is available, and do not take into account the degradation of an asset when predicting its life.

Model-based approaches Model-based approaches derive the explicit relationship between condition variables and degradation/lifetime via mechanism modeling. They typically use physics-based mathematical models and statistical models for an asset to be monitored, collecting input/output data of its operation. These approaches are traditionally used to understand the progression of a component's failure mode as a function of operating conditions, and are thus used to estimate the remaining useful life as a function of uncertainties in the component's stress properties. Typically, model-based prognostic approaches are only as good as their representative models for they require specific knowledge of the system's degradation mechanism and need many assumptions about the operating conditions of the asset. For statistical models, it is often impossible to collect data for all modes of system operating conditions in order to build a generalized model.

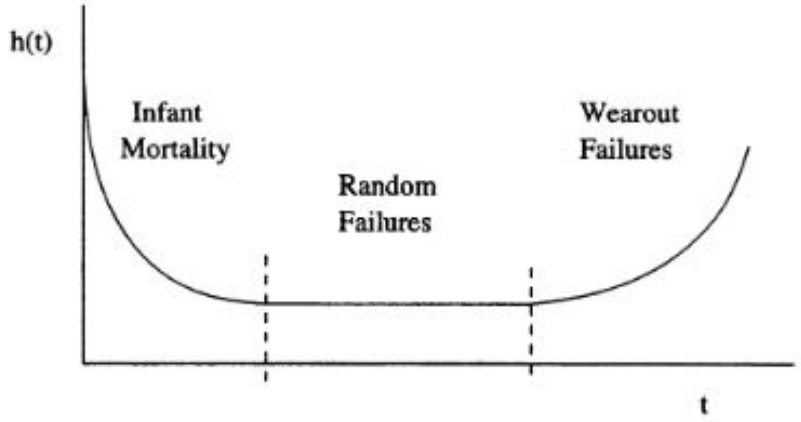

Figure 1.4: The classical bathtub curve based on a hazard Weibull distribution over time (from [120])

Knowledge-based approaches Knowledge-based approaches, such as expert systems and fuzzy logic systems, are algorithms written to solve problems usually solved by human specialists. These approaches do not require a model like the two previous approaches, but are based on the If-Then consequence for expert systems and on real world imprecision and non-statistical uncertainty for fuzzy logic systems. Knowledge-based approaches are generally used in the field of artificial intelligence, and are recently used in the field of fault diagnosis, where it is difficult to build accurate mathematical models, providing predictive decisions for maintenance as an expert would have done in a very humanlike and real-world manner. As much as these approaches have advantages, they also have limitations, as they are very dependent on the decision of an expert who may not have full domain knowledge, as fault cases are unique and human experts may not have encountered such situations before. Even though they require less computation than neural network systems, for example, they still present computational problems with the increasing number of rules to be considered.

Data-driven approaches Data-driven approaches are based on statistical and learning techniques like multivariate statistical methods, black-box methods, and graphical models. Neural networks (NNs) are the typical data-driven approach that is widely applied in prognostics because they can learn the normal conditions of the system and determine whether there are irregularities in the incoming data. They do not require distributional assumptions like traditional approaches, nor do they require prior knowledge of complex phenomena. Although approaches such as neural networks appear simple and easy to execute, they require a large amount of representative training data, including all operating conditions. The main problem with black box methods is their lack of transparency, as the reason for a certain decision is unknown, which could block any future maintenance.

This thesis will be based on model-driven approaches, as it is the main method used for degradation modelling. It is a mathematical and statistical approach used to quantify the dynamics of degradation and the effects of aging on it. Nonetheless it requires good understanding of the component's degradation mechanisms which will be presented in the following.

1.4 Survey of applications in electrical engineering

In electrical engineering, the applications of degradation are quite broad and can be divided into four main categories: Metals, semiconductors and microelectronics, dielectrics and insulators, energy storage and transformations.

1.4.1 Metals

Degradation of metal properties includes creep, crack initiation and propagation, wear, corrosion, oxidation and rust. Shipilov has written a very interesting article presenting cases of catastrophic failures in industry due to metal degradation, such as the failure of a steam turbine in a nuclear power plant at Hinkley, England, or Beznau, Switzerland, etc [194]. Metals have many applications beyond electrical engineering, but they play a major role in the failure of electrical motors for instance, due to rotor bar failure or degradation in their rolling bearing. Broken motor bars are caused by galvanic corrosion that distorts the current waveform and can even cause the metal to melt [125, 180]. Similarly, wear on induction motor bearings due to corrosion, contamination, friction and poor lubrication will increase their friction, causing speed and torque oscillations and reducing the average speed and torque of the motor [99, 154].

Other examples of metallic degradation of systems are magnetic recording media, where degradation of the metallic magnetic moment under thermal stress and high water concentration can affect system performance [148, 168]. Some capacitors have a ferroelectric layer that is very sensitive to hydrogen ions degrading its coercive field and causing an undesirable leakage current density [46]. Surge arresters experience some degradation due to the uncertainty of various electrical stresses and environmental pollution, so the return to the isolation mode is not perfect due to the degradation of their metal-oxide blocks [146]. Applications that involve a high power microwave pulse, such as HPM generators and linear electron gas pedal pedals, can cause mechanical stress on the metal present in these applications, and thus degrade its conductivity and mechanical properties [172].

Overall, electrical engineering applications containing metals are susceptible to aging if the metal is subjected to mechanical, thermal, electrical and environmental stresses like humidity and impurities in the environment. Fig. 1.5 shows different examples of metal degradation like corrosion, oxidation, rust, and cracks that can even cause a total breakage. Fig. 1.5a depicts a rusted metal that exhibits

(a) Rust expansion [36]

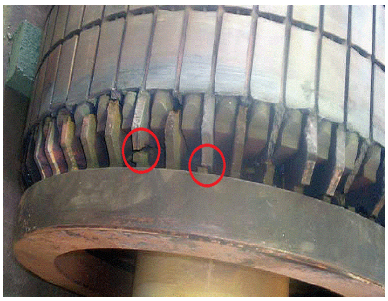

(b) Broken rotor bars [180]

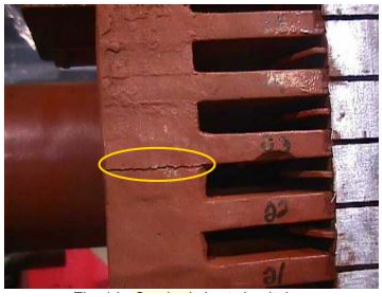

(c) Cracked short circuit ring [205]

Figure 1.5: Examples of degradation of metal properties

volume expansion as rust forms, which has undesirable effects [36]. Fig. 1.5b represents a broken rotor bar in squirrel-cage induction motors [180]. Finally, Figure 1.5c shows a crack in a shorting ring that can occur in motor and generator windings [205].

1.4.2 Semiconductors and microelectronics

The primary cause of failure of a semiconductor device is the movement of a material or charge from its designated location to an unfavorable position [216]. The degradation mechanism can be related

to oxide leakage current, oxide breakdown, over-voltage and electrostatic discharge, and other environmentally induced failures (most degradation mechanisms are thermally activated).

MOSFET devices, for example, are affected by oxide degradation, which increases the leakage current of their dielectric gate and leads to breakdown [141]. Integrated circuits (ICs) operating at high temperatures are susceptible to changes in their parameters over time, which significantly affect their proper operation. In this case, the power dissipation of the IC's base device, such as the complementary metal oxide semiconductor (CMOS), increases. In addition, the quality of operation (speed and accuracy) decreases, and finally, heat-induced latchup can lead to a total loss of functionality [76].

Flash memories are another example that tend to age over time due to many constraints related to their mode of operation. The program/erase (P/E) cycle would apply electrical stress that would cause P/E charge flow drift, and cause memory degradation [215]. There are also other mechanisms that affect flash memory performance, such as loss of electrical charge storage capacity due to tunnel oxides and many others. [50].

Microelectronics are generally a circuit of different electrical components associated with each other using a variety of metals. The interconnections between circuit elements are vulnerable to metal corrosion due to moisture (as discussed in the "Metal" section), which directly affects the reliability of the microelectronics by causing corrosion-induced degradation [164]. In the same concept, the current stress on microelectronics can cause mechanical degradation of solder joints due to Joule heating [228]...

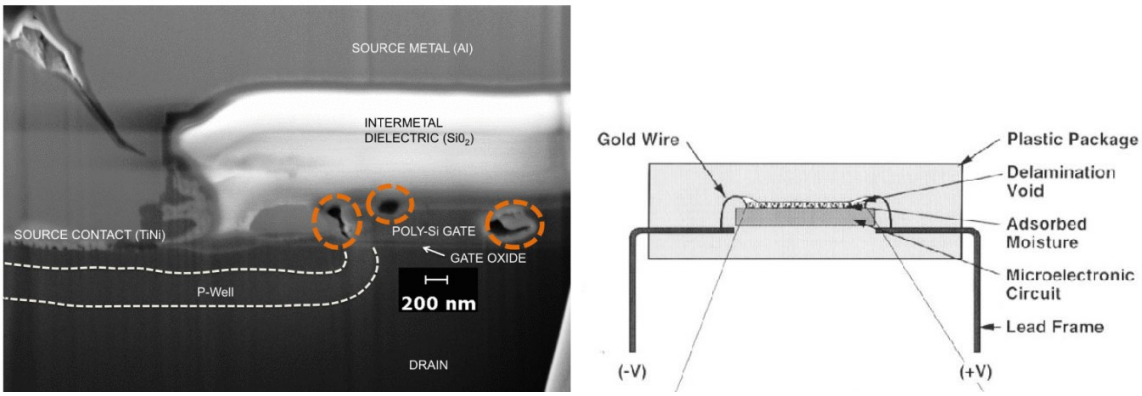

(a) SEM micrograph of a defective MOSFET [165] (b) Schematic diagram of microelectronics degradation by corrosion [164]

Figure 1.6: Examples of degradation of semiconductors and microelectronics

Fig. 1.6 shows two examples of degradation in semiconductors and microelectronics. Fig. 1.6a is a SEM (scanning electron microscope) of a defective MOSFET by gate current leakage [165]. Fig. 1.6b is part of a schematic of a polymer-encapsulated microelectronic device by Osenbach, where the polymer/passivation interface has delaminated, which could lead to moisture absorption and further corrosion of the circuit [164].

1.4.3 Energy storage

Energy storage is also a main field of electrical engineering, whose degradation is widely studied. There are many technologies in this area for different applications, such as storing renewable energy,

powering green electric vehicles or simply supplying mobile electrical systems.

Lithium batteries, which are considered as the long lasting electrochemical batteries, have many degradation mechanisms that reduce their capacity, increase their impedance causing a power fade, and reducing their charging/discharging performance [53, 200]. When aging, Lithium batteries exhibits the growth of solid electrolyte inter-phase, the loss of active material caused by mechanical stress and structural changes of electrodes, impedance increase and lithium plating [79].

Proton Exchange Membrane Fuel Cells (PEMFC) are used as clean regenerative fuel cells storing renewable energy production using water electrolyzers. [201]. Despite the advantages of this technology over conventional batteries, its performance is affected by its complex operating conditions. The aging of PEMFC is caused by degradation of PEM, degradation of catalyst, and aging of the diffusion layer, etc [231] These degradations are caused by dynamic electric loads, start-stop cycles, output temperature of the electrolyzer ... [190]

1.4.4 Dielectrics and insulation

As mentioned in the previous section, one of the main causes of semiconductor degradation is current leakage through their dielectric layers. Other applications that use dielectrics are generators and motors, transformers, capacitors, etc. Instead of evaluating the degradation of the entire electrical system, it may be better and more efficient to study the degradation of dielectrics directly. Measured properties of the insulators include breakdown voltage, elongation, tensile strength and flexural strength [160]. The deterioration factors of electrical insulators are mainly temperature (aggravating factor) and electrical stresses, as well as other secondary factors such as the effect of UV rays, mechanical stresses, radioactive environment, corrosive ambient conditions, oxidation, presence of solvents, etc.

In addition to the examples presented in the previous sections of metals, semiconductors, and microelectronics, where insulation breakdown was a primary cause of component degradation, other cases of insulation and dielectric degradation deserve mention. Insulation breakdown is common in high voltage applications such as high voltage transformers or capacitors in the power distribution system [31] (see Fig. 1.7b). It can also occur in overhead power lines, in underground power cables

(a) Insulation failure causing a fault in distribution line [9]

(b) The cores and coils of a 24 MVA transformer, and electrical insulation tearing in a HV coil [31]

Figure 1.7: Examples of insulation defects in high voltage electrical systems

or in lines that arc with nearby tree branches (see Fig. 1.7a). Because space is considered a partial vacuum environment, high voltage devices are subject to higher stressors such as operating pressure,

electrode geometry, and the frequency and voltage level of applied power within a power system, which cause cause breakdown at lower-level voltages [119].

Stator winding insulation breakdown can cause generator and motor failure [181]. One of the main applications of the degradation modeling studied in this thesis is the degradation of low voltage twisted pair insulation, and a much more detailed review is made for dielectric degradation in the following.

1.4.5 Common degradation mechanisms

All electrical systems have certain degradation mechanisms in common, and when identified, they can be incorporated as signs or outcomes in degradation modeling. These mechanisms include fatigue, creep, cracking, wear, corrosion/oxidation, variation in electrical parameters, and weathering.

- Fatigue is induced when materials are subjected to repeated mechanical loads and unloading, and is a major failure mechanism for bearings and electrical contacts [26].
- Creep is the slow plastic deformation of materials under constant mechanical load, and is one of the causes of failure of solder joints [155].
- Crack growth and initiation is one of the main applications for degradation modeling, especially using stochastic methods [196].
- Wear and tear is the result of friction that would remove part of the material, it often occurs on gears and bearings, as well as on machine tools.
- Corrosion and oxidation are generated by chemical reactions with either oxygen (oxidation and rust) or other chemicals like chlorine, acids, *etc.* These reactions are induced by temperature, humidity, and temperature changes. These reactions are induced by temperature, voltage or other activators, and are a major cause of failure for microelectronics, as discussed previously.
- Electrical parameter variation can be caused by typical operating conditions or accelerated stresses such as temperature and voltage. Variation in parameters can cause a voltage drop in a wiper [112], for example, or a change in the resistance of a rotor, which would require an adaptive control strategy [133].
- Weathering includes solar radiation, moisture, exposure to chemicals such as sulfur, and causes corrosion, rust, *etc.*

In general, when the degradation mechanisms are identified, it is possible to model their effects on the aging performance of the component for assessing its lifetime and eventually for health management. In this thesis, the aging of two components of different kinds, different models, different degradation phenomena and speed are studied. These components are organic LEDs, and insulation of low voltage twisted pair of copper, and in the following, a review of their degradation mechanisms and their particularity is made.

1.5 Focus on OLEDs and insulators

In this section, the degradation mechanisms of two components in the field of electrical engineering are presented: organic light-emitting diodes (OLEDs) and the dielectric insulation of low voltage twisted pairs of copper wire. Even though the degradation of each component is particular, and the physical reasoning behind this degradation might change, it is important to note that the aging factors are usually very similar for most components in the electric field, as presented previously.

1.5.1 OLED components

Organic light emitting diodes, OLED, or organic electro-luminescent devices, were effectively developed for industrial purposes in 1987 [212]. They are organic semiconductors, i.e. carbon-rich compounds whose structure is designed to optimize their luminescent properties [77].

They have developed rapidly over the past few decades due to their many advantages, like being a flat, uniform light source with excellent color rendering. They are thin-film multi-layer devices consisting of a substrate foil, film or plate, an electrode layer, layers of active organic materials, a counter electrode layer called cathode, and a protective barrier layer like glass [204] . The electrodes produces excitons like holes for the anode and electrons for the cathode, that recombine in the emissive layer to produce a photon (see Fig. 1.8a). The produced light naturally diffuses through thin

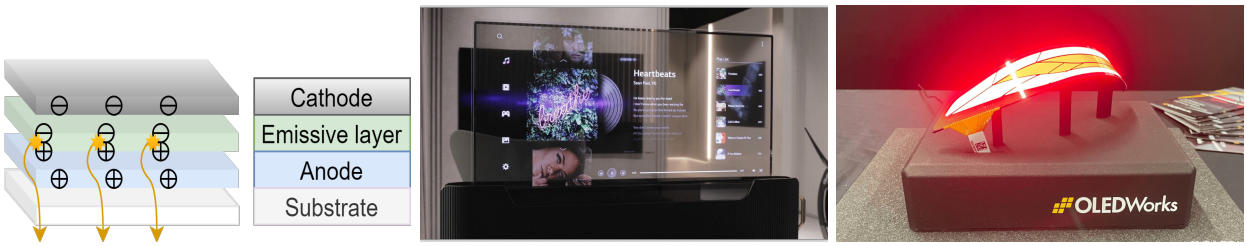

(a) 2D section diagram of a single layer OLED

(b) LG Smart Bed TV transparent display concept [21]

(c) Bendable automotive OLED lighting panel [6]

Figure 1.8: OLED technology: concept and applications

layers of material, and the OLEDs they have low power consumption and fast response time. OLEDs have a low operational temperature, unlike typical LEDs that generate a large amount of heat during operation and thus require additional heat sinking [166]. They have unique application compared to other lighting technologies, as organic layers can be deposited on several type of substrate, making it possible to create large-area, flexible or even transparent panels.

OLED technology is very used in display for TVs and smartphones, as it has a great image quality, exceptional contrast with good darkness representation as well as higher brightness, fuller viewing angle, wider color rendering than other display technologies. Fig. 1.8b represents an innovation idea of a transparent TV made from a transparent OLED screen presented at the 2021 Consumer Electronic Show (CES) [21].

OLED technology is also used for lighting, as it is very designer-friendly. Their panels are ultra-thin and lightweight, do not produce UV light and have a low heat emission [7]. They also have excellent uniformity, color consistency and low glare making them the perfect choice for museums for example, machine visions application and health-care [7]. Fig. 1.8c shows an application of flexible OLED panels in the automotive field [6].

Although OLEDs have many advantages, they have pronounced degradation mechanisms due to their organic composition. In order to make this technology reliable enough for mass production, their degradation mechanisms must be investigated. According to Aziz *et al.* , degradation of OLED have three different modes that will be detailed in the following based on the paper [24].

- dark-spot luminance degradation
- catastrophic failure
- intrinsic degradation

The degradation of the dark spots is related to the decrease of the luminance in a particular point because of the build-up of non emissive materials on the emissive layer of the OLED. These accumulations are caused by electrochemical mechanisms and by thermal heating due to manufacturing defects. As known, OLEDs are built by spin layer depositing technique, which results in homogeneous layers, but can sometimes add unwanted bumps that can turn into dark spots or even high-brightness spots later on.

On the other hand, during OLED operation, oxidation or delamination of the organic layer electrodes can occur due to absorbed moisture. In addition, structural deformation of OLEDs, i.e. local and lateral changes in the chemical structure, leads to lateral degradation of the bond strength of the layers. One probable explanation of this type of degradation degradation is the structural change of the polymers due to charge carrier transportation and therefore the heat formation [193].

Dark spots and delamination cause a high local current density that generates hot spots. In fact, electrical stress activates electrochemical reactions that expands polymer liquids, emits oxygen, CO2 or other gases, which results in bubble growth in the non-emissive areas, local high current density and local heating [116]. The organic layer, subjected to these hot spots, will also develop gas, resulting in bubble-like bumps that will eventually increase the hot spot until the thin organic layer is burned away. In this case, the electrodes will be in direct contact, causing electrical shorts and diffusion of metal into the polymers, resulting in the expansion of dark spots and eventual failure of the device. This mechanism is called the catastrophic failure from a structural-defect-related cause. Other catastrophic failures are caused by mechanical expansion when the operating temperature of the OLED is above the critical temperature of its organic layer.

Finally, the last degradation mode is the natural progressive evolution of the OLED characteristics during its operating time, called "intrinsic" degradation. It does not depend on the material, unlike the two previous degradation modes. The evolution of the OLED characteristics can be linked to the crystallization and the increase of the roughness of the organic layers with time, in particular for high temperature operating conditions. In addition, the recombination of holes and electrons with time can modify the characteristics of OLEDs, because the more the recombination is important, the less the mobility of excitons is important and their production is reduced. Furthermore, the anode can release some indium to the organic layer that changes the device's electro-luminescence. Ionic impurities from charge recombination and redistribution, and trapped positive charge at the emissive layer can increase the electrical impedance of the OLED with time. With time, the polymer layer will appear thinner due to degradation and the edge of the nonemissive area expand [116].

Although OLED main functionality is to produce light, it is important to note that OLEDs light emitting is reversible, which can have the same application as solar panels [38], or why not use it in a window application where it charges electricity from the daylight and act as a display in the evening for example [49]. However, this reversible characteristic can cause OLED aging, in such way that degradation of OLED might occurs when exposed to light, more particularly UV lights. When OLEDs with cathode made of magnesium is irradiated by UV, electron injection into the emissive layer deteriorates, increasing the resistance between the electrodes [128]. Overall, these are the main external factors for the OLED aging: temperature, current flow, UV light exposition, oxygen and moisture. Oxygen and moisture effects can be avoided by a good encapsulation of the OLED, and by choosing the right polymer material to avoid any internal chemical reactions that may produce oxygen or other gases. UV light exposure is avoided by adding a protection film on the glass substrate that absorbs the UV lights. In this manner, the aging of OLED is essentially caused by thermal and electrical stress.

1.5.2 Dielectric insulators materials

Another component used in electrical engineering applications is the dielectric around the cables. While OLEDs are a recent technology of about 30 years, winding insulation has been widely studied for more than a century, thanks to the important role it plays in the reliability of the overall machine. The stator and rotor windings of electrical machines are expected to have a long service life. In industrial applications, an electric motor or generator is expected to have a service life of at least 20 years.

Recently, electrical machines have been optimally designed to increase the efficiency of electrical production, reduce size and weight for aeronautical and automotive applications, or simply to reduce production cost. Optimal machine design changes many features, such as reducing the size of the air gaps, which results in a more concentrated flux, or reducing the thickness of the wires used, which reduces the thickness of the insulation around those wires. Most designs do not take into account the wear and tear of the insulation over time, as their optimum target is already listed. Nevertheless, designing a more compact machine would increase the stress on it, which would increase the risk of failure. In addition to the design, other factors also increase the stress on the machine, such as increasing PWM voltage, switching frequencies and reducing switching times. One of the main reasons for the failure of electrical machines is the failure of the insulation system. In what follows, the mechanisms of insulator aging are detailed, i.e., the types of stresses that can deteriorate dielectric materials and the indications of degradation.

The main stress factors that can cause an insulation deterioration and failure are joined under "TEAM" referring to the following factors [206]:

- Thermal
- Electrical
- Ambient
- Mechanical

Thermal stress can cause chemical reactions in the insulation, such as surface oxidation, or delamination due to loss of bonding strength. Thermal stress can be caused by machine overheating, due to core losses, losses in the copper conductors like I^2R, eddy current and stray load losses. The temperature increase could induce mechanical stress, as the temperature increase would cause the copper wire to expand more than the surrounding insulation. This expansion creates a shear stress and causes a bond break between the copper and its insulation. This type of stress is called thermo-mechanical stress because it is a mechanical stress induced by thermal causes, mainly by thermal cycling.

Electric stress factors can be power losses, high local resistance and capacitive currents because the coating impedance can be non-homogeneous. These factors lead to local overheating, oxidation of the insulation coating, sometimes even vaporization of the organic materials ([206], chapter 8.6), and air gap breakdown ([206], chapter 8.5) which can contribute to some discharge appearance. Partial discharges are the most influential factor that can cause deterioration. These are small electrical sparks that occur in the insulation and can cause the breakdown of certain chemical bonds within the insulation, the production of ozone gas, the perforation of the material and, sometimes, failure. Partial discharges are considered the main cause of insulator aging and premature failure under electro-thermal stress with high frequency voltage [65, 152]. Note that sometimes thermal stress can be beneficial because it removes any moisture from the winding, reducing the chance of electrical

failure. It can also cause some type of insulation to swell, reducing partial discharge in the swollen area.

On the other hand, moisture is one of the environmental conditions that can cause insulation failure. The common ambient abrasive factors, based on Stone et al. book, chapter 2.1 ([206], are moisture condensed on the windings, high humidity, aggressive chemicals, oil from other parts in the machine, pollution like dirt, debris and particles from the operating environment. Ambient conditions act as a catalyst to accelerate the degradation process caused by the other TEAM factors.

Finally, mechanical stresses such as centrifugal forces can distort or even crush the insulation. Vibrations due to magnetic forces induced by power frequency currents can abrade the insulation (if the windings are free to vibrate or come loose). Lastly, magnetic forces induced by high power transient currents, e.g. from motor start-up, can bend coils or bars and sometimes crack their insulation system.

In addition to the basic TEAM stresses and their interactions, nuclear radiation can cause abrasive chemical deterioration of the insulation surface if the application is in a nuclear power generation field [126].

In general, the most common stress factors between OLEDs and insulators are thermal and electrical factors. The degradation mechanisms of both electrical components have many common behaviors such as local impedance concentration, delamination, etc. Although each component has its own applications, operating modes, and degradation mechanisms, this thesis will focus on the common aging factors, and build a general methodology to model their degradation with these aging factors.

1.6 Degradation test methods

After understanding the degradation mechanisms of components, the second phase of model-based approach is to collect input/output data of its operation. For this purpose, the test method must be defined when planning for degradation; methods include destructive or nondestructive testing, as well as normal or accelerated testing.

1.6.1 Destructive vs non destructive degradation analysis

Degradation analysis is essentially measuring performance and degradation data, extrapolating them, and directly linking them to the suspected product failure. In order to establish a timely view of degradation, multiple measurements must be made on the same unit throughout the life of the product. Non-destructive measurements of degradation are collected in many examples, such as brake pad wear, crack size propagation, battery voltage decrease, LED bulb light output degradation... However, in some cases, measuring degradation would require destructive testing, which would affect the performance of the product so that it could not be returned to service for further aging. Examples of destructive testing include measuring corrosion in a chemical container or measuring the strength of an adhesive bond.

The evolution of breakdown voltage as a function of aging is a typical example of a destructive measurement used to assess degradation. Nelson was the first to study degradation using destructive testing [159]: he tested the degradation of electrical insulation under the same experimental conditions 8 times, for 8 different aging times ranging from 1 to 64 weeks. After each experiment has reached its expected initial aging time, the specimen is then subjected to a high voltage stress that

will cause a "destructive" breakdown of the insulation. The indicator of aging is therefore the breakdown stress which is modeled according to the thermal laws of the insulator and the given results. Similar studies have subsequently been conducted in numerous articles [207]. There are many other applications of destructive degradation analysis in the literature, such as measuring the strength of an adhesive bond. [74], or measuring corrosion in a chemical container.

Destructive measurements involve the tester interrupting operations to allow the test process to proceed, and potentially damaging valuable equipment used in or around the process. A non-destructive approach, such as ultrasonic inspection, Eddy current inspection, radiography/x-ray inspection, is the most effective approach, because it is more sensitive and can detect more aberrations in less time than destructive inspection. Destructive measurements are a one-measurement process, so using this single value, it is not possible to differentiate between initial defects caused by manufacturing and defects caused by aging. This is a case mentioned in the paper of Escobar *et al.* , where some measurements showed suspiciously low values, which were attributed to the manufacture of these units [74]. Data from these units were modeled using right-censored values with the assumption that the true value is unknown, but should be higher than recorded. In addition to the uncertainties caused by the one and only possible measurement, the destructive process costs companies a lot of time and money that can easily be saved with the non-destructive approach.

1.6.2 Accelerated degradation testing vs accelerated life testing

Shorter product development imposes a severe time constraint, which is not suitable for a life/degradation testing approach, especially if the product under test is highly reliable and has a long life. Accelerating the degradation would be a better solution than waiting for a failure that might not occur during a normal functional testing. According to Elsayed, there are three approaches to accelerated life testing [70]:

- To accelerate the "use" of a product under normal operating conditions. This mode is primarily tested for products that are not used continuously, such as home appliances and car tires that are used only a fraction of the time in a typical day.
- To accelerate aging of a product by imposing higher-than-normal operating conditions to accelerate failure. This approach is the most frequently used in the world of reliability assessment.
- To test under accelerated stress, defective or used products that have already exhibited some type of degradation, such as metal corrosion or mechanical component wear.

Although Elsayed considers the third approach to accelerated life testing (ALT) to be the accelerated degradation test (ADT), the second approach is the most widely used for both ALT and ADT modes. The difference between the two modes is based on the application, for example, if a highly reliable product with a long service life does not fail even with ALT, it is better to use the degradation approach. The difference lies in the outcome to be modeled, whether it is the mean time to failure MTTF or the degradation trajectory that would eventually lead to an estimate of the MTTF, and a reliability assessment. The latter is done by extrapolating the performance degradation to estimate when the performance reaches a failure level.

The main advantages of accelerated degradation over accelerated life testing are that performance degradation data can be analyzed earlier, before a product fails. Extrapolating lifetime data from degradation gives more options for using different design choices or assumptions about the level of performance leading to failure [160]. For example, some experts assume that an LED fails when its luminance reaches 50 % of its initial value and other schools consider a level of 70 %. Modeling the degradation instead of just the lifetime test would allow comparison of the two lifetime estimates,

selection of the better model, and increase the accuracy of the lifetime estimates.

Most reliability studies in the literature are based on accelerated testing, as these are the most time effective procedures. Note that the acceleration effect must be accounted for in the modeling in order to be able to predict lifetime under normal conditions.

Having stated the above comparisons, this thesis will use non-destructive accelerated degradation tests where measurements will be collected frequently. The input/output data of the collected measurement are then processed for modeling, where the processing methodology is presented in the following.

1.7 Data analysis

Results of degradation testing depend on whether they are destructive or not, whether they are accelerated or not, and if it is the performance that is desired for modeling or the lifetime *i.e.* the mean time to failure. As established in this chapter, we will be focusing on performance data, which will allow for good degradation modeling, while relating performance to age and stress.

1.7.1 Data types

Performance data consist of collecting data while looking for any degradation of objects, assets or systems. The group of objects to be studied are considered a **population** of interest. A **sample** is a subset of the population, for example, in the reliability domain, a sample is taken from the population in order to investigate the aging of that population under specific conditions.

Variables are changes in the characteristics of objects in the population. Variables can be categorical, such as the type of capacitor tested, or numerical, such as the operating temperature level. A univariate data set consists of observations made on a single variable, and a multivariate data set consists of observations made on more than one variable.

When desired information is available for all objects in the population, the data are called a census [63]. However, for performance data, which have constraints on data collection like time or money, complete information may not be available. Hence, data can be classified as [63]:

- Complete data includes performance data and the exact life (failure time) of each sample unit. Most of the performance data are incomplete, because failure may not occur during aging for reasons discussed previously.
- Censored data are of the type when some knowledge is missing.
  - The right-censored data are performance data with no failure time. So, if an aging process stopped before failure, the lifetime is known only to be beyond the process stop time. Sometimes, for maintenance purposes for example, failure may not occur and operation should not stop, so the data used for analysis are right-censored, and the lifetime is known only to be beyond the current running time. Other times, during data collection, some samples might fail due to uncontrolled accidents that are not related to the aging process, for example, a measurement error resulting in specimen failure. In such cases, data are also considered right censored.
  - Left censored data are performance data that failed before the assigned measurement time
  - Interval data are primarily performance data that are also left censored. For example, when inspections or measurements are performed regularly and a failure occurs between

two inspections, without knowing the exact time of the failure, the possibility of failure is then limited to a certain time interval.

- Competing data are data where sample units fail from different causes
- Quantal-response is a data type limited to life data only, as only one measurement is made during aging, to check if the specimen has already failed or not. This data are usually binary.

Fig. 1.9 summarizes these, and while some types of data are common to life and performance data, others are not, depending of several factors. The main data types that are used in the degradation

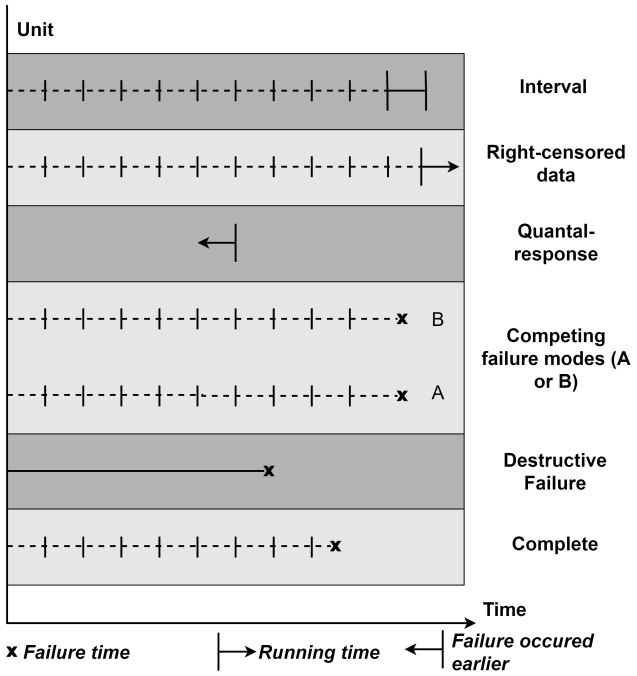

Figure 1.9: Types of data

modeling of this thesis are complete data where both performance and failure data are logged. In addition, when failure data are not recorded, only performance data is considered as right-censored data.

1.7.2 Descriptive statistics

Data analysis requires the interpretation of summary measures, by analyzing descriptive statistics such as the mean value and standard deviation of the sample or population. While these descriptive statistics are primarily applied to numerical data, similar concepts can be used for categorical data.

Descriptive statistics include the mean and median value of a sample or a population, and their standard deviation and variance. It also considers if the population is symmetric or skewed, and computes the confidence interval that groups a certain percentage of the population. It can also test if data are correlated or random (For more info on the descriptive statistics, see Appendix. A.1).

1.7.3 Data pre-processing

Data pre-processing can refer to the manipulation or dropping of data prior to its use to ensure or enhance performance. In most cases, the outcome of modelling is affected by data quality. The characteristics of data quality are:

- Validity, *i.e.* conformity to constraints or rules (a man cannot be pregnant for example, nor a resistance value can be negative)
- Accuracy, *i.e.* the closeness of the data to the actual true values
- Completeness, when all required data are known
- Consistency, when data from the same population are regular or consistent
- Uniformity, where data from the same population have the same unit of measure

When a data set lacks some of the data quality characteristics, some treatment should be performed to improve model fit and true representation to real life.

Data cleaning Data cleaning is the process of removing data that don't seem to belong in the data set. Data cleaning improves data quality by removing errors when multiple data sources are used. It also enhances the ability to use different models that does not usually consider incomplete or stochastic data... The basic steps of data cleaning are presented in Appendix A.2. Finally, after the cleaning process, the data must be validated by checking if the cleaned data have some signification, if they follow the appropriate rules for their domain, or if they show trends that can be modelled, *etc.*

Data integration Data integration is the process of combining data from multiple sources into a coherent data set. Metadata are the characteristics of the data that would aid in such error-free integration, like the name, meaning, data type, range of values permitted for the attribute and null rules handling missing values [87]. In data integration, data can be modified to fit the modelling rules, minimize fitting errors and enhance the total result, without changing their descriptive statistics. Normalization, standardization and transformation are operations that reshape data into a form that is practical for modelling.

Normalizing data involves scaling their values to fall within a small specified range. The concept of normalization is based on the fact that variables can have different units, types or sizes. If they are not scaled, some variables may weigh more than other variables in the modelling, misleading or distorting the results. There are three methods of normalization [87] that will be used in this thesis: min-max normalization, z-score normalization and normalization by decimal scaling (see A.3 for information).

On the other hand, when two or more variables have a nonlinear relationship, and the model to be used is only applicable for a linear relationship, transforming the dependent variable would linearize this relationship. If a variable y has a nonlinear relationship with a variable x such as $y = f(x) = alog(x) + b$, instead of using a nonlinear method to find the parameters a and b of the model, x would be transformed to $x' = log(x)$, so that y and x' would have a linear relationship f'.

1.7.4 Model selection

Different degradation models based on different modeling methods exist, which will be detailed in the next chapter. These methods are classified into several groups like physics-based or statistics-based models, etc [84]. Since many models are classified into several specific groups, some models may be better suited for degradation than others, as they may take into account factors that influence aging and increase the accuracy of the performance modeling, for example. Model selection methods are used to compare models and select the best candidate given the data. These methods can also be applied, not only on different models, but to check if the selected data are well adapted to the model

or not.

Model selection is widely used for machine learning, where the data are divided into three groups: training data that will estimate the parameters of the model; validation data that will predict results based on the fitted model, and estimate the prediction error, used for model selection; and test data that are used for assessment of the generalization error of the final chosen model. The data set is usually divided in the following ratio: 50 % for training data, 25 % for validation and 25 % for testing. In general, machine learning is applied to big data where such split is feasible, but the performance data for reliability consist mainly of small or medium sized data. In the case of degradation modelling, splits can be limited to just the training/learning set and the validation set.

As mentioned, model selection in machine learning uses the prediction error to assess model fit. The fit of a simple model is judged by the error sum of squares SSE, which measures the amount of variation in the data that is left unexplained by the model. The fit error is the primary indicator of a model quality, however, there are many better methods for testing the model fit. The main criteria suitable for comparing degradation models are presented in Table 1.1.

Table 1.1: Model selection criteria

Statistic	**Criterion**
R-squared R^2 and Adjusted R-Squared R^2_{adj}	Higher the better
F-Statistic and ANalysis Of VAriance (ANOVA)	Higher the better
Std. Error	Closer to zero the better
t-statistic	Should be greater 1.96 for p-value to be less than 0.05
Information criteria (Akaike information criterion AIC, etc)	Lower the better

For more details on these criteria, see Appendix A.5. Note that there are many other criteria which can help in the selection of models, depending on the modeling applications like cross validation (mainly used for big data), χ^2 tests, etc. These criteria are not used in this thesis as they are not suitable or needed for degradation modeling application .

1.8 Conclusion

This chapter presented the reliability study based on degradation modeling to assess the life of a product. It was considered preferable to use performance data rather than failure time data, for all the information that degradation data provides, especially for understanding the mechanisms behind failure modes.

Performance data can be modeled using different strategies, which have been presented above. In particular, degradation modeling based on a physical and empirical model approach was chosen as the best strategy to truly understand degradation. These models are thus detailed in depth in Chapter 2, and accompanied by some examples concerning their application in electrical engineering, and more particularly for OLEDs and insulators. For this purpose, the degradation mechanisms of several applications in electrical engineering are presented, in order to identify the common influencing factors on the degradation of electrical components in general.

Most of the models require experimental data to estimate their parameters (especially the empirical models), hence the model-based approach and the experimental approach are complementary.

In Chapter 3, the methodology of experimental design is presented in general, in order to optimize the cost of the experiments. Therefore, some test methods presented in this chapter will be used, where it is chosen to perform non-destructive and accelerated degradation experiments. In particular, the experimental design of OLEDs is detailed, where industrial OLEDs are aged for different stress conditions, including constant and dynamic cycling. In addition, the experimental design of the insulator is also carried out, where a twisted pairs of low voltage enameled copper are fabricated and aged under different thermal and electrical stress conditions.

Finally, some of the basic concepts concerning data treatment needed for the modeling in Chapter 2 are presented. Chapters 4 and 5, that analyze the performance data from the two experimental designs, also use some of the basic data concepts present in this chapter.

Chapter 2

Degradation models

Contents

2.1 Introduction

In chapter 1, it was established that in order to assess the reliability of a component, it is preferable to understand its degradation, and especially by using model-based approaches. This chapter details in depth the modeling of degradation in general, and in particular the degradation of electrical components. In the model-based approach of degradation learning strategies, there are mainly two types of models: physics-based models and statistics-based models [84]. These models can include stress factors related to their degradation mechanisms or can simply model the decay trajectory of a component regardless of their wear conditions. Finally models can reflect normal or accelerated degradation mechanisms.

- **Normal** degradation models are based on degradation data collected under normal operating conditions. **Accelerated** degradation models, on the other hand, use degradation data under accelerated time or stress conditions to assess reliability under normal conditions. These accelerated models are the most commonly used for reliability assessments, for reasons discussed earlier, and are therefore studied in this thesis.

- Models **without stress factors** like random process model [237] are applied in two cases; the first case is when the aging conditions are not known or measured. This is mainly the case of normal degradation when the aging circumstances are not surveyed. The second case is where aging conditions are known (because they are measured or imposed to accelerate the degradation), but are fixed at a level, so the stress factors do not vary with the experiments.

  Models **with stress factors** are models where the degradation is a function of the defined stress, when the aging conditions are known and the stress factors vary from one experiment to another.

- **Physics-based** models group the Arrhenius model for studying temperature effect on degradation, the Eyring model for accelerated aging with respect to thermal and non-thermal variables, the inverse power model for accelerated aging with respect to non-thermal variables, *etc* [84].

  Statistics-based models of degradation are mainly parametric models [160] and semi-parametric models with covariates to estimate the hazard of assets [54, 85].

In this chapter, the first two sections will discuss the two categories of degradation models: physics-based models, if the physics of degradation is known, or empirical data-based models, otherwise. Both categories are based on accelerated degradation where the stress factors are known. In particular, a review of the application of these degradation models to OLEDs and insulators is presented.

Considering that degradation is usually modeled using semi-empirical models, it is important to estimate their parameters. Therefore, deterministic estimation methods based on regression are fully detailed. A small review of advanced deterministic approaches such as neural networks and online modeling is also presented.

These models give an output for a single set of inputs and do not take randomness into account. Stochastic models, on the other hand, address randomness within the models. Thus, stochastic processes will be presented and an application of linear degradation using the Wiener process will be detailed.

Finally, the chapter will also address the modeling of degradation under dynamic variation of aging factors. More specifically, the modeling of cycling for OLEDs and insulators is presented, if available.

2.2 Physical-based degradation models

Degradation mechanisms have been discussed in 1.4.5, where they are attributed to multiple causes. Once the degradation mechanism of a product is thoroughly understood, it is possible to build a degradation model based on the physical process of the component or on chemical reaction laws. The most commonly used physical acceleration models are the Arrhenius model and the Eyring model, which have proven effective in modelling physical decays for a wide range of engineering applications [136].

2.2.1 Arrhenius model

The Arrhenius model accounts for the effect of temperature on the failure or degradation mechanism. The model was constructed to establish an inverse proportional relationship between chemical reaction rates and the applied temperature. The Arrhenius equation in Eq. 2.1 gives the dependence of the rate constant $R(T)$ of a chemical reaction on the absolute temperature T. For degradation applications, $R(T)$ is the behavioural decay rate of the component under high thermal stress. A is the pre-exponential temperature independent factor, E_a is the activation energy for the reaction and R is the universal gas constant [129].

$$R(T) = A \exp\{-\frac{E_a}{RT}\} \tag{2.1}$$

The Arrhenius model is applied to a wide range of applications, like modelling the power decay rate of photovoltaic cells, or the decay rate of their encapsulation discoloration with different temperature, moisture or UV levels [157, 199]. It is also used to model the degradation of Kraft paper insulation materials used in power transformers [60], or to distinguish the degradation mechanisms of MOSFETs as a function of temperature[22].

2.2.2 Eyring model

The Eyring model is another popular physical-based degradation model, which in addition to temperature, takes into account other stressors or covariates, like the effects of material properties, working conditions, activation energy and reaction dynamics. The Eyring model is based on a statistical mechanical justification, and is represented in Eq. 2.2, where R is reaction rate constant and T and X are respectively the temperature and other non-thermal covariate stressors [136]. k is the Boltzmann constant, k_1, k_2 and k_3 are the equation parameters, originally related to the chemical reaction but in the case of degradation, they can be related to the physical degradation process.

$$R(T, X) = \phi T^m \exp\{-\frac{k_1}{kT}\} \ \exp\{(k_2 X + \frac{k_3 X}{kT})\} \tag{2.2}$$

The Eyring model has been used to analyze the degradation of capacity of Li-ion batteries, based on temperature, current and depth of discharge [58]. It is also applied to model the degradation of LEDs under voltage and temperature stresses [121], or capacitor aging data [71], the thermo-electric degradation of motor insulation systems [235].

Eyring model does not specify the other stress factor X along with temperature, but the stress can be:

- A mechanical load (as in Weertman's model for creep rupture [86])
- Humidity (as in Peck's model for corrosion [171]);
- Current density (as in Black's model for electro-migration [30])

2.2.3 Peck's temperature–humidity model

Eyring model is widely used for constructing a relationship between the degradation rate $R_{Eyring}(T, rh)$ and temperature T and relative humidity rh (see Eq. 2.3, where E_a is the activation energy, k is the Boltzmann constant, A and b are the model's parameters)

$$R_{Eyring}(T, rh) = A \ \exp\{-\frac{E_a}{kT} - \frac{b}{rh}\} \tag{2.3}$$

Pecks model is another model that relates temperature and humidity to degradation rate (see Eq. 2.4, where B and n are the model's parameters)

$$R_{Peck}(T, rh) = B \ \exp\{ -\frac{E_a}{kT}\} \ (rh)^n \tag{2.4}$$

The previous two equations were mentioned in Park and Kim work [167], where they studied the effect of temperature and humidity on the power generation degradation rate of photovoltaic modules.

It is important to note that the original Peck's model considers the relationship between temperature, relative humidity and time-to-failure [171].

2.2.4 Black's model for current density

Black's model originally is used to estimate the mean time to failure of a semiconductor circuit due to electro-migration [30]. See Eq. 2.5 for Black's model, where $MTTF$ is the mean time to failure, j is the current density, T is the temperature, E_a is the activation energy and k is the Boltzmann's constant. $B(T)$ is related to the properties and geometry of the material and interconnection, but it can also be related to temperature, and more specifically, this stress can build-up over time according to Korhonen's model [61]. Thus, instead of a mean-time-to-failure model, a dynamic model can be constructed that includes the variation in stress. Note that even if dynamic stress was incorporated with the MTTF model, it is still not a degradation model, but it can help in understanding the relationship between current density and degradation.

$$MTTF = \frac{B(T)}{j^2} \exp\{\frac{E_a}{kT}\} \tag{2.5}$$

2.2.5 Solder based fatigue models

Solder fatigue is the mechanical degradation of the solder due to deformation under cyclic loading, such as cyclic temperature fluctuations [73], mechanical bending [45], etc. Most solder-fatigue models are failure-based approaches, as they relate the physical parameter to cycles to failure. They are based on Miner's rule [151], that constructed the simplest cumulative damage model of Eq. 2.6. C is the fraction of damage, or the fraction of life consumed by exposure to cycling at different stress levels. It considers that a failure occurs when the damage fraction tends to 1. k is the number of stress factors, and N_i is the average number of cycles to failure at the i^{th} stress S_i. n_i is the number of cycles accumulated at stress S_i.

$$C = \sum_{i=1}^{k} \frac{n_i}{N_i} \tag{2.6}$$

However, this equation requires several failure measurements in order to know the damage fraction, and it assumes that the damage rate is uniform, meaning that the first stress cycle at a constant stress level is as damaging as the last. More advanced models can be cited such as Engelmaier's model which takes into account the effects of frequency and temperature [72]. Another example is the Coffin-Manson model, which considers the effects of high cycle fatigue (HCF) mainly due to

elastic deformation and low cycle fatigue (LCF) mainly due to plastic deformation [95]. Nevertheless, all the previous models share the same problem, namely that they require failure measurements, in order to evaluate the damage rate for a certain number of cycles.

2.2.6 Conclusion on the physical-based models

Physics-based degradation models take into account stress covariates such as temperature and humidity, as well as additional stressors such as voltage or frequency. However, voltage, current, or other factors do not have a direct physical model to relate degradation to cause. Although there are many degradation models in the literature that take these stressors into account, such as the inverse power law model. In fact, the latter is an empirical model, or a data-driven model, that is not related to the physics of the degradation process.

In addition, all the models listed above consider the rate of degradation, and thus they do not provide a degradation path, as one can assume that degradation is linear with time and the indicator of this degradation y follows a linear equation $y = Rt + y_0$. This is not always the case, and to take into account nonlinear patterns, data-driven empirical models are used.

2.3 Data-driven empirical models

When the physical degradation process is difficult to handle, or the chemical reaction is not fully understood, the previous physical-based models are not suitable. Empirical models describe the aging processes without using chemical or physical explanations.

To model a degradation using empirical functions, Nelson imposed certain assumptions to follow, such as [160]:

- The model assumes that degradation is not reversible. If it is reversible, other methods, not included in this section, must be applied.
- The model applies to a single degradation mechanism, or failure mode. If there are simultaneous degradation processes, each requires its own model.
- The initial degradation of a sample is assumed to be negligible. That is, any degradation prior to the start of the aging tests is ignored.
- Performance is measured with negligible error.

From the models presented by Nelson [160], two parametric categories can be drawn: Simple constant rate models and exponential models. These two categories will be detailed below.

2.3.1 Typical degradation model

A general relationship of a simple constant rate model is represented in Eq. 2.7, where $\mu(t)$ can be the degradation measurements, or the performances, or the *log* of the performance over time t. α is the intercept coefficient, that is the degradation measurement at the beginning of the test. β is the degradation rate, and it has many representations depending on the applied stress, so it can have an Arrhenius dependence $\beta = \beta_0\ e^{\ -\beta_1/T}$, a power dependence $\beta = \beta_0 V^{\beta_1}$ or an exponential dependence $\beta = \beta_0\ e^{\beta_1 V}$ (V is the stress applied, β_1 and β_2 are the parameters of the dependency)

$$\mu(t) = \alpha - \beta t \tag{2.7}$$

Other typical form of a degradation function is presented in Eq. 2.8, where g is an specified function that is continuous, increasing, and differentiable at t [54].

$$\mu(t) = g(t, a) = e^{a_1}(1 + t)^{a_2} \tag{2.8}$$

2.3.2 The exponential model

The exponential model is the most commonly used model for nonlinear decay trajectories. Nelson named this model as the Weibull relation (to be distinguished from the Weibull distribution however), represented in Eq. 2.9, where α, β, γ and δ are the characteristics of the degradation process.

$$\mu(t) = \alpha\ e^{\ -(\frac{t}{\beta})^{\gamma}} + \delta \tag{2.9}$$

Similarly, Cox models degradation has an exponential rate model, when the aging behavior evolves exponentially with age (Eq. 2.10, where λ is the decay path, λ_0 is the initial decay value, β is the array of the unknown parameters, and z is the array of individual measurements in a sample) [55].

$$\lambda(t, z) = \lambda_0 e^{z\beta} \tag{2.10}$$

Meeker also represented the exponential degradation [150] (see Eq. 2.11), where $D(t; X)$ is the degradation with respect to time t and stress X, and D_∞ is the asymptote of the degradation path. $R(X)$ is the degradation rate, it can include an acceleration factor, and it can be a physical-based model if the physics is known.

$$D(t; X) = D_\infty(1 - e^{(-R(X)t)}) \tag{2.11}$$

Finally, a non-physical parametric model but not really a degradation model based on the inverse power law will be mentioned here because it is widely used to model electrical stress.

2.3.3 Inverse power law

The inverse power low is not really a degradation model as it is a relationship between lifetime L and non-thermal stressors X (mainly for electrical stressors). See Eq. 2.12, where K and n are the parameters of the model. Black's model is a particular application of the inverse power law, when the stress concerned is current density j, with $n = 2$. Yet, as mentioned for Black's model, the inverse power law is not a degradation model but if the lifetime is replaced with the damage rate, or the degradation level, it can be used as a model to relate degradation to most often the electrical stress. [104].

$$L(X) = \frac{1}{KV^n} \tag{2.12}$$

2.3.4 Conclusion on the Data-driven empirical models

To understand the real effect of stress factors on component aging, it is important to track the behavioural response of the components when subjected to the equivalent stress factors. It is important as well to analyse this behaviour and model the decay path of the component's aging, because degradation can be linear, exponential and much more. Understanding the degradation of a component can help in estimating its reliability, by predicting the lifetime or time to failure. The aging survey, can not only help estimates the lifetime, but gives an good indicator to any catastrophic deterioration that takes place while degrading.

The physical and empirical models presented above form the basis of all degradation modeling. There are limitations to the application of these models:

- It is not possible to take into account errors due to the measurement, the realisation of the experiment, the number of samples, the quality of the product, etc.
- It is not possible to take into account statistical properties such as sample distribution and bias.
- It is not possible to incorporate results from other studies with different technologies into the modeling, as they may have different physics or parameters.
- It is not possible to account for the randomness of degradation processes.

2.4 Degradation models of OLEDs and insulators

Physics-based and data-driven empirical models were presented to study the degradation of any component. This section presents a review on the degradation models that were applied to the OLEDs and insulators in the literature.

2.4.1 OLED degradation modelling

The degradation of OLEDs can be generally monitored by different indicators, such as electrical characteristics like the impedance of an equivalent circuit [162], Current-Voltage (CV) curve [69] or forward voltage [174]. The most commonly used aging indicator is optical luminance, since the main task of an OLED is to produce light. Brightness can be used as an indicator of aging, where the lifetime of the OLED can be defined as the time when the brightness reaches 50 % of its initial value [113]. However, this is not the best optical indicator because it is related to the distance of measurement. In the literature, most papers focus on luminance to predict lifetime or on electrical characteristics to design suitable drivers or compensate for luminance loss, as discussed afterwards.

The modeling of the luminance degradation and, consequently, the lifetime of the OLED will be presented in the following.

OLED lifetime modelling Modeling the aging of OLEDs has an essential objective: to predict their lifetime, or rather their life span, because the definition of the lifetime of an OLED is the moment when its luminance reaches a percentage of its initial value. Initially, newspapers considered a percentage of 50 % meaning half of the initial luminance. Half-life model, as the papers call it, is a typical model based on luminance and half-time, which was introduced by Wellmann [225] who noted that it could sometimes have an extrapolation error of 20 %.

$$L_0^n \times t_{1/2} = Cte \tag{2.13}$$

Eq. 2.13 represents the half-life model, where L_0 is the initial luminance, $t_{1/2}$ is the half-life or life where the luminance is at 50 % of its initial luminance, and n is the acceleration coefficient. It should be noted that the acceleration coefficient is applicable within certain limits, as excessive operating temperature would lead to intense chemical reaction and crystallization in organic solids, which would cause much faster failure of OLED devices [226].

Many papers have used this equation to model a constant stress lifetime. For instance, Li *et al.* used it to compare a continuous current wave to a pulsed current one, with 80 % lifetime level as defined in Eq. 2.14 [139]. They deduced that the effective 80 % lifetime of the pulsed current stressed OLED with less than 20 % duty cycle is shorter than the one of the constant current stressed OLED.

Otherwise, it has no effect, which is why they considered the OLED on time as the effective duty cycle.

$$EL = t_{0.8} \times duty\,cycle \tag{2.14}$$

Pang *et al.* modeled the lifetime of a small-area OLED as a function of its organic temperature, and then extrapolated the model to a large-area OLED with the same physical characteristics and current density aging conditions [166]. Their model is based on the relationship between the operational temperature rise of the device, which can be called organic temperature, and its induced voltage. The advantage of this method is to reduce cost and time, as small OLEDs are cheaper and have a shorter lifetime. The model in the paper is presented by a set of three equations relating the 80 % lifespan $LT(80)$ to luminance L (Eq. 2.15b), temperature T via the Arrhenius model (Eq. 2.15c), and and other lifetime values in Eq. 2.15a. The variables of these equations are similar to Eq. 2.13) where t_1 and t_2 are the equivalent lifespans of two OLEDs under different aging conditions, L_1 and L_2 are their respective initial luminance values, AF is the acceleration factor and a, b and α are the parameters of the model.

$$t_2 = t_1 \times (L_1/L_2)^{AF} \tag{2.15a}$$

$$LT(80) = \alpha \times L^{AF} \tag{2.15b}$$

$$ln(LT(80)) = a + b \times \frac{1}{T} \tag{2.15c}$$

All previous models tackled the modeling of lifetime with respect to no factor or at most one factor. Salameh *et al.* , on the other hand, incorporated several factors at a time [184]. They established a linear and quadratic relationship of lifetime with temperature, current density and their interaction using a design of experiment method. Eq. 2.16 represents an example of their modeling methodology, where $L70$ is the lifespan when the luminance reaches 70 % of its initial value, T and J are respectively the temperature and the current density applied, E and I are respectively the effect of the stress applied and the interaction between stress factors, and X is the level of the stress applied.

$$L70 = Mean(L70) + E_T X_T + E_J X_J + I_{TJ} X_T X_J \tag{2.16}$$

This method can be useful for estimating lifetime under any given condition, unlike previous models that only predicted OLED lifetime under one stress condition at a time. The work in this thesis will be a continuity of the methodology presented above, as it is important to model the degradation and eventually the lifetime with more than one factor to mimic a real situation.

OLED pre-existing degradation model As mentioned earlier, modeling luminance degradation is very useful because it improves the reliability of OLEDs. For example, luminance can be kept constant during aging by considering a linear relationship between current and luminance, and letting the OLED drivers compensate for luminance decline whenever the luminance level drops through this relationship [44].

The most commonly used luminance decay model is the stretched exponential decay, presented in Eq. 2.17, where L and L_0 is the luminance and its initial value, t is the aging time, τ and β are the parameters of the model. It was first introduced by Ishii and Taga to study the effect of temperature and current on OLEDs with high glass transition temperature [101]. Using the model parameters, they were able to prove that neither temperature nor current density changes the shape of the decay curves.

$$L(t) = L_0 exp\{-(\frac{t}{\tau})^{\beta}\} \tag{2.17}$$

Fan *et al.* were able to build a luminance degradation model including the influence of ambient temperature [75], by combining the accelerated lifetime relationship (Eq. 2.13) and the stretched exponential decay model (Eq. 2.17). Since luminance degradation increases with temperature, they modelled the acceleration n with temperature, using an increasing exponential relationship, which leads to a full time and thermal variant luminance degradation model (see Eq. 2.18, where α is the normalized luminance $L(t)/L_0$ and the constant k is $K = C/ln2^{1/\beta}$ from the previous equations).

$$\alpha = exp\{-(\frac{tL_0^{n(T)}}{K})^{\beta}\} \tag{2.18}$$

Zhang *et al.* built a model of luminance degradation with time and current intensity for small areas OLED [233]. The model is based on the stretched exponential decay and on the physical knowledge of the polymers used. It is presented in Eq. 2.19 where I_0 and I are respectively the normal working stress current and the accelerated current, β being the acceleration coefficient and m and η are the shape and scale parameters of the luminance decay.

$$L(t) = L_0 exp\{-(\frac{t}{\eta(\frac{I_0}{I})^{\beta}})^{m}\} \tag{2.19}$$

A luminance degradation model called a nonlinear mixed exponential model based on the estimation of 4 parameters as a function of time is considered to model the luminance increase during the first hours of aging of a flexible OLED display [51].

Overall, only luminance-based lifetime, and subsequent luminance degradation, were modeled over time and mostly against one single constraint. Although there are many interesting indicators to model as a function of time, such as the electrical impedance of the OLED for example, the modeling in the literature is limited to only the luminance decay aspect. Furthermore, in the literature, the decay is limited to empirical exponential models incorporating only one physics-based constraint relation at most.

2.4.2 Insulation degradation modelling, limited to lifetime

Insulation reliability has been studied extensively over the past century, and a review of mean time to failure modeling is presented in this section. The lifetime of insulation is generally modeled as a function of temperature according to the Arrhenius law [59] (see Eq. 2.20 where L is the life of the insulation , T is the temperature in Kelvin, A and B are the parameters of the model).

$$L = A \cdot e^{\frac{B}{T}} \tag{2.20}$$

The insulation life is also modelled with electrical stress using an inverse power model [8] (see Eq. 2.21, where L is the insulation time to failure at applied voltage stress level V, k and n are the model parameters).

$$L = k \cdot V^{-n} \tag{2.21}$$

An exponential model is also used for modeling the life of insulation [8] (see Eq. 2.22, where V is the electric voltage stress and c, k are the model parameters).

$$L = c \cdot e^{-kV} \tag{2.22}$$

The above equations are used to calculate the lifetime of the insulation using the accelerated aging method, where the stress levels are above a certain threshold, considering that below this threshold, no aging is observed [206]. For an electrical stress, the threshold is called PDEV or partial discharge

extinction voltage. Similarly, each insulating material has its own thermal threshold below which no aging due to thermal stress occurs. For example, the thermosetting threshold for insulating materials is near the glass transition temperature [206].

Since insulation aging can be caused by multiple reasons (see TEAM factors in 1.5.2), it is important to build a valid model that contains most of the causes of failure, as there might be direct and indirect interactions between the stress factors. The multi-factor aging models for insulators presented below are abundant in the literature, and they are very well detailed in the paper by Gjerde [81]. Simoni, Ramu, Fallou and Crine models are examples of these multi-factor models, according to Gjerde, and they are explained below.

Simoni's model considers the amount of aging at the time of failure as a characteristic parameter of an insulation system. Thus, it combines thermodynamics to construct the expression of Eq. 2.23, where R is the aging rate, T and E are the temperature and the electrical field respectively, a, b, A and B are the model parameters and $f(E)$ is a function that takes into consideration a reference E_0 where there is no aging below its level.

$$R = Aexp\{-\frac{B}{T}\}exp\{(a + \frac{b}{T})f(E)\} \tag{2.23}$$

Ramu's model multiplies the classical single-constraint models presented earlier to construct an electric field and temperature dependent model (see Eq. 2.24). The model considers the parameters of the inverse power law, k and n to be temperature T dependent. $\Delta(T) = \frac{1}{T} - \frac{1}{T0}$ uses a threshold temperature below which no thermal aging occurs. The $\Delta(T)$ is also considered for the temperature dependent parameters k and n, thus creating a kind of electrical threshold.

$$L = c(T)E^{-(n(T)}exp\{-B\Delta(\frac{1}{T})\} \tag{2.24}$$

Similarly, Fallou's model considers the parameters of the Arrhenius model as dependent on the electric field. On the other hand, Crine's model uses material physics to construct the insulation lifetime model, with lifetime defined as the amount of energy required to crack the insulation.

After the basic models were detailed, many papers used and developed their own life models depending on their application, whether it was a high or low voltage application, etc.However, all of the previously presented models and their continuity are limited to the lifetime of the insulation only, and no degradation has been modeled. Some papers have studied the degradation of insulators, but again, no models have been performed.

Overall, insulator and OLEDs lifetime modeling has focused on empirical exponential and power models. Insulation reliability in particular, has never used degradation modeling to estimate a mean time to failure.

For all of the reasons mentioned above, it is necessary to have an appropriate strategy for modeling degradation. This is not to say that the above models are not relevant, but that on their own they are simply not sufficient to model degradation.

These strategies can be deterministic such as regression modeling, where many stressors and covariates can be included in the modeling. The effect of sample size, sample population and many other parameters can be taken into account.

Stochastic modeling is another group of strategies, widely used for modeling and predicting degradation. These strategies take into account the randomness of degradation and other factors such as stage changes in the degradation process.

The last strategy is online degradation modeling, as it is mandatory to monitor the degradation of systems in order to limit the failure points. In the following, the three main strategies will be explained in detail.

2.5 Regression-based models

Regression-based models primarily consider the empirical models listed above, and apply them to data extracted from a degraded population, which is aged under certain defined stressors. In what follows, the basic path approach of regression modeling will be discussed, as well as robust regression, some details on biased populations, how to incorporate data from different populations, and finally a graphical approach.

2.5.1 Degradation path curve approach

The degradation path curves are based on the degradation trajectories over time. The degradation process, and its decay level are assumed to be observed at any time. The products being monitored come from a population, each of which exhibits the same degradation path.

According to Meeker *et al.* [150], a degradation model considers a decay path $D(t, \beta)$ with a random deviation ϵ from the path representing measurement errors (Eq. 2.25). The decay path $D(t, \beta)$ is modelled over time t with unknown parameters β to be estimated for each specimen. Even though t denotes time (operating or real time), it can represent other factors if the time is not the main aging abscissa. In case of automobile tires, t designate miles, and number of cycles for batteries or capacitors ...

$$Y(t) = D(t, \beta) + \epsilon(t) \tag{2.25}$$

The parameters of the decay path can be found by applying a regression method: linear or not, uni- or multi-variate, ... In fact, the regression concept is based on describing a relationship between a quantitative response variable y and one or more explanatory variables x [40, 189]. Explanatory variables are known as regressors, predictors, inputs or independent variables. A multi-linear regression (MLR) model is represented in Eq. 2.26, where one response variable y has k explanatory variables x, linearly bonded through $k + 1$ parameters $\beta_{0\to k}$. Y is an $(n \times 1)$ vector of observable random variables, to be modelled or explained by X. X is an $(n \times k)$ matrix of observable random variables called the design matrix with $k < n$, and has a full rank when its columns are linearly independent (the rank of X is k). ϵ is an $(n \times 1)$ vector of unobservable random variables designating the random error, and its values are assumed to be independently normally distributed with zero mean and constant variance σ^2.

$$Y = \Phi(X, \epsilon) = X\beta + \epsilon = \beta_0 + \beta_1 X_1 + \ldots + \beta_k X_k + \epsilon \tag{2.26}$$

The multi-linear model groups many sub-models, like a simple linear regression (SLR), where it has one regressor ($k = 1$). Other sub-models like curvilinear models or interaction terms can be assessed using the MLR method if some additional transformations of the explanatory variables are done. Curvilinear models for instance, have polynomial values that are presented in the MLR as $X_j = X^j$. If variables are not independent, interactions between predictors can be expressed as another predictor term $X_3 = X_1 \times X_2$. This is an advantage of regression-based models where

interactions between the stressors can be included as input variables.

It should be noted that categorical variables, like the manufacturer source of the product for example, can be transformed as well so they can be included in the MLR. Additionally, a transformation of the output response variable can be done to respect the linearity specification of the MLR. The Cox model for instance, which is an exponential model, can be linearized by transforming the decay path, so that $Y = log(\lambda) = log(\lambda_0) + z\beta$ is a log-linear model.

There are basically two regression methods to estimate a model's parameter: the least square and the maximum likelihood methods [189].

The method of least squares is used to obtain the estimate of β, a $(k \times 1)$, as it consists of minimizing the square sum of errors $\epsilon = Y - X\beta$ with respect to β. It can be estimated using Eq. 2.27, that is obtained from differentiating $\epsilon'\epsilon$ with respect to β and solving $\frac{\partial \epsilon'\epsilon}{\partial \beta} = 0$. However, to apply this method, columns of the matrix X should be linearly independent, for $\hat{\beta}$ to have a unique solution.

$$\hat{\beta} = (X'X)^{-1}X'Y \tag{2.27}$$

The maximum likelihood estimation method is based on the assumption that the errors are normally distributed $\epsilon \sim N(0, \sigma^2)$. The likelihood function $L(\beta, sigma^2)$ is given by the probability density function of Y (see Eq. 2.28). As the likelihood is exponential, it is usually transformed into a log-likelihood, where its maximum is calculated by solving the differential equation with respect to β: $\frac{\partial logL}{\partial \beta} = 0$, which is equivalent to the least squares estimate of β.

$$L(\beta, \sigma^2) = \frac{1}{\sqrt{(2\pi\sigma^2)^n}} exp\{-\frac{1}{2\sigma^2} \|y - X\beta\|^2\} \tag{2.28}$$

The basic methods to calculate least-square regression fits are solving the normal equations that would lead to Eq. 2.27 based on the sum of squares and cross-products (SSCP) matrix $X'X$ using mathematical methods like Gaussian elimination, the sweep operator or the Cholesky decomposition.

Otherwise, a QR decomposition [1] of X can be applied, by employing algorithms like Gram-Schmidt or Householder reflections ...[1] For a more stable numerical results, the singular value decomposition can be used, but this is the most computationally expensive approach. More details about the algorithms cited above can be found in Seber and Lee's book, Chapter 11 [189]. However, they will not be developed in this thesis as they exist in many statistics software like matlab ($mdl = fitlm(X, y)$) or R ($lm = (Y \sim X)$).

2.5.2 Confidence bounds

Considering the multiple methods of fitting a model listed previously, and considering that the results data do not 100 % fit to the model (because of the error factor), each fitted model requires some confidence intervals. A confidence interval indicates the percentage of the results observations that follows the model. It can be used as a model selection method, because if the interval is too big, it may be a sign that observations have a big variance, and do not entirely fit the model.

For degradation modelling, there are two main aspects for using confidence intervals:

- To predict a safety margin for the mean time to failure

[1] In linear algebra, a QR decomposition, also known as a QR factorization or QU factorization, is a decomposition of a matrix A into a product A = QR of an orthogonal matrix Q and an upper triangular matrix R , Wikipedia

- To predict the evolution of variability in degradation with time

The first aspect is to predict a confidence interval for the mean time to failure, or when the degradation reaches its threshold level. As said previously, degradation modelling is used for maintenance purposes, and since observations do not 100 % fit to the model (due to the error), a component degradation indicator might reach its threshold level before the predicted value of the model. This might cause a serious problem like the cable car accident that crashed one day before its maintenance date [2].

Fig. 2.1 illustrates some simulated degradation data, that are used to discuss the second aspect of using the confidence interval for degradation modelling. The simulation tackles $i = 4$ specimens

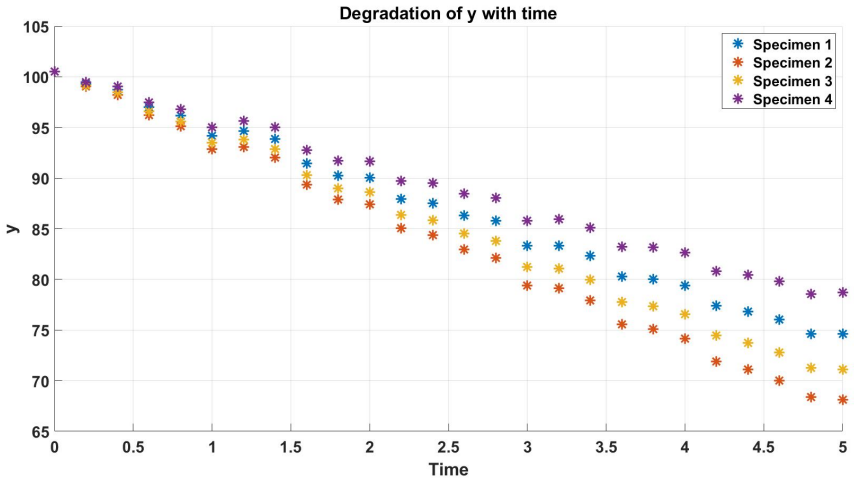

Figure 2.1: A simulated data of a linear degradation of random component

that are supposedly aged under the same conditions, for a period of time. $j = 26$ inspections are made along the aging process, making the total number of observations $n = 104$. The degradation path is linear and the model of the degradation to be fitted is $y_i = \beta_0 + \beta_1 x_{ij}$, where $\beta = [\beta_0\ \beta_1]$ is the array of parameters of the model. x_i is the time of the j^{th} inspection for the i^{th} specimen.

As it is seen in the figure, each specimen has its own degradation path, which implies that there might be a missing covariate. Nonetheless, the aging process could be divided into different stages, where the degradation of all specimens in the first stage (up to time $x_j \leq 1$) follows the same path. The second stage, where $1 < x_j \leq 2$, is when each specimen starts having its own path. The last stage, $x_j > 2$, is when the variability between paths is more pronounced. This type of degradation occurs quite often in real life, as a lot of insignificant factors progressively develop effects with the aging of each specimen. For example, if the impedance of an electrical component subject to thermal and electrical stress increases with aging, it might enlarge the Joule losses. This progressive heat dissipation increases the local thermal stress on the individual component, which accelerate the evolution of the impedance and etc.

In regression modelling, confidence intervals are calculated for the coefficient estimates and for the predicted values of the results. The equations presented below are taken from Seber and Lee's book, that detailed many ways of computing confidence bounds for regression surfaces [189].

The confidence interval for coefficient estimates follows Eq. 2.29, where t is the inverse of Student's t cumulative distribution function, for a confidence level $1-\alpha$, and $n-k$ degrees of freedom; n being

the total number of observations, and k is the number of regressors. $s^2 = \left(\sum_{i=1}^{n}(y_i - \hat{y}_i)^2\right)/(n-k-1)$ is the variance or the mean squared error (similar to Eq. A.3). $X = [1\ x]$ is the regressor matrix (in the case of the example presented, the regressors are only the time), and $(X'X)^{-1}$ is the covariance matrix.

$$CI(\beta) = \hat{\beta} \pm t_{\alpha/2,(n-k-1)}\sqrt{s^2(X'X)^{-1}} \tag{2.29}$$

The confidence interval for the predicted values of y, for a given regressors values x_0, according to the fitted model using the estimated parameters $\hat{\beta}$ is presented in Eq. 2.30. The confidence interval for only the model without the error of observation is called CI_{func}, or the functional confidence interval. When the observations errors are considered (which is the case wanted for degradation), the confidence interval is called CI_{obs}, where the mean squared error term is added.

Moreover, there are two ways of computing a confidence interval for y: simultaneous and non simultaneous. The simultaneous way would consider all the regressors values at once, for example the CI of the data of Fig. 2.1 would consider all the time array at once. The non simultaneous way would measure the confidence only for a single regressor value each time. The confidence interval equations presented here are non-simultaneous, to illustrate the evolution of the variability of observations with aging.

$$\begin{aligned} CI_{func}(y_0) = &\quad \hat{y_0} \pm t_{\alpha/2,(n-k-1)}\sqrt{s^2 x_0'(X'X)^{-1}x_0} \\ CI_{obs}(y_0) = &\quad \hat{y_0} \pm t_{\alpha/2,(n-k-1)}\sqrt{s^2 + s^2 x_0'(X'X)^{-1}x_0} \end{aligned} \tag{2.30}$$

Fig. 2.2 shows the fitting of the simulated data to a linear model $y = a\ time + b$, where the parameters $a = -5.64\ \pm 0.31$ and $b = 100.36\ \pm 0.9$ are found according to the Least square linear regression fitting method. It also shows the functional and observational confidence interval, found according

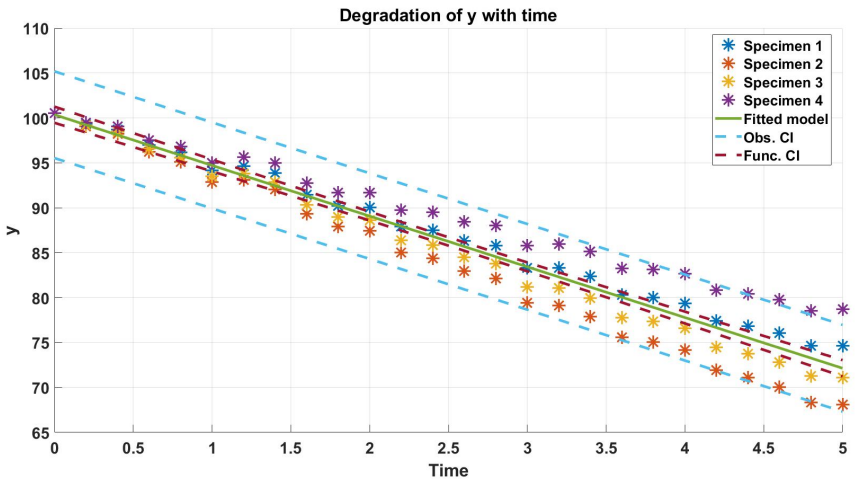

Figure 2.2: Model fitting and confidence intervals for the simulated data of Fig. 2.1

to Eq. 2.30. The functional confidence interval, does not consider the variability of measurements for each inspection, but its width does vary with the input variables, that is $x_0 = [1\ time]$. The observational confidence interval however, considers the standard deviation of measurement errors $s^2 = 5.7$, which is very big compared to the covariance term "$s^2 x_0'(X'X)^{-1}x_0$" that has a maximum value of 0.83. That's why the observational CI, computed with non-simultaneous fitting, seems to not change with time, and is very similar to a one computed with a simultaneous fitting.

Lastly, a regression fitting considers several assumptions like the error elements follow a normal distribution $\epsilon \sim N(0, \sigma^2)$ with a mean= 0 that makes them unbiased, and a constant variance σ^2.

There is no correlation between the residual elements, making them independent, meaning that the explanatory variables are not random variables. According to these assumptions, a confidence interval can be built for the parameters estimate and for the fitted function and the observations.

When one of the four assumptions

1. $\epsilon \sim$ Normal distribution
2. $E[\epsilon] = 0_{n\times 1}$
3. $Var[\epsilon] = \sigma^2 I_{n\times n}$
4. $Corr[\epsilon_i, \epsilon_j] = 0$

is not respected, additional techniques can be incorporated during the modelling, to enhance the estimation. Some techniques (explained in the following) reduce over-fitting, differentiate between significant and random explanatory variables, and select the minimum sample size to be allowed to use assumptions like normal distribution, etc.

2.5.3 Robust regression

When the errors are normally distributed, ordinary least square estimation is the most efficient regression method, as it is called BLUE or Best Linear Unbiased Estimator [78]. However, when outliers exists causing extreme errors, and making the distribution of errors long-tailed, or biased, a robust fitting that ignores such outliers is the preferable method.

In fact, the typical ordinary least square (OLS) regression uses the "mean" least square method to minimize the mean of the squared residuals ($\min_{\beta} \frac{1}{n} \sum_{i=1}^{n} \epsilon_i^2(\beta)$). However, the average of the squared errors depends on two factors, this first of which being the size. An outlier having a large estimation error, and thus larger squared residual, would have a higher impact on the total sum than the other observations. The second factor is the criterion chosen to minimize the least square, which is commonly the mean, that would inflate when the square of an outlier is added.

The robust regression will solve the problems faced with outliers by replacing the square of residual ϵ^2 by another function $\rho(\epsilon)$ that reflects the size of the residual in a moderate way. This function would have the same proprieties of the square of errors like being symmetrical, positive and monotone. Additionally, the mean criterion can be replaced by a median or a trimmed mean criterion that is more robust towards outliers. Functions of the robust fitting are the M-estimators, bound influence estimators, S-estimators and R-estimators, that sanction outliers by adding further weight on them, or by scaling the residuals or by measuring their dispersion. Once again, robust fitting and its estimators are very well detailed in Seber and Lee's book [189]. Nonetheless, it is important to note that when data have a normal distribution, a least square is sufficient, as some of the robust functions like the M-estimators are very inefficient compared to least squares.

2.5.4 Bias

Bias in estimation occurs when the mean of the errors is not zero due to under-fitting or over-fitting. Under-fitting and over-fitting can be detected through verification data that assess how well the model fits observations that were not used to estimate the model. A model that has poor prediction results cannot be generalized to the entire population, and thus further steps are required.

Under-fitting A model is under-fitted when the explanatory variables do not illustrate all the response values. A least square method usually follows the estimation of $E[Y] = X\beta$, with $E[\epsilon] = 0$, but in the case of under-fitting, the true model would need additional parameters like shown in Eq. 2.31, where Z is an $(n \times t)$ matrix, whose columns are linearly independent from X, and γ is the vector of associated parameters.

$$E[Y] = X\beta + Z\gamma \tag{2.31}$$

The real estimation of $\hat{\beta}$ is then shown in Eq. 2.32, where $L = (X'X)^{-1}X'Z$. Note that the added term $L\gamma$ makes a biased estimation of β. Reducing the bias can be done by increasing the number of explanatory variables so that the under-fitting term L would be reduced.

$$\begin{aligned} E[\hat{\beta}] &= (X'X)^{-1}X'(X\beta + Z\gamma) \\ &= \beta + L\gamma \end{aligned} \tag{2.32}$$

Over-fitting In the case of over-fitting, the number of explanatory variables X is more that what is needed and can be divided in two sub-matrix $X = [X_1\ X_2]$ where X_1 are the significant explanatory variables only, and X_2 cause the over-fitting. The true model therefore is $E[Y] = X_1\beta_1$ where β_1 is the unbiased estimation of $\hat{\beta}$, based on the demonstration done in Eq. 2.33 [189].

$$\begin{aligned} E[\hat{\beta}] &= (X'X)^{-1}X'X_1\beta \\ &= (X'X)^{-1}X'X \begin{pmatrix} \beta_1 \\ 0 \end{pmatrix} \\ &= \begin{pmatrix} \beta_1 \\ 0 \end{pmatrix} \\ &= \beta_1 \end{aligned} \tag{2.33}$$

Since the estimate of $\hat{\beta} = \beta_1$ is unbiased, the estimate of $E[\hat{Y}] = X_1\beta_1$ is also unbiased. However the bias would be pronounced in the variance of the elements of $\hat{\beta}$, where the apparent variance is higher then the true one (Further demonstration can be found in Seber et Lee's book, Chapter 9 [189]).

To limit the over-fitting, it is advised to make an ANOVA test to identify the significant explanatory variables A.5, and thus limit unimportant regressors that do not contribute in the real model. Another way to avoid over-fitting is to do a regularization (explained in the following), which adds penalty to complex models that usually tend to over-fit.

2.5.5 Regularized regression

Regularization constrains the estimates of the coefficients, penalizing their magnitude as well as that of the error term. There are two types of regularization in regression, the first being Ridge regression. It is a way to create a parsimonious model when the number of predictors in a set exceeds the number of observations, or when a data set has multi-collinearity (correlations between predictors). The other type is Lasso regression, a linear regression based on shrinkage. Shrinkage involves reducing the values of the data to a central point, such as the mean. This type is very useful when there are high levels of muti-collinearity or to improve model selection techniques, including variable selection/parameter elimination [83].

As mentioned above, regularization is very useful when the order of the model increases, so hereafter a regularization example on a polynomial regression, taken from Wan *et al.* is presented [222]. Three models are compared, with and without regularization, to test the effect of regularization on over-fitting ($(\beta = a_0, a_1, \ldots, a_n)$:

- linear model, $h(x, \beta) = a_0 + a_1 x$
- quadratic model, $h(x, \beta) = a_0 + a_1 x + a_2 x^2$
- quadratic curve model, $h(x, \beta) = a_0 + a_1 x + a_2 x^2 + a_3 x^3 + a_4 x^4$

The criterion chosen to minimize the ordinary least squares, or the mean squared error, is otherwise called the cost function $J(\beta)$. Regularization consists in introducing a penalty term λ for the higher order coefficients, and thus the higher the order of the model, the higher the cost function that must be minimized (see Eq. 2.34).

$$J(\beta) = \frac{1}{2}\left[\frac{1}{n}\sum_{i=1}^{n}(y^{(i)} - \beta x^{(i)})^2 + \lambda \sum_{j=1}^{D} a_j^2\right] \tag{2.34}$$

2.5.6 Sample size determination

Usually the variance of the error is unknown, and it can be estimated from the data as $\sigma^2 = \frac{1}{n}\sum_{i=1}^{n}\epsilon_i^2$. ϵ is an unobservable variable, that is unknown as well, so it can be replaced by the residual values of the OLS estimation $e_i = y_i - \hat{\beta} x_i$. Since OLS objective is to make the sum of the e_i^2 as small as possible, e_i are generally smaller than ϵ_i. The estimated variance is then presented in Eq. 2.35, where the sum of squared errors is divided by the degrees of freedom $n - k$ rather than n to maintain the same size as the actual variance [78]. Hence the first constraint on the sample size, as n should be greater than the number of regressors $n > k$ for the estimator of the variance $\hat{\sigma}^2$ to be defined. The consequence of an undefined variance would be misleading results, for example, the R^2 value would be $R^2 = 1$ indicating that the model has a perfect fit, though it is not the truth but the real cause is the lack of observations.

$$\hat{\sigma}^2 = s^2 = \frac{1}{n-k}\sum_{i=1}^{n} e_i^2 = \frac{1}{n-k}\sum_{i=1}^{n}(y_i - \hat{\beta} x_i)^2 \tag{2.35}$$

One can say that the more observation a sample has, the more it is reliable, however, more samples require more effort and cost. Defining the minimum sample size needed for a study is a criteria for optimal modeling, as it will affect the model outcome. The more information available, the best a model is able to give a general unbiased representation of the population, however it might be a waste of resources. Small sample size would give inconclusive or contradictory results, especially when the sample variation is high [100].

In default, to be able to have a variance, a sample must have at least two observations $n > 2$. However, some papers require that a minimum sample size per group to be $n = 5$, for the statistical analysis to be reliable [39]. It is more likely that an ANOVA test will erroneously accept non-significant effects for a small sample size [57]. Others base the sample size on the number of predictors of the regression, $n \sim 50 \times k$. Such numbers are not feasible in many electrical engineering applications, and standards typically define the sample size for each electrical product. For example, for accelerated reliability testing of energy measurement equipment, the standard states that aging tests should be performed with as many samples as available [98].

Sample size can be chosen by selecting the minimum sample number that gives the best model selection criterion, like adjusted R^2 or AIC. After several studies based on these two criteria, Jenkins et Quintana recommended a minimum sample size of $n = 8$ for a tight data pattern (i.e., very low variance value) and $n \geq 25$ for high variance value, to clearly match a model to the data pattern [107].

Sample size determination (SSD) methods fall into two groups: frequentist methods and Bayesian methods, which generate debate about which group is more reliable, especially for small sizes [12]. The aim of all SSD methods is to allow the investigator to determine the sample size by specifying a target level of accuracy or by maximizing a specified objective function. Note that these approaches require preliminary studies that may be harmless when the objective of determining the minimum sample size is to increase accuracy. If, on the other hand, the goal is to reduce the cost of the experiment, doing preliminary studies is not the best solution, and the scientist should refer to standards or devices available on hand.

2.5.7 Meta-regression

Regression has a very wide range of applications, and therefore has many subgroups. If multiple studies have common or conflicting results, a method called "meta-regression analysis (MRA)" combines, compares, and synthesizes the results of these investigations while adjusting for the effects of available predictors on the response variable.

Meta-regression does not build a general model of the response y with respect to the explanatory variables x, but constructs a model of effect size θ of a study. It is usually very used in economics [105] and medicine [131], for example, a meta-analysis combines 28 studies to estimate the effect of cholesterol reduction in reducing the risk of heart disease, regardless of the other test conditions within each study [88]. Instead of testing if the effect estimate of each study is statistically significant, it is better to group all studies and determine an effect size as it can be more generalized into a population.

In the case of degradation, MRA can be used to combine actual aging research with previous similar studies to estimate the overall effect of a particular aging factor. Previous studies could include degradation data of the same electrical component but with a different technology, or subjected to additional aging factors, or similar factors but at different stress levels, etc.

For example, the modeling of OLED degradation in one study may end up assuming that the effect of electrical stress is not significant on luminance degradation, due to lack of samples or bias in the modeling, etc. In order to really test this hypothesis, a meta-analysis would incorporate various other studies, to increase the accuracy of the estimation of the effect of electrical stress on OLED aging and have a more generalized degradation model.

Meta-regressions are similar in essence to simple regressions, in which an outcome variable is predicted according to the values of one or more explanatory variables [91]. The outcome variable of a meta regression is the effect of one aging factor, and the explanatory variables are the characteristics of each study.

$$\hat{b}_j = \beta + \sum_{k=1}^{K} \alpha_k Z_{jk} + e_j \tag{2.36}$$

Eq. 2.36 presents the general estimation of a particular effect $\hat{b}$ [202] where

- β is the intercept value or the true value of the parameter of interest
- Z_{jk} is the meta-independent variable which explains the heterogeneity between studies, it indicates relevant characteristic of the j^{th} study out of the K combined studies
- α_k is the meta-regression coefficient which reflects the biasing effect of particular study characteristics

- e_j is the meta-regression disturbance term

Meta-regressions are very interesting for having a generalized degradation model independent of the particular aging factors, controlled and uncontrolled, that influence a specific study. However, they are not recommended when the number of studies is greater than 10. In this case, heterogeneity across studies can be added as an explanatory categorical variable (e.g., study number), along with the other unified regressors in the degradation model.

2.6 Advanced algorithms: machine learning models

In most cases, basic regression models work just as effectively for small degradation problems, but they are not suitable for more complex problems. Modeling the degradation of a complete system, for example, requires in-depth knowledge of the degradation of its subsystems and their causes (in many cases unobservable or unknown). If a system's weak points are identified and measurable, many output performance results can be tracked, making it difficult to incorporate them into a simple regression model. The third problem with a simple regression model is the need for a threshold, to model a mean time to failure distribution. In many cases, due to the complexity of a system, this is not easy to detect.

More advanced regression algorithms can solve some of the problems listed above. These algorithms are based on machine learning strategies, which are the most effective at accurately predicting a model. However, they have a big disadvantage as they are referred to as black box processes, since the mechanism that transforms input into output is obscured by an imaginary box.

In what follows, neural networks and support vector machines, the two most common machine learning algorithms, are presented, along with other examples.

2.6.1 Neural Networks

Neural networks (NN) are one of the main techniques used in artificial intelligence. It is based on the imitation of the biological neural network of the brain, as it consists of interconnected processing elements, called "neurons", through three main layers: an input layer, one or several hidden layers and an output layer (see Fig. 2.3a). The hidden layers can have as many intermediate variables or neurons as needed (depending on the complexity of the model).

As said, they are widely used in artificial intelligence, due to their ability to handle complex modeling, and can therefore be used in predictive modeling. NNs build a complex regression function between a set of network inputs and outputs, so they can be used for degradation prediction without the need to actually understand the physics leading to degradation or the actual model of degradation. The advantage of using neural networks lies in their ability to model the evolution of complex multidimensional degradation signals [80].

Neural networks are gaining popularity in degradation modeling because of their efficiency in prediction. Zhu *et al.* modeled the degradation of an epoxy resin adhesive using a tri-variate regression model and a neural network, with a small sample of data [239]. The neural network did indeed predict with a higher R^2 value the lifetime of the validation set, but again, the method did not show what were the reasons for the degradation, or more importantly, how the adhesive behaves when faced with stress factors. Gebraeel and Lawley they used neural networks to predict the times of degradation of bearings, and ultimately predict the distribution of the remaining life of bearings [80].

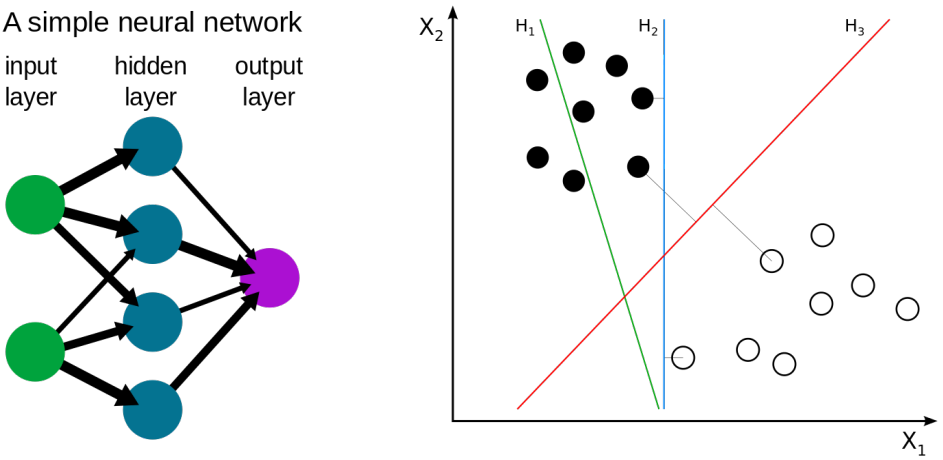

(a) Neural network example from Wikipedia (b) SVM example from Wikipedia

Figure 2.3: Machine learning methods

They integrated this technique with an empirical exponential model based on their experimental observations to better understand the degradation results. Zhang *et al.* modeled the degradation of mechanical components using a back propagation neural network algorithm[236]. The paper actually accentuates the drawbacks of neural networks and attempts to provide solutions. The authors tested the use of small samples for prediction, using the first n degradation indicators (let's say a time-series of $[y_1, \ldots, y_n]$) to predict the next n degradation indicators $[y_{n+1}, \ldots, y_{2n}]$. Three important bits of information are extracted from this paper:

- The NN is a black box that gets an output based on the input, regardless of the mechanism between the input and the output.
- Long-term predictions are poor (in their case).
- The size of the training sample affects the output, as the NN may converge to a local value. This was also confirmed in the paper by Dong and Luo, compared to other learning algorithms like SVMs [66].

For insulation, neural networks are widely used for diagnosis, as they can assess the aging state of electrical insulation based on acoustic techniques [82], or recognition of partial discharges [224], and even predict their breakdown voltage strength [198]. They are also applied to predict the degradation of insulators by predicting the variation in electrical resistance [195], or the degradation of their tensile strength [33]. However, the main objective of neural networks is the prediction of the output, and not the modeling of the degradation behavior.

Neural network algorithms tend to achieve excellent prediction results when using a large amount of diverse training data. They are expensive and cannot be applied to degradation modeling, because most degradation data are small to medium in size and therefore not sufficient. Furthermore, this type of algorithm is used for more complex systems where the failure mechanisms are not known. NN algorithms can only predict the failure cases that are included in their training set, and fail to identify other possible failure modes. Finally, neural networks do not show the relationship between the output to be modeled, whether it is a level of degradation or a lifetime value, and the corresponding explanatory variables, because the role of the hidden layers is to associate the output with their explanatory variables.

2.6.2 Support vector machines

Neural networks became popular in mid 2010 but previously, support vector machines SVM were used for high dimensionality regression problems [106]. SVMs are learning algorithms used primarily for classification (of data) and regression analysis. They classify the input data into several categories or kernels, as they are called. Classification is performed by finding a certain hyperplane as in Fig. 2.3b, which best separates two or more categories. In Fig. 2.3b, two hyperplanes $H2$ and $H3$ make this separation, however, the SVM chooses the hyperplane that has the greatest distance to the training data, so $H3$ is considered the best separator.

According to Vapnik [218], the hyperplane has the equation of Eq. 2.37, where Ψ is a feature space that transforms the variables, for an easier separation (see Fig. 2.4a). w is a vector of weights

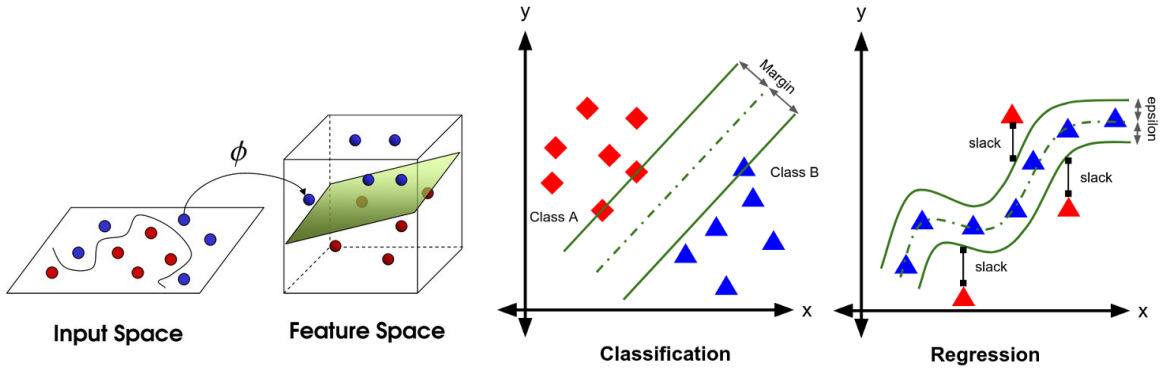

(a) Feature space concept from [209] (b) Regression vs classification application from [11]

Figure 2.4: SVM perception

determining the hyperplane in the transformed space. The SVM will find the hyperplane that separates the training data without error with a minimum norm $|w|$, i.e., the margin length between the hyperplane and the nearest data point of Fig. 2.4b (Eq. 2.38).

$$H : \Psi(x)w + b = 0 \tag{2.37}$$

$$y_i \left[(\Psi(x_i)w) - b\right] \geq 1 \tag{2.38}$$

SVM is mainly used to classify data, for example to detect spam or for handwriting recognition. However, for regression applications, SVM does not look for the hyperplane that best separates the data, but the one that is closest to the value of y_i. Its goal is to find a function $f(x, \alpha) = (wx) + b$, by minimizing the empirical risk R_{emp} that the data are outside the margin of the hyperplane. In this manner, the SVM separates two groups of data, so that the measures within the function are grouped into one class and the outliers are considered as the other class (see Fig. 2.4b). More equations about the minimization of the empirical risk can be found in [218].

$$R_{emp}(w, b) = \frac{1}{n} \sum_{i=1}^{n} |y_i - (wx_i) - b|_\epsilon \tag{2.39}$$

SVM is mainly used for fault diagnosis, for example to identify defects in OLED panels [197]. For degradation modeling, however, Sun and Li performed SVM extrapolation of performance data to determine the lifetime of a microwave assembly [209]. They considered the performance data as a time-series where the next performance value can be predicted based on the previously recorded data $\hat{x}_i = f(\{x_{i-h}, \ldots, x_{i-1}\})$, where h is the embedded order of the time series. The SVM would

automatically identify the f and use it to predict the i^{th} value. Here, it was used as a "black box" technique, which does not show how the prediction is made, even though it has high prediction accuracy.

SVM was used to predict the bearing degradation process [66], where the characteristics of the vibration signals are extracted and iterative algorithms are applied to predict the next value based on only 7 previous inputs (inputs are collected as time series every 10 minutes). The method performed very well, compared to neural networks, especially because it requires very little input data compared to other learning methods. Once again, the SVM did not give the direct path of degradation, but predicted future values without really understanding the changes in degradation, and in the case of Dong *et al.* [66] or even other papers [208], only one future value was predicted by the algorithm. Since SVM uses time series for degradation processes, the future values depend on the time series inspection unit, so it can only predict a few minutes or hours ahead. This could limit the planning of any preventive or maintenance action, which is basically one of the reasons why degradation modeling is studied in the first place.

2.6.3 Online models

One of the important reasons for degradation modeling is to study the performance of the device. In some cases, degradation modeling based on the methods presented earlier is sufficient for scheduling maintenance and interventions. However, in real life, accidents tend to happen, and if not detected early, systems or devices can suffer catastrophic damage.

Online modeling, based on advanced machine learning-based algorithms, can be applied. However, they are more complicated than the other solutions and require many calculations. Kalman filters are the best way to continuously monitor system degradation. They are very popular for control applications, and signal processing. For degradation modelling, their advantage is its adaptability to change in degradation paths/trajectories. A Kalman filter is used to evaluate the dynamic bearing degradation and estimate its failure (that was possible to do 50 minutes before failure) [177]. It can be used to predict the change in chromaticity of LEDs, which has a big variance with aging [130]. The extended Kalman filter is used to monitor the health of electro-hydraulic servo-valves, used to power transportation systems like aircraft [140]. An extended Kalman filter is used for an online estimation of the degradation of a proton exchange membrane fuel cell [134].

Nonetheless, the aim of online models (including artificial intelligence algorithms) is to predict an outcome. The model may be known in the case of Kalman, filter, but it continuously changes with the aging time. These changes are solely based on previous data, and do not take into account external factors.

2.6.4 Others

Other complex models can be used for modeling degradation, depending on the case, such as the fuzzy logic system. When degradation is a vague phenomenon, where the degradation indicators have a large variability, it is preferable to use a fuzzy regression model. Thus, the parameters of the regression do not follow a certain distribution but the model considers a set of fuzzy parameters [211].

For example, fuzzy logic systems have been incorporated with neural networks for the prediction of the remaining useful life of a ball nose milling cutter [138]. The proposed hybrid method was found to have better prediction results with higher learning speed than each technique separately or even compared to ordinary multiple regression, but it is still expensive, and the efficiency gain might

not be worth the amount of computational effort.

All the methods proposed in this paragraph are based on a black box concept, they have a high prediction accuracy, but at the cost of understanding the real model that leads to this degradation. They also need a large amount of training data for their algorithms, which is very expensive for degradation experiments. Another approach to model the degradation of complex systems is the stochastic approach. This approach, presented in the following, is very different from the regression approach, because it includes the randomness of the degradation in the model.

2.7 Stochastic modelling

Electrical components failure can lead to system failure, resulting in downtime losses and additional unplanned maintenance actions, not to mention the risks to people and the environment. Previously, deterministic degradations have been studied for inspection planning and maintenance decisions. Deterministic methods were able to give an exact degradation value, for a particular set of input variables. However, deterministic models do not include uncertainties caused by random or uncontrolled factors. That is, uncertain factors are represented by a random error factor in deterministic models that result in only one solution to a problem.

In order to adequately predict the evolution of a component's behavior for better maintenance decision making, modeling degradation under uncertainty must be considered. Therefore, stochastic methods that present data and predict outcomes which account for certain levels of unpredictability or randomness, will be applied to model degradation. Stochastic modeling is inherently random, and uncertain factors are built into the model. The model produces many responses, estimates, and results to see their different effects on the solution. The same process is then repeated many times under different scenarios [117].

The applications of stochastic modeling are very broad. In the following, some examples of stochastic modeling of degradation in electrical engineering are listed.

- Fatigue crack growth: Fatigue crack growth is generally modeled by a Brownian motion degradation process [196, 229].
- Battery degradation: Differences in lithium-ion battery production processes and materials were incorporated into the modeling of cut-off voltage degradation by a Wiener process [93].
- Machine degradation: There are three stages of machine performance degradation: normal operation, fault occurrence and accelerated degradation. Wanf *et al.* assigned a stochastic Lévy degradation process to each stage, such as Brownian motion to model gradual time-varying deterioration and the Poisson process to incorporate transient performance drops [223].
- Physical degradation in microelectronics: An interesting application of stochastic modeling is in microelectronics, where the aging of trapping/untrapping properties is considered a stochastic process [169].
- Storage Degradation: Stochastic degradation considers a random initial degradation, where the initial degradation may not be zero. Shen *et al.* integrated the initial random decay into the three basic decay processes: Wiener, Gamma and inverse Gaussian [191]. The paper then applied these models to modeling the blocking error rate of magneto-optical data storage disks. This application is characterized by a random degradation process and, more interestingly, by random initial values due to storage problems.

- Dynamic degradation: Degradation processes can include stages for dynamic covariates, like a step-stress degradation process [62]. One application of multi-step degradation processes are processes that include abrupt jumps in degradation pathways, where the timing of the abrupt jump is also unknown [124].

The stochastic approach is widely used for modeling degradation, especially when several degradation scenarios are possible. The technique is applied for systems with a lot of randomness, i.e. real life systems. For example, a stochastic modeling of battery degradation allows to compute the energy management of an off-grid electrical system,... This thesis tackles the degradation of a single component, where it is preferable to use deterministic approaches, because the aging conditions are known and fixed.

2.8 Modelling with dynamic covariates

Static stress is a stress that does not or slowly changes with time. **Dynamic** stress is a stress that has change or progress within its time of application.

So far, degradation modeling, including general trajectory models and stochastic degradation processes, has considered degradation under certain fixed covariates. However, as mentioned in the degradation mechanisms of the previous chapter 1.4.5, the causes of degradation are not always constant.

Dynamic stress may take various profiles, explained below, and summarized in Fig. 2.5.

- Step stress consist of multiple level constant stress that are increasing with time
- Cyclic stress consist of alternating stress levels in a cyclic way.
- Ramp stress consist of increasing gradually the stress level. It is used to detect the stress level that causes failure for example. Ramp stress can also be associated with step and cyclic stress, in order to not abruptly change between two levels (mainly thermal stress is concerned as its time response is slow). It can only be applied in a cyclic way, in a triangular shape (dwelling time of the cyclic stress is null).

In fact, the degradation caused by the environment, such as temperature, solar radiation or humidity, is not constant, and can change with the day and night or with the season. The various operating environments and actual workloads of systems vary in operation, e.g. dimming for lighting systems, variable speed for electric motors... mean that the rate of degradation varies throughout the life cycle. Zhang *et al.* cited many examples of dynamic degradation, such as the change in operational status of a missile weapon system from storage to transportation to maintenance [238]. The paper notes that the state change of the system is a stochastic process, as it has many uncertainties around the state transitions. Thus, it cites many continuous-time stochastic models to represent state commutations, between storage and operation for example, etc.

If the dynamic operating model of the system workload is scientifically constructed and incorporated into the degradation model, maintenance planning can be improved and the accuracy of the remaining useful life estimate can be increased. However, this is a much more complicated modeling process that requires advanced statistical knowledge.

Of course, Meeker, a pioneer in degradation modeling, studied modeling degradation with dynamic covariates [92]. Considering the general degradation path of Eq. 2.25, the degradation with dynamic covariates will become as represented in Eq. 2.40

$$y_i(t_{ij}) = D[t_{ij}; x_i(t_{ij})] + R(t_{ij}; w_i) + \epsilon_i(t_{ij}) \tag{2.40}$$

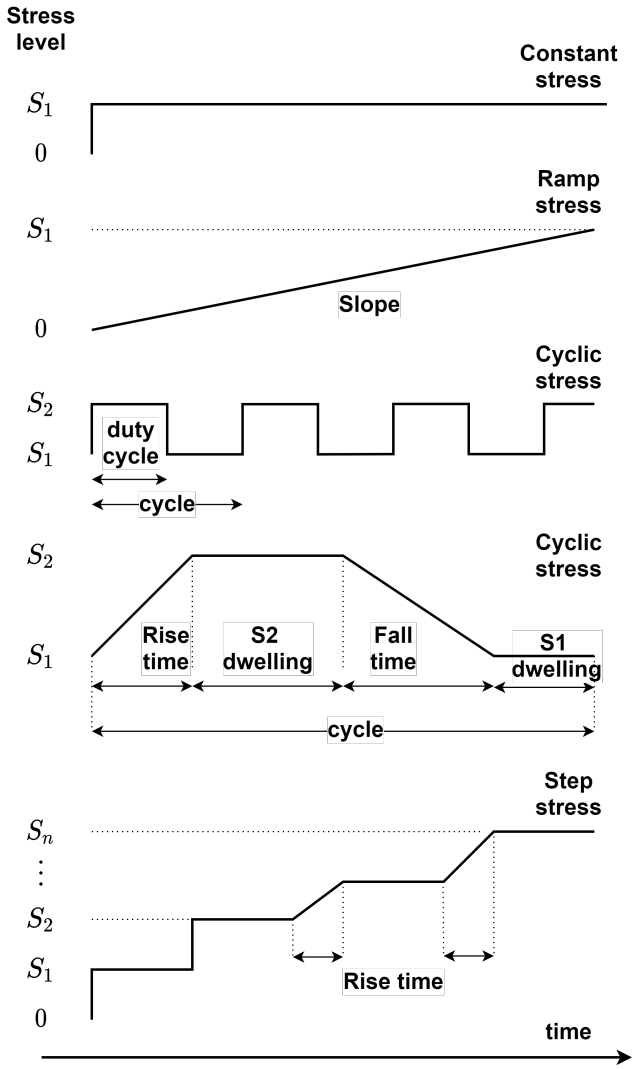

Figure 2.5: The possible constant and dynamic stress profiles

- $y_i(t_{ij}$ is the j^{th} observation of degradation of the i^{th} realisation at time t_{ij}.
- $D[t_{ij}; x_i(t_{ij})]$ is the degradation path that includes the dynamic covariates x_i as follows:

$$D[t_{ij}; x_i(t_{ij})] = \beta_0 + \sum_{l=1}^{p} \int_0^{t_{ij}} f_l[x_{il}(\tau); \beta_l] d\tau \tag{2.41}$$

  - β_0 is the initial level of degradation
  - It is supposed that the model has p covariates
  - $f_l(.)$ is the covariate-effect function, for $l = 1, \ldots, p$
  - β_l are the parameters of the covariate function $f_l(.)$

  $f_l[x_{il}(\tau); \beta_l]$ represents the effect of $x_{il}(\tau)$ at time τ on the degradation process. It is usually considered as a linear combination of spline bases.

  $\int_0^{t_{ij}} f_l[x_{il}(\tau); \beta_l] d\tau$ is the cumulative effect of x_l on the degradation process up to time t.

- $R(t, w_i)$ represents the random departure from the mean structure $D[t; x_i(t)]$, to account for unit-to-unit variability caused by unobservable factors. $w_i \sim \mathcal{N}(0, \sigma_w)$ is the effect of the random factor, that is modelled by zero-mean normal distribution.

- $\epsilon_i(t_{ij}) \sim \mathcal{N}(0, \sigma_\epsilon^2)$ is the independent and identically distributed noise term (similar to Eq. 2.25)

Similarly, there is a physical failure-based modeling method, called the cumulative exposure model (CEP), used to analyze lifetime data obtained from a step-stress experiment [158]. The CEM is based on the cumulative probability of physical failure or damage over time, so it will not be detailed in this thesis as it focuses primarily on a lifetime analysis.

This thesis will focus on one type of dynamic stress, namely cycling. In what follows, a review of cycling modeling for electrical components in general, and OLEDs and insulators in particular, is presented.

2.8.1 OLED cycling

Self-heating of OLEDs occurs when some of the input electrical power is converted to heat rather than light. It causes reactions such as charge traps, nonradiative recombination centers, and luminescence quenchers, especially if there are original defects such as metal ion diffusion and environmental contaminants. To avoid this self-heating, Li *et al.* studied the effect of pulsed stress on OLEDs [139] and observed that short pulses with a duty cycle of $10 \sim 20\%$ significantly reduced the total injection power, and thus largely eliminated the effects of self-heating on OLED stability. In other words, the actual impact of the pulsed current is smaller than the constant stress because the accumulated ions and carriers have the opportunity to redistribute during the off cycles.

Similarly, Cao studied the effect of thermal and non-thermal stress factors on OLEDs [43]. To differentiate between the two effects, the current pulse was used because, in this case, the effects of heating would be significantly reduced because the total power injected is reduced (especially if the duty cycle is less than 10 %).

Similar work has been done on blue phosphorescent OLEDs with different fabrication technologies, and it stated that pulsing can suppress Joule heating of the recombination region[227]. The reduction in self-heating, and thus power dissipation, would result in a slight increase in lifetime. The work also attempted applying a reverse voltage while pulsing at 100 Hz and 1 % duty cycle, where an increase in lifespan of about 15 % was observed. It was deduced that the reverse bias voltage can release carrier accumulation in the recombination region and fixed charge trapping at the defect states, leading to a small recovery.

Li also studied the reverse cycling by applying a negative voltage during the reverse cycle of the pulsed stress while maintaining the current density in the forward cycle [139]. Adding a reverse component to the pulsed current can indeed lead to performance recovery.

On a slower scale, Azrain *et al.* tested an on/off cycle of a few seconds to study the effect of discharge time on the luminance of OLEDs [25]. They tested the OLEDs under the same current density, and for 1 s turn-on time and several turn-off time values starting from 1 to 40 s, for 25 on-off cycles. First, it was found that this cycling increases the luminance of the OLED, and the shorter the off-time, the more luminance is increased. The increase in luminance during the off-time is explained by the additional luminance produced due to the energy stored in the OLED. In other words, when the OLED is turned on, the charged excitons of the anode and cathode act as a parallel capacitance to store energy. These excitons will have the ability to rebalance and neutralize each other by reducing the stored energy when the OLED is turned off. The longer the OLED is in its off state, the more stored energy is dissipated, so when the OLED is in its on state, the luminance changes less and after a turn-off time of 40 s, the luminance remains constant.

Similarly, Rao and Mohapatra stated that there are two types of degradation mechanisms in OLEDs, permanent and recovery degradation [178]. To prove the recovery mechanism, they subjected the OLEDs to a dynamic pulsed voltage, i.e., the pulse width is kept constant for 10 minutes, but the relaxation time between each pulse increases (see Fig. 2.6). The luminance value is measured

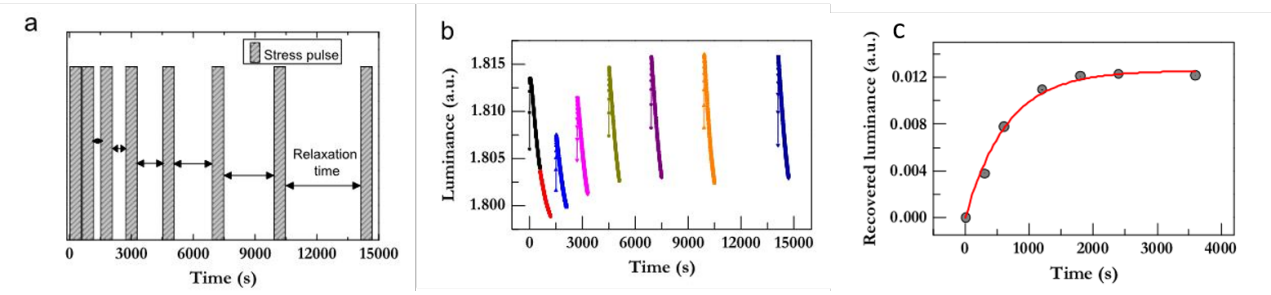

Figure 2.6: Cyclic profile applied to OLEDs: (a) 10 min bias voltage pulse, with varied relaxation time in between successive pulses, (b) its luminance response and (c) its recoverable luminance as a function of relaxation time [178]

parallel to the pulse stress, and it is found that the luminance value increases with increasing relaxation time. This type of luminance evolution is caused by the recovery mechanism where trapped charges are released due to the relaxation time. Finally, cyclic stress is modeled using the relaxation time factor, where luminance is shown to have an exponential relationship with this quantitative variable.

Lastly, Zhang and his team studied the aging of OLEDs under constant current step stress to accurately estimate the half-life of OLEDs under accelerated stress. Each stress step is then transformed into a constant stress using the acceleration factor equation that relates MTTF and initial luminance [234]. The step stress is actually an excellent way to reduce the number of samples to be tested, because a sample can be tested at different levels, if no failure occurs.

2.8.2 Insulators cycling

As presented previously, few papers studied the aging of OLEDs under dynamic, and in more particular, cyclic stress. In fact, even general aging standards of OLEDs does not exists. This is not the case for insulators, as many standards describe very precisely how to test the insulation, depending on its application, and its physics and size, and whether it is under constant or dynamic stresses. Generators usually transition between low and high power loads, inducing thermal variations, leading to additional dynamic electrical and thermal stress. In the following, some cycling modelling of the insulation in the literature is presented.

Kokko studied the effect of thermomechanical power control cycles on the life of stator windings in hydroelectric power plants. [122]. Since power regulation results in thermal heating and cooling, and thus expansion of the wire and insulation, the effect of cycling was modeled using an electro-thermo-mechanical aging model presented in Eq. 2.42), where t_s is the lifetime consumption for each cycle, E_w is the electric field stress, l_e is the maximum relative thermal expansion during the cycle. t_r, E_{re} and l_r are respectively the reference lifetime, electric field stress and thermal expansion, based on previous studies, and m and n are the model parameters.

$$t_s = t_r \left(\frac{E_w}{E_r e}\right)^{-m} \left(\frac{l_e}{l_r}\right)^{-n} \tag{2.42}$$

Mazzanti studied the effect of electro-thermal step-stress with load cycling on high voltage AC cables, because as explained earlier in the physics of degradation of insulation, thermal stress can

cause the insulation and wire to expand differently, resulting in insulation cracking [149]. He considered three models to represents the electro-thermal stressing, Zhurkov, Crine and Arrhenius-IPM models. Zhurkov's model usually represents thermal fluctuations caused by mechanical stress on general solids, but Mazzanti replaced mechanical stress with electrical stress, and so the model proposed in Eq. 2.43 combines electrical and thermal stress, with the presence of a cyclic load. In Eq. 2.43, τ is for the insulation lifetime, τ_0 is the reference lifetime when the exponential of the equation is equal to 1, w is the activation energy of structural failure, R is the universal gas constant, χ is a generic structural parameter related to the thermal fluctuation, E is the electrical field and T is the stress temperature.

$$\tau = \tau_0 e^{\frac{w - \chi E}{RT}} \tag{2.43}$$

(Crine and Arrhenius were explained earlier) Only the loss of lifetime per day, e.g. per cycle was modeled, and to incorporate the daily dynamic effect of the loads, this loss of lifetime was divided into small time intervals, where the transient temperature caused by the dynamic load can be considered constant. The lifetime is then integrated for each step of the dynamic load.

2.8.3 Dynamic aging of other components

In real applications, dynamic stresses in general, and cyclic stresses in particular, can have a great influence on component aging. In fact, it is very important to model component aging with dynamic stress, mainly for energy management, as they may have other effects on component degradation that are not accounted for with constant stress, which could sabotage any energy management plan.

Batteries are one of the most important dynamically stressed electrical components. Their application can vary from vehicle batteries to cell phone batteries to solar power plant batteries and much more. Their applications are based on the state of the charge-discharge cycle which causes them to age with each cycle. In the field of batteries, there are mainly two types of aging, cyclic aging and calendar aging. Cyclic aging is related to the decrease of the battery's capacity during its operation. Calendar aging is related to the decrease of its capacity when it is stored and not used. Battery health can be assessed using the State of Charge (SoC) and Depth of Charge (DoD) indicators. The first parameter is the current capacity of the battery relative to its initial capacity, and the DoD is the discharged capacity relative to the initial capacity. Narayan *et al.* modelled the battery lifetime L with respect to the DoD, the cycle-life n, the nominal battery capacity E_{nom}, and the total energy throughput of the battery $E_{thr,tot}$ in Eq. 2.44 [156].

$$L = n \times DOD_{avg} \times \frac{2E_{nom}}{E_{thr,tot}} \tag{2.44}$$

Super-capacitors are another excellent example where aging due to power and thermal cycling has been studied [23, 214]. Kreczanik *et al.* modeled the lifetime of super-capacitors under power cycling aging [170], considering it is proportional to the inverse of the dynamic stress, and it is presented in Eq. 2.45, where τ_d is the lifetime, $T_c(t)$ and $v(t)$ are the dynamic voltage and temperature, and (t_{init} and t_{end} are the beginning and ending time of the experiment.

$$\tau_c\left(T_c(t); v(t)\right) = \frac{t_{end} - t_{init}}{\int_{t_init}^{t_end} \left(\frac{1}{\tau_s\left(T_C(t); v(t)\right)} \right) dt} \tag{2.45}$$

Photovoltaic ribbon wires are also subjected to dynamic stresses, such as thermal fatigue, thermal shock by current, moisture, etc. Jeong *et al.* studied the degradation mechanism of photovoltaic wire under cyclic thermal stress [108]. Although no modeling was performed, it is interesting to note that, according to their results, the strength of the photovoltaic ribbon remained constant until a number

of cycles where a crack caused by thermal expansion significantly decreased its value. Therefore, dynamic cycling may not lead to direct degradation of electrical component characteristics, but it can cause catastrophic degradation and premature failures.

As in other previous examples, the reliability of LEDs is related to electrical, thermal and environmental factors such as humidity. Transient thermal stress, for example, can cause LEDs to de-laminate, which enhance moisture absorption[94]. Hu *et al.* modeled the transient stress temperature with the LED surface, as seen in Eq. 2.46, where T is the temperature, t is the time, x, y and z are the spatial coordinates and α is the thermal diffusivity of the component [94]. Thermal stress σ, considered to mechanically expand the LED, was also modelled in Eq. 2.47 using the coefficient of thermal expansion α and the elastic modulus E that are relative to each component and the difference between the initial temperature T_{ref} and the actual temperature T.

$$\frac{\partial^2 T}{\partial^2 x} + \frac{\partial^2 T}{\partial^2 y} + \frac{\partial^2 T}{\partial^2 z} = \frac{1}{\alpha}\frac{\partial T}{\partial t} \tag{2.46}$$

$$\sigma = E\alpha(T - T_{ref}) \tag{2.47}$$

Overall, dynamic stress, if it has been studied at all, has only been studied to estimate a lifetime. Also, if dynamic stress has been modeled, it has generally been transformed into an equivalent constant stress where known models can be applied. Few real-time modeling was done, but no modeling of "degradation" over time was done, as the main interest of most papers was to estimate component life. More importantly, no general method can be applied to all components, as most models are application specific.

2.9 Conclusion

This chapter has presented the various physical and empirical models that are used in electrical engineering in general, and for OLEDs and insulators in particular. Each model has its own characteristics, with physical models representing the relationship between degradation rate and stress factors. The empirical models define the degradation trajectories, where the degradation rate is included. In order to model the components of degradation with time and stress factors, a combination of the two models can be made to have a semi-empirical model.

This chapter has also listed the different approaches to estimate the parameters of the decay models, from a first theoretical point of view. Each approach has its own advantages and inconvenience. For instance, regression methods are easy to use and have very well known variables and fixed parameters. They are not quite efficient in cases of complex systems however, where unknown variables are the majority, or where big sources of randomness exists.

Machine learning algorithms tackle complex systems degradation, in a high accuracy level. These methods however are far more complicated than basic regression analysis and are based on black box concept, where the degradation process, or the causes of such degradation are unknown. This is inconvenient for designing a highly reliable product.

Online models, like Kalman filtering, tend to give a very close-up monitoring solution for maintenance planning. These models however are very costly, as the data are required to be collected frequently, and computation is done repeatedly. Moreover, their objective is to monitor the evolution of degradation, which can change depending on the data. However, this is not the objective of this thesis, since the components are aged under constant or dynamic, but fixed factors through the aging time.

Stochastic processes solve the lack of incorporating the randomness in basic regression models. They are best suited to address the modeling of the degradation of a component in a global system for design optimization or energy management, where different degradation scenarios must be taken into account. Again, this is not the case in this thesis because the degradation modeling only addresses the individual electrical components, where they are subject to very few uncontrolled random factors.

The methods of the degradation models have been detailed, it is now time to apply them, if possible, to motivating examples. Two motivating examples will be used in this thesis, the first being the degradation of organic light emitting diodes, which are very sensitive to stressors due to their organic layers. The other example is the degradation of the insulation of twisted pairs of enameled copper wires at low voltages, which has been rarely studied before, unlike their mean time to failure studies. For this purpose, a design of experiments will be performed to evaluate the aging of components under multiple stress factors. Finally, the test benches and measurement procedures will be explained. However, the data collected will not be treated in the following chapter.

Chapter 3

Experimental design

Contents

3.1 Introduction

In the previous chapter, physics-based and empirical models were presented. It was established that semi-empirical models that combine both models, include the stress factors and capture the decay trajectories. To estimate the parameters of the semi-empirical models, experimental data are required. For this purpose, the experimental design methodology is presented, in order to optimize the cost of the experiments and to produce the most reliable performance data.

The experimental design procedure is then applied to two experimental designs: The OLEDWorks experimental design and the insulator experimental design. The OLEDWorks experimental design includes aging of industrial OLED panels using a test bench that already exists for previous OLED studies. Therefore, the test bench is presented, along with the added part regarding the application of dynamic electrical stress. The measurement procedures are then identified, in order to collect as much data as possible, for the modeling of the degradation and the understanding of the degradation mechanisms. Finally, the experimental plan selecting the experiments to be performed under different levels of accelerated, thermal and electrical, constant and cyclic stresses, is presented.

As for the experimental design of the insulator, it consists of aging twisted pairs of enamelled copper manufactured in the laboratory for low voltage applications. Also, the degradation test bench is presented, where it includes temperature, voltage and frequency constraints. Therefore, an experimental plan selecting the experiments to be performed under these constraints is designed. Periodic inspections are performed, where the partial discharge inception voltage is measured. The measurement procedure is also detailed.

3.2 Design of experiments

"The only way to learn anything about a system is to disturb it and then observe it" [68]. An experiment is a scientific procedure undertaken to make a discovery, test a hypothesis or validate a known fact. Experiments have been conducted since the beginning of time, and while Newton did not need an experiment to discover the law of gravity, most scientists need to conduct experiments to understand their research. In the case of this thesis, experiments are needed to test the aging of electrical components in order to apply degradation modeling methods to their results. In the following paragraphs, the terms of the experiments are explained and the steps in designing an experiment are presented.

Firstly, an outcome is always expected from an experiment, and it may vary depending on the conditions of the experiment. Although experiments can be natural (uncontrolled), the term "experiment" generally implies a controlled experiment that has a specified goal combining the outcome and the desire to adjust it. In other words, the conditions of the experiment are controlled by certain "factors" or "variables", which are modified to influence the outcome. These factors can be qualitative or categorical, such as the type of variable or its presence, and they can be quantitative, meaning that the amount of the factor applied varies from experiment to experiment.

Since a large number of tests can be a waste of time and resources, it is important to conduct the experiments in an efficient manner, i.e., to obtain the maximum amount of information by doing the minimum amount of work. To plan an experiment, five steps are necessary [115]:

1. Establish the Goal
2. Develop a Strategy

3. Create a plan
4. Implement the plan
5. Observe and analyse the results

3.2.1 Establish a goal

The first step of the experiment is to assign an objective; In the field of reliability, and in particular in degradation modeling, the objective is to maximize the lifetime and to accurately predict the lifetime or the mean time to failure. For instance, in Jin *et al.* paper, their goal was to predict the lifetime of a flywheel in long-life satellites by estimating the amount of lubricant lost [109]. In Lall and Wei paper, their goal was to predict a 70 % lifespan by tracking the luminous flux degradation and color change of a solid-state light. In addition, the objective is related to the factors used, e.g., if the objective is to maximize lifespan, experiments must test several conditions in order to achieve this objective. Therefore, when planning an experiment, factors that reflect the stress applied under real-world conditions should be considered.

3.2.2 Develop a strategy

The next step is to develop a strategy: The first strategy that comes to mind for testing the effect of a factor on the outcome is to conduct several experiments with that factor at different levels. This is called the OFAT (one-factor-a-time) method, where each factor is tested alone. This method is very expensive because if n factors have to be studied at k levels each, the number of experiments to be tested will be a total of $n \times k$. In addition to the cost of the experiments, the interactions between the factors will not be considered, since only one factor at a time is tested. The interaction between factors is a phenomenon that occurs in real life, for example, which can not be ignored when studying all the system. This is where the experimental design comes in, which includes three main techniques: the factorial design, the D-optimal design and the Latin hypercube design [153].

The factorial experimental design allows for the study of the interactions between factors, which is not possible with a one-factor-a-time (OFAT) method. Fisher introduced the design by considering each factor to be independent of the others, and classified it into full and fractional factorial designs [34]. The full factorial design requires k^n experiments to be performed, and generally the factors are considered orthogonal, i.e. the number of levels for n factors at k levels each is optimally assigned to two, with two values, high and low. The level depends on whether the factor used is quantitative or qualitative. When the factor is quantitative, the terms "high" and "low" refer to the highest and lowest quantity of the factor applied, respectively. Whereas for the qualitative case, the level can be attributed to the type of factor used or simply its presence or not in the experiment. The effect of high and low levels of one factor should balance out (cancel) against the effects of the other factors for an orthogonal experimental design.

The fractional factorial design could be the first option for selecting which experiments to perform when the effects of the factors are unknown, as it is less expensive and labor intensive. As the name implies, the fractional factorial design consists of an adequate fraction (half or 1/4) of the combination of factors that allows the most important factors to be estimated, and higher order interactions to be neglected.

Fig. 3.1 presents a three-factor full and fractional factorial design. The full design consists of 8 experiments placed orthogonally, to combine all levels. The fractional design, on the other hand, is a reduction of the full design, where the experiments are carefully chosen so that their projection onto

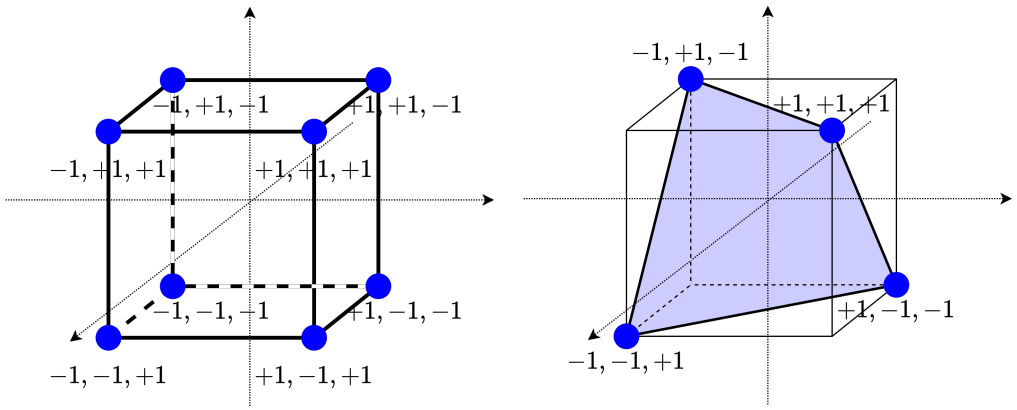

(a) full factorial design (b) fractional factorial design

Figure 3.1: Three factors factorial designs

a two-dimensional plan gives the same results as a full two-factor design. This allows the prediction of the effect of the main factors, without interactions. In fact, the combination of levels for each factor can be confounded by the interaction between the other two factors. An example is presented in Tab. 3.1, where the table represents the factor combinations for each experiment in the full and fractional factorial design. It can be seen that the levels of factor F3 for the fractional design ex-

Table 3.1: Levels distribution of three-factor factorial designs

	Full factorial design			
	Experiments	Factors		
		F1	F2	F3
Levels	1	−1	−1	−1
	2	+1	−1	−1
	3	−1	+1	−1
	4	+1	+1	−1
	5	−1	−1	+1
	6	+1	−1	+1
	7	−1	+1	+1
	8	+1	+1	+1

Fractional factorial design				
Experiments	Factors			Interactions
	F1	F2	F3	F1×F2
2	+1	−1	−1	−1
3	−1	+1	−1	−1
5	−1	−1	+1	+1
8	+1	+1	+1	+1

periments are the same as the interactions between factors F1 and F2. This phenomenon is called aliasing, because the effect of the factor F3 includes the effect of the interaction between factors F1 and F2. Nevertheless, it still is a great solution for a primarily study because it reduces the number of experiments to be made. Instead of 2^k experiments, a fraction of this number is needed which can be extracted from the trade-off table in Fig. A.6.

In addition to the factorial design, center points that are halfway between the high and low levels can be added to confirm the linearity of the model or to test for curvature and switch to response surface designs for example (presented below). The center points also serve as a reference for other experiments and indicate the stability and variability of the process. They should be tested at the beginning and end of the experiment, and a few times during the experiments. Sometimes it is worthwhile to test a three-level factorial design to estimate a second-order model, but it is best to split factorial designs with more than three levels into two or more two-level factorial designs.

Optimal designs focus on optimizing a criterion, e.g., an A-optimal design minimizes the mean variance of the parameters, and D-optimal designs minimize the general variance of the parameters, etc [110]. A full factorial design with two levels for each factor is already an optimal design. The Placket-Burman design is a different model to use for experimental designs, when only the main effects of the factors are sought, thus reducing the total number of experiments to a multiple of four instead of a power of two [176]. The Latin hypercube design consists of assigning a single sample for each level of the equally divided "p" parts of each of the "d" dimensions. It is mainly used for computer experiments for sampling and modeling strategies providing good uniformity and covering the entire surface to be modeled [220]. It is very advantageous when there are nuisance factors but it does not take into account the interactions between the factors and the number of levels for each factor must be the same as the number of conditions.

The response surface method is another good strategy to implement for experimental design. It is mainly applied to test the quadratic or cubic order of the relationship between a factor and the result. For this purpose, more than two levels are needed for a single factor, in the same way as for factorial designs with more than two levels for each factor. However, the total number of experiments required for factorial designs will be very high, even with a modest number of factors.

On the other hand, the total number of experiments in a response surface strategy is based on the design itself. The first design is the central composite design, which consists of a basic factorial design (in blue), central points (in red), and another group called "star points" (see Fig. 3.2). For each factor, two star points are placed on its axis, where the experiments of the star points consider only one factor at a time. Considering that the distance between the center point and the points of the factorial design is ± 1, the distance between the center and each star point is a certain *alpha* computed based on whether the factorial points actually reach the limits of the experiments or not.

If the design can exceed the limits of the experiment, it is called a central composite circumscribed design CCC, and $\alpha = \left(2^k\right)^{1/4}$ is greater than one.

If the design cannot exceed the boundaries of the experiment, the design is referred to as a CCI-listed central composite design and the actual alpha would be $\frac{1}{\alpha} < 1$.

In both designs, five levels are required for each factor, however, if it is not possible to have more levels, a design where $\alpha = 1$ called a central composite face CCF can solve the problem.

All possible response surface designs are shown in Fig. 3.2. The overall number of runs needed

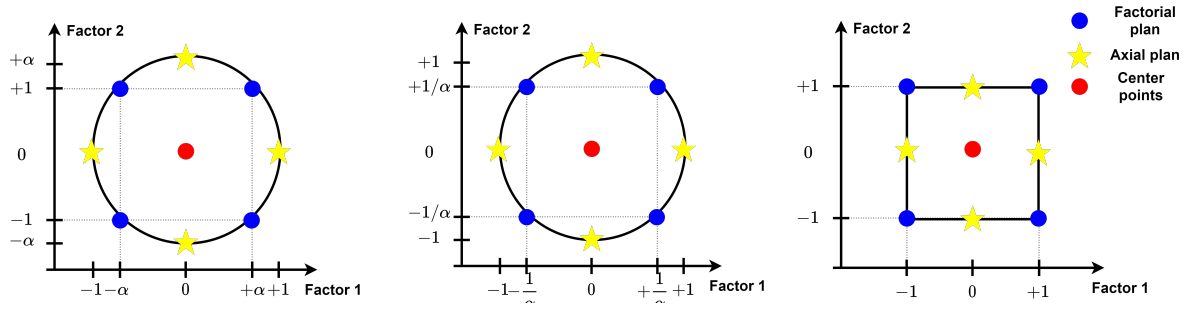

(a) CCC (b) CCI (c) CCF

Figure 3.2: Two factor response surface designs

by the response surface designs would be 2^k for the factorial plan, $2k$ for the star points and $n0$ for the central points (see Eq. 3.1).

$$n = 2^k + 2k + n0 \tag{3.1}$$

Finally, the design of experiments, as Fisher introduced it, is based on the principles of replication, randomization and blocking [35]. **Replication**, or repeating each experiment under the same experimental conditions but at a different time, is essential for statistical purposes to estimate measurement variance, significance of results, and measurement uncertainty.

By **randomizing** the timing of the experiments and repeating the samples for each experiment, a normal distribution for the variance of the results is simulated, allowing the significance of the results to be tested by considering them as "independent". In addition, randomization can minimize perturbations caused by some unknown or uncontrollable factors. When some uncontrolled factors take place, for example two scientist that alternate in doing the measurements, or experimental devices are ordered in several batches, or an uncontrolled "pandemic" occurs and interrupts the experimental process, or in case of weather variations, etc., the **blocking** principle can be applied to solve the problem.

Usually, interactions between three or more factors can be ignored, so blocking would be a variable that replaces third degree interactions. For example, when two scientists alternately perform the measurements, and considering that the experiment has three factors A, B, and C, one scientist will perform the experiment when the ABC interaction is at its lowest value and the other will perform it when it is at its highest value. Since the ABC interaction is small and generally ignored, the disturbance caused by the measurement operator is compensated by blocking. In this case, blocking is an additional categorical factor that represents the scientist making the measurement.

Finally, validation and testing experiments must be added randomly to validate the good fit of the model, as presented previously. This is done to test the ability of the model to predict other outcomes since the experimental designs have no or very few degrees of freedom.

3.2.3 Create a plan

There are two choices for conducting reliability experiments, namely the evolution of quality over time. Lifetime data is the best way to determine the reliability of a product, while the other choice is to monitor the degradation of a component through aging. It is preferable to record both data because they provide the complete aging performance history of the product. However, there are many challenges that need to be addressed according to Chiao *et al.* [48]:

- Testing to failure may not be feasible for highly reliable products, even using censored data, and is very costly
- Failure can be accelerated at high stress levels and may not reflect true behavior under nominal conditions

These challenges are solved by planning a "degradation" experiment instead of a mean time to failure experiment. The design of a degradation experiment, according to Yu and Tseng [232], implies posing the following decision problems:

- How many devices must be used to perform a life test?
- How do you determine an appropriate inspection frequency and interval?
- How long should the experiment last before it is terminated if no failure occurs?

These questions are answered by consulting previous work or the literature, or by conducting preliminary tests if no previous studies are available. They also depend on the model in situ, as some models require more samples for the statistical computation. They also rely on the strategy chosen, e.g. the number of experiments to be tested for k-factor full factorial design with two levels per factor is 2^k, and for each experiment, a certain number of repetitions is necessary. In addition, they are dependent on resources, time, and cost, and responses must take into account whether resources allow for replication and repetition of experimental conditions, and for designing validation and testing sets.

The inspection time depends on the nominal lifetime of the product, and the model used, for example if the decay is modelled with a logarithmic scale of time, the inspection interval increases with time. Inspection frequency depends on the model desired, for example stochastic modelling requires more measurements than an ordinary regression. Finally, ending an experiment before failure depends on several conditions, and is mainly restricted by time. For example, if a scientist has 6 months to execute a full batch of let's say 12 experiments, and has three stress equipment (three thermal ovens for example), experiments should not age for more than two months, because other experiments need to be done. This is a crucial constraint to test an experimental process in a three year PhD thesis. Now, if there is no analogous constraint, and no failure is happening, it is possible to set a termination rule based on an on-line real-time procedure that is related to the convergence of the accuracy prediction of MTTF, specially for highly reliable products because of their regularity and their relatively slow decay [192].

3.2.4 Implement the plan and analyse the results

The fourth step in planning an experiment is to implement the previous plan foreseen, and this consist of the physical application of the design previously. Lastly results are collected an analysed to obtain the goal setted at the early stage of the planning.

Studying the main factors that could affect the aging of any component in electrical engineering, and in particular the OLEDs and insulators were studied firstly. The possible aging models were studied as well to be considered while choosing stress levels, and inspection frequency and time. Lastly, several experimental strategies were presented to choose from.

In the following sections, experiments testing the aging of OLEDs and insulation of twisted pairs are detailed as following:

- Components specifications
- test benches
- Measurement procedures
- Results

The results will be analysed in the next chapter following several degradation modelling methods.

3.3 OLED experiments

The first component tested is organic light-emitting diodes. As presented in Chapter 1, the degradation mechanisms of OLEDs are activated when the panels are subjected to external factors such as temperature and current. Other external factors such as UV light and moisture can be avoided by adding a UV protection film on the glass substrate or by sealing the OLED hermetically. The OLEDs used in this thesis are industrial panels already sold on the market, so they are assumed to be very reliable against external stress factors. Two types of OLEDs are tested, and in the following the experimental setup of these OLEDs are presented.

3.3.1 GL55 experimental campaign

In the LAPLACE laboratory, the aging of OLEDs has been studied in several ways: luminance, impedance, CV characteristics.

An experimental campaign testing the aging of OLEDs has already been performed before the beginning of the thesis. The previous OLEDs used were large area lighting panels from Philips (see Fig. 3.3.1) with the characteristics presented in Tab. 3.2.

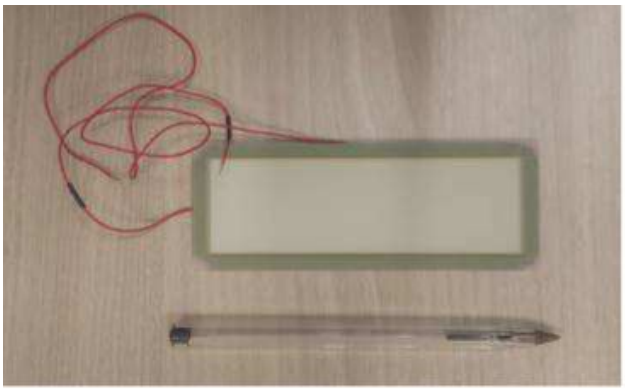

Figure 3.3: OLED panel GL55, compared to a pen in size

Name	Philips Lumiblade OLED Panel GL55
Color	White
Color temperature	3200 K
Dimensions	130.2 mm × 47.8 mm
Light emitting area	116.7 mm × 35.2 mm
Rated current	390 mA
Maximum current	450 mA
Rated voltage	7.2 V
Maximum voltage	7.5 V
Lifetime at rated current	10 000 h
Nominal luminance	4200 cd m^{-2} @ rated current

Table 3.2: Technical characteristics of OLED panel GL55

Aging due to temperature only, without electrical stress, was also tested. One OLED was tested for each stress condition, and the experimental design is shown in Fig. 3.4. The choice of experimental design was based on the design of experiments method, specifically the full factorial design plus the response surface methodology, which was explained earlier. The purpose of the experimental campaign was to assess the reliability of OLEDs using accelerated life testing, as the life at rated current was a long period of 10 000 hours. Therefore, considering that the nominal current density is equal to 9.494 mA cm^{-2}, three current densities above the nominal level were chosen with a ratio of 1.18, 1.37 and 1.58. The temperature also had three levels, the ambient temperature 23 °C, a medium level at 40 °C and a high level at 60 °C below the maximum organic temperature of the OLED.

The campaign was employed in two different theses where several aspects of aging were studied; these aspects are presented below.

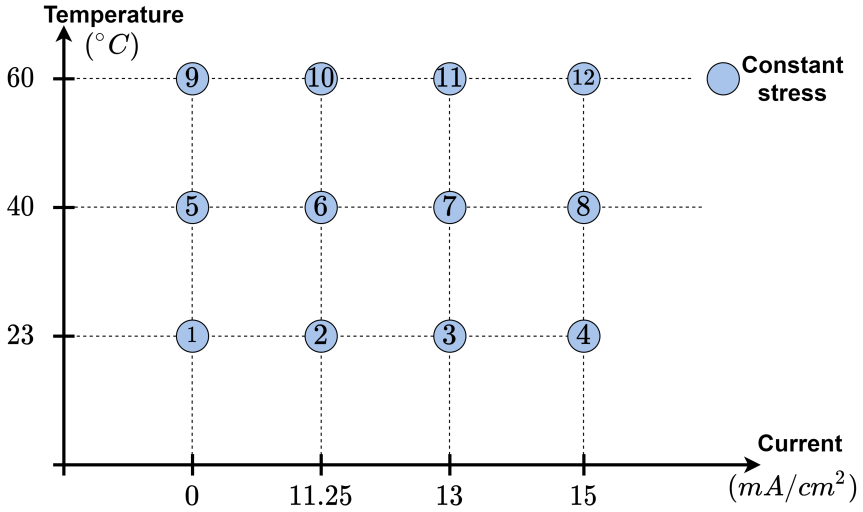

Figure 3.4: Experimental design for GL55 OLED panels

Luminance aging Modeling the lifetime of large area OLEDs based on the GL55 experimental design has been studied previously [182]. The modeling involved several OLED lifespans, which correspond to the time when luminance decreases by a specified percentage. For example, $L85$ is the lifespan of the OLED when its luminance has a decay of 15 %, and reaches 85 % of its initial value. The luminance data of the aging set is presented in Fig. 3.5.

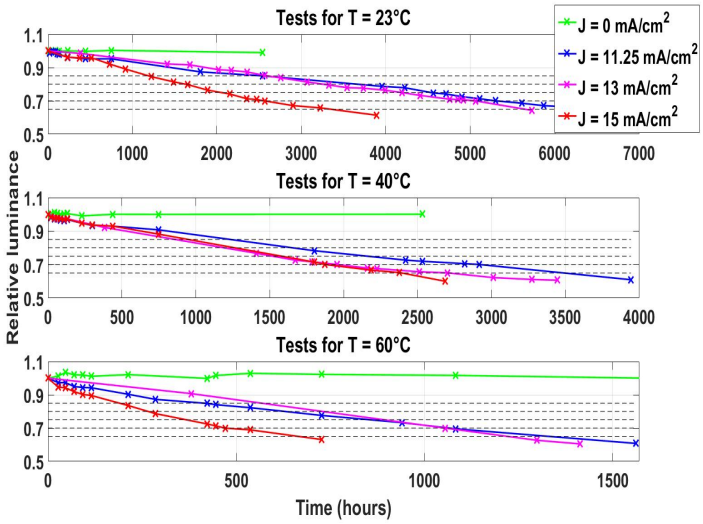

Figure 3.5: Luminance aging data of OLED GL55

Despite the recording of several luminance decay values over time, the main objective of the previous thesis was the modeling of the OLED lifetime or the 70 % lifespan $L70$. Lifetime modeling of $L70$ included the effects of applied stress, using different methods such as experimental designs and regression trees to understand the impact of stress conditions and their interaction on lifetime. Eq. 3.2 presents a first order semi-empirical model of the lifetime $L70$ with the current density J, the temperature T and their interaction. The model is based on a linear relationship between lifetime and current density, and an inverse exponential relationship between lifetime and temperature (based on the Arrhenius model). The physical relationships between stressors and lifespan were then combined using a basic multi-linear regression that also allowed the estimation of the interaction effect between

electrical and thermal stress. Nonetheless, since the physical relationship between temperature and lifetime is exponential, a transformation of variables was performed to linearize the equation. Finally, it was deduced that both stress factors have a negative effect on the lifetime, i.e., they decrease the lifetime, and that temperature has the most significant effect on the aging of the OLED.

$$Log(L70) = 3.206 - 0.173log(J) - 0.352/T - 0.007log(J)/T \tag{3.2}$$

The same luminance data was used in another thesis, to model the degradation of the OLED separately for each given stress condition [19]. The modeling was based on the accelerated lifetime equation (see Eq. 2.13), and the stretched exponential decay equation (see Eq. 2.17). Eq. 3.3 represents the fitted SED model of the luminance L of the OLED aged at 23 °C and 11.25 mA cm^{-2}.

$$L = 3639 \cdot exp\{-(\frac{t}{17024})^{0.9298}\} \tag{3.3}$$

The two previous thesis have used different methods according to their studies purposes. Dr. Salameh, for example, has worked on semi-empirical models to estimate the effects of stress conditions on lifetime without considering dynamic aging [182]. Dr. AlChaddoud worked on modeling the decay in a time-varying equation without incorporating the effects of stress [19]. This thesis integrates the two approaches to build a time-varying luminance degradation model that includes the stress constraints.

Impedance aging indicator In addition to luminance, the degradation of OLEDs can be monitored using electrical characteristics. The electrical impedance of OLEDs has been studied previously based on the equivalent electrical circuits of OLEDs [19]. In fact, there is a wide variety of equivalent electrical circuits of OLEDs that depend on the materials used (phosphorescent or fluorescent diodes), the type (display or panels), the application (flexible), or other objectives like designing drivers to compensate for any degradation in luminance. Studying the equivalent capacitance of the OLED can help in understanding the transport and trapping of charge carriers, which helps in designing OLEDs and optimizing layer thickness for example [37, 89, 175].

The basic equivalent circuit of an OLED consists of a resistor in series with a block of capacitors and resistors in parallel [111] (see Fig. 3.6a). The series resistor is used to model the induction current flow inside the OLED, and the block of capacitors and resistors in parallel is used to model the capacitance between the layers, and then the subsequent light output.

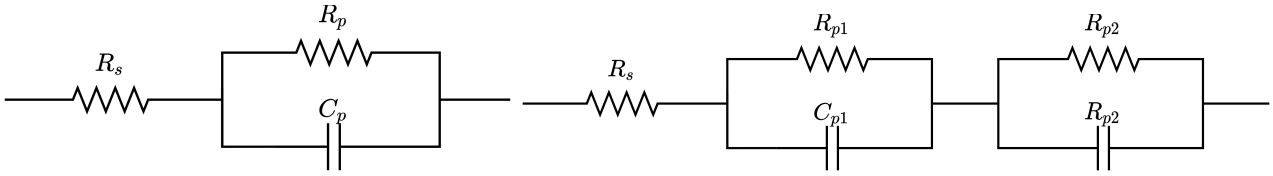

(a) OLED basic equivalent electrical circuit (b) OLED equivalent electrical circuit adopted in AlChaddoud thesis [19]

Figure 3.6: Equivalent electrical circuits of OLEDs in literature

Lee identified the three components of this circuit using the very fast transient response of voltage and current (less than one microsecond) [132]. Similarly, Li *et al.* was able to compute the equivalent capacitance of an organic single-layer OLED using this fast transient voltage and current and their derivatives [135]. In another approach, Campbell identified the capacitor and the resistor in parallel using a Bode diagram for frequencies ranging from 100 Hz till 1 MHz, and fitting the result to the equivalent circuit using a least squares fit[42]. Similarly, Ahn *et al.* used a Cole-Cole plot for their impedance spectroscopy with two voltage bias levels to identify the same equivalent circuit

[13]. Drechsel *et al.* added two additional blocks of parallel resistors and capacitors to model the intrinsic interlayering and the depletion layer [67]. After identifying the elements of the proposed circuit by impedance spectroscopy, they used the identified values to determine the geometric thickness of each layer, and the charge density distribution within those layers. In the same approach, Chulkin *et al.* added another parallel block for OLEDs with high operation voltage (5 to 10 V) and used impedance spectroscopy to estimate the mobility and concentration of charge carriers in the transport layers. [52].

The typical current-voltage curve C-V, which is related to the diode family, has also been used to identify the equivalent electrical circuits of OLEDs. Bender *et al.* dissected the C-V curve into three regions: the first region does not produce light, but a small current begins to flow through the OLED [28]. The second region corresponds to the first light emission around the threshold voltage and the third region shows the OLED in operation where the current flow and luminance production are very important. Each region was modeled with a set of capacitors, resistors, and diodes, and the model was experimentally verified by simulating the C-V curve and transient voltage.

The evolution of impedance with aging was also studied in Dr. AlChaddoud's thesis. The OLED panels in the GL55 experimental design were modeled using an equivalent circuit consisting of one resistor in series and two blocks of capacitors and resistors in parallel (see Fig. 3.6b). The Bode diagram was plotted at three stages of the OLED life, before aging, at 30 % of degradation or at the lifespan L70 and at the half-life where there is 50 % of degradation. It was deduced that the parallel resistance increased with aging and the parallel capacitance decreased with aging. However, no modeling of the impedance evolution was performed because only three measurement points were taken. The current density-voltage curve was also studied for the three stages of aging, and it was deduced that the threshold voltage, that is capable of generating 1 cd cm^{-2} of luminance, increased with aging (see Fig. 3.7). This measurement made it possible to estimate the evolution of the energy

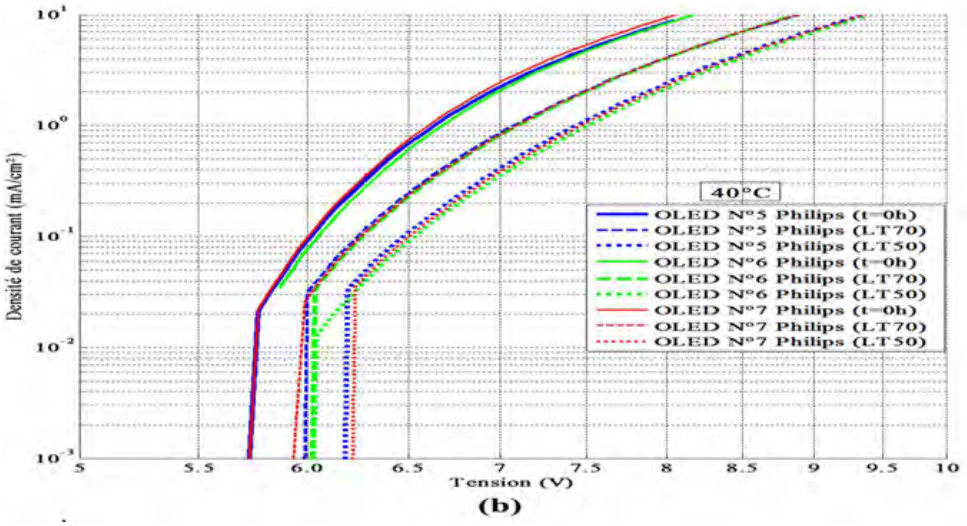

Figure 3.7: Evolution of the threshold voltage of the IV curve of OLED GL55 at three current densities and one temperature (from [19])

required by the trapped charges to produce light.

3.3.2 OLEDWorks experimental campaign

The second campaign is made during this thesis where large area commercial OLED panels from OLEDWorks were chosen to test their aging. They are warm white large area OLED panels called

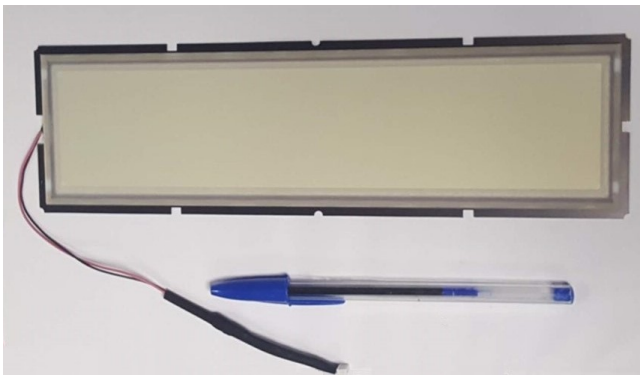

Figure 3.8: OLED panel OLEDWorks FL300 L ww, compared to a pen in size

"OLED Panel Brite FL300 L ww level 2" that can be seen in Fig. 3.8). Their technical characteristics are presented in Tab. 3.3, from the corresponding data sheet [143].

Table 3.3: Technical characteristics of the OLED panel OLEDWorks FL300 L ww

System	
Name	Brite FL300 L ww level 2
Application	Indoor buildings
Carrier material	Glass
Color	White
Dimensions($l \times w \times h$)	248 mm × 70 mm × 21 mm
Weight	69 ± 0.8g
Light emitting area	222 mm × 46 mm, 102.1 cm^2
Operational conditions	
Ambient temperature	$+5 \cdots 40$ °C
Maximum internal	$\leq$80 °C
operation temperature	
Rated current	0.368 A
Maximum current	0.390 A
Initial rated voltage	20 V
Voltage at end of life	25 V
Nominal luminance	8300 cd m^{-2} @ $I_{in\ rated}$ =0.368 A

Similar to the previous GL55 experimental campaign, the main external two factors for OLED aging are then the thermal and electrical stress. Additionally, to study the effect of the discharge phenomena on the OLED lifetime, the electrical stress factor will be applied constantly or in a cyclic way.

The test bench that was built by Dr. Alchaddoud for the GL55 experimental campaign is used for this thesis as well. It consists of thermal ovens with electrical wiring for the supply [19]. The temperature inside these ovens is kept constant using PID controllers, and is well diffused using fans to ensure a homogeneous distribution in all ovens. In addition to the previously built bench, mechanical supports were designed to fit the size of the large OLEDs used, and to allow good air circulation inside the ovens. Each OLED panel is connected to a Wellman DC power source that has a maximum voltage of 30 V and a current of 5 A.

Furthermore, to take into account the cyclic behavior of the electric current, a solid state relay is connected to each DC power source, placed on a metal board acting as a cooling system. The relays

are controlled by DLP design modules which are connected to a LabVIEW program. Moreover, for each thermal oven, an electronic board connects the power sources, relays and OLEDs to manually switch from constant to cyclic mode. The boards can also switch between two power sources, mainly to perform electrical measurements of OLEDs inside thermal ovens. Finally, some thermocouples read the organic temperature of the OLED inside the oven to detect any unwanted local heating for example. The test bench and a diagram of the wiring are shown in Fig. 3.9.

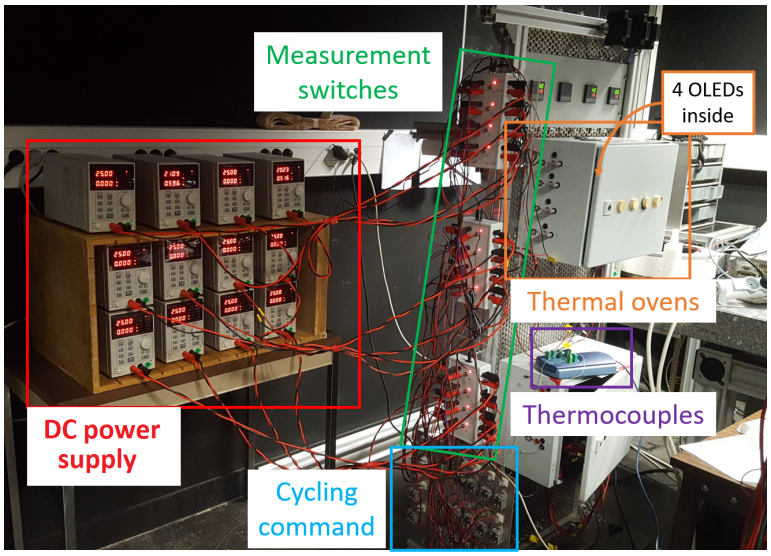

(a) Test bench figure

(b) OLED on a mechanical support inside the thermal oven

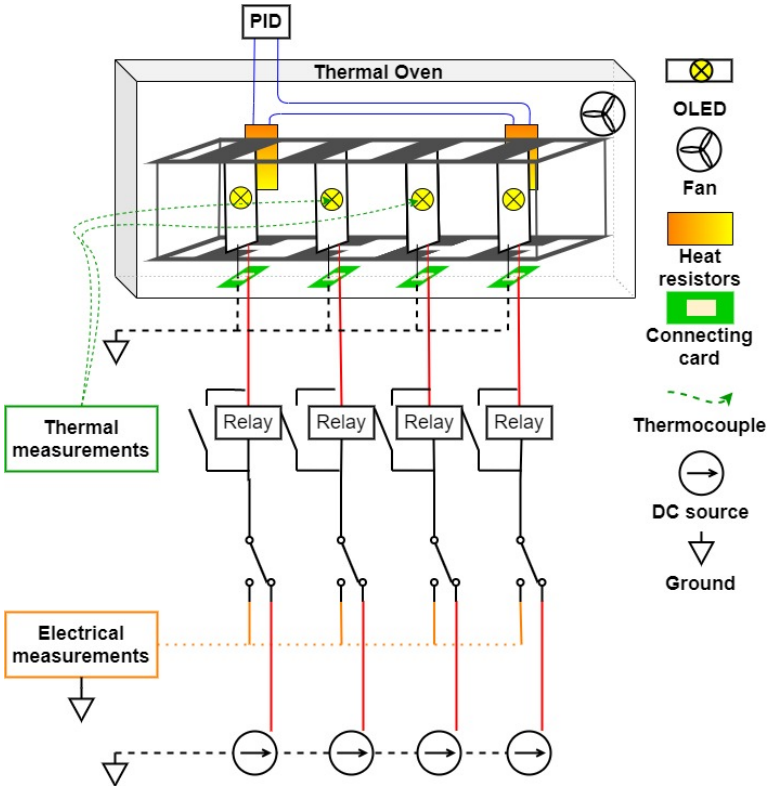

(c) Thermal oven with wiring drawing

Figure 3.9: Aging test bench for OLED panels under thermal, constant and cyclic electrical stress

For the OLEDWorks experimental campaign, several types of optical and electrical measurements

are performed to track the evolution of the OLED over time. Optical measurements include luminance, spectrum and colorimetric parameters such as correlated color temperature CCT, distance to the black body-locus Duv, chromaticity (x,y) and (u',v') and color rendering coefficient (Rf,Rg) (For more details on the measured optical parameters, please refer to the US Department of Energy report [217]). Photos of the very low current OLEDs are taken to detect any super bright or dark spots that could lead to an unwanted failure. As for electrical measurements, they include impedance measurement, CV curve and voltage evolution versus time. Finally, thermal measurements were made with a thermal camera occasionally and thermocouples. All these measurements are detailed in the following parts.

3.3.2.1 Transient response of voltage and temperature

The current that flows in the OLED when it is turned on generates with the luminance, a small heat that will gradually warm up its organic temperature. At the same time, current diffusion and thermal resistance decrease the electrical resistance and reduce the voltage level. In fact, as the temperature increases, the energy required for exciton recombination decreases and therefore a lower forward voltage is required to power the OLEDs [187]. It is important to wait for the end of this transient behavior before performing other measurements based on supplying the OLED with constant current (mainly optical measurements).

The study of the transient response of voltage and organic temperature is also very important for dynamic aging, such as the choice of the electrical stress cycle time or its duty cycle. The study of the transient temperature and voltage, thus the study of the thermal resistance of the different anode materials, is very useful to improve the luminance efficiency and thus increase its reliability [174]. The study of transient temperature is also important to study transient luminance, which is very important for OLED displays for example, since one of the great advantages of OLEDs is their fast turn-on time [47]. The study of the thermal degradation of OLEDs allows understanding the electrical properties, such as electron injections for example, and improving their performance [127].

Fig. 3.10 displays the transient luminance response of an unaged OLED at nominal current (368 mA) and ambient temperature (23 °C). The curves are fitted to a degree 6 polynomial function

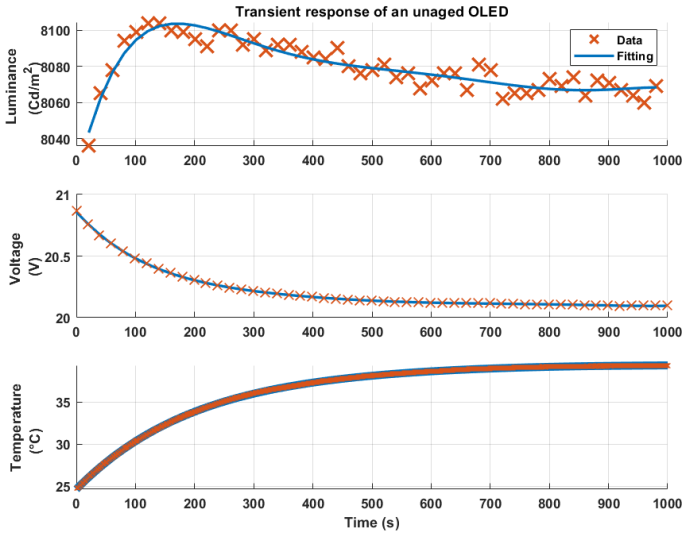

Figure 3.10: Transient response of an unaged OLED at ambient temperature and nominal current

for a clearer visual reading. The luminance in the first 120 seconds increases with time, but then decreases slowly and exponentially to a static state after about 700 s or 11 min. However, the variation of luminance in this transient state is very small since it fluctuates around a difference of 40 cd m^{-2}, which is less than 0.5 % of the measured luminance.

Fig. 3.10 also shows the transient voltage and temperature of the OLED. The voltage has a decreasing exponential curve with a time constant of 550 s or 9 min. The temperature has a rising exponential curve with a time constant of 600 seconds or 10 minutes. The evolution of the three curves can be linked as explained above, because when the OLED is heated, the electrical resistance decreases, which leads to a decrease in voltage. This decreasing voltage will decrease the luminance consequently. However, even though the time constants are about 10 minutes, the OLED characteristics can be measured before reaching the steady state in about 20 % because their variation is minimal compared to their actual value. In fact, the luminance has only a 0.5 % variation and the voltage has an overall change of 3.8 %.

The transient temperature is also measured for higher current and temperature levels to select the dynamic stress time. Fig. 3.11 represents the temperature evolution for two cycles including the OLED in its on state and its off state. When the OLED is turned on, its organic temperature

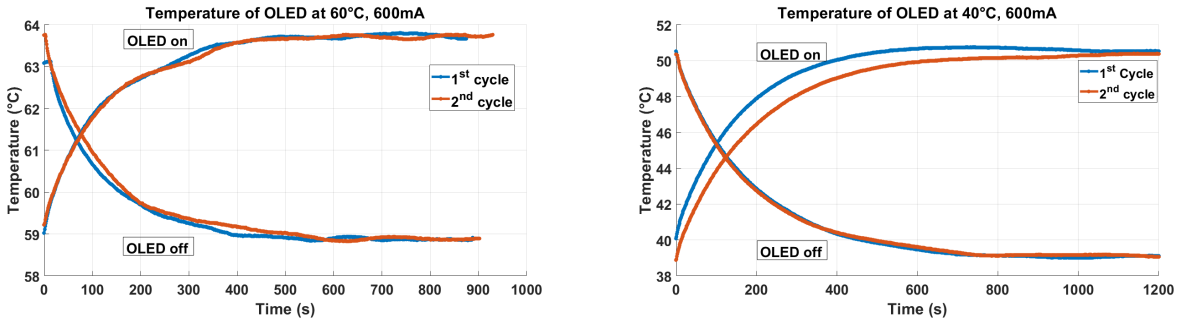

(a) 60 °C (b) 40 °C

Figure 3.11: Transient response of OLEDs at 600 mA and different temperature

increases, but when it is turned off, its organic temperature also decreases exponentially. It is therefore important to study the temperature evolution in the on and off states. Tab. 3.4 represents the time response of the organic temperature of OLEDs at different current levels and different ambient temperature levels. The higher the ambient temperature, the less time it takes for the organic temperature of the OLED to reach its steady state. In addition, the higher the ambient temperature, the smaller the difference between the initial temperature and the organic temperature at the steady state.

Table 3.4: 5 % response time of the organic temperature of OLEDs

Ambient temperature (°C)	current (mA)	State	5 % Time response (s)
23	368	on	600
40	600	on	525
40	600	off	614
60	600	on	372
60	600	off	424

Again, this type of measurement is performed before starting the aging campaign, as it is useful for designing the measurement protocol performed during each aging inspection.

3.3.2.2 Optical measurements

As in the previous GL55 experimental campaign, luminance is the main indicator to evaluate the degradation of OLEDs. In addition to luminance, other optical measurements can be taken in parallel, such as spectrum and colorimetric parameters. These optical characteristics are measured using a Minolta CS-1000 spectrometer (see Appendix C.2). The OLEDs used are rectangular panels of large surface, whose photometric characteristics can vary from one spot to another. Thus, three location areas are considered, "low" at the injection area, " middle" in the center and "high" at the other end of the OLED, as shown in Fig. 3.12. For the measurement, the OLED is placed perpendicular to

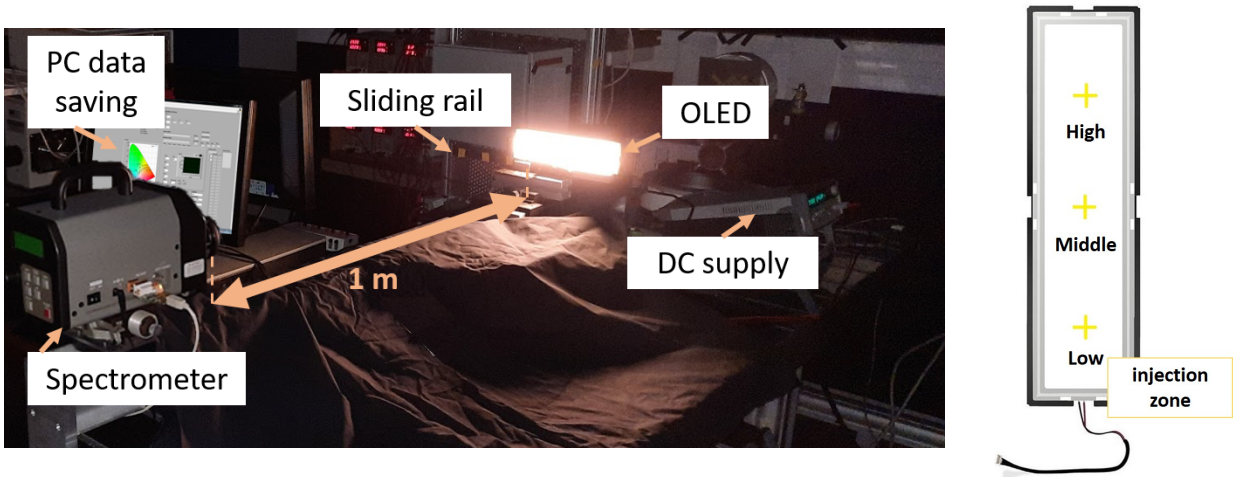

Figure 3.12: Photometric measurement

the spectrometer, so that the measurement axis has a 0° angle. The distance of the measurement can be chosen as described in [161], or following the common rule that the measuring distance should be at least 10 times the size of the light source. Therefore, the OLED is placed at a distance of 100 meter, to have a complete coverage of the measurement areas of the OLED which has a 5 cm × 5 cm area.

The measurements are performed periodically, while the OLEDs are aging. For each inspection, the OLEDs are removed from the ovens and allowed to cool for at least 5 min on heat dissipating pads before starting the measurement procedure. The latter consists of turning on the OLED at its rated current, and waiting 5 minutes until the voltage is almost stabilized (based on the above study of the transient response of voltage and temperature). For each of the three locations, 22 measurements of the optical characteristics are then made consecutively in a dark room for a period of about three minutes to eliminate any measurement uncertainty.

In this thesis, only the luminance is used, but the aging of OLEDs based on the other colorimetric characteristics are analyzed in a separate study [27].

3.3.2.3 Electrical characterization

Electrical characterisation is made to understand the physical mechanisms behind the aging of OLEDs. It includes the study of impedance spectroscopy, the CV curve and the fast transient response of current and voltage.

Impedance spectroscopy The impedance can be extracted from the equivalent electrical circuit of the OLED presented in Fig. 3.6b, which is identified from a Bode diagram. The Bode diagram is plotted using the Modulab XM MTS device for electrochemistry and photovoltaic measurements from Solartron analytical (see Appendix C.1). The device has a measuring system with 4 connection terminals (two for the supply of the electrical component and two for the measurement of current and voltage). It has an internal impedance of 50 Ω which is connected to a Faraday cage, where the OLED is placed to limit any additional noise.

It is connected to a software called Xm-studio MTS which applies a frequency sweep from 1 Hz to 100 kHz of an AC voltage of 100 mV, plus a constant bias voltage. Consequently, it records the magnitude and phase at a rate of 50 samples per second, and plots the Bode diagram. The results of the Bode diagram are then used to estimate the parameters of an equivalent circuit chosen by the user using a specific written algorithm that takes into account the internal impedance of the device (Fig. 3.13).

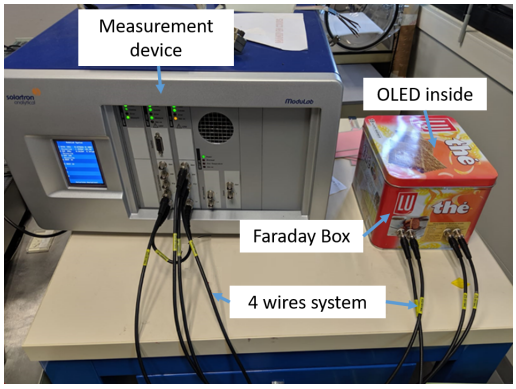

Figure 3.13: Impedance spectroscopy set-up

Impedance is specifically measured at a bias of 20 V, which is the nominal operating voltage. However, Bode plots of several other bias levels are recorded, for later study that is not included in this thesis. For example, the equivalent circuit at a bias voltage of 10V is purely capacitive because the OLED is not in its conducting state. In Fig. 3.14, 6 levels of constant voltage were applied, 10 V simulating the blocking state of the OLED, 12.5 V the first light production of the OLED, [15 V 17.5 V 20 V 22.5 V] chosen for different levels of light production. Note that the applied voltage bias is split between the internal resistance and the OLED, so when the current starts to flow through the circuit, the OLED voltage would be less than the actual voltage bias (see the step voltages above 15 V in Fig. 3.14a)

The correlation between impedance and luminance is investigated in a separate study, in which we studied the possibility of predicting lifetime using only the electrical characteristics [16]. In this study, we showed that the impedance has two time constants (from the parallel capacitance and resistance blocks), which are strongly correlated with the luminance. By tracking the evolution of these time constants, and using the correlation between luminance and time constant, it is possible to predict the lifespan of OLEDs.

CV curve The current-voltage curve (known as the CV curve) is an important characteristic for any light-emitting diode in general, and for OLEDs in particular, as it is used to build an equivalent circuit, or to track the degradation of OLEDs over time. Measuring the CV curve can be very tricky because it not only has the typical exponential shape of any diode, but contains many operating sections that can identify a certain electrical impedance. Thus, two measuring devices were used to

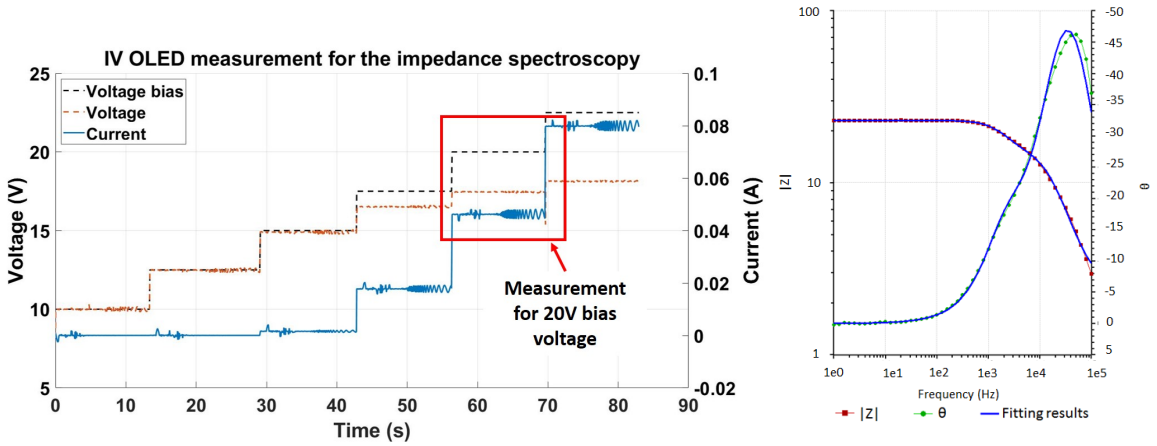

(a) Measurement voltage conditions

(b) Bode diagram impedance for a 20 V bias voltage with fitting to an equivalent circuit

Figure 3.14: Impedance spectroscopy measurement by applying several bias voltage levels and fitting the measurement to the equivalent circuit of Fig. 3.6b

measure the CV curve:

- Modulab XM MTS
- Keithley 2602A source-meter

The first device is the Modulab XM MTS which has a high accuracy with a fast sampling rate allowing the detection of all small sections useful for any further identification. However, the Modulab XM MTS device is not designed to generate a current greater than 100 mA, so it cannot cover all stages of the CV curve. For this reason, a Keithley 2602A source meter was used to measure the CV curve specifically for the operating section above 100 mA till the maximum allowed current 390 mA. This interval is included in the exponential section because the organic diode will be in its pass state for these current levels and will produce light at high luminance levels.

As can be seen in Fig. 3.15, the two plots are equal; however, the difference between the plots is clear when zooming in on the beginning of the exponential area. Fig. 3.15b accentuate this area,

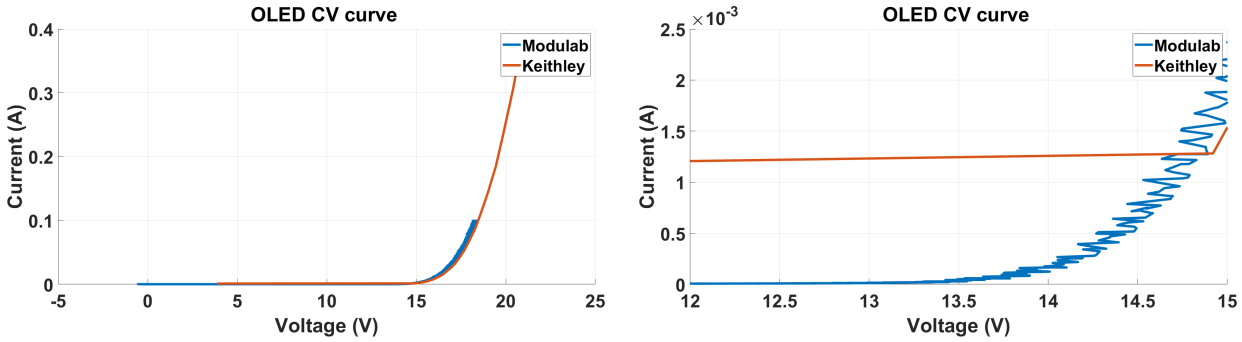

(a)

(b) zoom of the CV curve

Figure 3.15: CV curve using two measurement devices: the Modulab with high sampling rate and noise, and the Keithley with high precision but low sampling rate

where the Keithley has a low precision sampling rate, unlike the Modulab which has higher noise but

fast sampling. Keithley's CV plot would identify the threshold voltage at 15 V while Modulab's CV curve is more accurate and indicates that the exponential region begins before 14 V.

The CV curve is used to extract the characteristics of the equivalent circuit. Nevertheless, it will not be employed in this thesis, because the main objective of this study is the modeling of the degradation of OLEDs.

Transient response of current and voltage There are two aspects to consider for transient current and voltage measurements. The first is the slow transient voltage which is related to the thermal self-heating of the OLED (presented above). The second is measuring the rapid turn-on of the light, in about a few microseconds. Therefore, the fast transient current and voltage response are measured with the Modulab XM MTS device, because it has a fast sampling rate. A voltage step should be applied to the OLED to measure these characteristics. However, applying a voltage step from zero to its nominal value is not recommended for several reasons. First, the OLED does not provide enough light below about 13 V, and the jump from zero to full light output, will cause the OLED to go through different states that are not needed. Second, the Modulab cannot cope with this fast step to measure the transient response of the OLED.

The solution is to turn on the OLED at the nominal voltage level, then increase the voltage for several steps of 0.4 V peak to peak (see Fig. 3.16a). After each step, the voltage is then reduced

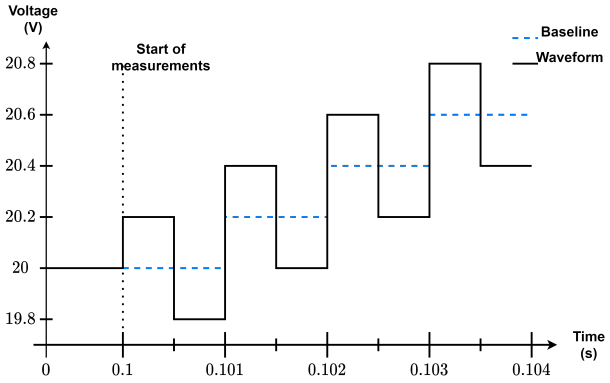

(a) Step command to measure transient response of the OLED

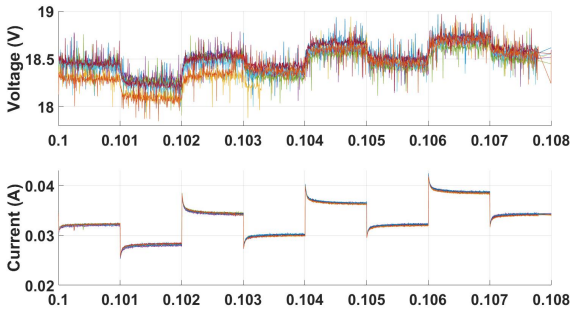

(b) Transient current and voltage response of the OLED, repeated for 10 times

Figure 3.16: Fast electrical transient response of large-area OLED panels, measured repeatedly at different voltage levels

to also measure the turn-off response of the OLED. This will verify if the transient response has the same characteristics for different current levels. If so, this will increase the certainty around the estimate of the OLED equivalent model. However, to increase the certainty and accurately estimate the variance of the measurement, the step command is repeated 10 times. The results of the step command are shown in Fig. 3.16, where the current has an impeccable replica of its response. The first repetition of the voltage response differs from the others, and this could be due to the OLED not being heated enough at the beginning. The voltage response would then be equal for all other repetitions, but with a lot of noise (due to fast sampling).

This fast transient current and voltage response can also be used to track the aging of the OLED. In fact, all of the previous measurements required a special device to perform them, and sometimes these devices can be bulky or expensive. Therefore, companies may not be able to integrate these measurement procedures into a real time diagnostic of their components.

An industrial solution to monitor the aging process is to design an electrical board capable of performing this type of measurement. This electrical board must be inexpensive, simple, and capable of accurately measuring the rapid transient response of the OLED current and voltage with fast sampling. This equipment can be sold with the OLED driver for real-time diagnosis of the OLED aging state.

3.3.2.4 Surface characterisation

OLEDs are first checked for defects using a luminance mapping method. This method involves taking high quality photos at different exposure times to detect all luminance levels. The photos are then analyzed using specific software to obtain a surface luminance distribution around the OLED panel. Fig. 3.17 presents four different OLEDs at 20 µA, and 1″ exposition time. Fig. 3.17a, Fig. 3.17b, Fig. 3.17c and Fig. 3.17d respectively present a homogeneous panel, a multitude of bright spots in the center of the panel, a vertical luminous line and a double dark spot in the lower middle of the panel. Note that this non-homogeneity is only observed at very low current levels, and at low luminance

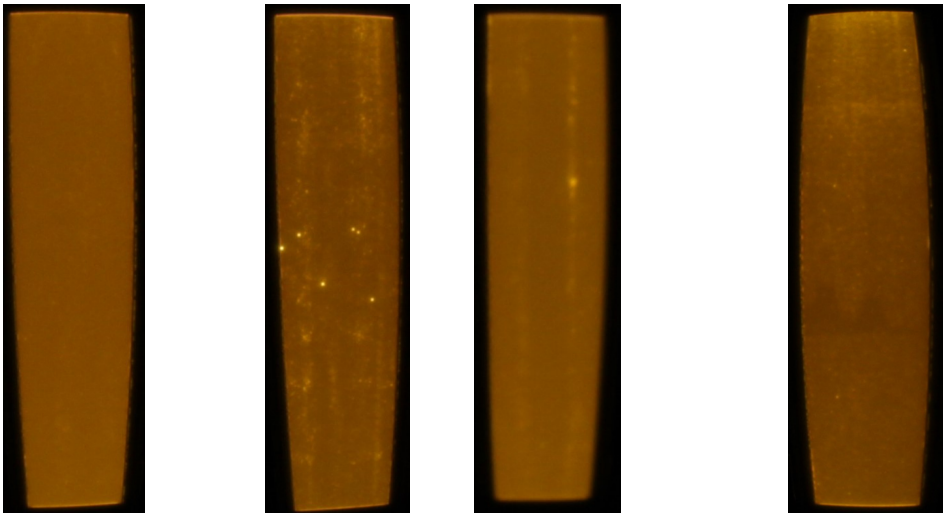

(a) (b) (c) (d)

Figure 3.17: Photos of different OLEDs at 20 µA, and 1″ exposition time

generation, because when the OLED generates more luminance, the non-homogeneity is not noticed by the naked eye. The bright and dark spots are caused by manufacturing defects while spin coating for example, where the electrode and polymer layers in some areas have slight bumps increasing or reducing the luminance production locally.

The pictures are taken with a Canon EOS 50D camera whose sensor is calibrated pixel by pixel. The camera is equipped with a Sigma EX Circular fisheye with an F 1:2:8 opening. The OLED was powered at a current of 20 µA, which is the minimum current producing light high enough for the camera to detect, and not generating transient heat thus transient voltage response. Photos at ten different exposition times (4″, 2″, 1″, 0.5″, 1/4″, 1/8″, 1/15″, 1/30″, 1/60″, 1/125″) were taken to detect all luminance levels.

Next, the photo series were analyzed with Photolux software to create an accurate mapping of the luminance surface. In Fig. 3.18, the OLED was burned directly when placed in the thermal oven at 60 °C and turned on at 520 mA. By retrieving the initial luminance mapping, it was found that the burnt spot was an initial high luminance spot. This means that the local current density at this

location was very high, that it generated an organic temperature above the tolerated temperature, which caused the polymer layers to burn. The burning of the organic material generated gas that formed a bubble around the dark spot, as can be seen in Fig. 3.18a.

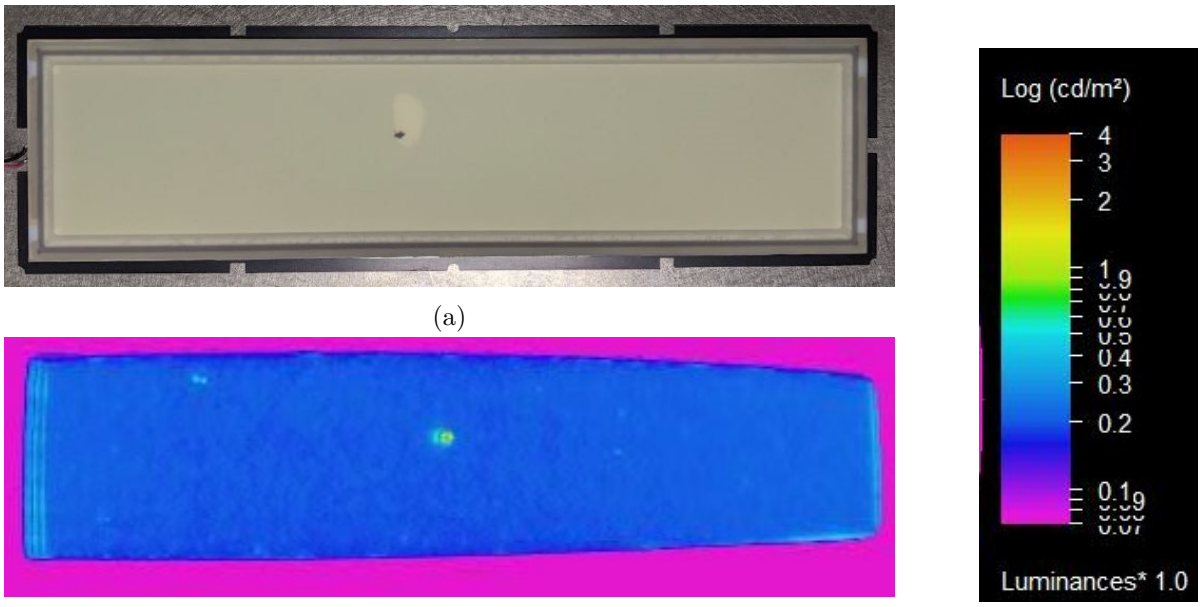

(a)

(b)

Figure 3.18: Photos of a burned OLED with its luminance mapping

This initial measurement justified several accidental burn-ins of some of the first stressed OLEDs. After these incidents, only OLEDs with a homogeneous luminance surface were selected for accelerated stressing. In addition, periodic photos were taken of several aging OLEDs to track the evolution of the bright spots over time, but this will not be addressed in this thesis. It could be a future perspective for anyone interested in image analysis.

3.3.2.5 Experimental conditions

Initial characterization of all industrial OLEDs was done before starting the experiment. The experiments are organized according to the factorial designs and surface response methodology (explained earlier). The levels of the stress factors are based on their nominal characteristics, and are chosen to be consistent with the previous GL55 experimental design in order to compare the two results. The experimental design is shown in Fig. 3.19, where three stress factors are considered: Current, temperature and cycling mode.

The first stress factor is temperature, and its values are the same as in the GL55 experimental plan. The lowest temperature level is assumed to be the room temperature, which is always maintained at23 °C. However, the OLEDWorks panels were larger than the GL55 OLEDs, and despite the fact that 4 devices fit in one thermal chamber, the self-heating of the OLEDs increased the temperature of the thermal chamber to 30 °C.

Current is the chosen electrical stress factor, unlike the previous GL55 experimental design where current density was the chosen stress. In fact, the OLEDWorks panels are almost twice as large as the GL55 panels, so the same current density would result in half the power input. In addition, the nominal current of OLEDWorks OLEDs is much higher than the nominal current of GL55 OLEDs. Therefore, it is not possible to consider the same current density levels as the GL55 experimental

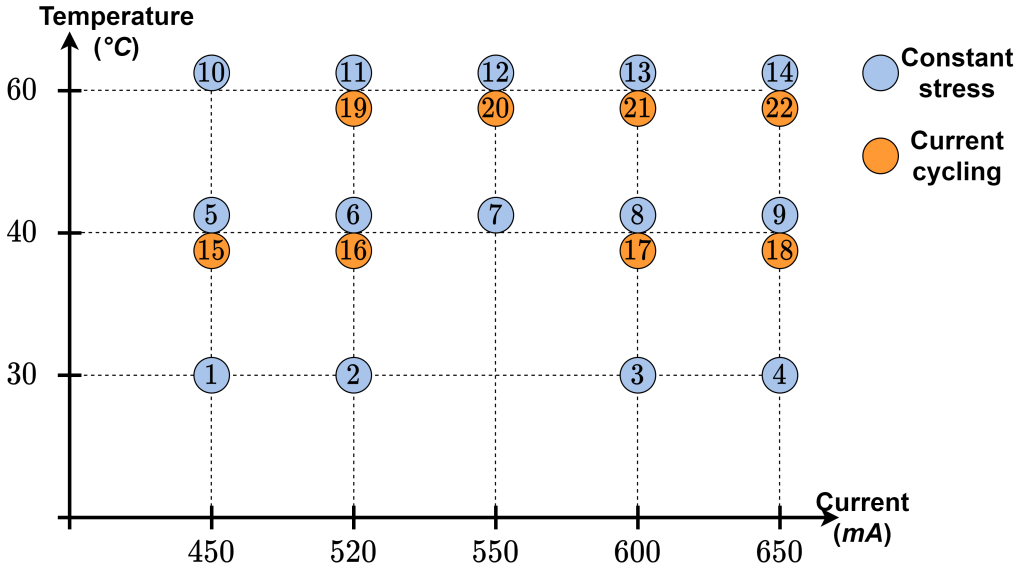

Figure 3.19: The experimental aging conditions for OLEDWorks OLED panels

design, as these values will not cause accelerated aging. Therefore, the ratio of the nominal current to the applied current is chosen as the mutual electrical stress between the GL55 and OLEDWorks experimental designs.

The third stress factor is the type of electrical stress applied, whether it is a constant or dynamic stress. The dynamic constraint was chosen to be an on-off cyclic current, to mimic the daily lighting of lamps. This type of cycling tests whether the period when the OLED is turned off has a recovery effect on the luminance or electrical characteristics of the OLED. The on-off states can also cause thermal self-heating and cooling, resulting in additional thermal and/or mechanical stress that can increase OLED degradation.

The daily on-off cycle is very slow, the dwell time for the on-state and off-state should be reduced to accelerate this stress (For more information on cyclic stress, please refer to Fig. 2.5). Nevertheless, the dwell time should not interfere with the self-heating and self-cooling of the OLED to distinguish between the effect of thermal stress and the effect of electrical dynamic cycling on OLED aging. Therefore, the transient thermal response related to self-heating and self-cooling of the OLED for each thermal stress is measured. The transient voltage, which is correlated with self-heating, is also measured. The maximum rise time for the temperature and voltage to reach their steady state is about 15 minutes. The maximum fall time for the OLED to cool to the ambient temperature of the thermal chamber is just under 20 minutes.

Therefore, a cycle consists of two phases: the online phase and the offline phase, where the current is turned on for 20 minutes and off consecutively for 20 minutes. As a result, a current cycle will be 40 minutes with two states, on and off, and with a 50 % duty cycle. he cycling chronogram is shown in Fig. 3.20a, where one cycle is presented. As it is seen in the figure, the cycling stress is alternated between two successive OLEDs, in other words, when one is switched on, the adjacent OLED is turned off. This is done to ensure an even temperature inside the oven, because as explained earlier, the self-heating of the OLEDs can increase the overall temperature of the oven. Even though the PID controller is able to consider the increase in OLEDs as a disturbance, it will take longer to warm up the oven when all four OLEDs are turned off. Therefore, alternating will minimize this disturbance,

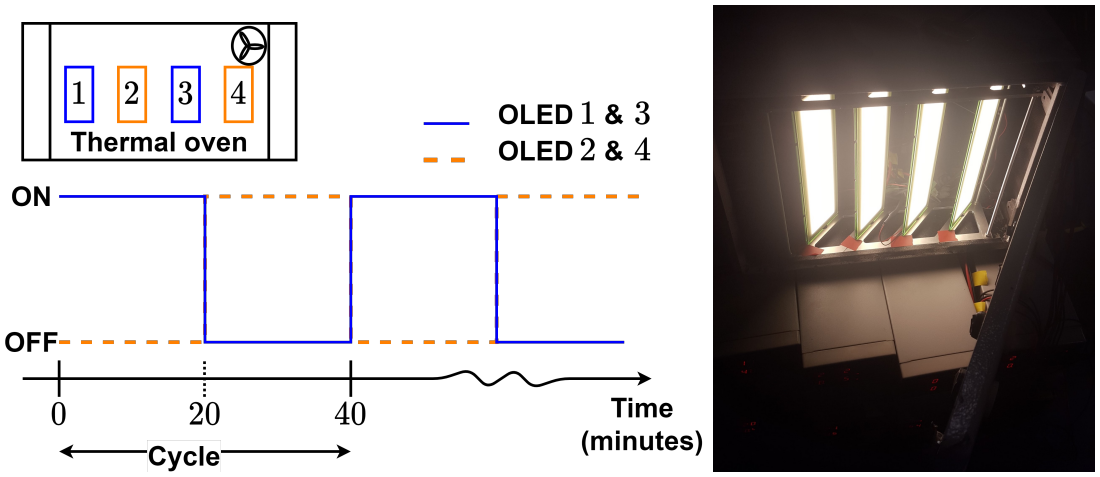

(a) Chronogram of one current cycle inside the thermal oven

(b) OLEDs on a mechanical support inside the thermal oven (from Fig. 3.9)

Figure 3.20: The current cycling profile of the OLEDWorks experimental design

and help the PID maintain a constant temperature in the oven.

3.3.3 Conclusion on OLED experiments

After having designed the OLEDs experimental aging campaign, and selected the measurements to be performed frequently during the aging, the data are then collected in a regular way, to be treated in the following chapters. In order to generalize the degradation modeling approach proposed in this thesis, another type of electrical components will also be aged under thermal and electrical stress. This type consists in aging an insulation system, which will be presented below.

3.4 Insulators experiments

In the LAPLACE laboratory, the insulation of twisted pairs of enamelled copper wires has been studied to test its dielectric life [210]. Twisted pairs are used for the stator and rotor windings of low voltage electrical machines. Dr. Szczepanski has developed methods to test the insulation system of low voltage motors operating under partial discharges. Organic polymer enamelled twisted wires are tested under accelerated aging using three stress factors (temperature, voltage and frequency). The study of insulation life is based on destructive testing: a high voltage above the partial discharge inception voltage is applied to the twisted pair for a period of time until the insulation and electrical current break down. Insulation life is then modeled at high stress levels, but extrapolated to low stress levels below the PDIV using a statistical Weibull distribution.

Dr. Salameh also studied the life of twisted pairs of various enameled wires, using the same destructive accelerated aging under the same stresses [182]. The objective of the thesis was to study the effects of applied stresses and their interaction on the overall life of the insulation. The lifespan modeling used parametric methods such as design of experiments and non-parametric methods such as regression trees.

However, the main concern of this thesis is the aging of twisted pair insulation and the modeling

of its degradation. Therefore, no destructive methods must be used to test the dielectric characteristics of the insulation. In other words, aging should not be performed at high voltages, where partial discharges already exist, but below the PDIV level. This is relatively a new approach, as only one research has corresponded to this idea by following the evolution of the PDIV of twisted pairs in a similar way [186]. In fact, they followed the evolution of the PDIV and the capacitance of a 210 °C thermal class twisted copper wires with different diameter size at 280 °C following the standard EN 60172. They were able to prove that indeed PDIV changes with time, nevertheless, no modeling was done, and no correlation with capacitance evolution is made.

In the following, the aging of twisted pairs insulation experiment will be presented in the following order:

- Production of the twisted pairs
- The aging test bench
- The measurement procedure
- Experimental plan

3.4.1 Production of the twisted pairs

Enamelled copper wires from Acebsa were used for the twisted pairs (see Appendix B.2). Their specifications are presented in Tab. 3.5.

Table 3.5: Specification of the enamelled copper wires used for the twisted pairs

name	IBERFIL C
thermal class	H 210
Base coat	Polyamide-imide
Temperature index 20 000 h	210
Breakdown voltage	180 V µm^{-1}
Diameter	0.5 mm

The manufacture of twisted pairs of enamelled copper wire is based on the European standard NF EN 60851-5:2008-12.

- A piece of 40 cm wire is cut
- Removing the enamelling from 5 mm of each end
- Cleaning the wire with ethanol, to remove sanded insulation particles
- Hang the wire by both ends to a rotating device, and hold it at a load of 3.4 N
- Twisting the wire for 16 complete turns
- Cut the middle of the twisted wire to create two wires of 20 cm each, twisted together.

After the twisted pairs are manufactured, the bare terminals of the twisted pair are attached to a banana plug. The twisted pair is cleaned one last time with ethanol to remove any unwanted residue that may be attached to it and which could affect its characteristics. Fig. 3.21 represents the equipment used to make these twisted pairs. Fig. 3.22 represents the twisted pairs manufactured, before their aging and inside a thermal oven.

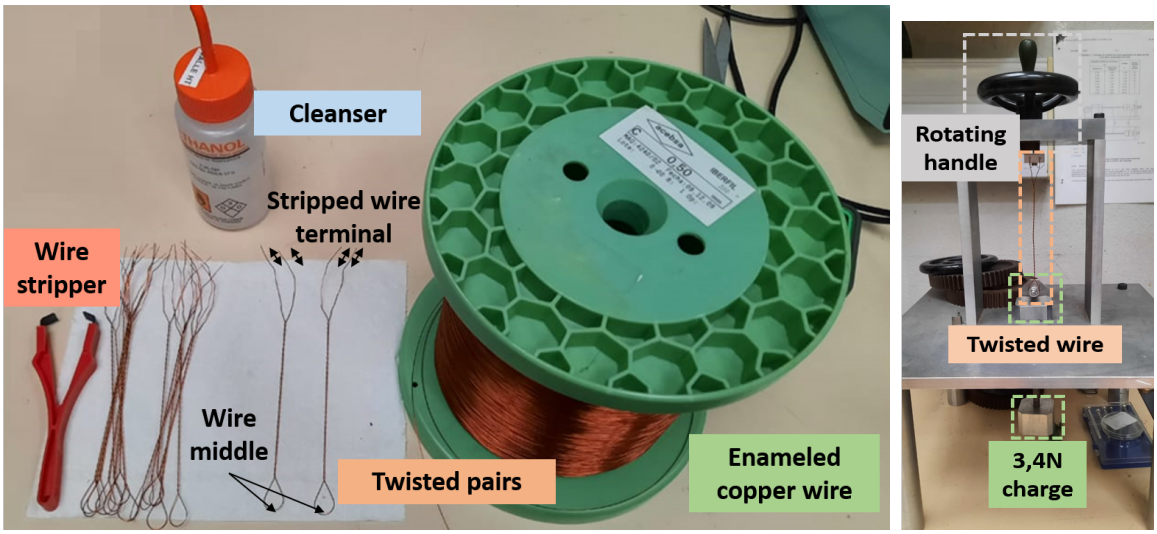

(a) The equipment used

(b) The rotating device

Figure 3.21: Fabrication of twisted pairs of enamelled copper wires

(a)

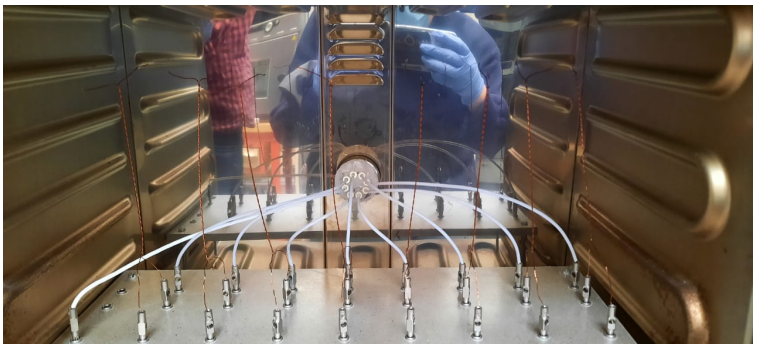

(b) Eight twisted pairs inside ovens

Figure 3.22: Photos of the twisted pairs

3.4.2 Test bench

A test bench based on the application of thermal and electrical stress to twisted pairs, already existing in the LAPLACE laboratory, is used (see Fig. 3.23). It consists of a thermal oven connected to an electrical system capable of generating pulsed high voltage signals. The signal is produced by alternating two voltage levels using two power switches controlled by a waveform generator to regulate the frequency and waveform of the overall signal.

In this thesis, to realize the electric voltage square wave, the two voltage sources generate the

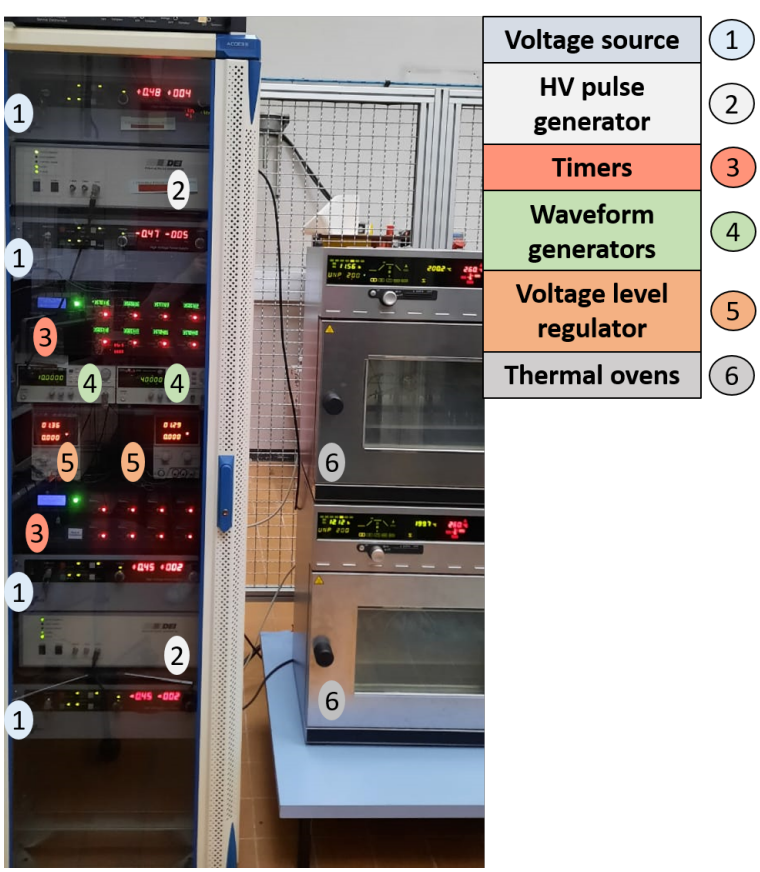

(a)

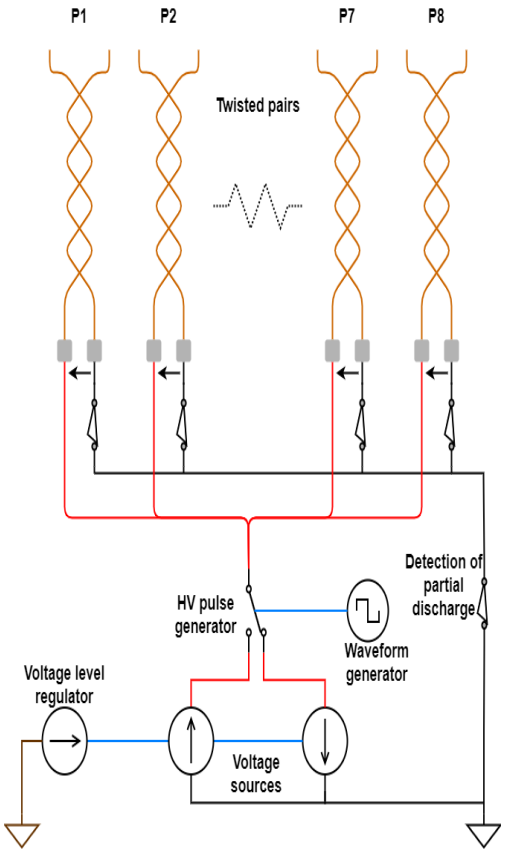

(b) Drawing of the electrical wiring of one oven

Figure 3.23: Aging test bench of twisted pairs under thermal and electrical stress

same levels but with different polarity. The HV pulse generator will then alternate between the two signals according to the frequency defined by the waveform generator. A low voltage source is connected to the HV voltage sources, in order to change both voltage levels at the same time. This is a necessary option for the periodic partial discharge initiation voltage measurements that will be performed later. Sensors are placed in series with each twisted pair to detect any current leakage due to wire insulation failure that could cause a short circuit and damage the power sources. Finally, three thermal chambers of a maximum temperature of 250 °C, that can contain up to 8 twisted pairs, and can be regulated to apply constant or dynamic thermal stress are used.

3.4.3 Measurement procedure

The voltage at the beginning of partial discharge is a very delicate characteristic to measure. First of all, the discharge current for the type of materials used is very low (less than 1 mA). Secondly, the discharge current is a high-frequency phenomenon that can be confused with other parasitic signals from measuring devices, cabling or surrounding noise. Also, the measurement of the partial discharge inception voltage must be extremely fast so as not to add another aging factor, high voltage, which would play a huge role in insulation failure. As twisted pairs are aged by the effect of partial discharge, accidental failures due to high voltage are not desired. Thus the criteria for measuring the PDIV would be

- High sensitivity and high bandwidth current probe

- High bandwidth oscilloscope

- Fast sampling rate and fast FFT computing time

Partial discharges can add fluctuation to the measured transient current, increase the noise of the electrical discharges, and produce ozone, resulting in a change in odor[145]. These three indicators can certainly confirm the presence of partial discharges, but they are not as accurate in detecting the first occurrence of partial discharges.

The ideal solution after several trial and error with several current probes, oscillators and cables was to measure the current that flows in the ground wire. The current is measured by two current probes from Pearson electronics called current monitor model 4100 that has a $1\,\mathrm{V\,A^{-1}}$ sensitivity, maximum RMS current of 5 A, a 10 ns usable rise time and a high frequency 3 decibel point of 35 MHz. The second probe is always from Pearson Electronics but has higher bandwidth of 250 MHz, a $1\,\mathrm{V\,A^{-1}}$ sensitivity, maximum RMS current of 10 A, a 1.5 ns usable rise time (see Appendix C.3). The measurement is visualized and analysed using a digital phosphor oscilloscope MSO 5204 from Tektronix that has a 2GHz bandwidth and maximum of 10 GSample/s sampling rate.

The transient response of the current is then analyzed with each rise of the square wave signal using a fast Fourier transform (FFT), which generates a frequency spectrum related to the measured current. In order to detect the first partial discharges, one twisted pair at a time is supplied with a low voltage level, which is then slowly increased in 3.3 V steps using the voltage regulator. The FFT of the measured transient current remains the same until the appearance of the partial discharge, where the overall amplitude of the high frequencies changes drastically, and precisely at frequencies between 40 MHz and 50 MHz. The reason for this change in the FFT measurement may be the overall circuit of the bench which increases the currents around these frequencies by a form of resonance.

Most of the time, the amplitude around these frequency levels increases a lot, but in some cases, this frequency does not change for some random reason. Nevertheless, the spectrum still changes somehow at the PDIV, because in some cases where the 40 to 50 MHz amplitude does not change, the spectrum still fluctuates greatly after the PDIV voltage level is reached. Therefore, the FFT spectrum at very low voltage level is saved, and then when the PDIV is detected, the voltage level at the twisted pair sides and that of the voltage level regulator are noted, and the FFT spectrum is saved. The PDIV would then be the first voltage applied to the twisted pairs that changes the shape of the leakage current FFT spectrum.

Fig. 3.24 presents the current and FFT spectrum measured by a Pearson 4100 of a twisted pair, which is placed in a thermal oven at 150 °C for 24 hours without applied electrical stress. The blue curves of Fig. 3.24 presents the leakage current and its FFT spectrum of the twisted pairs at a voltage square signal of 310 V amplitude and 4 kHz was applied. There is no partial discharge under these conditions, but when the amplitude of the voltage is gradually increased to 570 V (± 3 V) (the red curves), the current signal starts to fluctuate. Additionally, the spectrum around 50 MHz shows a very obvious increase in level, indicating the occurrence of a partial discharge. In this case, the partial discharge inception voltage is 570 V. The same results are obtained with the wider bandwidth oscilloscope, but with more noise. Still, for more precision, the current will be measured by the two oscilloscopes in order to have the right inception voltage which causes the partial discharge.

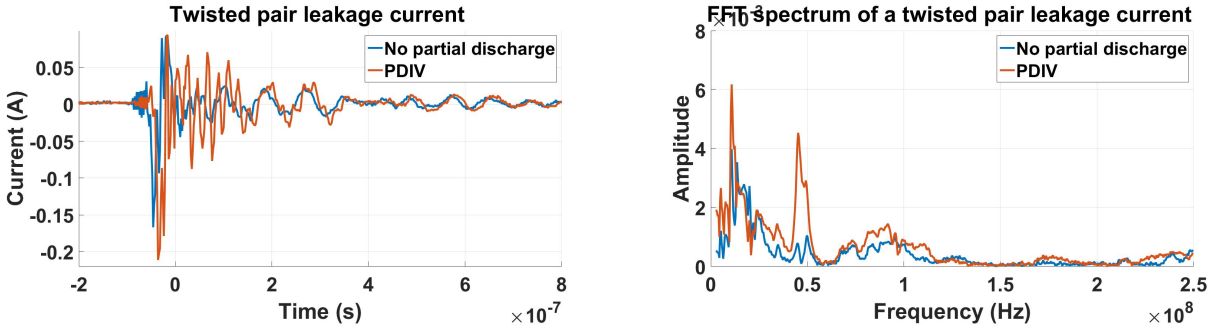

(a) Current (b) FFT spectrum

Figure 3.24: Electrical characterization of a twisted pair before and after a partial discharge

3.4.4 Experimental conditions

The aging factors that were chosen for this experiment are similar to the factors used for destructive methods in previous studies [210]. The stress factors are voltage, frequency, and temperature, as these are the most common and influential factors listed in the literature. The main objective of this experimental campaign is to follow the aging of the twisted pair insulation. To achieve this goal, non-destructive methods must be used, where low levels of stress are applied. Low stress levels are a combination of stress factors that place the insulating material below its PDIV. Note that for high stress levels, insulation breakdown occurs within minutes or at most hours, which would not allow periodic measurement of the dielectric characteristic.

On the other hand, if low stress levels are applied, aging will take years to reach breakdown voltage. It is then necessary to establish a compromise between aging below PDIV levels and accelerated aging, keeping in mind that the experiments must be performed in a limited time of 6 months maximum. The experimental conditions that were tested are presented in Fig. 3.25.

The first strategy used, just to have a good understanding of the evolution of PDIV, was to test the runs from 1 to 3 from the experimental plan of Fig. 3.25. For each run, num8 twisted pairs were stressed at three temperatures below the thermal class of copper wire (that is 210 °C) including ambient temperature. Besides the thermal stress, a low voltage level below the minimum measured PDIV value of the copper wires and a 4 kHz frequency were applied. These runs were tested for 1000 h, and then stopped, as no breakdown happened, to allow further experiments.

New runs were then tested at high temperature and voltage levels 500 V level and alternating between 4 kHz and 10 kHz frequency. The runs were numbered from 4 to 9 from the experimental plan of Fig. 3.25. The six runs were conducted in two batches, where the first batch at high temperature levels failed immediately or after a few hours at most. The solution for the second batch was to reduce the temperature level to see if it was thermal stress that caused this failure, but a rapid failure also occurred.

Since the high voltage caused the breakdown, the next runs from number 10 to 12 were subjected to medium voltage and temperature stresses, but were shut down after one month because no failure occurred.

Finally, runs from number 13 and more are tested at high temperature levels, above thermal class, and at low and moderate voltage levels. Breakdowns in these runs occurred after several weeks of testing, which gives a good censored data that is useful in the modelling later on. Therefore, a

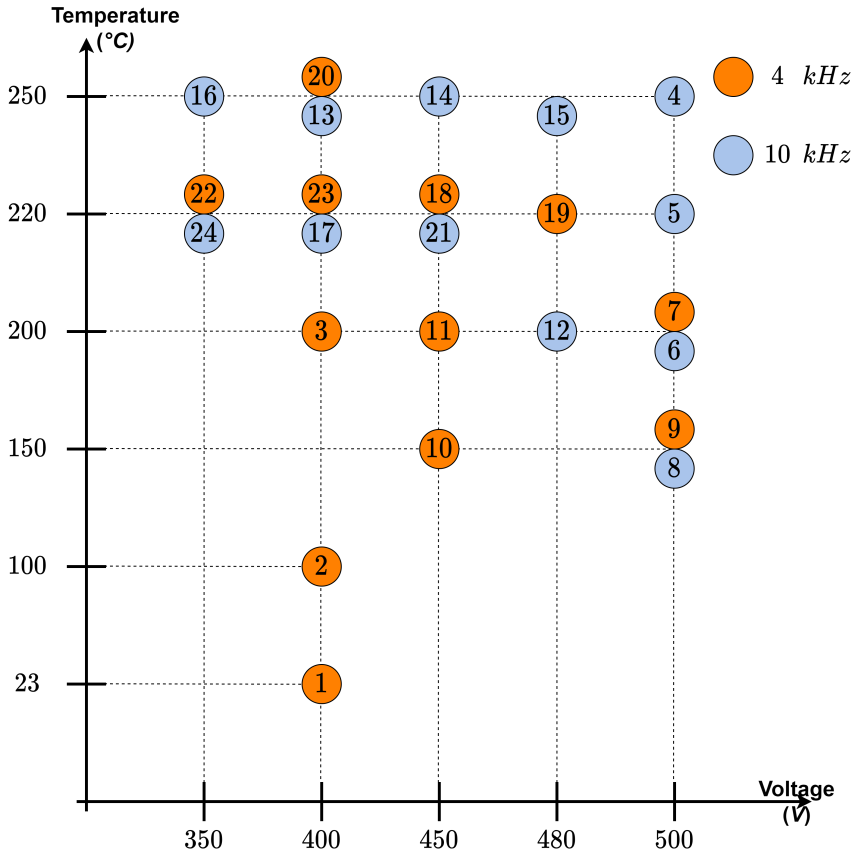

Figure 3.25: The experimental aging conditions for the twisted pairs insulation

three-factor, two-level factorial design is designed by considering two temperature levels of 220 °C and 250 °C, two voltage levels 400 V and 450 V and two frequency levels 4 kHz and 10 kHz.

In order to be able to compare different factorial designs, experiments at 350 V and at different temperature and frequency levels are also tested. Note that due to time constraints, it was not possible to perform full factorial designs, and thus only experiments of fractional factorial designs are be conducted.

3.5 Conclusion

This chapter presented the design of experiments technique, according to different steps; the first one is to define an objective which is the optimization of the lifetime by modeling the effect of stress factors on the degradation rate of components. The second step was to develop a strategy based on experimental designs such as factorial designs and response surface methodology. Such strategies allow for the optimization of the cost of experiments by performing experiments on multiple stress factors at once. The third step was to create a plan to perform the experimental design, which consists of optimizing the duration of the experiment and accurately selecting the inspection times, etc. This step is necessary to have a controlled environment for the thesis, which eliminates any source of randomness and ensures clean and unbiased data.

The last step was to implement the experiments; In this step, two electrical components were tested separately. The first component was the organic light emitting diode, where an experimental campaign performed by previous studies using different industrial OLED panels was presented. This campaign was used as a guideline for the campaign done in this thesis, where two objectives were sought: the first one was to estimate the lifetime of OLEDs by measuring the time it takes for its luminance to decrease to a certain level. The second objective was to understand the physical mechanisms behind the luminance degradation, by performing impedance spectroscopy and electrical characterization.

On this basis, the main objective of this thesis, would be to model the degradation of OLEDs, under constant and cyclic, thermal and electrical stress factors. For that, the test bench used for this experimental campaign was presented. Moreover, the degradation of OLEDs can be modeled by following the degradation of their luminance or by measuring some electrical characteristics. Other measurements were also chosen to obtain additional information, which could be used for other studies, such as the colorimetric analysis of OLEDs [27].

Lastly, the strategies chosen for this experimental design were a combination of several factorial and response surface designs, in addition to some randomized experiments, which could be used to validate the modeling procedure. The experiments are performed, and the timeline of the experiments will be presented in the next chapter.

As for the second component, it consisted of twisted pairs of enamelled copper wires used for low-voltage applications. The objective of this experimental campaign was to model the degradation of the insulation under temperature, frequency and voltage. Therefore, a test bench providing these stress factors is presented. This idea of modeling the degradation is new, as no previous measurements have been performed periodically. Therefore, the objective of the insulator experiments is to measure the partial discharge initiation voltage (PDIV) of twisted pairs periodically over time. Thus, the PDIV measurement procedure used in this thesis is presented. Lastly, due to time constraints, the strategy is based solely on factorial designs with some additional experiments to validate the modeling procedure.

Finally, the data collected during these experimental campaigns are processed and analyzed in the following chapters for modeling degradation without stress factors (Chapter 4), and with stress factors (Chapter 5).

Chapter 4

Degradation modeling methods without covariates, with application to OLEDs and machine insulators

Chapter 5

Degradation modeling methods with covariates, with application to OLEDs and machine insulators

Contents

Conclusion and outlook

Overall conclusion

The work carried out during this thesis has demonstrated an effective method for assessing the degradation of electrical components. The objective of the thesis was to model the degradation of electrical components under multiple stress factors in order to estimate their lifetime. The electrical components used as an example in this thesis were large area OLED panels which have many advantages in the lighting industry, but are sensitive to many factors due to their organic characteristic. The second electrical component used is the twisted pair of enameled copper wires, which is concerned with the insulation of low-voltage electrical machines powered by inverters that are subject to several stress factors. The reliability of the insulation has always been evaluated by destructive methods. This thesis proposed a promising new methodology to evaluate insulation degradation by monitoring their partial discharge.

A **state of the art** concerning the study of reliability, and more particularly failure analysis was presented. Since failure often occurs after degradation, the study of degradation was chosen to assess reliability. In the study of degradation, the model learning approach was chosen because it requires a good understanding of the degradation mechanisms. In general, the degradation mechanisms in electrical engineering are fatigue, wear, variation of electrical parameters, etc. They are mainly caused by electrical, thermal, mechanical and climatic conditions. The model-based approach required the definition of some test methods to identify the result to be modeled. Non-destructive methods of accelerated degradation were then selected, for measurements to be performed periodically.

In the **second chapter**, different physics-based models were presented. Physics-based models require the identification of the main reaction causing the degradation, which is not always possible, especially for industrial components. Therefore, empirical models have also been presented that focus on modeling degradation trajectories as a function of time without any stress factors. To incorporate stress factors into these empirical models, semi-empirical models have been proposed. These are based on measured data, which require some estimation. Therefore, estimation methods based on linear and nonlinear deterministic regression have been presented. Another data-based approach for modeling degradation, which does not require a model, was briefly presented. This approach is based on black-box models that are not useful, if a degradation model is sought, for lifetime estimation. Another type of estimation method based on a stochastic approach was briefly presented. It is useful for modeling component degradation for global systems, where there is a lot of randomness. However, this is not the case in this research. Finally, an estimation method based on dynamic covariates is modeled, where it was found that no serious dynamic modeling has been done for OLEDs.

The **third chapter** was to design the experimental procedure to be followed for aging of OLED panels under constant and cyclic thermal and electrical stressors. It was then decided to monitor the degradation of OLEDs by performing optical and electrical measurements such as luminance measurement and impedance spectroscopy. The experimental design of this campaign tested different experimental design strategies, such as factorial designs or response surface methodology. It

allocated some experiments for validation sets that were used to evaluate the performance of the models . Similarly, the experimental procedure for aging twisted pairs of enameled copper wires was also detailed, from specimen fabrication to experimental design. As this type of experiment is new, several experiments were performed before the actual aging campaign in order to define the stress values that will be used for aging. Therefore, the experimental design consisted only of split factorial designs as well as a few experiments that could be used for the validation set.

The **fourth chapter** studied the modeling of the degradation of electrical components without using stress factors. This was done mainly to identify the degradation trajectories of each of the tested components (OLEDs and insulators). For OLEDs, several estimation methods were applied, for both linear and exponential decay models. These estimation methods were confronted with several problems specific to certain experiments, such as the variable number of observations per specimen, or abrupt changes, etc. Based on the model selection criteria, it was found that ordinary linear regression was the best estimation method to model the luminance decay of OLEDWorks OLED panels. Similarly, two nonlinear models, were chosen to model the evolution of the insulator PDIV. Several estimation methods were applied to identify the parameters of the nonlinear PDIV evolution. Some methods penalized outliers while others included the few stress factor observations in the decay models. Based on the model selection criteria, it was found that the ordinary power model estimate was the most likely to illustrate the PDIV evolution.

In the **last chapter**, the selected models for OLEDs and insulators were used to estimate the effect of stress factors on the degradation rate of the electrical component in question. Indeed, few previous studies have included multiple constant and dynamic stress factors in the lifetime or degradation rate estimation, which was one of the objectives of this thesis. For OLEDWorks, only the degradation slope parameters found by ordinary linear regression were used. The intercept was shown to follow a normal distribution, which is not related to stressors, as it represents the initial state of the OLEDs. The decay slope was modeled with each stressor alone to identify the relationship it has with these stressors. It was found that the current has a non-linear relationship with the decay rate (which can be attributed to Eyring's physical model). The relationship between decay slope and temperature and the categorical factor, cycling, has not been identified however, due to lack of experiments. The identified relationship is used to normalize the current into a covariate. The temperature and cycling covariates were normalized using a linear relationship due to lack of experimental data.

The decay slope was modeled with these covariates and their interaction using several full and fractional factorial designs. The effectiveness of the estimates of these models was calculated by predicting the lifetime of the experiments in the validation set. It was found that the smaller the current range for the training set, the more efficient the effect estimates. This is due to the fact that no quadratic current covariate was incorporated, which assumes that the decay current-rate relationship is linear (even with normalization).

The quadratic current covariate was incorporated using response surface designs for the training set. This is also a novelty, since in the response surface planes there is a categorical factor that is cycling. The efficiency of the RSM estimates was also calculated by predicting the lifetime of the experiments in the validation set. It was found that the wider the current range of the training set, the more effective the prediction. Overall, the RSM models performed better in prediction than the factorial models, primarily because they include a quadratic term for the current. This quadratic term was attributed to Joule losses that increase with OLED degradation, as seen in an impedance analysis.

On the other hand, it was found that cycling had a positive effect on the OLED decay rate, indicating that cycling reduces the self-heating of the panel, which in turn is caused by Joule losses. Temperature and current always had a negative impact on the luminance decay rate, which confirms what has been found in the literature.

As with the insulators, the parameters of the power and exponential models that are responsible for the decay rate were identified. The relationships between decay rates and stress factors separately, however, have not been identified due to lack of experiments. Therefore, the factors are normalized using a linear relationship for voltage and frequency (based on Eyring's law), and an inverse relationship for temperature (based on Arrhenius' law). The power and exponential decay rates were modeled with the covariates using two fractional factorial designs for the training set. These were the only designs possible in this experimental campaign due to time constraints. The effectiveness of these models was then calculated using a mutual validation set for both training sets. It consisted of predicting the evolution of the decay and checking if it was within the confidence interval of the measured IVDP. It was found that the power decay rate could not really predict the evolution of the insulator PDIV for the validation experiments. This is in contradiction with what was found in the previous chapter, which indicates that modeling the decay trajectory by experiment without covariates tends to over-fit the decay data. On the other hand, the estimates of the effects of the two training sets for the exponential models were contradictory, which could not be attributed to physical significance. The training set with the lower voltage range was more effective, and the reason for this is that it estimated a positive effect for temperature. However, this has no physical explanation, and further experiments proving the relationship between temperature and decay rate are needed.

Perspectives

Finally, the study could not cover all aspects of degradation modeling, as this is a very broad area. However, it proved that the degradation methodology was valid for two of the electrical components. It would be interesting to test this methodology on other electrical components, which show more variation in degradation, for example, or which are part of a larger electrical system, etc.

In terms of prospects, since it was proven that the models tend to overfit if no stress covariates are included, it would be interesting to verify which of the linear and nonlinear models has the best prediction results for the OLEDWorks experimental design.

Another perspective would be to consider adding more covariates to the model to study the evolution of light inhomogeneity during aging of OLED panels. This can be done by adding the luminance measurements that were made at different locations on the light emitting surface.

The effect of dynamic cycling on OLED panels also needs to be studied in more detail, by changing the duty cycle or cycle time, etc. Its impact on aging indicators other than luminance, such as electrical impedance, should also be studied to link the degradation effect to the physical mechanisms involved.

Also, it was not possible to apply many statistical tests such as significant ANOVA estimation. It would be interesting to add more variation to the OLEDs decay patterns either by artificially introducing it or by increasing the number of specimens per experiment.

Furthermore, can the conclusion that all large area OLED panels exhibit linear decay also be drawn? The study of aging of other types of OLEDs could help generalize what is found in this PhD thesis.

With respect to insulators, the methodology proposed in this thesis is promising, but not complete. A relationship between each factor and the decay rate is required, hence the need for additional experiments at different stress levels. In addition, a threshold is still needed to define the level at which an insulator is highly likely to fail. This threshold requires further failure observations, which in turn require allowing the twisted pairs to age longer. In addition, it was not possible to increase the temperature above 250 °C, which extended the life of the insulators. Aging the insulators at excessive temperature could be an interesting prospect, as it could show higher indications of degradation.

Finally, the identification of the PDIV procedure could be improved by turning it into an automatic detection instead of a manual detection as it is currently.

Appendix A

Data

A.1 Descriptive statistics

Mean value The average value $\bar{x}$ of n observations observation in a sample, or the population mean μ is

$$\mu = \bar{x} = \frac{x_1, x_2, \ldots, x_n}{n} = \frac{\sum_{i=1}^{n} x_i}{n} \tag{A.1}$$

Median value The sample median $\tilde{x}$, the population median $\tilde{\mu}$, or the middle value of observations that are ordered from smallest to largest, is

$$\tilde{x} = \begin{cases} \left(\frac{n+1}{2}\right)^{th} \text{ ordered value,} & \text{if } n \text{ is odd} \\ \text{average of } \left(\frac{n}{2}\right)^{th} \text{ and } \left(\frac{n}{2}+1\right)^{th} \text{ ordered values} & \text{if } n \text{ is even} \end{cases} \tag{A.2}$$

Standard deviation and variance Sample variability can be measured by the sample range, which is the difference between the largest and smallest values in the sample. However, the range is not exactly representative to the variability of the system, as it does not take into account the dispersion of the value of other observations. The variability is then represented by the sum of squares of deviation from the mean, in order to equally represent the deviation to the left and right of the mean. The sample variance s^2, or population variance σ^2 is represented in Eq. A.3. The sample standard deviation is $s = \sqrt{s^2}$ and the population standard deviation is $\sigma = \sqrt{\sigma^2}$.

$$s^2 = \frac{\sum(x_i - \bar{x})^2}{n-1}, \sigma^2 = \sum_{i=1}^{N}(x_i - \mu)^2/N \tag{A.3}$$

Skewness The population may have a negatively or positively skewed distribution respectively where the observations are concentrated on the right or left side (Fig. A.1). The data are skewed when the population does not have a symmetric distribution, so the mean and median of the population are not equal.

Confidence interval The confidence interval (CI) is a method of checking for outliers when it surrounds the majority of the population. It is also used to check if an estimate fits the population, as its value must fall within the CI. It has a confidence level α that measures how reliable the interval is. The higher the level, the more likely it is that a value will fall within the range. In this sense, if the confidence level is high and the interval is narrow, the value of the variable is accurate, and vice versa, where there would be uncertainty about its value.

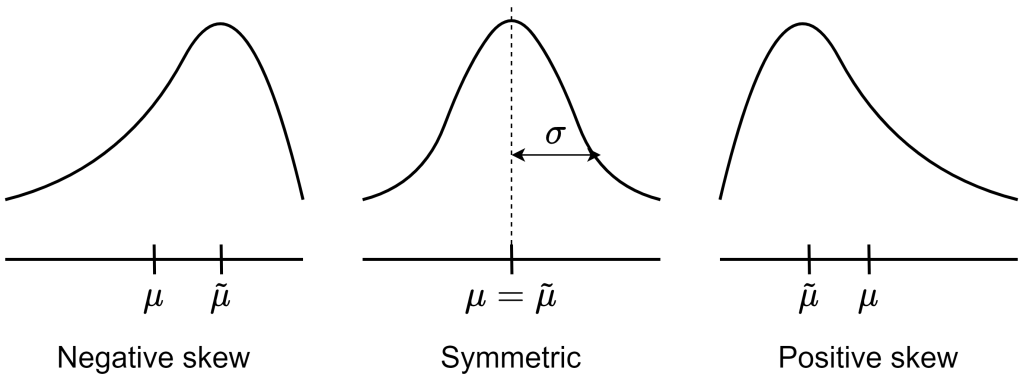

Figure A.1: Shapes of population distribution

When a population has a normal distribution, with a mean value μ and standard deviation $\sigma/\sqrt{n}$, the mean variable of a sample from this population would have a 95% confidence interval of $\left[-1.96\frac{\sigma}{\sqrt{n}}, 1.96\frac{\sigma}{\sqrt{n}}\right]$. $1.96 = z_{\alpha/2}$ is the value of the normal distribution with $\alpha = 0.95$ however, when a population does not follow a normal distribution, $z_{\alpha/2}$ is replaced by a t-critical value $t_{\alpha,v}$, where v is the number of degrees of freedom for Student's t-distribution . The α confidence interval of a sample with n observation is then

$$CI_\alpha = \left[-t_{\alpha/2,n-1}\frac{s}{\sqrt{n}}, t_{\alpha/2,n-1}\frac{s}{\sqrt{n}}\right] \tag{A.4}$$

Correlation A numerical summary of the relationship between measured variables is the Pearson product-moment correlation coefficient $r_{x,y}$ (Eq. A.5, where x and y are different variables). The range of r is between $-1 \leq r_{x,y} \leq +1$, and when it is positive or negative respectively, the variables are positively or negatively correlated. Independent variables have a zero value, or close to 0, and the higher the value, the stronger the correlation is.

$$r_{x,y} = \frac{\sum_{i=1}^{n}(x_i - \bar{x})(y_i - \bar{y})}{[\sum_{i=1}^{n}(x_i - \bar{x})^2 \sum_{i=1}^{n}(y_i - \bar{y})^2]^{1/2}} \tag{A.5}$$

A.2 Data cleaning

The basic steps of data cleaning are [5]

- Removal of duplicate or irrelevant observations. Duplication usually occurs when data from several data sets are combined, such as when a client's data are present twice ... Redundancy when one variable is derived from another is another kind of duplication, and is measured by the coefficient of correlation r: the higher the value, the stronger the relationship between the variables (Eq. A.5). Irrelevant observations are data that do not fit the problem at hand. For example, if the problem is to model the aging of white LEDs, the data for blue LEDs are irrelevant.

- Fixing structural errors, so that the data follow a certain naming convention, and the data analysis software can read them.

- Filtering out unwanted outliers, like when measuring the luminance of an LED and someone turned-on other external light sources, the value would be erroneous. This type of outliers can be removed, however, outliers do not mean that the data is incorrect, as they can be useful in understanding the problem, and checking the good model fit.

- Handling missing data because some algorithms do not accept missing values. An example of missing values is a lost measurement due to a malfunction of the measuring device, or necessary inspections that were not performed because of other constraints or simply lack of planning, etc. If the modelling methodology allows it, missing data can be replaced by its estimation, assuming that data are consistent. Another solution is to eliminate all the observations that have missing values but it will be a waist of resources.

  This is a case that has already occurred in this thesis, where observations from the first experiments were lost due to the change of measurement devices. Two operations have been made, where the first operation is to remove all performance data made by the old measurement device as it is considered as inefficient. However, an initial value was needed for all the degradation methodology, thus the second operation consisted of estimating the initial value based on measurements of new components made by the new measurement device. This estimation assumes that all components have no prior degradation before aging, and that the initial data of all components must follow a normal distribution around a the mean value of the new initial measurements.

A.3 Normalization

The main three methods of normalization are [87]:

Min-max normalization consists of performing a linear transformation on the original data. If a variable x with a range of $[x_{min}, x_{max}]$, needs to be resized to a lower range $[x'_{min}, x'_{max}]$, to be coordinated with the ranges of the other variables, the transformed variable x' would be

$$x' = \frac{x - x_{min}}{x_{max} - x_{min}}(x'_{max} - x'_{min}) + x'_{min} \tag{A.6}$$

Z-score normalization is based on the concept zero-mean normalization, where the variable is normalized based on the population mean and standard deviation. It is used when data have a pronounced dispersion and the min-max normalization would consider outliers. The process is called standardization and the normalized value x' would be

$$x' = \frac{x - \mu}{\sigma} \tag{A.7}$$

Decimal scaling consists in reducing the size of the variables. For example, an aging process may last for several months, and the time variable is represented in hours. In this case, it is better to consider the $khours$ unit and reduce the size of time following the equation Eq. A.8, where j is the smallest integer such that $x'_{max} < 1$.

$$x' = \frac{x}{10^j} \tag{A.8}$$

A.4 Anderson-Darling test for goodness of fit

The Anderson-Darling test for goodness of fit is a non-parametric test that verify if a data set has a specific distribution, like a normal or exponential distribution.

The demonstration of the Anderson-Darling test is based on the electronic engineering statistics handbook [1]. The Anderson-Darling test is defined as:

- The null hypothesis H_0: The data follow a specified distribution.

- The alternative hypothesis H_a: The data do not follow the specified distribution
- The test statistic:

$$A^2 = -N - S \tag{A.9}$$

where

$$S = \sum_{i=1}^{N} \frac{(2i-1)}{N} [lnF(Y_i) + ln(1 - F(Y_{N+1-i}] \tag{A.10}$$

N is the number of data samples, Y_i is the ordered samples from smallest to largest, and F is the cumulative distribution function of the tested distribution

- The significance level is α
- The critical values at the significance level α depend on the specific distribution that is tested. The hypothesis that the distribution is of a specific form is rejected if the test statistic A^2 is greater than the critical value.

The critical value can be found using the tables found in [203], or in the code provided by [147]. The critical value of the AD test for normal distribution is presented in Fig.A.2.

Case	n	15%	10%	5%	2.5%	1%
0	≥ 5	1.621	1.933	2.492	3.070	3.878
1			0.908	1.105	1.304	1.573
2	≥ 5		1.760	2.323	2.904	3.690
3	10	0.514	0.578	0.683	0.779	0.926
	20	0.528	0.591	0.704	0.815	0.969
	50	0.546	0.616	0.735	0.861	1.021
	100	0.559	0.631	0.754	0.884	1.047
	∞	0.576	0.656	0.787	0.918	1.092

Figure A.2: The critical value of the AD test for normal distribution, at different significance level (from Wikipedia)

A.5 Model selection criteria

The model selection criteria are parametric tests to verify the goodness of fit of the data to a certain model.

R-squared and adjusted R-squared The R-square (R^2) is the simplest criterion to check the goodness of fit of mainly a regression model, where it is between 0 and 1, with 1 being the best fitting value. Mathematically, it is called the coefficient of determination or Pearson's coefficient and its definition is *"the proportion of the variation in the dependent variable that is predictable from the independent variable(s)"* [63].

R-squared is then given by Eq. A.11 where

$$R^2 = 1 - \frac{SSE}{SST} \tag{A.11}$$

- $SSE = \sum(y_i - \hat{y}_i)^2$ is the error sum of squares, or the residual sum of squares; y_i is the i^{th} data measured, and $\hat{y}_i$ is its estimated value based on the fitted model.
- $SST = \sum(y_i - \bar{y}_i)^2$ is the total sum of squares, or the total amount of variation observed; $\bar{y}_i$ is the mean value of all observation data $y_{1\to n}$
- The ratio SSE/SST is the proportion of total variation that cannot be explained by the fitting; Fig. A.3 represents the graphical error versus the prediction (for the SSE) and versus the total mean of data (for the SST).

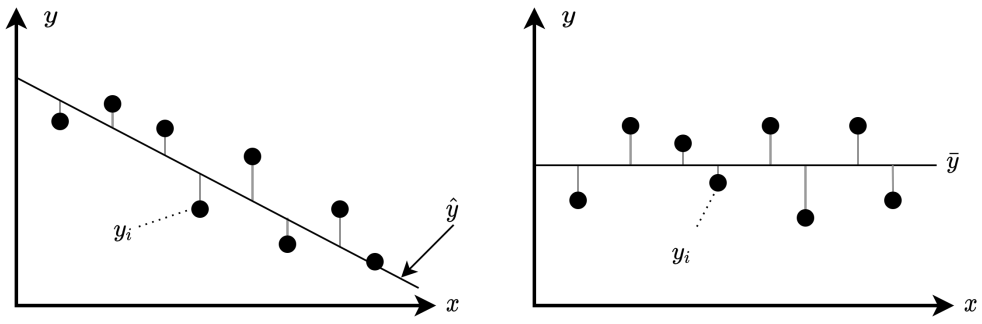

(a) SSE (b) SST

Figure A.3: Graphical representation of sum of squared deviations from the prediction (SSE) and from the mean value of data (SST)

The major drawback of R^2 is that its value increases with each added factor even if the factor is not as significant, or correlated to the outcome being modelled. When the model has a number of parameters $p \geq 2$, it is preferable to use the adjusted R-squared, because it is less sensitive to the number of parameters, and thus, models of different numbers of parameters can be compared using the R^2_{adj}. The R^2_{adj} follows the same concept of R^2, but it can take negative values! The adjusted coefficient of multiple determination (R^2_{adj}) is given by Eq. A.12, where n is the total number of data observations and k is the number of parameters in the model.

$$R^2_{adj} = 1 - \frac{n-1}{n-(k+1)} \cdot \frac{SSE}{SST} \tag{A.12}$$

R^2 is not a suitable model selection criterion for multivariate data, where a model has multiple predictors k. Instead of identifying a general R^2 that would consider all predictors, it is better to identify the model with the optimal number of predictors *i.e.* identify the smallest number k that would give an R^2_k that is nearly as large as the general R^2.

Rationale for the third criterion C_k A criterion widely used by data analyst called *"the rationale for the third criterion C_k"* can be applied also for multivariate data. Eq. A.13 represents the formula of C_k where SSE_k is the error sum of squares for k predictors and n observations; $s^2 = \hat{\sigma}^2 = \hat{V}(\epsilon)$ is the variance estimate of the error ϵ based on the model that includes all predictors for which data is available. The concept is based on normalizing SSE_k, in order to compare models with different values of k, and since σ^2 is not known, its estimate is used. However, this criterion requires a tedious computational work because, normally, a combination of predictors must be tested to check the best model, and it is recommended to be applied when $k \leq 5$.

$$C_k = \frac{SSE_k}{s^2} + 2(k+1) - n \tag{A.13}$$

Analysis of Variance For multivariate data, when graphical representation is not available, a formal test of model utility, based on the analysis of variance and Fisher test, called ANOVA, is most appropriate, because the value of R^2 can be deceptive as it is strongly influenced by the number of predictors.

The basic F-test is based on the null hypothesis H_0, which assumes that there is no useful relationship between the data and their k predictors. To test the null hypothesis, the statistical value of the test f is compared to a particular Fisher distribution value $F_{\alpha,k,n-(k+1)}$, where k is the number of variables or predictors, n is the number of observation, α is the significance level; if f is higher than the Fisher critical value (see Fig. A.5), the null hypothesis is rejected and the variable or predictor is useful to the model (Fig. A.4). The value of the statistical test is given by Eq. A.14, where R^2 is the coefficient of determination of the model, $SSR = SST - SSE$ is the regression sum of squares.

$$f = \frac{R^2/k}{(1-R^2)/[n-(k+1)]} = \frac{SSR/k}{SSE/[n-(k+1)]} \tag{A.14}$$

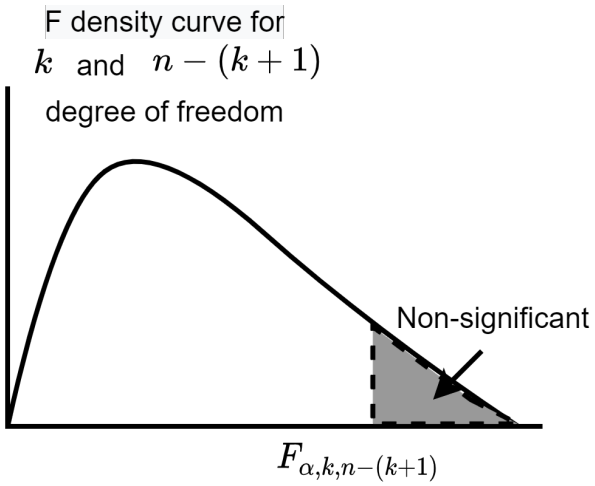

Figure A.4: F density curve and the critical value for F-tests

ANOVA is an advanced F-test, which can be either single-factor or two-factors test. The single-factor test consists of comparing the means of several n populations, so that the null hypothesis is that all means are equal ($H_0 : \mu_1 = \mu_2 = \ldots = \mu_n$), and the relevant hypotheses are many, depending on the number of populations to be compared, but they claim that at least two of the means are different (for example, $H_a = \mu 1 \neq \mu 2 = \mu_3 = \ldots = \mu_n$). The ANOVA method is well presented in Devore's book, chapter 10 [63].

ANOVA can be useful for checking whether samples tested under different conditions have different values or not. It is also useful for checking the significance of predictors, and finally for model selection by comparing their f-value.

The ANOVA will deal with a data set consisting of I populations, with J observations for each population. $x_{i,j}$ would then be the observed value of the j^{th} measurement for the i^{th} population. The statistical test for the single-factor ANOVA is presented in Eq. A.15, where

$$F = \frac{MST_r}{MSE} \tag{A.15}$$

- $MST_r = \frac{J}{I-1}\sum_i(\bar{X}_i - \bar{X})^2$ is the mean square for treatments
  - $\bar{X}_i = \frac{\sum_{j=1}^{J} X_{ij}}{J}$ is the individual population mean.
  - $\bar{X} = \frac{\sum_{i=1}^{I}\sum_{j=1}^{J} X_ij}{IJ}$ is the average of all $I \times J$ observations
- $MSE = \frac{\sum_{i=1}^{I} S_i^2}{I}$ is the mean square for error
  - $S_i^2 = \frac{\sum_{j=1}^{J}(X_{ij}-\bar{X}_i)^2}{J-1}$ is the variance of the i^{th} population

The computation of the ANOVA is summarized in an *"ANOVA table"* (Tab. A.1). The comparison between populations or models is based on the highest f-value. To check whether the effect of the predictors is significant or not, Tukey's method consists in comparing the f-value to a Student's t-test distribution $Q_{\alpha,m,v}$ (similar to $F_{\alpha,k,n-(k+1)}$) where m and v are respectively the degrees of freedom of the numerator and denominator of Eq. A.15.

Table A.1: ANOVA table

Source of variation	**Degree of Freedom**	**Sum of Squares**	**Mean Square**	**f**
Treatments	$I-1$	$SSTr$	$MSTr = SSTr/(I-1)$	$MSTr/MSE$
Error	$I(J-1)$	SSE	$MSE = SSE/[I(J-1)]$	
Total	$IJ-1$	SST		

A two factor ANOVA is an extension of the single-factor method, where several factors are of simultaneous interest. Two-factor ANOVA will study the combination of such factors, and tests which combination is significant. It is mainly applied to design of experiments where the model generally consists of p factors having 2 levels and the interactions between those factors. More details about the design of experiments are found in Chapter 3.

0.95 quantiles for F distributions ($f_{0.05,d_1,d_2}$ values)

This table gives $f_{0.05,d_1,d_2}$ values for different (d_1, d_2)'s, where f_{a,d_1,d_2} is defined such that $P(F(d_1,d_2) > f_{a,d_1,d_2}) = a$ and $F(d_1,d_2)$ is the F distribution with (d_1,d_2) degrees of freedom.

	d_1 *(degrees of freedom for the numerator)*															
	1	2	3	4	5	6	7	8	9	10	12	15	20	24	30	40
1	161	200	216	225	230	234	237	239	241	242	244	246	248	249	250	251
2	18.5	19.0	19.2	19.2	19.3	19.3	19.4	19.4	19.4	19.4	19.4	19.4	19.4	19.5	19.5	19.5
3	10.1	9.55	9.28	9.12	9.01	8.94	8.89	8.85	8.81	8.79	8.74	8.70	8.66	8.64	8.62	8.59
4	7.71	6.94	6.59	6.39	6.26	6.16	6.09	6.04	6.00	5.96	5.91	5.86	5.80	5.77	5.75	5.72
5	6.61	5.79	5.41	5.19	5.05	4.95	4.88	4.82	4.77	4.74	4.68	4.62	4.56	4.53	4.50	4.46
6	5.99	5.14	4.76	4.53	4.39	4.28	4.21	4.15	4.10	4.06	4.00	3.94	3.87	3.84	3.81	3.77
7	5.59	4.74	4.35	4.12	3.97	3.87	3.79	3.73	3.68	3.64	3.57	3.51	3.44	3.41	3.38	3.34
8	5.32	4.46	4.07	3.84	3.69	3.58	3.50	3.44	3.39	3.35	3.28	3.22	3.15	3.12	3.08	3.04
9	5.12	4.26	3.86	3.63	3.48	3.37	3.29	3.23	3.18	3.14	3.07	3.01	2.94	2.90	2.86	2.83
10	4.96	4.10	3.71	3.48	3.33	3.22	3.14	3.07	3.02	2.98	2.91	2.85	2.77	2.74	2.70	2.66
11	4.84	3.98	3.59	3.36	3.20	3.09	3.01	2.95	2.90	2.85	2.79	2.72	2.65	2.61	2.57	2.53
12	4.75	3.89	3.49	3.26	3.11	3.00	2.91	2.85	2.80	2.75	2.69	2.62	2.54	2.51	2.47	2.43
13	4.67	3.81	3.41	3.18	3.03	2.92	2.83	2.77	2.71	2.67	2.60	2.53	2.46	2.42	2.38	2.34
14	4.60	3.74	3.34	3.11	2.96	2.85	2.76	2.70	2.65	2.60	2.53	2.46	2.39	2.35	2.31	2.27
15	4.54	3.68	3.29	3.06	2.90	2.79	2.71	2.64	2.59	2.54	2.48	2.40	2.33	2.29	2.25	2.20
d_2																
16	4.49	3.63	3.24	3.01	2.85	2.74	2.66	2.59	2.54	2.49	2.42	2.35	2.28	2.24	2.19	2.15
17	4.45	3.59	3.20	2.96	2.81	2.70	2.61	2.55	2.49	2.45	2.38	2.31	2.23	2.19	2.15	2.10
18	4.41	3.55	3.16	2.93	2.77	2.66	2.58	2.51	2.46	2.41	2.34	2.27	2.19	2.15	2.11	2.06
19	4.38	3.52	3.13	2.90	2.74	2.63	2.54	2.48	2.42	2.38	2.31	2.23	2.16	2.11	2.07	2.03
20	4.35	3.49	3.10	2.87	2.71	2.60	2.51	2.45	2.39	2.35	2.28	2.20	2.12	2.08	2.04	1.99
21	4.32	3.47	3.07	2.84	2.68	2.57	2.49	2.42	2.37	2.32	2.25	2.18	2.10	2.05	2.01	1.96
22	4.30	3.44	3.05	2.82	2.66	2.55	2.46	2.40	2.34	2.30	2.23	2.15	2.07	2.03	1.98	1.94
23	4.28	3.42	3.03	2.80	2.64	2.53	2.44	2.37	2.32	2.27	2.20	2.13	2.05	2.01	1.96	1.91
24	4.26	3.40	3.01	2.78	2.62	2.51	2.42	2.36	2.30	2.25	2.18	2.11	2.03	1.98	1.94	1.89
25	4.24	3.39	2.99	2.76	2.60	2.49	2.40	2.34	2.28	2.24	2.16	2.09	2.01	1.96	1.92	1.87
30	4.17	3.32	2.92	2.69	2.53	2.42	2.33	2.27	2.21	2.16	2.09	2.01	1.93	1.89	1.84	1.79
40	4.08	3.23	2.84	2.61	2.45	2.34	2.25	2.18	2.12	2.08	2.00	1.92	1.84	1.79	1.74	1.69
60	4.00	3.15	2.76	2.53	2.37	2.25	2.17	2.10	2.04	1.99	1.92	1.84	1.75	1.70	1.65	1.59
120	3.92	3.07	2.68	2.45	2.29	2.18	2.09	2.02	1.96	1.91	1.83	1.75	1.66	1.61	1.55	1.50
∞	3.84	3.00	2.60	2.37	2.21	2.10	2.01	1.94	1.88	1.83	1.75	1.67	1.57	1.52	1.46	1.39

Figure A.5: Fisher critical value for 5 % significance level (from [4])

Akaike information criterion and the corrected information criterion The Akaike information criterion (AIC), as its name suggests, is based on information criterion where it estimates the relative amount of information lost by a given model. It is particularly applied for the estimation of maximum likelihood models, like linear regression and logistic regression *etc.* The AIC follows Eq. A.16, where $\tilde{L}$ is the maximum value of the likelihood function for the model, and k is the model parameters. The better the fitness of the model, the lower the criterion is. However, the fitness of the model is penalized by twice the number of its parameters.

$$AIC = -2log(\tilde{L}) + 2k \tag{A.16}$$

When the sample size n is relatively small, or when the ratio of the number of parameters k to observations n is big, *i.e.* $n/k < 40$, the AIC will select over-fitting models [96]. In such case, it is better to use corrected AICc that adds a term to the original AIC that would converge to zero when n tends to infinity (Eq. A.17) .

$$AICc = AIC + \frac{2k(k+1)}{n-k-1} \tag{A.17}$$

Bayesian information criterion BIC The bayesian information criterion (BIC) has the same concept as AIC, but it has a larger penalty term for the number of parameters than the AIC (Eq. A.18) [188]. It is also less efficient for small number of samples, as n should be much larger than k^2 [221].

$$BIC = -2log(\tilde{L}) + klog(n) \tag{A.18}$$

A.6 Trade-off table for fractional factorial models

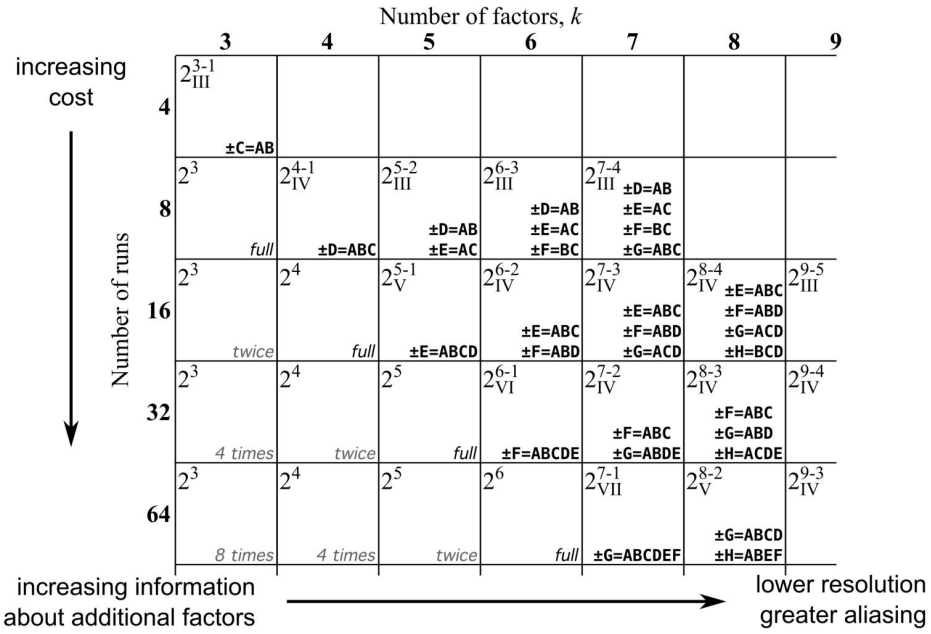

Figure A.6: Trade off table of the design of experiment to accurately choose the number of experiments for a full and fractional factorial design depending on the number of factors [68]

Appendix B

Data sheets

B.1 OLEDWorks FL300L ww OLED panel Datasheet

System

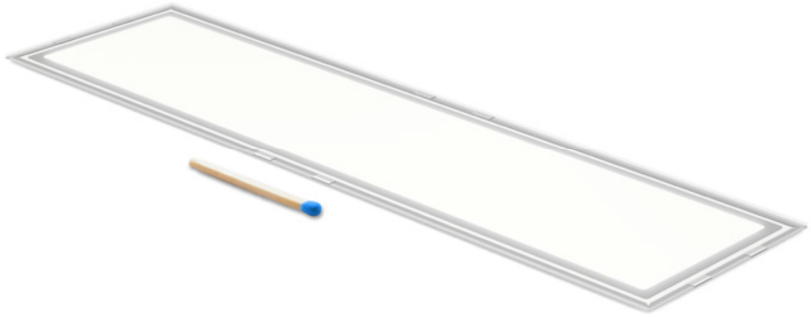

Figure 1: OLED Panel Brite FL300 L ww N w/o Rset

	Description	Remark
Indoor / outdoor	Indoor buildings	location with insignificant shock and vibration
Ingress protection		not applicable for OLED components
Classification	Applicable in applications with Class III protection	Application standard IEC61140
OLED color	White	
Carrier material	Glass	
Cable	AWG 26	Brite FL300 L ww Level 2 Brite FL300 L wm Level 2
Connector	5-pin Molex Picoblade	
RoHS conform	Yes	2011/65/EU

ENVIRONMENTAL

Operational environmental conditions*

Specification item	Value	Unit	Condition
Ambient temperature	+5 … +40	°C	
Relative humidity	20 … 80	%rH	no dew, no water spray, a maximum %rH of 60 is recommended.
Recommended internal operation temperature (temperature of OLED emission side)	≤ 50	°C	local temperature
Maximum internal operation temperature (temperature of OLED emission side)	≤ 80	°C	local temperature, for t > 50 °C lifetime will be reduced.

* please refer to Thermal Characteristics on page 24 for more information.

The Brite FL300 L is designed for indoor use only. Do not expose to water or excessive moisture.

OLEDWorks
Naturally Illuminating

Storage conditions*[1]

Specification item	Value	Unit	Condition
Ambient temperature	-40 … +60	°C	
Relative humidity	5 … 85	%rH	no dew, no water spray

*[1] Recommended storage temperature is between 15 ... 25 °C with a humidity < 65 %rH.

Transport conditions

Specification item	Value	Unit	Condition
Ambient temperature	-40 … +60	°C	
Relative humidity	5 … 85	%rH	no dew, no water spray

MECHANICAL DIMENSIONS

Specification item		Value	Unit	Condition
Brite FL300 L ww Level 1 w/o Rset Brite FL300 L wm Level 1 w/o Rset	length	240.6 ±0.2	mm	
	width	62.7 ±0.2	mm	
	height	1.4 ±0.15	mm	
	weight	36.4 ±0.5	gram	
Brite FL300 L ww Level 2 Brite FL300 L wm Level 2	length	248.1 ±0.15	mm	dimensions excluding cable
	width	70.2 ±0.15	mm	
	height	2.1 ±0.2	mm	excluding Molex Picoblade plug
	diameter screw opening	3.2	mm	for fixation with M3 screws
	distance screw openings	123.8 ±0.2 247.5 ±0.2 69.6 ±0.2	mm	
	weight	69 ±0.8	gram	
Light emitting area	length	222 ±0.2	mm	Brite FL300 L ww Level 1 w/o Rset Brite FL300 L wm Level 1 w/o Rset Brite FL300 L ww Level 2 Brite FL300 L wm Level 2
	width	46 ±0.2	mm	
	area	102.1	cm^2	

ELECTRICAL AND OPTICAL CHARACTERISTICS - OLED

Electrical characteristics

Specification item	Value	Unit	Condition
OLED rated current, $I_{in\ rated}$	0.368	A	
OLED maximum current, $I_{in\ max}$	0.390	A	
OLED voltage at t=0, U_{in}	20.0 + 0.5/– 1.0	V DC	$I_{in\ rated}$
OLED voltage at end of life, $U_{EOL} = U_{in\ max}$	25.5	V DC	$I_{in\ max}$
Power consumption at t=0, P_{in}	7.4	W	$I_{in\ rated}$
Power consumption at end of life, $P_{EOL} = P_{in\ max}$	10.0	W	$I_{in\ max}$

All data nominal at stabilized conditions after 5 min warm-up, $T_{organic}$ = 50 °C.

OLED drivers

Use of power supplies with dedicated controls for turning off output power if an OLED fails is recommended when operating the OLED Panel Brite FL300 L ww and wm. Recommended drivers are shown in the table below. These drivers all have sockets compatible with the Molex Picoblade connector.

Product	Supply voltage	Output channels	Product Code
Driver D230V 80W/0.1-0.5/1A/28V TD/A 8CH	120, 220-240, 277 V AC	8	9254.000.10200
Driver D024V 10W/0.1A-0.4A/28V D/A	24 V DC	1	9254.000.10100
Driver D024V 10W/0.1A-0.4A/28V DMX	24 V DC	1	9254.000.12000

Dimming

Both pulse width modulation (PWM) and amplitude modulation (AM) techniques can be used to dim the OLED. More detailed information can be found in the design-in guide for the Brite FL300 family.

OLED connection

The OLED Panel Brite FL300 L is available at different integration levels. At integration level 1, no cable is attached to the device. Integration levels 2 provide a cable with a Molex Picoblade connector type compatible with the Lumiblade OLED driver electronics.

At integration level 1 the Brite FL300 L features contact areas on the rear side (see Figure 6). Area A provides contact pads A1, 3, 5, 7, 9 (plus) and A2, 4, 6, 8, 10 (minus). The individual signals for the 5-wire connector are shown in Figure 7. Only one of the interface areas must be used for electrical contact.

Optical characteristics FL300 L ww*[2]

Specification item	Value	Unit	Condition
Luminance, nominal	8300	cd/m²	@ $I_{in\ rated}$ = 0.368 A, perpendicular, center
	3150		@ 0.135 A, perpendicular, center
Luminous flux	300 ± 10 %	lm	@ $I_{in\ rated}$ = 0.368 A with L70B50 = 10khrs
	115 ± 10 %		@ 0.135 A with L70B50 = 50khrs
Luminous efficacy, nominal	42	lm/W	@ $I_{in\ rated}$ = 0.368 A
	46		@ 0.135 A
	50		@ 0.040 A
Color	White		
Chromaticity x, nominal	0.4415		integral measurement, CIE 1931
Chromaticity y, nominal	0.4016		
Chromaticity u', nominal	0.2546		integral measurement, CIE 1976
Chromaticity v', nominal	0.5211		
Duv	-0.0016		center of color box with respect to BBL
Color spec limits CIE xy	0.4290 0.3934 0.4490 0.3997 0.4544 0.4097 0.4337 0.4034		corner coordinates of area in colorspace
Color spec limits CIE u'v'	0.2500 0.5159 0.2604 0.5215 0.2594 0.5262 0.2488 0.5206		corner coordinates of area in colorspace
CCT	2,900	K	@ $I_{in\ rated}$ = 0.368 A
Color Rendering Index: CRI / R9	80 / 0		@ $I_{in\ rated}$ = 0.368 A
color instability over angle (CSF)	≤ 0.004		0 .. 75°, □=5°, Ta = RT, I = 0.368 A
Homogeneity	≥ 80%		9 point measurement, min/max, $I_{in\ rated}$ = 0.368 A

*[2] all data for stabilized electrical conditions of the device after 5 min warm-up period, integration level 1.

Lifetime

Luminous flux reduces with lifetime of the OLED. The luminous flux of the Brite FL300 L decreases to approximately 70% after 10,000 hours at rated current.

Brite FL300L ww

Specification item	Value	Luminous flux	Condition
OLED Panel Lifetime L70B50	10,000 hours	300lm	@ $I_{in\ rated}$ = 0.368 A, $T_{organic}$ = 52 °C
OLED Panel Lifetime L70B50	50,000 hours	115lm	@ 0.135 A, $T_{organic}$ = 35 °C

Brite FL300L wm

Specification item	Value	Luminous flux	Condition
OLED Panel Lifetime L70B50	10,000 hours	190lm	@ $I_{in\ rated}$ = 0.368 A, $T_{organic}$ = 52 °C
OLED Panel Lifetime L70B50	50,000 hours	74lm	@ 0.135 A, $T_{organic}$ = 35 °C

Voltage increases over lifetime of the OLED; color and homogeneity of the panel may also change.

General handling recommendations and care

Cleaning
Please avoid scratching the front side with any hard or sharp objects. OLEDs can be cleaned with any soft textile. If required use a damp cloth but avoid extensive moisture.

Use of a compressed air spray to remove regular dust from the individual panels is advised for everyday cleaning. Should fingerprints or more persistent contamination occur, isopropanol applied to a lint-free cloth can be used to gently clean the surface of the OLED. Clean using circular movements beginning at the center of the OLED and moving outwards towards the edges. Contact with water is to be avoided.

Storage and operating
Please note that the recommended storage temperature is 15 °C to 25 °C. The recommended relative storage humidity is 65% or lower. Avoid exposing OLEDs to UV light.

Safety
Please be careful when handling OLEDs. The edges of the OLED panels may be sharp and can chip or break.

In the unlikely event that an OLED fails, the temperature may rise locally to high levels. To avoid this the OLED should be turned off immediately.

Disposal
OLEDs should be disposed of according to local legislation

B.2 Iberfil C Datasheet

SPECIFICATIONS OF ENAMELLED COPPER WIRES

	"IBERFIL C"
SPECIFICATIONS:	
	Very high temperature resistant thermical resistents
Thermal class	H-210
Base coat	Polyamide-imide
Overcoat	--
Temperature index 20.000 h.	210
Intersection point Tang. Delta	210ºC
Heat shock	260ºC
Cut-through	380ºC
Breakdown voltage	180 V/µm.
Continuity of insulation	0 – 2
Flexibility and adherence	60 %
Abrasion bidirectional	100
Abrasion unidirectional	20 gr/µm.
Resistance to solvents	4 H
Winding-Ability	Excellent
Resistance to humidity	Excellent
Resistance to transformer oil	Excellent
Resistance to refrigerants	Excellent
Resistance to styrol	Excellent
Solderability	--
Heat bonding	--
Risoftening temperature	--
MAIN APLICATION AREAS:	Special motors, Pumps, Nuclear industry
STANDARDS:	
IEC-	60.317-26
UNE - EN	60.317-26
DIN -	--
NEMA -	--
UTE -	NFC 31676
HOMOLOGATIONS:	
DIAMETER RANGE:	
Gr 1 mm.	0,20 – 1,00
Gr 2 mm.	0,20 – 1,00

Edición: Mayo 2000.

B.3 Philips Lumiblade Oled panel GL55

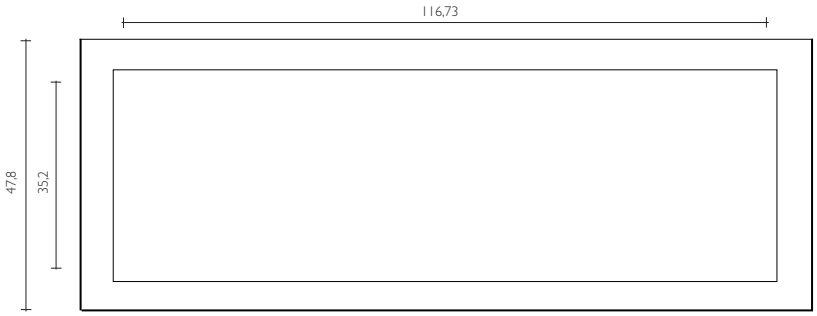

Type	Color / CCT CIE x/y	Lum. Flux[1]	CRI	Voltage	Rated Current
L0022 CE32 ILO 9254.000.033	white 3200K	55.0 lm	86	7.2 V	390 mA

Notes:
All values are nominal values measured at standard temperature and pressure.

Connectors

OLEDs of this product family are shipped with minimal 100mm long red cables, finished with Molex Picoblade connector: 51021-0500.

Electrical

Rated voltages

Type	Rated Current	Max Current	Minimum voltage	Nominal voltage	Maximum voltage
L0022 CE32 ILO	390 mA	450 mA	7.0 V	7.3 V	7.6 V

Rated voltages and maximum values apply to new OLEDs. Voltage can increase over lifetime. Philips strongly recommend the usage of SCP 1002, see page 32.

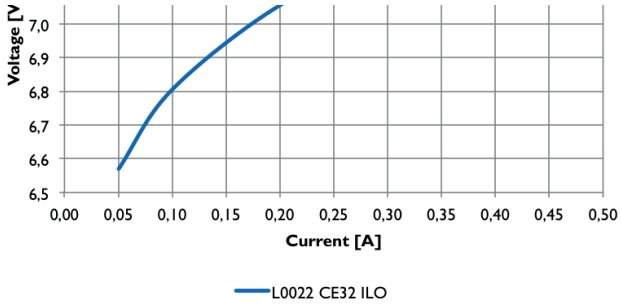

Luminous flux

Rated luminous flux

Type	Rated Current	Luminous flux min	Luminous flux nominal	Luminous flux max
L0022 CE32 ILO	390 mA	49.0 lm	55.0 lm	61.0 lm

Luminous flux versus forward current

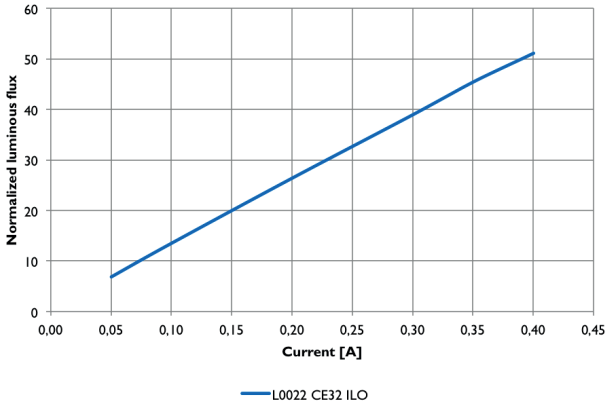

Lifetime

Lifetime

Type	Lifetime
L0022 CE32 ILO	7000 h[1]
L0022 CE32 ILO	20000 h[2]

[1] Until 50% decrease in luminance or defect (L50B50) at nominal current

L0022 CE32 ILO	390 mA	80%

Luminance

Luminance

Type	Rated Current	Luminance min	Luminance nominal	Luminance max
L0022 CE32 ILO	390 mA	3750 cd/m²	4200 cd/m²	4650 cd/m²

Luminance versus current

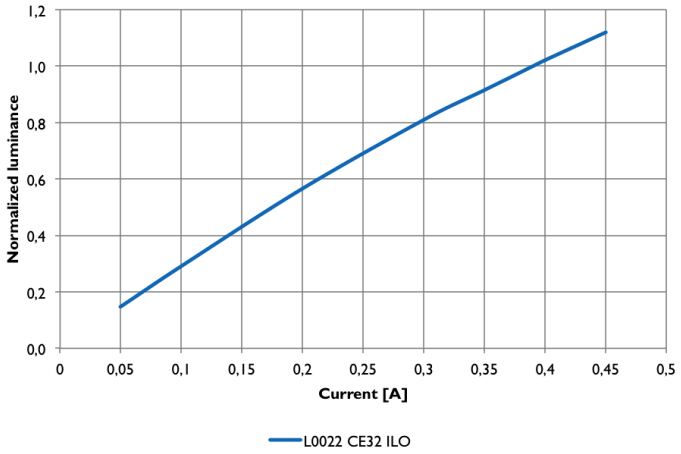

Luminance versus angle

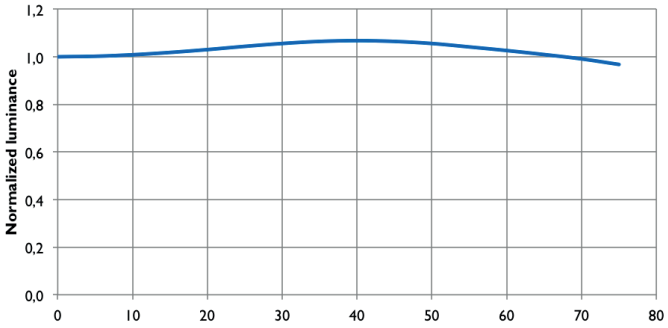

Appendix C

Measurement devices

C.1 Modulab XM MTS

ModuLab® XM mts
state of the art
solartron analytical
mXm

Electronic Materials

Displays | Solar/PVs | Semiconductors | Nanomaterials

LED, LCD, OLED, MEMs, Perovskite materials
OPV, Si, DSSC, OFET, Ge, GaAs

the XM difference

- ***Market leading impedance analysis***
- ***Widest voltage and current range available***
- ***Time domain and impedance analysis in a single system***

ModuLab® XM MTS is the only electronic materials test system that combines an accurate time domain analyzer and a high performance impedance analyzer into a single "plug and play" modular chassis. Purpose built for electronic materials research the ModuLab XM provides:

- High-performance impedance analysis throughout the entire frequency range and across all three modes of operation
  - Swept sine (highest accuracy and repeatability)
  - Multi-sine/FFT (for increased test throughput especially at low frequency)
  - Harmonic analysis (to study non-linear materials)
- 100 V option module enables tests of operating range and linearity/breakdown properties of materials
- Low frequency <10 Hz impedance/C-V measurements for material purity and degradation studies
- Multi-component system calibration for ensured measurement accuracy
- Market leading frequency range and resolution for analysis of carrier mobility/concentration (1 in 65,000,000)
- Staircase or smooth 'analog' ramp waveforms. Important for I-V, hysteresis and polarization measurements.
- Wide current measurement range (over 16 decades of current from 0.1 fA to 2 A) needed for electronic materials that transition between conduction states depending on applied voltage
- All time domain techniques (fast pulse, I-V etc.) use the same 'core' hardware module ensuring minimum cabling to the sample and consistency of results
- Available voltage and current amplification modules (100 V amplifier, femto ammeter, 2A booster) for the greatest flexibility in application
- XM hardware and software is compatible with highly efficient, low cryogen usage cryostats and probe stations
- User friendly software with simple three step test setup/run, built-in live waveform displays, connection diagrams and equivalent circuit/ IV fit functions.
- Compatibility with potentiostat modules for Dye-Sensitized Solar Cells (DSSC)

C.2 Konika Minolta CS1000 A

KONICA MINOLTA

SPECTRORADIOMETER

CS-1000A (STANDARD MODEL)
CS-1000S (SMALL MEASURING AREA MODEL)
CS-1000T (SMALL MEASURING ANGLE MODEL)

ISO 9001 CERTIFIED ISO 14001

Konica Minolta manufactures

reliable optical lens

via integrated

production syste

starting from R&D

and melting glass

to the final production.

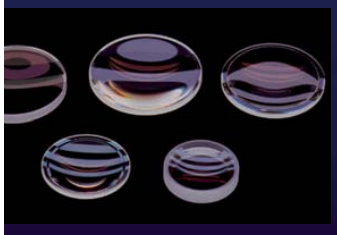

High Performance Spectroradiometer

With the increased emphasis on ISO 9001, product quality has become a focal point in many companies. At the same time, in-house production departments are requiring systems that calibrate their measurement instruments. CS-1000 series Spectroradiometer supports these activities.

High-Speed

- Use of polychromator enables high-speed measurements. ➲1
- Fast measurement for the low luminance target.➲2

➲1 Measurement speed varies depending on the luminance of the light source.
➲2 Fast Mode. Using CS-S1W

High-Accuracy

- Repeatability of 0.1%+1digit for Luminance, 0.0002➲3 for Chromaticity.

➲3 Normal Mode. Using Standard Lens.
The other measurement conditions : based on Minolta standard test method.

- Measurements can be synchronized with a display device.
- Low polarization error-ideal for measuring LCD's.
- Aperture mirror eliminates misalignment between the finder target and actual measuring spot.

Low Luminance

- Specifications are guaranteed even at 1cd/m^2.(Repeatability for illuminant A)
- Sensor cooling improves S/N ratio, enabling measurement of low-luminance subjects.

C.3 Pearson current monitor model 6585

PEARSON ELECTRONICS, INC.

PEARSON™
CURRENT
MONITOR
MODEL 6585

Sensitivity	1 V/A ±1% 0.5 V/A into 50 Ω
Output resistance	50 Ω
Maximum peak current	500 A
Maximum rms current 10 A	
Droop rate	0.3 %/μs
Useable rise time	1.5 ns
Maximum I•t	0.002 A s with bias
Low frequency 3 dB cut-off	400 Hz
High frequency ±3 dB	250 MHz (approximate)
Maximum I²t / pulse	5 A² s
Output connector	BNC (UG-290A/U)
Operating temperature	0 to 65 °C
Weight	0.68 kg

* Maximum current-time product can be obtained by using core-reset bias as described in the *Application Notes*. 0.0005 Ampere-second is typical without bias.

Dimensions in inches

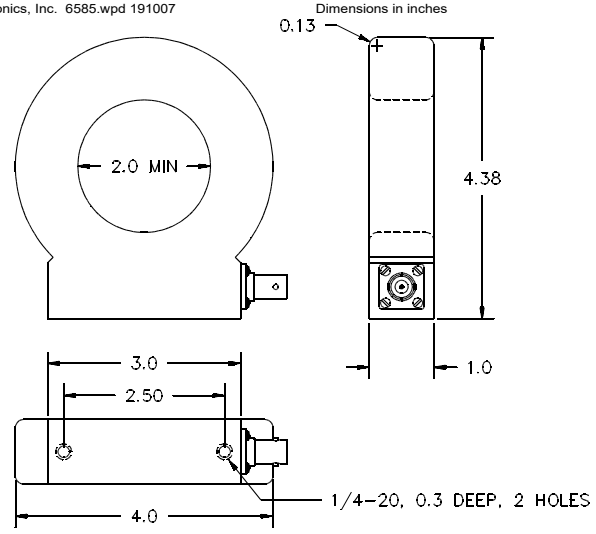

Pearson Electronics, Inc. • 4009 Transport Street • Palo Alto, CA 94303
Telephone 650-494-6444 • FAX 650-494-6716 • www.pearsonelectronics.com

Appendix D

Abrupt change algorithm

D.1 Abrupt change algorithm

Linear degradation of an electrical component is caused by defined stress factors, usually constant. However, as previously said, accidents tend to happen, and the linear path will have a catastrophic degradation not predicted previously. A power cut of the test bench is an example of accidents that might occur, and will change the electrical stress applied. A bad contact in the thermo-couple of the heat regulator of a failure in the fan assuring a homogeneous temperature all along the test bench, will change the local heat stress applied to the electrical component. These accidents will cause different degradation decays during an interval of time before being detected and resolved. The uncontrolled factors added might not be harmful (in the case of no stress applied due to the power cut), but the might cause a catastrophic degradation when the additional stress is added like the increase of local temperature around the asset might cause a failure.

Even with catastrophic degradation, the stressed asset might not have reached the failure limit and thus the operation shall continue. However, like said, the decay path changes during the interval of the accident, and if not considered in the modelling, the overall linear degradation will change causing false predictions. In this case, data after any abrupt change can be cleaned by the process described previously in chapter 1, and shall be considered as rightly censored, because the failure is not a true representation of the real value when it is caused by uncontrolled stress. If the component did not fail, but there is a change in the slope, data after the change can be eliminated and only rightly censored data is taken.

However if there is enough degradation data before and after the abrupt change, and if the degradation is linear for example, and the decay slope is the subject of interest, data can be divided into two subgroups, adding a "fictive" sample to study. We developed an algorithm based on the confidence intervals to extract an adequate degradation slope from a degradation path with abrupt change as it can be seen in Alg. 1.

The algorithm studies the degradation in the following way: It applies a robust linear regression to the first three degradation measurements (as $i = 3$ is the minimum number for a sample size) to estimate a preliminary degradation parameters $\{a_i, b_i\}$. A confidence interval is then generated with the fitting characteristics using the Student law equation from Eq. A.4, where $\alpha/2 = 0.05$, $n = k - i - 1$ and s is the standard deviation of the model from true data (based on Eq. A.3). When a new measurement is acquired, the confidence interval is extended till the $i + 1^{th}$ point: $y_{(i+1),CI} = \hat{y}_{i+1} \pm CI_i$, where $\hat{y}_{i+1} \sim a_i + b_i x_{i+1}$. If the measurement is inside the confidence interval, it means the degradation is following the previously modelled path, and there is no fault detected.

Nevertheless, if it is not the case, it can be either due to measurement error and stochastic variation, or due to catastrophic degradation discussed above. To differentiate the two cases, one more measurement is taken (if possible), and this measurement is also tested to the confidence interval built by the i^{th} iteration. If the second new measurement does not fit inside the confidence interval neither, an abrupt change has happened surely indicating catastrophic degradation. In this case, if the electrical component is still working, and new degradation measurements can be acquired, the algorithm re-initializes the data to the moment after the i^{th} iteration and studies a new degradation path starting from the $k = i + 1$ measurement. If the second measurement fits however inside the i^{th} confidence interval, no change is declared, and the first measurement can be considered simply as an outlier. The online modelling path would continue to incorporate those two measurements and further ones into the algorithm, considering that that no change in the decay path had occurred.

Algorithm 1 Recursive algorithm based on confidence intervals to detect abrupt changes

Data: {x,y}
Result: decay parameters

initialisation:
  n=size(x)
  k=1 ; // start the fit from $\{x_k, y_k\}$
while $k < n - 2$ **do**
  $i = k + 2$
  repeat
    Robust linear regression $Y_{k \to i} \sim a(i) + b(i) X_{k \to i}$
    Student confidence interval CI for $t_{(0.05, i-k-1)}$
    if $y_{i+1} > |CI_{i+1}|$ **then**
      Student confidence interval CI for $t_{(0.05, i-k)}$
      if $y_{i+2} > |CI_{i+2}|$ **then**
        save a_k and b_k ; // Abrupt change detected
        $k = i + 1$
      else
        $i \leftarrow i + 1$
      end
    else
      $i \leftarrow i + 1$
    end
  until *(*$i == n$*)*;
end

Appendix E

Stochastic processes

E.1 General processes

A stochastic process has many statistical definitions (refer to [64]), but in terms of engineering, it is a random function $X(t)$ that is defined as a family of random variables, for $t \in \mathcal{R}$. The distribution of the stochastic process is determined by some characteristics, such as

- The mean function $\{a_X(t) = EX(t)\}$
- The covariance function $R_X(t,s) = cov(X(t), X(s))$
- A characteristic functions set $\{\phi^X_{t1,\ldots,t_m},\ m \geq 1\}$, that satisfy the below conditions

  i $\phi(0) = 1$

  ii ϕ is continuous in the neighborhood of 0

  iii For any $m \in \mathbb{N}$, $z_1, \ldots, z_m \in \mathbb{R}$ and $c_1, \ldots, c_m \in \mathbb{C}$:

$$\sum_{j,k=1}^{m} \phi(z_j - z_k) c_j \bar{c}_k \geq 0$$

A stochastic process can have many properties like being measurable, continuous, stochastically differentiable, integrable, etc. It can have independent increments, that is $X(t_0), X(t_1) - X(t_0), \ldots, X(t_m) - X(t_{m-1})$ are jointly independent, $\forall t_0 < \ldots < t_m$ and $m \geq 1$. if the independent increments have the same distribution, the process is called homogeneous.

Since a degradation process is an additive accumulation of decay, it can be related to a stochastic process with independent increments. In the following, a Lévy process that has this feature will be defined, and examples of Lévy processes that can be assigned as degradation processes will be mentioned.

E.2 Lévy processes

A Lévy process is a stochastic continuous process $X = X_t, t \geq 0$ with stationary and independent increments [10], that is:

(i) The distribution of $(X_{t+s} - X_t)$ is independent of t

(ii) The process is additive, that is for every $t \geq 0$ and $s \geq 0$, $P\{X_{t+s} - X_t \in A | X_u, u \leq t\} = P\{X_{t+s} - X_t \in A\}$

(iii) The process is continuous, that is for every $t \geq 0$ and $\epsilon \geq 0$, $lim_{s \to t} P\{|X_t - X_s| > \epsilon\} = 0$

The distribution of a Lévy process is characterized by its characteristic function, which is described in Eq. E.1, where $a \in \Re$, $b \geq 0 \in \Re$, $\nu(0) = 0$ is called the Lévy measure of X on $\Re$ which has the property $\int_{\Re \setminus \{0\}} min(1, x^2)\nu(dx) < \infty$ i.e., $X_0 = 0$ almost surely; A Lévy measure represents the intensity of the jumps of a Lévy process, for when a Lévy process is continuous, a Lévy measure is null everywhere.

$$ln(\Phi_X(z)) = t\{iza - \frac{z^2 b}{2} + \int_{\Re \setminus \{0\}} [e^{izx} - 1 - izx I_{\{|x|<1\}}]\nu(dx)\} \tag{E.1}$$

Following the above characteristics, a degradation process where data are measured continuously and degradation increments constantly can be associated to Lévy processes. Lévy processes include several processes that, according to the case studied, might be the best fitted to the situation. The most important processes for degradation modelling are the Brownian motion or the Wiener process, the Gamma process and the compound Poisson process.

The Brownian motion A Brownian motion is a Lévy process where the increments have a normal distribution $(X_{t+s} - Xt) \sim \mathcal{N}(s\mu, s\sigma^2)$, for $t \geq 0$, and $s \geq 0$. A Brownian motion path is non-differentiable, continuous and has finite variations, or increments. Since a Brownian motion has continuous trajectories, its Lévy measure is zero everywhere.

A Wiener process $W(t)$ is a standard Brownian motion which increments follow a standard normal distribution i.e., $(W_{t+s} - W_t) \sim \mathcal{N}(0, s)$. Note that the independent increments are defined on the $\mathbb{R}^+$, and $W(0) = 0$.

Gamma process A Gamma process is an increasing Lévy process, that is the sample paths are increasing. A Gamma process is an increasing Lévy process where the Lévy measure of $(X_t)_{t \geq 0}$ is

$$\nu(dx) = \delta \frac{e^{-\eta x}}{x} dx$$

where $\delta > 0 \in \Re$ and $\eta > 0 \in \Re$. The characteristic function for a Gamma process is in Eq. E.2. For more proof, please refer to [142].

$$\Phi_{X_t}(\xi) = \frac{\beta^{\alpha t}}{(\beta - i\xi)^t} \tag{E.2}$$

Poisson process A Poisson process $N(t)$ is a process with independent increments, where the increment $N(t) - N(s)$, $\forall t > s$ has the Poisson distribution [64], whom the probability mass distribution is $f(k; \lambda) = \Pr(X{=}k) = \frac{\lambda^k e^{-\lambda}}{k!}$, for $\lambda > 0$.

A compound Poisson process is a Lévy process, where the distribution F of the increments is characterised by the Lévy measure $\nu(dx) = \lambda F(dx)$ is finite. The Gamma process is the limit of a compound Poisson process with the Poisson arrival rate λ tending to infinity.

The stochastic modeling of the degradation follows a stochastic process and more particularly a Lévy process (see Appendix E). In the following, a degradation process is presented based on a Wiener process, the most common process used for the degradation application.

E.3 Degradation processes

A degradation process is an additive accumulation of degradations with a defined wear intensity. [114]. It adds modeling uncertainty to a degradation trajectory by including a stochastic process, as the degradation itself may have multiple trajectory options due to random effects caused by unknown or uncontrolled variables. It can be modeled by Eq. E.3, where $Y(t)$ is the observation of the degradation process, $D(t, \beta)$ is similar to the degradation path of a deterministic model, and $S(t)$ is a stochastic process that considers the randomness of the paths. $D(t)$ is a typical degradation function that can be based on common relationships, or physical conclusions, presented earlier. $S(t)$ can be any of the Levy processes presented in Appendix E, depending on the case of study.

$$Y(t) = D(t, \beta) + S(t) \tag{E.3}$$

Fig. E.1 presents a degradation process where two realizations are tracked, and for each realization, m_i observations are recorded. Note that the number of observations and the corresponding

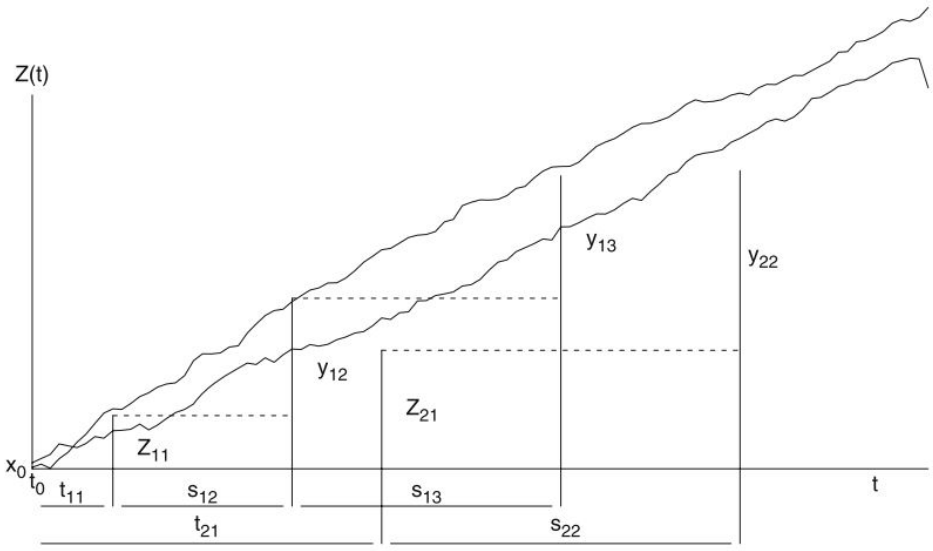

Figure E.1: A degradation process example from [114]

time for each realization can be different.

The observations of the degradation process are characterized by certain variables (which are sketched in Fig. E.1). Note that the denotation used in the following is different from that used for Eq. E.3. The degradation process here is called $Z(t)$ and has a valid range of $t \geq t_0$, where t_0 is the beginning of the degradation. It has n realisations and for each realisation, m_i observations are recorded at times t_{ij} ($i = 1, \ldots, n$ is the number of realisation in question, and $j = 1, \ldots, m_i$ is the number of observation in question)

- $y_{ij} = Z_i(t_{ij}) - Z_i(t_{ij-1})$ are the increments of the process, for $j = 2, \ldots, m_i$
- $s_{ij} = t_{ij} - t_{ij-1}$ are the distance between time points of observation, for $j = 2, \ldots, m_i$
- $Z_{i1} = Z_i(t_{i1})$ are the observations at the first recorded times of each realisation, for $i = 1, \ldots, n$
- $\bar{Z_1} = \frac{1}{n} \sum_{i=1}^{n} Z_{i1}$ is the average value of the first observed values of each realisation
- $\bar{Z_m} = \frac{1}{n} \sum_{i=1}^{n} Z_{im_i}$ is the average value of the last observed values of each realisation

- $\bar{t}_1 = \frac{1}{n}\sum_{i=1}^{n} t_{i1}$ is the average value of the first recorded times
- $\bar{t}_m = \frac{1}{n}\sum_{i=1}^{n} t_{im_i}$ is the average value of the last recorded times
- $\bar{m} = \frac{1}{n}\sum_{i=1}^{n} m_i$ is the average value of the number of observations in one realisation

In an analogue with a typical regression problem, a device would fail if its degradation process reaches some threshold h, which is generally unknown in the stochastic world (unlike the threshold defined in deterministic models). The lifetime of the device T_h is then defined as the first time the degradation process exceeds the threshold level: $T_h = inf\{t \geq t_0 : Z(t) \geq h\}$

In order to construct the likelihood for estimating the parameters of the degradation process, certain assumptions must be made. The first assumption is to define the degradation path (linear, exponential, etc). The second assumption is to choose the stochastic process that the degradation follows, as it will define the probability distribution around the uncertainties.

The most common stochastic process associated with the degradation process is the Wiener process because the degradation starts at 0, and the increments of the degradation follow a normal distribution. Gamma processes are also widely used for monotonically growing degradation, but this study will focus on modeling degradation based on the Wiener process. Nevertheless, some works related to the application of the Gamma process for the application of degradation will be quickly mentioned.

E.4 Wiener modelling

Several studies have discussed Wiener modeling, however these studies have advanced statistical equations, which are not within the knowledge of an electrical engineer. Kahle and Lehmann were among the few to propose a simple approach to quantify the parameters of a Wiener process used for modeling degradation [114]. Therefore, this section will present the modeling of the Wiener process from the perspective of the Kahle and Lehmann publication. A degradation process can be modeled by a standard Wiener process (see in Eq. E.4), where

$$Z(t) = z_0 + \sigma W(t - t0) + \mu(t - t_0), t \geq 0 \tag{E.4}$$

- z_0 is the constant initial degradation,
- t_0 is the beginning of the degradation,
- μ is the decay drift parameter,
- $\sigma > 0$ is the variance parameter,
- $W(t)$ is the standard Wiener process on $[0, \infty)$

The degradation path in Eq. E.4 is a linear path, and the degradation increments follow a normal distribution $Y_{ij} \sim \mathcal{N}(s_{ij}\mu, \sigma^2 s_{ij})$. Similarly, the first observed increment follows a normal distribution $Z_{i1} \sim \mathcal{N}(z_0 + (t_{i1} - t_0)\mu, \sigma^2(t_{i1} - t_0)$.

T_h in the case of a Wiener process follows an inverse Gaussian distribution with the density function f_{T_h} of Eq. E.5 [114].

$$f_{T_h}(t) = \frac{h - z_0}{\sqrt{2\pi\sigma^2(t - t_0)^3}} exp^{-\frac{(h - z_0 - \mu(t - t_0))^2}{2\sigma^2(t - t_0)}}, \forall t > t_0 \tag{E.5}$$

Since a degradation process can have a record of degradation increments, failure times, or both, the likelihood function of the degradation process for each scenario is different. Kahle and Lehmann considered the case where increments are observed with and without the recorded failure times.

The likelihood function of the scenario where only degradation increments are observed is in Eq. E.6, where ϕ is the density function of the standard normal distribution.

$$L = \prod_{i=1}^{n} \frac{1}{\sqrt{\sigma^2(t_{i1} - t_0)}} \phi\left(\frac{z_{i1} - z_0 - \mu(t_{i1} - t_0)}{\sqrt{\sigma^2(t_{i1} - t_0)}}\right) \prod_{j=2}^{m_i} \frac{1}{\sqrt{\sigma^2 s_{ij}}} \phi\left(\frac{y_{ij} - \mu s_{ij}}{\sqrt{\sigma^2 s_{ij}}}\right) \tag{E.6}$$

The resolution of the likelihood function leads to Eq. E.7, which is a set of four equations, that when solved numerically, give the estimated parameters of the degradation process ($\hat{t}_0$, $\hat{z}_0$, $\hat{\mu}$,$\hat{\sigma}^2$). One may ask why estimate a t_0 or the initial degradation z_0, since normally it is the initial values that are supposed to be known. In some cases, a certain degradation process does not start at the beginning of a device's life, as it may be stored for some time. It may also be subjected to some stress that does not immediately cause degradation, and degradation occurs after some time. Thus t_0, and its corresponding degradation level z_0 in these cases are unknown and must be estimated.

$$\begin{aligned}
\hat{\mu} &= (\bar{z}_m - \hat{z}_0)/(\bar{t}_n - \hat{t}_0) \\
\hat{\sigma}^2 &= \frac{1}{\bar{m}n} \left(\sum_{i=1}^{n} \left(\frac{(z_{i1} - \hat{z}_0)^2}{t_{i1} - \hat{t}_0} + \sum_{j=2}^{m_i} \frac{y_{ij}^2}{s_{ij}} \right) - \hat{\mu} n (\bar{z}_m - \hat{z}_0) \right) \\
\hat{z}_0 &= \left(\frac{1}{n} \sum_{i=1}^{n} \frac{z_{i1}}{t_{i1} - \hat{t}_0} - \frac{\bar{z}_m}{t_m - \hat{t}_0} \right) \Big/ \left(\frac{1}{n} \sum_{i=1}^{n} \frac{1}{t_{i1} - \hat{t}_0} - \frac{1}{t_m - \hat{t}_0} \right) \\
\hat{\sigma}^2 \sum_{i=1}^{n} \frac{1}{t_{i1} - \hat{t}_0} &= \sum_{i=1}^{n} \frac{(z_{i1} - \hat{z}_0)^2}{(t_{i1} - \hat{t}_0)^2} - \hat{\mu} n
\end{aligned} \tag{E.7}$$

Other modeling scenario are considering the degradation process with only the failure times, when observed and the threshold is known. Another approach is to consider both degradation increments and failure times when they are recorded for realization. For more information on the likelihood function for these scenarios, see [114].

E.5 Application of a Wiener process to OLEDWorks experimental design

So far, deterministic models have been studied where a single model is generated from a particular set of data. The main objective of stochastic degradation modeling is to generate different scenarios, where for a set of aging conditions, the degradation trajectory of the electrical component changes hazardously. The stochastic degradation modeling is done to include all uncontrolled and immeasurable factors in the modeling, in order to expand the prediction area.

The stochastic method of degradation modeling is presented in section 2.7, where the degradation process is supposed to follow a Wiener Gaussian process. Since a Wiener process is part of the Lévy processes, it is important to respect the limits of a Lévy process $X(t)$, that is it is

(i) The distribution of an increment $(X_{t+s} - X_t)$ is independent of t

(ii) The process is additive, that is for every $t \geq 0$ and $s \geq 0$, $P\{X_{t+s} - X_t \in A | X_u, u \leq t\} = P\{X_{t+s} - X_t \in A\}$

(iii) The process is continuous, that is for every $t \geq 0$ and $\epsilon \geq 0$, $lim_{s \to t} P\{|X_t - X_s| > \epsilon\} = 0$

(iv) The start point of the value is null, i.e. $X_0 = 0$.

The degradation modeling in this section will consider the luminance degradation of OLEDWorks panels. Note that these are commercial OLEDs where the degradation based on a set of conditions does not vary greatly. However, they are used here only to get a general idea of a stochastic degradation process. Previously, for deterministic approaches, luminance degradation was modeled directly with time. But for stochastic modeling, the degradation increments are needed and not the luminance evolution. The degradation process of specimen i at inspection time t_ij is the subtraction of the initial luminance value at inspection time t_{i0} from the luminance value at inspection time t_ij: $D_i(t_{ij}) = L_i(t_{ij}) - L_i(t_{i0})$. To simplify the fitting algorithm, the initial inspection time are supposed to be null: $t_{i0} = 0, \forall\ 1 \leq i \leq n$.

As an example, two experiments from the OLEDWorks experimental design will be used: experiment #14 and experiment #10. Each experiment has its own particularity which will be detailed later. Note that this analysis can be done for all experiments in the OLEDWorks experimental design.

At first, experiment #14 is used to study the degradation process. Experiment #14 has two replications (i.e. the experiment was repeated twice, for the same aging conditions, but in a different time zone). The second replication consists of aging 4 specimens, in the same oven, at 60 °C, 650 mA, and without cycling. The second replication of this experiment is chosen because the inspection times are uniform, and the stress interval between two inspections is always 7 days. Each of the 4 specimens has its own degradation process $Z(t)$, but these processes have the same incremental time (that is the stress interval between two inspections): $s_{i,j+1} = t_{i,j+1} - t_{i,j} = 7$ days or 168 hours, $\forall\ 1 \leq i \leq 4$ and $\forall\ 0 \leq j \leq (m_i - 1)$. m_i is the number of observations for the process i.
The incremental data of the degradation processes $Z(t)$ are represented in Tab E.1.

Table E.1: Increments of the degradation process $Z(t)$ of the second replication of OLEDWorks experiment #14

Name / Number	OLED 14a	OLED 14b	OLED 14c	OLED 14d
i	1	2	3	4
$z_{ij} - z_{i,j-1}$ ($\mathrm{cd\,m^{-2}}$)	373	207	478	379
	202	253	277	269
	383	361	412	304
	271	237	312	239
	370	282	466	352
	285	372	312	263
	327	296	343	207
	337	382	293	392
	332	227	312	254
	147	340	195	233

The degradation process $Z(t)$ presented in Section 2.7 is used

$$Z(t) = z_0 + \sigma W(t - t0) + \mu(t - t_0) \tag{E.4}$$

The estimates of its parameters are based on the set of equations in Eq. E.7 that must be solved numerically. It was impossible however to solve all four equations, as the values were not reasonable, like $\hat{\sigma}^2$ had negative value. Since all the degradation processes started at $t_0 = 0$, it is not mandatory

to "estimate" a t_0 and can be directly considered as $\hat{t}_0 = 0$. Moreover, the stochastic approach does not give a single parameter estimate, but a set of parameters around a kernel. The kernel of the parameter estimate is found by numerically computing the set of equations in Eq. E.7.

$$\begin{aligned}
\hat{\mu} &= (\bar{z}_m - \hat{z}_0)/(\bar{t}_n - \hat{t}_0) \\
\hat{\sigma}^2 &= \frac{1}{\bar{m}n}\left(\sum_{i=1}^{n}\left(\frac{(z_{i1}-\hat{z}_0)^2}{t_{i1}-\hat{t}_0} + \sum_{j=2}^{m_i}\frac{y_{ij}^2}{s_{ij}}\right) - \hat{\mu}n(\bar{z}_m - \hat{z}_0)\right) \\
\hat{z}_0 &= \left(\frac{1}{n}\sum_{i=1}^{n}\frac{z_{i1}}{t_{i1}-\hat{t}_0} - \frac{\bar{z}_m}{t_m - \hat{t}_0}\right) \Big/ \left(\frac{1}{n}\sum_{i=1}^{n}\frac{1}{t_{i1}-\hat{t}_0} - \frac{1}{t_m-\hat{t}_0}\right) \\
\hat{\sigma}^2 \sum_{i=1}^{n}\frac{1}{t_{i1}-\hat{t}_0} &= \sum_{i=1}^{n}\frac{(z_{i1}-\hat{z}_0)^2}{(t_{i1}-\hat{t}_0)^2} - \hat{\mu}n
\end{aligned} \tag{E.7}$$

The joint confidence region for parameter estimation is found using a concept similar to the regression confidence interval. The joint confidence region is presented in Eq. E.8, where θ is the set of parameters, and $\hat{\theta}$ is its estimate. I_θ is the Fisher information matrix used to get the covariance matrix for Bayesian analysis, and a^2 is the quantile of the χ^2 distribution, with k degrees of freedom (k being the number of parameters of the vector θ)

$$(\hat{\theta} - \theta)^T I_\theta^{-1}(\hat{\theta} - \theta) < a^2 \tag{E.8}$$

The confidence region for only the two parameters of interest μ and σ^2, and equal first observation time for all specimens t_1 is represented in Eq. E.9 (the demonstration is found in [114]).

$$\frac{(\hat{\mu}-\mu)^2}{\sigma^2}(t_m - t_1) + \frac{(\hat{\sigma}^2 - \sigma^2)^2}{2\sigma^4}(\bar{m} - 1) \leq \frac{a^2}{n} \tag{E.9}$$

The parameters estimate are $\hat{\theta} = [\hat{\mu};\ \hat{sigma}^2;\ \hat{z}_0] = [1.744;\ 35.6;\ 64.8]$ (they are found by numerically computing Eq. E.7).

The 95 % and the 90 % joint confidence regions are represented in Fig. E.2.

As seen in Fig. E.2, the confidence interval of the decay slope μ and the variance of the Wiener process σ^2 are correlated. The largest confidence interval for μ and σ^2 is for the kernel estimate. The confidence interval for σ^2 becomes narrower when the values of μ move away from its kernel (in a symmetric manner). The analysis is similar to the confidence interval of μ. To understand what this means, the decay slope of the kernel is also plotted in Fig. E.2. This means that the confidence interval at the kernel level is very wide because it must take into account 90 % or 95 % of all observations. When the decay slope is larger or smaller than the kernel estimate, the stochastic process will have a smaller variance, i.e. there is less chance that the decay trajectory of the #14 experiment will follow this path.

Fig. E.2 also represents a comparison between the fits of an ordinary linear regression and the deterministic part of the process, i.e. $\hat{\mu}(t - t_0) + \hat{z}_0$. The two models are very similar and have the same decay path. The difference is that the OLR method gives only one decay trajectory, unlike the many decay trajectories estimated by the degradation process.

The lower the σ^2 is, the wider the confidence region of μ, and the opposite is true. This means that either the modeling has a high value of randomness by the stochastic process, or high random estimation error.

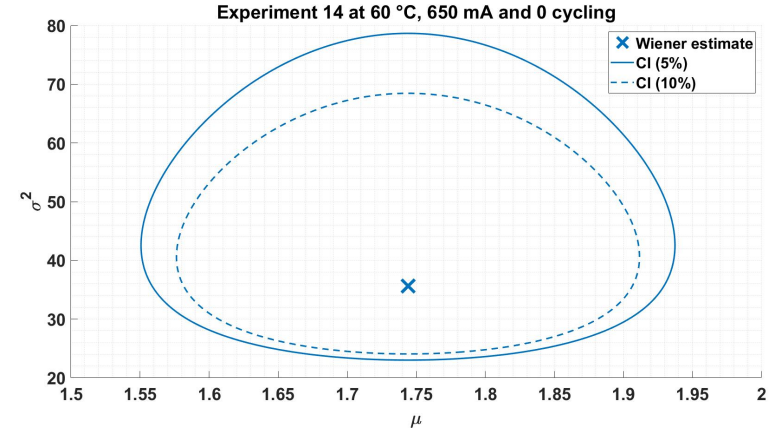

(a)

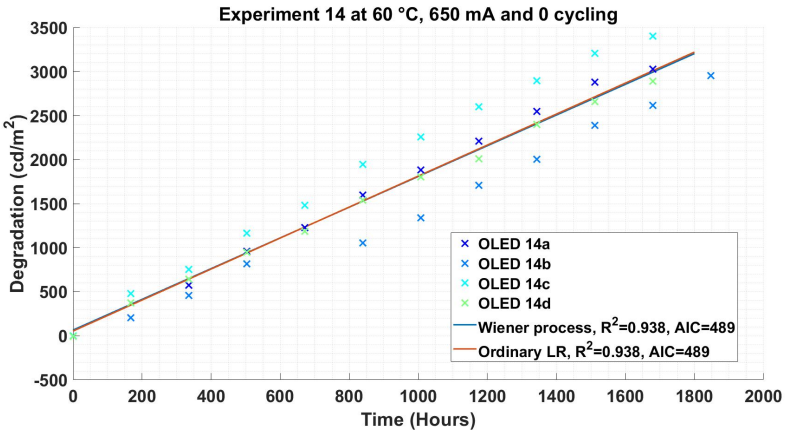

(b)

Figure E.2: Stochastic degradation modeling of the second replication of experiment 14 of OLEDWorks experimental plan: (a) The joint confidence interval of the estimated parameters of interest $\hat{\mu}$ and $\hat{\sigma}^2$ (b) Comparison between the deterministic part of the process and the ordinary linear regression

Another examples of stochastic modeling is shown in Fig. E.3, where luminance degradation data from experiment #10 in the OLEDWorks experimental design are presented: Experiment #10 also includes several specimens and thus several degradation pathways. However, it has an in-homogeneous inspection times or stress intervals, this is why is chosen, to prove the validity of the stochastic model in all cases. The Kernel estimate of the degradation process is also compared to a deterministic ordinary linear regression. The OLR tried to reduce the maximum error between the model and the data, and thus had better model selection criteria values than the stochastic model. However, the Wiener process distributed the weights fairly among each repetition of the experiment and had a decay path similar to a WLR model.

Finally, the stochastic approach is another way to model degradation, which is based on random statistical processes. This approach is used to estimate the degradation of a component within a whole system, where there are many interactions between stressors, and many uncontrolled variables. However, this thesis models the degradation of electrical components, where aging occurs in a controlled environment. In this case, the stochastic approach is overestimated and traditional deterministic methods are sufficient to model the degradation of OLEDs for example.

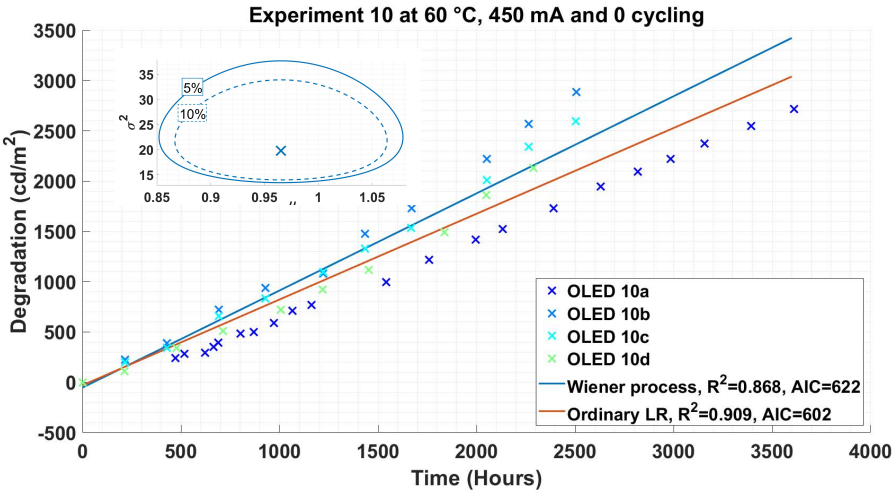

Figure E.3: Stochastic degradation modeling of data from experiments #10 and #2 of the OLED-Works experimental plan

Appendix F

Online Models

F.1 Kalman filter

Kalman filtering, also known as linear quadratic estimation (LQE), is an algorithm that uses a series of measurements observed over time, including statistical noise and other inaccuracies, and produces estimates of unknown variables by estimating a joint probability distribution over the variables for each time-frame. It is very popular for control applications, and signal processing.

In what follows, the basic concepts of the Kalman filter and its application to degradation modeling are presented.

State space Kalman filters are used to estimate states based on linear dynamical systems in a state space format. [118]. It uses the state space system of Eq. Eq. F.1, where x_k, y_k and u_k are respectively the state, measurement and control input vectors of the process. A_k is the state transition matrix applied to the previous state vector x_k and C_k is the measurement matrix. α_k and β_k are noise vectors that are assumed to be zero-mean Gaussian, and independent, i.e., α_{k1} and α_{k2} (or β_{k1} and β_{k2}) are independent if $k_1 \neq k_2$. $\alpha_k \sim \mathcal{N}(0, Q)$ is the process noise vector with the covariance Q, and $\beta_k \sim \mathcal{N}(0, R)$ is the measurements noise vector with the covariance R. Although covariance matrices are supposed to reflect the statistics of the noises, the true statistics of the noises are not known or are not Gaussian in many practical applications. Therefore, Q and R are typically used as tuning parameters that the user can adjust to achieve the desired performance [118].

$$\begin{cases} x_{k+1} = A_k x_k + u_k + \alpha_k \\ y_k = C_k x_k + \beta_k \end{cases} \tag{F.1}$$

A Kalman filter algorithm consists of two stages: "correction/update" and "prediction". Suppose that the system has already k measurement points $y_0, y_1, \ldots, y_{k-1}$. The Kalman filter has already estimated/predicted the state space vector $\hat{x}_{k|k-1}$ at time k given the $(k-1)^{th}$ one, that was computed based on the $(k-1)^{th}$ measurements vector. This vector has a covariance matrix of $\Gamma_{k|k-1}$. When the y_k measurement is collected, the state space vector is updated to become $x_{k|k}$, that is different of $x_{k|k-1}$. The correction of this vector is based on the set of equations in Eq. F.2.

$$\begin{aligned}
&(i) && \hat{x}_{k|k} &&= \hat{x}_{k|k-1} + K_k \tilde{y}_k && \text{(corrected state estimate)} \\
&(ii) && \Gamma_{k|k} &&= \Gamma_{k|k-1} - K_k C_k \Gamma_{k|k-1} && \text{(Corrected error covariance)} \\
&(iii) && \tilde{y}_k &&= y_k - C_k \hat{x}_{k|k-1} && \text{(Innovation/ Measurement residual)} \\
&(iv) && S_k &&= C_k \Gamma_{k|k-1} C_k^T + \Gamma_{\beta_k} && \text{(Innovation covariance)} \\
&(v) && K_k &&= \Gamma_{k|k-1} C_k^T S_k^{-1} && \text{(Kalman gain)}
\end{aligned} \tag{F.2}$$

$$\begin{aligned} (i) \quad \hat{x}_{k+1|k} &= A_k \hat{x}_{k|k} + u_k && \text{(Predicted state estimate)} \\ (ii) \quad \Gamma_{k+1|k} &= A_k \Gamma_{k|k} A_k^T + \Gamma_{\alpha_k} && \text{(Predicted covariance)} \end{aligned} \tag{F.3}$$

Degradation modelling The Kalman filter is used for linear modeling while for non-linear degradation paths, the extended Kalman filter must be used. This thesis focuses on the application of the basic Kalman filter for linear degradation prediction. First, a degradation model must be chosen, for example a linear or log-linear degradation model $D = d_0 + \mu t$. The parameters to be estimated and updated with each new measurement constitute the state space vector, for example $x = \begin{bmatrix} d_0 \\ \mu \end{bmatrix}$. The Kalman filter system will then be :

$$\begin{cases} x_{k+1} = \begin{bmatrix} 1 & 0 \\ 0 & 1 \end{bmatrix} x_k + \begin{bmatrix} 1 \\ 1 \end{bmatrix} u_k + \alpha_k \\ y_k = \begin{bmatrix} 1 & t_k \end{bmatrix} x_k + \beta_k \end{cases} \tag{F.4}$$

y_k are the performance measurements at time t_k. If multiple measurements are performed at once, the covariance value of β_k, is easily measured, otherwise β_k and the parameters covariance α_k are chosen manually, to optimize predictions results. u_k are the aging stress factors (in the case presented here, only one input is considered).

Previously presented models considered data all along aging time. In some cases, the aging process might change, due to some known factors, or to some uncontrollable variables. Experiment #2 of the OLEDWorks experimental plan is a good example of uncontrollable degradation process, where temperature stress level fluctuated, and thus the decay path was not totally linear. Adaptive modeling methods in this case is needed, as the mean time to failure might change depending on the instantaneous stress applied. the most used adaptive online modeling method is the Kalman filter, as it is flexible and adaptive to changes in decay paths. The Kalman filter model used is presented in Eq. F.4 or the equation below, where no inputs are considered in the model since this chapter only focuses on modeling degradation without covariates.

$$\begin{cases} x_{k+1} = \begin{bmatrix} 1 & 0 \\ 0 & 1 \end{bmatrix} x_k + \begin{bmatrix} 0 \\ 0 \end{bmatrix} u_k + \alpha_k \\ y_k = \begin{bmatrix} 1 & t_k \end{bmatrix} x_k + \beta_k \end{cases}$$

The algorithm is based on the set of correction equations and prediction equations presented in Chapter 2 (see Eq. F.2 and Eq. F.3).

$$\begin{aligned} (i) \quad \hat{x}_{k|k} &= \hat{x}_{k|k-1} + K_k \tilde{y}_k && \text{(corrected state estimate)} \\ (ii) \quad \Gamma_{k|k} &= \Gamma_{k|k-1} - K_k C_k \Gamma_{k|k-1} && \text{(Corrected error covariance)} \\ (iii) \quad \tilde{y}_k &= y_k - C_k \hat{x}_{k|k-1} && \text{(Innovation/ Measurement residual)} \\ (iv) \quad S_k &= C_k \Gamma_{k|k-1} C_k^T + \Gamma_{\beta_k} && \text{(Innovation covariance)} \\ (v) \quad K_k &= \Gamma_{k|k-1} C_k^T S_k^{-1} && \text{(Kalman gain)} \end{aligned} \tag{F.2}$$

$$\begin{aligned} (i) \quad \hat{x}_{k+1|k} &= A_k \hat{x}_{k|k} + u_k && \text{(Predicted state estimate)} \\ (ii) \quad \Gamma_{k+1|k} &= A_k \Gamma_{k|k} A_k^T + \Gamma_{\alpha_k} && \text{(Predicted covariance)} \end{aligned} \tag{F.3}$$

The variables used at the beginning of the algorithm, and at each iteration are defined below

- Firstly, initial value of x_k are needed for the algorithm. For this purpose, and since a linear model with two parameters needs at least two points for fitting, a basic linear regression is done for measurements data of the first three inspections $y_{1\to3} = b + at_{1\to3}$, with $x_0 = [b\ a]^T$.

  The choice of the number of data for the initial fitting does affect the convergence of the Kalman filter.

- The error covariance or the parameters covariance is set to be an identity matrix of the size of parameters to be estimated $\Gamma_k = \begin{bmatrix} 1 & 0 \\ 0 & 1 \end{bmatrix}$. This covariance will be updated at each data acquisition.

- For each inspection time, 21 consecutive measurements are taken, to reduce the uncertainty, and thus the variance of each inspection time is taken as the measurement covariance value Γ_{β_k}. The initial value is taken as the maximum of the variance of the measurements at each inspection time from $0 \to 3$.

- The covariance matrix of the parameters error estimation is set to be null $\Gamma_{\alpha_k} = \begin{bmatrix} 0 & 0 \\ 0 & 0 \end{bmatrix}$. It is set arbitrarily, and it will be modified to test its influence later on.

- $A_k = \begin{bmatrix} 1 & 0 \\ 0 & 1 \end{bmatrix}$ is also an identity matrix of the size of parameters to be estimated.

The algorithm runs in the following order:

1. When a new data measurement is acquired, the innovation covariance S_k and then the Kalman gain K_K are computed first.

2. The innovation residual $\tilde{y}$ is computed, then the state estimate $\hat{x}_{k|k}$ and the parameters covariance $\Gamma_{k|k}$ are corrected.

3. After correcting the variables, new parameters $\hat{x}_{k+1|k}$ and their covariance matrix $\hat{\Gamma}_{k+1|k}$ are predicted.

The predicted measurement data $Y_{k+1|k}$ at time t_{k+1} follows the normal distribution

$$Y_{k+1|k} \sim \mathcal{N}(C_{k+1}\hat{x}_{k+1|k}, C_{k+1}\Gamma_{k+1|k}C_{k+1}^T + \Gamma_{\beta_k})$$

where $C_{k+1} = [1\ t_{k+1}]$, and the covariance of $Y_{k+1|k}$ is computed in a similar form as the prediction interval of a regression [56].

Data from experiments #3 and #13 of OLEDWorks are used as a motivating example of the adaptive Kalman filter modeling. The first repetition of experiment 13 had a very pronounced abrupt change between inspection number $j = 10$ and $j = 11$ (see Fig. F.1). Since the Kalman filter is an online modeling method that requires less computation than online linear regression, it can be used to monitor the degradation trajectory to detect and adapt to any abrupt changes. Figure F.1 represents the update of the modeling that the Kalman filter performs at each inspection when new measurements are acquired. It includes the prediction of the time it will take to reach the decay level of the next inspection and the relative error of this prediction, that is $\epsilon_{j+1}(\%) = (t_{j+1} - \hat{t}_{j+1})/t_{j+1}$. It can be seen that until 800 hours, or until the 10^{th} inspection, the prediction error is very minimal ($< 4\%$). However, when an abrupt change occurs, it is normal that the prediction did not consider such rapid decay, so the prediction error reached 30 %. It then re-adapted to the new path after two

new measurements acquisitions, to reach a minimal prediction error again.

Figure F.1 also includes ordinary linear regression (OLR) using measurements from all inspections to compare its performance to online Kalman filter modeling. What can be noted here is that the

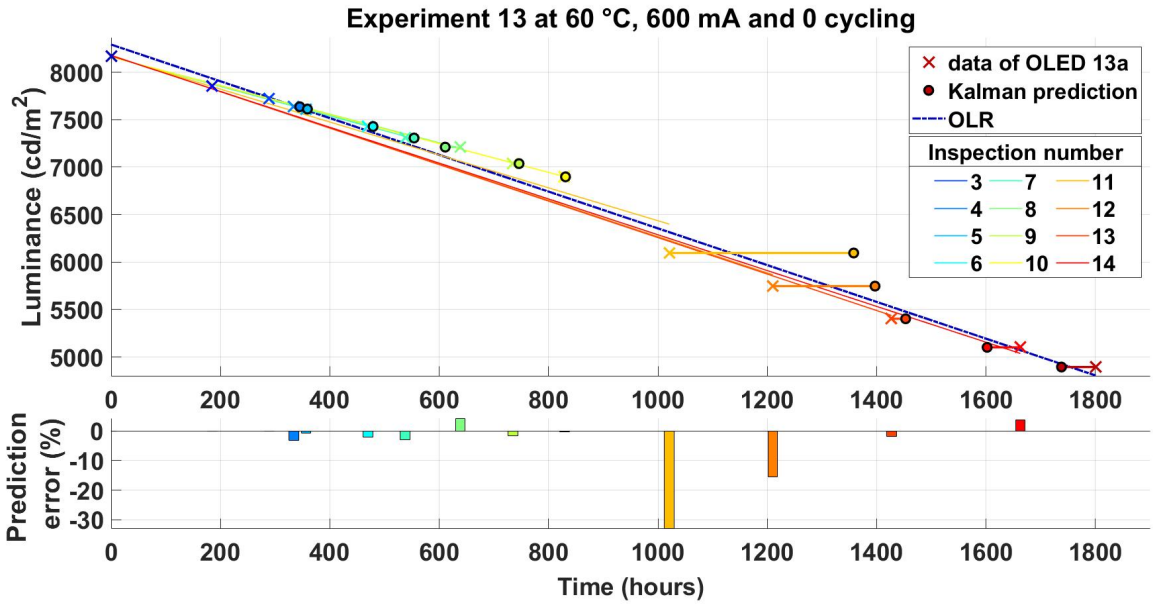

Figure F.1: Online Kalman prediction of experiment #13 from the OLEDWorks experimental plan

Kalman filter respected the initial luminance value, since the 14 decay paths had the same intercept, in contrast to the OLR which had a slightly higher intercept than the initial luminance value, in order to reduce the residuals and improve the regression fit.

The second case studied is experiment #3 from the OLEDWorks experimental plan. This experiment resembles experiment #2 as its OLED was stressed at 30 °C, meaning that the thermal stress was not constant and had fluctuations. Experiment #3 is chosen for Kalman filter modeling as it has more pronounced quadratic decay than experiment #2. Figure F.2 represents the online modeling and prediction of the Kalman filter at each inspection. It also compare the modelled path to the OLR of all data at once. The predicted values along time also had some sort of quadratic path, which implies that the Kalman filter did adapt to this quadratic path, even though the relationship between y and parameters x is linear. In fact, the progressive trajectories were replicating the tangents of the real decay curve, which is usually done for linearizing a quadratic path on a small interval. The more the decay had a quadratic curve shape, the more the prediction error increased though and it reached a maximum value of 15 %.

Keeping in mind that these results were achieved while G_α is set to zero, the Kalman filter did not adapt as needed to the quadratic change. To adjust this problem, G_α is chosen as the uncertainty around the estimated coefficients of the ordinary linear regression applied to the first three data points (found by Eq. 2.29). In the case of experiment #3, the covariance of the process noise factor is $G_\alpha = \begin{bmatrix} 0.031 & 0 \\ 0 & 81.9 \end{bmatrix}$, which is related to the covariance matrix of the linear regression of the first three data measurements. In this case, the adaptive Kalman Filter results are presented in Fig. F.3 where the Kalman filter predictions were very flexible and the prediction errors were extremely reduced to less 5 % per inspection.

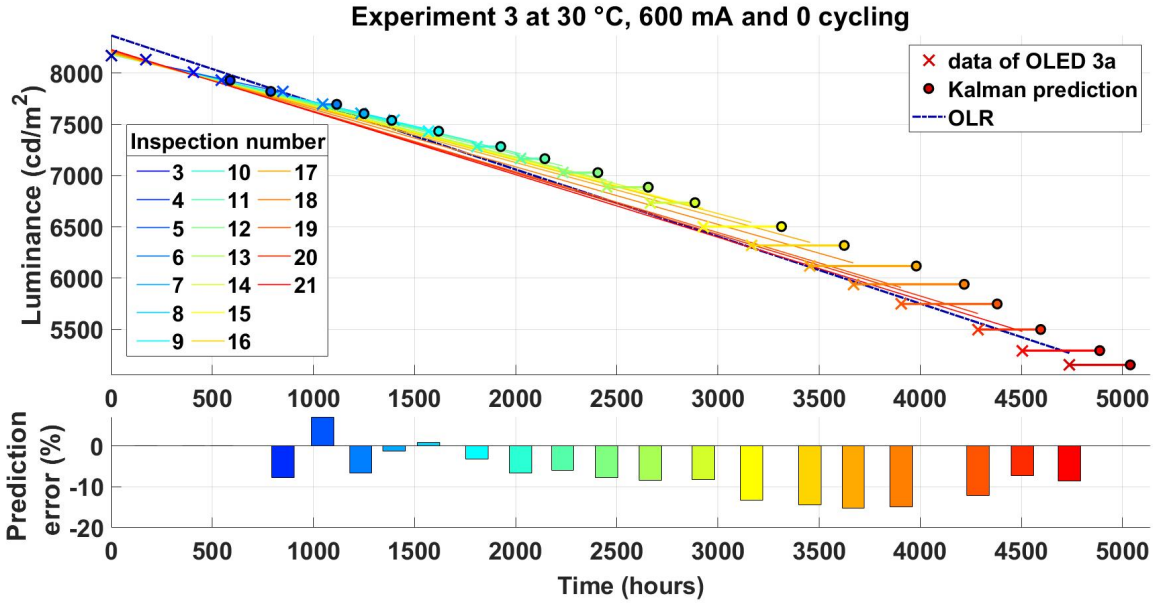

Figure F.2: Online Kalman prediction of experiment #3 from the OLEDWorks experimental plan

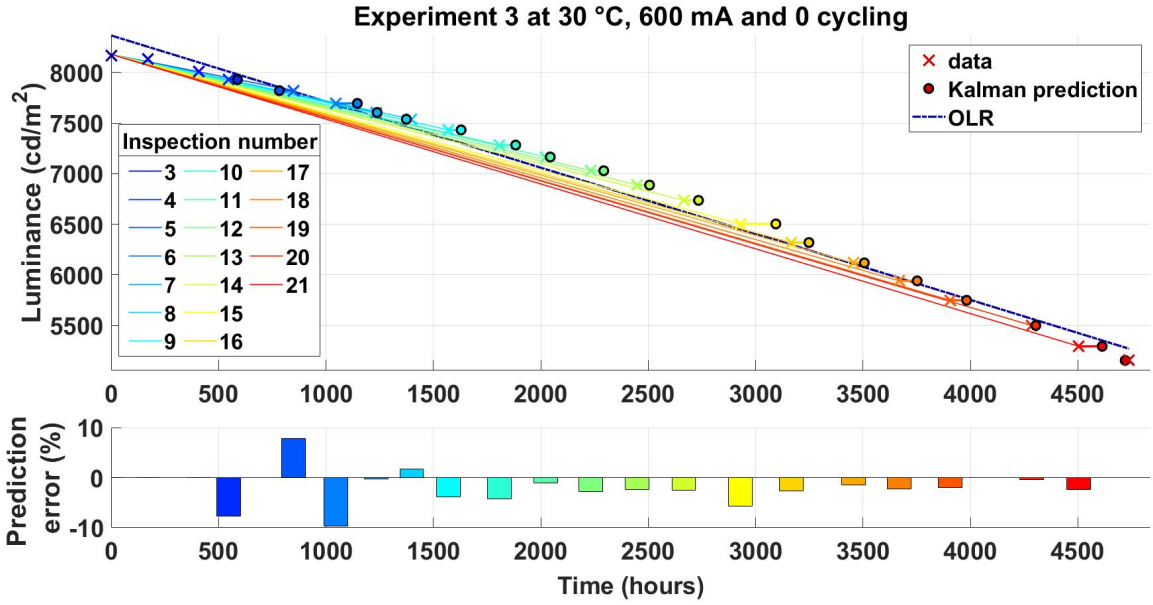

Figure F.3: Online Kalman prediction of experiment #3 from the OLEDWorks experimental plan, when the covariance of the process noise factor is not null.

Lastly, more complex online models based on machine learning algorithms are widely used in the degradation modeling field, as presented in Chapter 2. It may be advantageous to apply these methods to the data, especially if the decay trajectory is not clear, to increase the prediction reliability. However, these models often do not explain how the prediction was made, as they are data-driven black box models. As for nonlinear decay paths, such as the exponential decay of the insulation PDIV, it is recommended to use an extended Kalman filter that takes into account the non-linearity of the model. This is not tested in this thesis but it is a new perspective for future research.

Appendix G

Additional information for chapter 5

G.1 OLEDWorks experimental design: Current and temperature relationship with the intercept

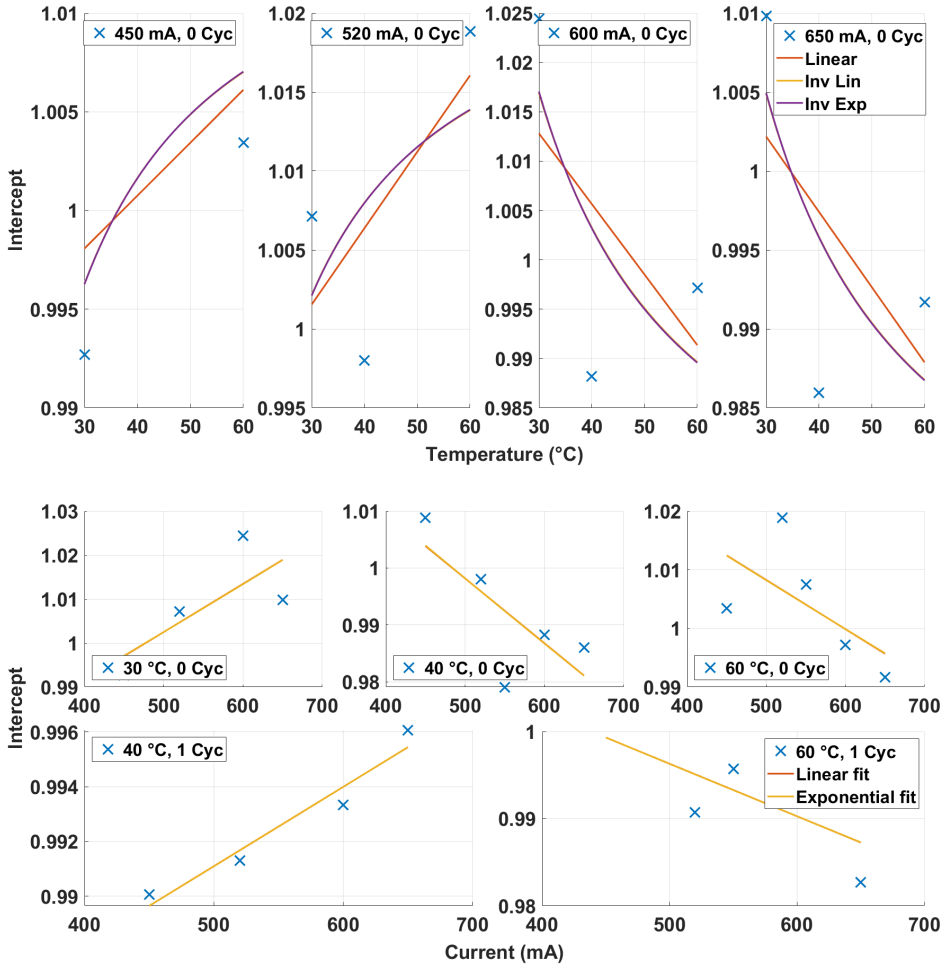

Figure G.1: OLEDWorks experimental plan: Relationship between the estimated intercept of OLR model and temperature, and current for each other stress level

G.2 OLEDWorks experimental design: Model 2 with variation

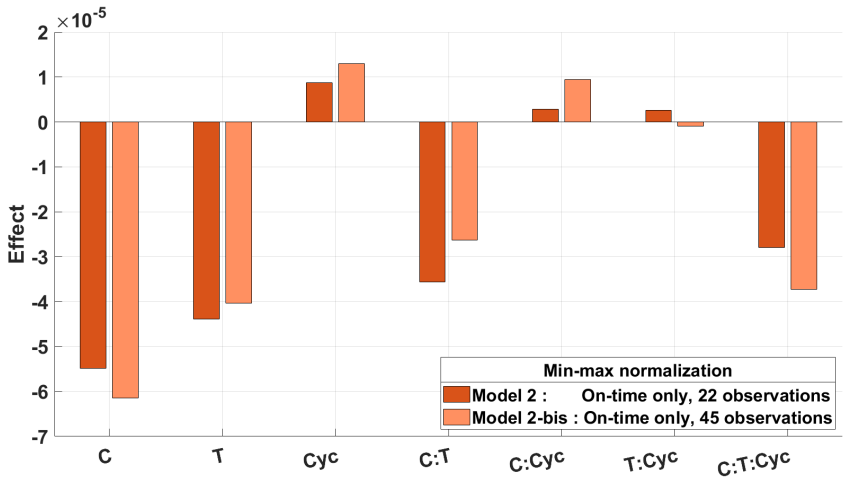

(a)

Covariates	Sum of squares	Degrees of freedom	F
Current	1.2×10^{-7}	1	103.4
Temperature	3.8×10^{-8}	1	32.7
Cycling	2.3×10^{-9}	1	1.98
C:T	2.6×10^{-9}	1	0.23
C:Cyc	5.3×10^{-10}	1	0.45
T:Cyc	3.4×10^{-10}	1	0.8
C:T:Cyc	6.2×10^{-9}	1	5.29
Error	4.3×10^{-8}	37	

(b)

Figure G.2: OLEDWorks experimental design: Effect estimates of model 2, with 45 observations, and its ANOVA table

G.3 Insulator experimental plan: Prediction of PDIV evolution for some experiments below 200 °C

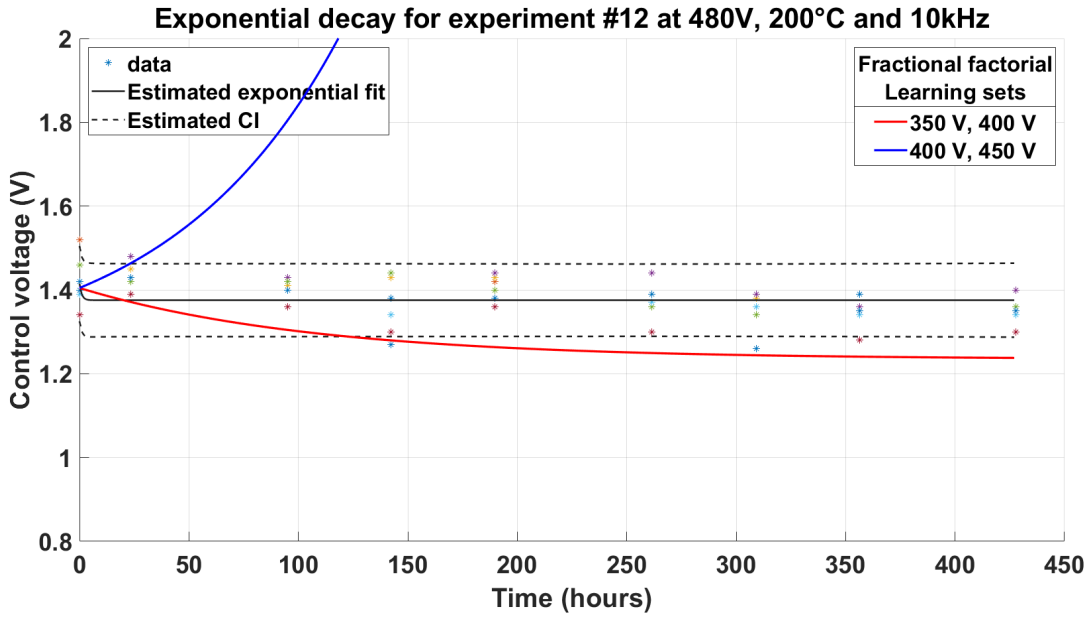

Figure G.3: Insulator experimental design: Prediction of PDIV evolution for experiment 12 at 480 V, 200 °C and 10 kHz

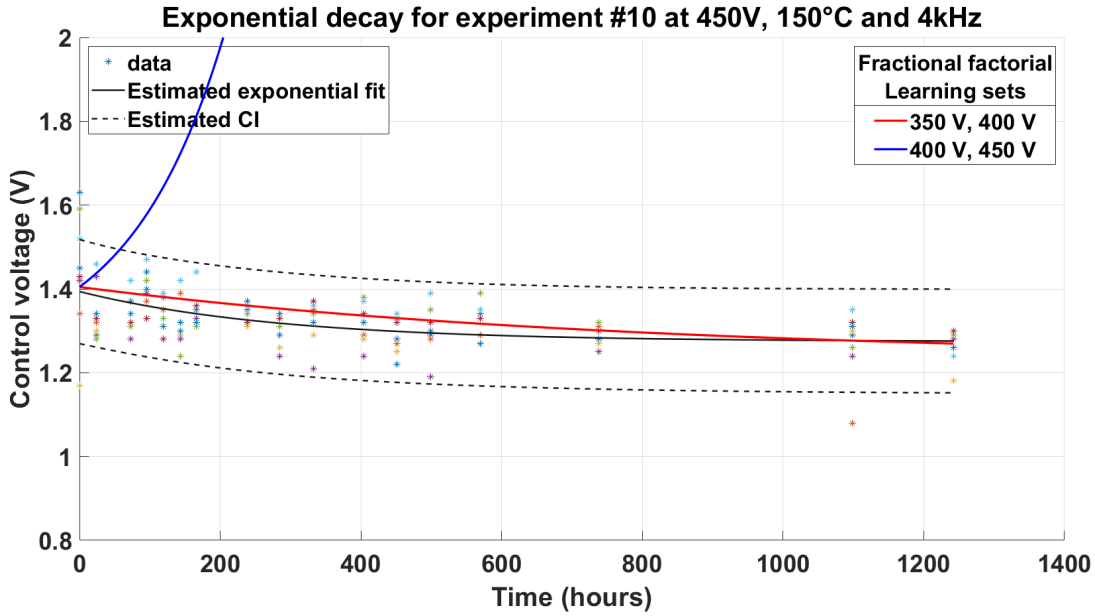

Figure G.4: Insulator experimental design: Prediction of PDIV evolution for experiment 10 at 450 V, 150 °C and 4 kHz

Bibliography

[1] Anderson-darling test, e-handbook of statistical methods, NIST/SEMATECH. url=https://www.itl.nist.gov/div898/handbook/eda/section3/eda35e.htm.

[2] Czech cable car crashes to ground, kills one. https://p.dw.com/p/42PN8. Accessed: 03-05-2022.

[3] Failure mode and effects analysis (fmea). https://asq.org/quality-resources/fmea. Accessed: 06-09-2021.

[4] Fischer tables. http://www3.nccu.edu.tw/~tmhuang/teaching/statistics/tables/f.pdf.

[5] Guide to data cleaning: Definition, benefits, components, and how to clean your data. https://www.tableau.com/learn/articles/what-is-data-cleaning. Accessed: 11-12-2021.

[6] Isal highlights – oled technology and the automotive lighting revolution. https://www.oledworks.com/news/blog/isal-highlights-oled-technology-and-the-automotive-lighting-revolution/. Accessed: 20-05-2022.

[7] Oled light 101. https://www.oledworks.com/resources/oled-light-101/. Accessed: 18-4-2021.

[8] Ieee guide for the statistical analysis of electrical insulation voltage endurance data. *ANSI/IEEE Std 930-1987*, pages 1–28, 1987.

[9] Types of faults in electrical power systems. https://www.electronicshub.org/types-of-faults-in-electrical-power-systems, 2015. Accessed: 11-12-2021.

[10] Mohamed Abdel-Hameed. *Degradation Processes: An Overview*, pages 17–25. Birkhäuser Boston, Boston, MA, 2010.

[11] Beny Maulana Achsan. Support vector machine: Regression. https://medium.com/it-paragon/support-vector-machine-regression-cf65348b6345, December 2019. Accessed: 05-01-2022.

[12] C. J. Adcock. Sample size determination: A review. *Journal of the Royal Statistical Society Series D: The Statistician*, 46(2):261–283, 1997.

[13] J Ahn, D Chung, J Lee, G Lee, M Song, W Lee, W Han, and T Kim. Equivalent circuit Analysis of ITO/Alq 3/Al Organic Light emitting Diode. *Journal of the Korean Physical Society*, 46(2):546–550, 2005.

[14] Andrea Al Haddad, Laurent Canale, Antoine Picot, Georges Zissis, Pascal Maussion, and Pascal Dupuis. Degradation of the luminance and impedance evolution analysis of an oled under thermal and electrical stress. In *IECON 2019 - 45th Annual Conference of the IEEE Industrial Electronics Society*, volume 1, pages 4260–4267, 2019.

[15] Andrea Al Haddad, Antoine Picot, Laurent Canale, Pascal Dupuis, Georges Zissis, and Pascal Maussion. Modeling oled luminance decay under thermal, constant and cyclic electrical stress. In *2021 IEEE Industry Applications Society Annual Meeting (IAS)*, pages 1–6, 2021.

[16] Andrea Al Haddad, Antoine Picot, Laurent Canale, Pascal Dupuis, Georges Zissis, and Pascal Maussion. Prediction of oled luminance using impedance measurements. *IEEE Transactions on Industry Applications*, 58(1):996–1004, 2022.

[17] Andrea al Haddad, Antoine Picot, Laurent Canale, Georges Zissis, and Pascal Maussion. Parametric degradation model of oled using design of experiments (doe). In *2019 IEEE 12th International Symposium on Diagnostics for Electrical Machines, Power Electronics and Drives (SDEMPED)*, pages 432–438, 2019.

[18] Andrea Al Haddad, Antoine Picot, Laurent Canale, Georges Zissis, Pascal Maussion, and Pascal Dupuis. Oled luminance prediction using impedance measurements. In *2020 IEEE Industry Applications Society Annual Meeting*, pages 1–6, 2020.

[19] Alaa Alchaddoud. *Etude du comportement électrique et photométrique des diodes électroluminescentes organiques pour l'éclairage ayant subi un vieillissement accéléré*. PhD thesis, Université Toulouse 3, 2017.

[20] Lee Andresen, David Boud, and Ruth Cohen. Experience-based learning. *Understanding Adult Education and Training*, pages 225–239, 1995.

[21] Tanguy Andrillon. Ces 2021 – lg display : un téléviseur oled transparent et un autre incurvable à l'envi. https://www.lesnumeriques.com/tv-televiseur/ces-2021-lg-display-un-televiseur-oled-transparent-et-un-autre-incurvable-a-l-envi-n159 html, 2021.

[22] D.S. Ang, S. Wang, and C.H. Ling. Evidence of two distinct degradation mechanisms from temperature dependence of negative bias stressing of the ultrathin gate p-mosfet. *IEEE Electron Device Letters*, 26(12):906–908, 2005.

[23] Mohamed Ayadi, Olivier Briat, Richard Lallemand, Gerard Coquery, and Jean-michel Vinassa. Influence of thermal cycling on supercapacitor performance fading during ageing test at constant voltage. In *IEEE 23rd International Symposium on Industrial Electronics (ISIE)*, pages 1823–1828. IEEE, 2014.

[24] Hany Aziz and Zoran D. Popovic. Degradation phenomena in small-molecule organic light-emitting devices. *Chemistry of Materials*, 16(23):4522–4532, 2004.

[25] M M Azrain, M R Mansor, L M Lim, S Zambri, B Cosut, and D Sivakumar. Effect of Discharge Time on the Luminance Output of Organic Light Emitting Diode (Oled). *Journal of Advanced Manufacturing Technology (JAMT)*, 14(2 (1)), 2020.

[26] Claude (1938-2015) Bathias. *Introduction to Fatigue: Fundamentals and Methodology*. ISTE : J. Wiley, London Hoboken (N.J.), 2013.

[27] Oussama Ben Abdellah, Andrea Al Haddad, Mustapha El Halaoui, Pascal Dupuis, Laurent Canale, Adel Asselman, and Georges Zissis. Colorimetric characterizations of large area white oleds under thermal and electrical stress using tm-30-18 method. In *2020 Fifth Junior Conference on Lighting (Lighting)*, pages 1–6, 2020.

[28] Vitor C. Bender, Nórton D. Barth, Fernanda B. Mendes, Rafael A. Pinto, J. Marcos Alonso, and Tiago B. Marchesan. Modeling and characterization of organic light-emitting diodes including capacitance effect. *IEEE Transactions on Electron Devices*, 62(10):3314–3321, 2015.

[29] K.M. Blache and A.B. Shrivastava. Defining failure of manufacturing machinery and equipment. In *Proceedings of Annual Reliability and Maintainability Symposium (RAMS)*, pages 69–75, 1994.

[30] J.R. Black. Mass transport of aluminum by momentum exchange with conducting electrons. In *2005 IEEE International Reliability Physics Symposium, 2005. Proceedings. 43rd Annual.*, pages 1–6, 2005.

[31] Chongrag Boonseng, Repeepornpat Boonseng, and Kunyanuth Kularbphettong. Electrical insulation testing and dga analysis for the diagnosis of insulation faults and failures in 24 mva transformers for distribution systems. In *2020 8th International Conference on Condition Monitoring and Diagnosis (CMD)*, pages 70–73, 2020.

[32] Steven Borris. *Total productive maintenance*, volume 148. MsGraw-Hill, 2005.

[33] L. Boukezzi and A. Boubakeur. Comparison of some neural network algorithms used in prediction of xlpe hv insulation properties under thermal aging. In *2012 IEEE International Conference on Condition Monitoring and Diagnosis*, pages 1218–1222, 2012.

[34] G. E. P. Box and J. S. Hunter. The 2 k-p Fractional Factorial Designs Part I. *Technometrics*, 3(3):311, 1961.

[35] Joan Fisher Box. R . A . Fisher and the Design of Experiments , 1922-1926. *The american statistician*, 34(1):1–7, 1980.

[36] Richard Brown. Degradation of materials. University Lecture, 2007.

[37] W. Brütting, H. Riel, T. Beierlein, and W. Riess. Influence of trapped and interfacial charges in organic multilayer light-emitting devices. *IBM Journal of Research and Development*, 45(1):77–88, 2001.

[38] Kevin Bullis. Tinted windows that generate electricity.

[39] Katherine S. Button, John P. A. Ioannidis, Claire Mokrysz, Brian A. Nosek, Jonathan Flint, Emma S. J. Robinson, and Marcus R. Munafò. Power failure: why small sample size undermines the reliability of neuroscience. *Nature Reviews Neuroscience*, 14(5):365–376, May 2013.

[40] Javier Cabrera and Andrew McDougall. *Statistical Consulting*. Springer-Verlag New York, 1 edition, 2002.

[41] Mara Calvello. How to Go From Product Conception to Manufacturing: A Step-by-Step Guide, 2019.

[42] I. H. Campbell, D. L. Smith, and J. P. Ferraris. Electrical impedance measurements of polymer light-emitting diodes. *Applied Physics Letters*, 3030:3030, 1995.

[43] X. A. Cao, X. M. Li, R. Y. Yang, and Y. M. Zhou. Effects of Localized Heating at Heterointerfaces on the Reliability of Organic Light-Emitting Diodes. *IEEE Electron Device Letters*, 36(8):847–849, 2015.

[44] G. Reza Chaji, Clement Ng, Arokia Nathan, Ansgar Werner, Jan Birnstock, Oliver Schneider, and Jan Blochwitz-Nimoth. Electrical compensation of OLED luminance degradation. *IEEE Electron Device Letters*, 28(12):1108–1110, 2007.

[45] F.X. Che, H.L.J. Pang, W.H. Zhu, and Anthony Y. S. Sun. Cyclic bend fatigue reliability investigation for sn-ag-cu solder joints. In *2006 8th Electronics Packaging Technology Conference*, pages 313–317, 2006.

[46] Y. Q. Chen, X. B. Xu, Z. F. Lei, C. Zeng, X. Y. Liao, Y. F. En, Y. Huang, and W. X. Fang. Effect of hydrogen on electrical properties of metal-ferroelectric (srbi₂ta₂o₉)–insulator (hftao)–silicon capacitor. *IEEE Electron Device Letters*, 36(8):763–765, 2015.

[47] Frederique Chesterman, Bastian Piepers, Tom Kimpe, Patrick De Visschere, and Kristiaan Neyts. Influence of Temperature on the Steady State and Transient Luminance of an OLED Display. *Journal of Display Technology*, 12(11):1268–1277, 2016.

[48] Chih-hua Chiao and Michael Hamada. ROBUST RELIABILITY FOR LIGHT EMITTING DIODES USING DEGRADATION MEASUREMENTS. In *QUALITY AND RELIABlLITY ENGINEERING INTERNATIONAL*, volume 12, 1996.

[49] Takayuki Chiba, Daichi Kumagai, Kazuo Udagawa, Yuichiro Watanabe, and Junji Kido. Dual mode OPV-OLED device with photovoltaic and light-emitting functionalities. *Scientific Reports*, 8(1):1–7, 2018.

[50] A. Chimenton, P. Pellati, and P. Olivo. Analysis of erratic bits in flash memories. *IEEE Transactions on Device and Materials Reliability*, 1(4):179–184, 2001.

[51] Kanghyun Choi, Jongwon Lee, and Jongwoo Park. Nonlinear Mixed Model and Reliability Prediction for OLED Luminance Degradation. *IEEE International Reliability Physics Symposium Proceedings*, 2019-March:1–4, 2019.

[52] P. Chulkin, O. Vybornyi, M. Lapkowski, P. J. Skabara, and P. Data. Impedance spectroscopy of OLEDs as a tool for estimating mobility and the concentration of charge carriers in transport layers. *Journal of Materials Chemistry C*, 6(5):1008–1014, 2018.

[53] Kuan-Jung Chung and Chueh-Chien Hsiao. Accelerated degradation assessment of 18650 lithium-ion batteries. In *2012 International Symposium on Computer, Consumer and Control*, pages 930–933, 2012.

[54] Vincent Couallier. *Comparison of Parametric and Semiparametric Estimates in a Degradation Model with Covariates and Traumatic Censoring*, pages 81–96. Birkhäuser Boston, Boston, MA, 2004.

[55] D. R. Cox. Regression Models and Life-Tables. *Journal of the Royal Statistical Society.1*, 34(2):187–220, 1972.

[56] Philippe Crochet. Adaptive kalman filtering of 2-metre temperature and 10-metre wind-speed forecasts in iceland. *Meteorological Applications*, 11(2):173–187, 2004.

[57] Michael J Curtis, Richard A Bond, Domenico Spina, Amrita Ahluwalia, Stephen P A Alexander, Mark A Giembycz, Annette Gilchrist, Daniel Hoyer, Paul A Insel, Angelo A Izzo, Andrew J Lawrence, David J MacEwan, Lawrence D F Moon, Sue Wonnacott, Arthur H Weston, and John C McGrath. Experimental design and analysis and their reporting: new guidance for publication in bjp. *British Journal of Pharmacology*, 172(14):3461–3471, 2015.

[58] Haifeng Dai, Xiaolong Zhang, Weijun Gu, Xuezhe Wei, and Zechang Sun. A semi-empirical capacity degradation model of ev li-ion batteries based on eyring equation. In *2013 IEEE Vehicle Power and Propulsion Conference (VPPC)*, pages 1–5, 2013.

[59] Thomas W Dakin. Electrical Insulation Deterioration Treated as a Chemical Rate Phenomenon. *AIEE Transactions*, 67:113–122, 1948.

[60] M. Darveniza, D.J.T. Hill, T.T. Le, T.K. Saha, and B. Williams. Chemical degradation of cellulosic insulation paper for power transformers. In *Proceedings of 1994 4th International Conference on Properties and Applications of Dielectric Materials (ICPADM)*, volume 2, pages 780–783 vol.2, 1994.

[61] R.L. de Orio, H. Ceric, and S. Selberherr. Physically based models of electromigration: From black's equation to modern tcad models. *Microelectronics Reliability*, 50(6):775–789, 2010. 2009 Reliability of Compound Semiconductors (ROCS) Workshop).

[62] Lin Deng, Zegui Huang, Zhongyi Cai, and Yunxiang Chen. Step-stress accelerated degradation modeling based on nonlinear wiener process. In *2016 11th International Conference on Reliability, Maintainability and Safety (ICRMS)*, pages 1–5, 2016.

[63] Jay L. Devore. *Probability statistics for engineering and sciences*. Eighth edi edition.

[64] Alexey Kulik Yuliya Mishura Andrey Pilipenko (auth.) Dmytro Gusak, Alexander Kukush. *Theory of Stochastic Processes: With Applications to Financial Mathematics and Risk Theory*. Problem Books in Mathematics. Springer-Verlag New York, 1 edition, 2010.

[65] Guojing Dong, Tao Liu, Minhao Zhang, Qingmin Li, and Zhongdong Wang. Effect of voltage waveform on partial discharge characteristics and insulation life. *Proceedings of the IEEE International Conference on Properties and Applications of Dielectric Materials*, 2018-May:144–147, 2018.

[66] Shaojiang Dong and Tianhong Luo. Bearing degradation process prediction based on the pca and optimized ls-svm model. *Measurement*, 46(9):3143–3152, 2013.

[67] J. Drechsel, M. Pfeiffer, X. Zhou, A. Nollau, and K. Leo. Organic Mip-diodes by p-doping of amorphous wide-gap semiconductors: CV and impedance spectroscopy. *Synthetic Metals*, 127(1-3):201–205, 2002.

[68] K. Dunn. *Process Improvement Using Data, Version: Release*. Number March. 2019.

[69] Pascal Dupuis, Alaa Alchaddoud, Laurent Canale, and Georges Zissis. OLED ageing signature characterization under combined thermal and electrical stresses. *Proceedings of the International Symposium on Electrical Insulating Materials*, pages 311–314, 2014.

[70] Elsayed A. Elsayed. Overview of reliability testing. *IEEE Transactions on Reliability*, 61(2):282–291, 2012.

[71] H. Endicott, B. Hatch, and R. Sohmer. Application of the eyring model to capacitor aging data. *IEEE Transactions on Component Parts*, 12(1):34–41, 1965.

[72] W. Engelmaier. Fatigue life of leadless chip carrier solder joints during power cycling. *IEEE Transactions on Components, Hybrids, and Manufacturing Technology*, 6(3):232–237, 1983.

[73] W. Engelmaier. The use environments of electronic assemblies and their impact on surface mount solder attachment reliability. In *InterSociety Conference on Thermal Phenomena in Electronic Systems*, pages 8–15, 1990.

[74] Luis A. Escobar, William Q. Meeker, Danny L. Kugler, and Laura L. Kramer. Accelerated Destructive Degradation Tests: Data, Models, and Analysis. pages 319–337, 2003.

[75] Rui Fan, Xiaoning Zhang, and Zhentao Tu. Influence of ambient temperature on OLED lifetime and uniformity based on modified equivalent lifetime detection. *Journal of the Society for Information Display*, 27(10):597–607, 2019.

[76] Denis Flandre. Silicon-on-insulator technology for high temperature metal oxide semiconductor devices and circuits. *Materials Science and Engineering: B*, 29(1):7–12, 1995. European Materials Research Society 1994 Spring Meeting Symposium E: High Temperature Electronics: Materials, Devices and Applications.

[77] Stephen R. Forrest. Electronic Appliances on Plastic. *Nature*, 428(6986):911–918, 2004.

[78] David A. Freedman. *Statistical Models: Theory and Practice*. Cambridge University Press, 2 edition, 2009.

[79] Ahmed Gailani, Rehab Mokidm, Mo'ath El-Dalahmeh, Ma'd El-Dalahmeh, and Maher Al-Greer. Analysis of lithium-ion battery cells degradation based on different manufacturers. In *2020 55th International Universities Power Engineering Conference (UPEC)*, pages 1–6, 2020.

[80] Nagi Z. Gebraeel and Mark A. Lawley. A neural network degradation model for computing and updating residual life distributions. *IEEE Transactions on Automation Science and Engineering*, 5(1):154–163, 2008.

[81] Anne Cathrine Gjerde. Multifactor Ageing Models - Origin and Similarities. *IEEE Electrical Insulation Magazine*, pages 6–13, 1997.

[82] H. Gleizer, J.K. Nelson, S. Azizi-Ghannad, and M.J. Embrechts. Application of ultrasonics and neural network techniques to the evaluation of stator bar insulation. In *Proceedings of 1995 Conference on Electrical Insulation and Dielectric Phenomena*, pages 250–253, 1995.

[83] Stephanie Glen. Regularized regression. https://www.statisticshowto.com/regularized-regression. Accessed: 12-08-2021.

[84] Nima Gorjian, Lin Ma, Murthy Mittinty, Prasad Yarlagadda, and Yong Sun. A review on degradation models in reliability analysis. *Engineering Asset Lifecycle Management - Proceedings of the 4th World Congress on Engineering Asset Management, WCEAM 2009*, (September):369–384, 2009.

[85] Nima Gorjian, Lin Ma, Murthy Mittinty, Prasad Yarlagadda, and Yong Sun. A review on reliability models with covariates. In *Proceedings of the 4th World Congress on Engineering Asset Management*, number September, pages 28–30, 2009.

[86] W.V. Green, J. Weertman, and E.G. Zukas. High-temperature creep of polycrystalline graphite. *Materials Science and Engineering*, 6(3):199–211, 1970.

[87] Jiawei Han and Micheline Kamber. *Data Mining: Concepts and Techniques, Second Edition (The Morgan Kaufmann Series in Data Management Systems)*. Morgan Kaufmann, 2006.

[88] Roger M. Harbord and Julian P. T. Higgins. Meta-regression in stata. *The Stata Journal*, 8(4):493–519, 2008.

[89] Yutaka Harima, Kazuhiko Takeda, and Kazuo Yamashita. Molecular solid of zinc tetraphenylporphyrin as a model organic semiconductor with a well-defined depletion layer. *Journal of Physics and Chemistry of Solids*, 56(9):1223–1229, 1995.

[90] E. Henley and H Kumamoto. *Reliability Engineering and Risk Assessment*. Prentice Hall, Upper Saddle River, 1981.

[91] Jpt Higgins, J Thomas, J Chandler, M Cumpston, T Li, M J Page, and V A Welch. *Cochrane Handbook for Systematic Reviews of Interventions version*, volume 6. Cochrane, 2022.

[92] Yili Hong, Yuanyuan Duan, William Q. Meeker, Deborah L. Stanley, and Xiaohong Gu. Statistical methods for degradation data with dynamic covariates information and an application to outdoor weathering data. *Technometrics*, 57(2):180–193, 2015.

[93] Yandong Hou, Datong Liu, and Yu Peng. Accelerated degradation wiener model for lithiumion battery considering individual difference. In *2020 IEEE International Instrumentation and Measurement Technology Conference (I2MTC)*, pages 1–6, 2020.

[94] Jianzheng Hu, Lianqiao Yang, Woong Joon Hwang, and Moo Whan Shin. Thermal and mechanical analysis of delamination in GaN-based light-emitting diode packages. *Journal of Crystal Growth*, 288(1):157–161, 2006.

[95] YanDong Hu, ZhiZhong Hu, and ShuZhen Cao. Theoretical study on manson-coffin equation for physically short cracks and lifetime prediction. *Science China Technological Sciences*, 55(1):34–42, Jan 2012.

[96] Clifford M Hurvichl and Chih-ling Tsai. Model Selection for Extended Quasi-Likelihood Models in Small Samples. *Biometrics*, 51(3):1077–1084, 1995.

[97] International Electrotechnical Vocabulary, Chapter 191 Dependability and quality of service . Standard, International Standards Organization, Geneva, 12 1990.

[98] Electricity metering equipment - Dependability - Part 31-1: Accelerated reliability testing - Elevated temperature and humidity. Standard, International Electrotechnical Commission, Geneva, CH, October 2008.

[99] JunHyuk Im, JunKyu Park, and Jin Hur. Accelerated life test of bearing under electrical stress. In *2018 21st International Conference on Electrical Machines and Systems (ICEMS)*, pages 2501–2504, 2018.

[100] John P. A. Ioannidis. Why most published research findings are false. *PLOS Medicine*, 2(8):null, 08 2005.

[101] Masahiko Ishii and Yasunori Taga. Influence of temperature and drive current on degradation mechanisms in organic light-emitting diodes. *Applied Physics Letters*, 80(18):3430–3432, 2002.

[102] Quality Vocabulary . Standard, International Standards Organization, Geneva, 1986.

[103] Information technology - Vocabulary - Part 14: Reliability, maintainability and availability. Standard, ISO/IEC JTC 1, 12 1997.

[104] C. Iyyappan and C.C. Reddy. Inverse power law based inclusive life model for dc polarity reversal stresses. *IEEE Transactions on Dielectrics and Electrical Insulation*, 28(2):586–593, 2021.

[105] Hevel Jean-Baptiste, Meikang Qiu, Keke Gai, and Lixin Tao. Meta meta-analytics for risk forecast using big data meta-regression in financial industry. In *2015 IEEE 2nd International Conference on Cyber Security and Cloud Computing*, pages 272–277, 2015.

[106] Manikandan Jeeva. The scuffle between two algorithms -neural network vs. support vector machine. https://medium.com/analytics-vidhya/the-scuffle-between-two-algorithms-neural-network-vs-support-vector-machine-16abe0eb418 September 2018.

[107] David G. Jenkins and Pedro F. Quintana-Ascencio. A solution to minimum sample size for regressions. *PLoS ONE*, 15(2):1–15, 2020.

[108] Jaeseong Jeong, Nochang Park, Wonsik Hong, and Changwoon Han. Analysis for the degradation mechanism of photovoltaic ribbon wire under thermal cycling. In *Conference Record of the IEEE Photovoltaic Specialists Conference*, 2011.

[109] Guang Jin, David Matthews, Youwen Fan, and Qiang Liu. Physics of failure-based degradation modeling and lifetime prediction of the momentum wheel in a dynamic covariate environment. *Engineering Failure Analysis*, 2013.

[110] R C St John, N R Draper, and R C St John. D-Optimality for Regression Designs : A Review. 17(1):15–23, 2016.

[111] Christoph Jonda and Andrea B. R. Mayer. Investigation of the electronic properties of organic light-emitting devices by impedance spectroscopy. *Chemistry of Materials*, 11(9):2429–2435, 1999.

[112] V. Roshan Joseph and I. Tang Yu. Reliability improvement experiments with degradation data. *IEEE Transactions on Reliability*, 55(1):149–157, 2006.

[113] Chang-jung Juan and Ming-jong Tsai. Implementation of a Novel System for Measuring the Lifetime of OLED Panels. *2 IEEE Transactions on Consumer Electronics*, 49(1):1–5, 2003.

[114] Waltraud Kahle and Axel Lehmann. *The Wiener Process as a Degradation Model: Modeling and Parameter Estimation*, pages 127–146. Birkhäuser Boston, Boston, MA, 2010.

[115] Bill Kappele. *Blind Analysis for Design of Experiments and Response Surface Methodology*. 2017.

[116] Lin Ke, Soo Jin Chua, Keran Zhang, and Peng Chen. Bubble formation due to electrical stress in organic light emitting devices. *Applied Physics Letters*, 80(2):171–173, 2002.

[117] Will Kenton. Stochastic modeling. https://www.investopedia.com/terms/s/stochastic-modeling.asp, 2021. Accessed: 06-01-2022.

[118] Youngjoo Kim and Hyochoong Bang. Introduction to kalman filter and its applications. In Felix Govaers, editor, *Introduction and Implementations of the Kalman Filter*, chapter 2. IntechOpen, Rijeka, 2019.

[119] H. Kirkici. Electrical insulation in space environment. In *2001 Annual Report Conference on Electrical Insulation and Dielectric Phenomena (Cat. No.01CH37225)*, pages 16–19, 2001.

[120] Georgia Ann Klutke, Peter C. Kiessler, and M. A. Wortman. A critical look at the bathtub curve. *IEEE Transactions on Reliability*, 52(1):125–129, 2003.

[121] S. Koh, Willem Van Driel, and G.Q. Zhang. Degradation of epoxy lens materials in led systems. In *2011 12th Intl. Conf. on Thermal, Mechanical Multi-Physics Simulation and Experiments in Microelectronics and Microsystems*, pages 1/5–5/5, 2011.

[122] Voitto I.J. Kokko. Ageing due to thermal cycling by power regulation cycles in lifetime estimation of hydroelectric generator stator windings. *Proceedings - 2012 20th International Conference on Electrical Machines, ICEM 2012*, pages 1559–1564, 2012.

[123] Alice Y. Kolb and David A. Kolb. Experiential learning theory: A dynamic, holistic approach to management learning, education and development. *The SAGE Handbook of Management Learning, Education and Development*, (May 2015):42–68, 2009.

[124] Dejing Kong, Narayanaswamy Balakrishnan, and Lirong Cui. Two-Phase Degradation Process Model With Abrupt Jump at Change Point Governed by Wiener Process. *IEEE TRANSACTIONS ON RELIABILITY*, 66(4):1345–1360, 2017.

[125] J.D. Kueck, J.C. Criscoe, and N.M. Burstein. Assessment of valve actuator motor rotor degradation by fourier analysis of current waveform. In *IEEE Conference on Nuclear Science Symposium and Medical Imaging*, pages 694–696 vol.1, 1992.

[126] D. M. Kulawansa and E. R. Menzel. Diagnostics of Radiation Exposure of Dielectrics by Fluorescence Techniques. *IEEE Transactions on Dielectrics and Electrical Insulation*, 2(3):503–505, 1995.

[127] Kiyeol Kwak, Kyoungah Cho, and Sangsig Kim. Analysis of thermal degradation of organic light-emitting diodes with infrared imaging and impedance spectroscopy. *Optics Express*, 21(24):29558, 2013.

[128] Sun Kap Kwon, Ji Ho Baek, Hyun Chul Choi, Seong Keun Kim, Raju Lampande, Ramchandra Pode, and Jang Hyuk Kwon. Degradation of OLED performance by exposure to UV irradiation. *RSC Advances*, 9(72):42561–42568, 2019.

[129] Keith J. Laidler. The development of the arrhenius equation. *Journal of Chemical Education*, 61(6):494–498, 1984.

[130] Pradeep Lall, Junchao Wei, and Lynn Davis. Prediction of lumen output and chromaticity shift in leds using kalman filter and extended kalman filter based models. In *2013 IEEE Conference on Prognostics and Health Management (PHM)*, pages 1–14, 2013.

[131] Debbie A Lawlor and Stephen W Hopker. The effectiveness of exercise as an intervention in the management of depression: systematic review and meta-regression analysis of randomised controlled trials. *BMJ*, 322(7289):763, 2001.

[132] Soon-seok Lee. Parameter Analysis of an Organic Light-Emitting Diode (OLED). *Journal of the Korean Physical Society*, 53(2):840–844, 2008.

[133] E. Levi and M. Wang. Impact of parameter variations on speed estimation in sensorless rotor flux oriented induction machines. In *1998 Seventh International Conference on Power Electronics and Variable Speed Drives (IEE Conf. Publ. No. 456)*, pages 305–310, 1998.

[134] Chao Li and Yanyan Hu. On-line degradation estimation of proton exchange membrane fuel cell based on imm-ekf. In *2020 Chinese Automation Congress (CAC)*, pages 6668–6672, 2020.

[135] Nuo Li, Xindong Gao, Baofu Ding, Xiaoyu Sun, Xunmin Ding, and Xiaoyuan Hou. Determination of capacitance-voltage characteristics of organic semiconductor devices by combined current-voltage and voltage decay measurements. *Science China Technological Sciences*, 54(4):826–829, 2011.

[136] Song Li, Zhiyong Chen, Qiaobin Liu, Wenku Shi, and Kunheng Li. Modeling and Analysis of Performance Degradation Data for Reliability Assessment: A Review. *IEEE Access*, 8:74648–74678, 2020.

[137] Wenjian Li and Hoang Pham. Reliability modeling of multi-state degraded systems with multi-competing failures and random shocks. *IEEE Transactions on Reliability*, 54(2):297–303, 2005.

[138] X. Li, M. J. Er, B. S. Lim, J. H. Zhou, O. P. Gan, and L. Rutkowski. Fuzzy regression modeling for tool performance prediction and degradation detection. *International Journal of Neural Systems*, 20(5):405–419, 2010.

[139] Xiaomeng Li and Xian An Cao. Degradation of phosphorescent organic light-emitting diodes under pulsed current stressing. *Organic Electronics*, 14(10):2523–2527, 2013.

[140] Wlamir Olivares Loesch Vianna, Luiz Gonzaga de Souza Ribeiro, and Takashi Yoneyama. Electro hydraulic servovalve health monitoring using fading extended kalman filter. In *2015 IEEE Conference on Prognostics and Health Management (PHM)*, pages 1–6, 2015.

[141] Salvatore Lombardo, James H. Stathis, Barry P. Linder, Kin Leong Pey, Felix Palumbo, and Chih Hang Tung. Dielectric breakdown mechanisms in gate oxides. *Journal of Applied Physics*, 98(12):121301, 2005.

[142] Huang Lorick. Lecture notes in Introduction to Lévy Processes, 2021.

[143] Lumiblade OLED Panel Brite FL300 ww, E353273 datasheet. *OLEDWorks LLC*, 2016.

[144] B. O.Y. Lydell. Pipe failure probability - the Thomas paper revisited. *Reliability Engineering and System Safety*, 68(3):207–217, 2000.

[145] Cartlidge D. M., Casson D. W., Franklin D. E., Macdonald J. A., and Pollock B. C. *Machine Condition Monitoring : Ozone Monitor for Air Cooled Generators*. Canadian Electrical Association, 1994.

[146] K.P. Mardira, M. Darveniza, and T.K. Saha. Search for new diagnostics for metal oxide surge arrester. In *Proceedings of the 6th International Conference on Properties and Applications of Dielectric Materials (Cat. No.00CH36347)*, volume 2, pages 947–950 vol.2, 2000.

[147] George Marsaglia and John Marsaglia. Evaluating the anderson-darling distribution. *Journal of Statistical Software*, 9(2):1–5, 2004.

[148] M.C.A. Mathur, G.F. Hudson, R.J. Martin, W.A. McKinley, and L.D. Hackett. Kinetic studies of iron metal particle degradation at various temperature and humidity conditions. *IEEE Transactions on Magnetics*, 27(6):4675–4677, 1991.

[149] G. Mazzanti. The combination of electro-thermal stress, load cycling and thermal transients and its effects on the life of high voltage ac cables. *IEEE Transactions on Dielectrics and Electrical Insulation*, 16(4):1168–1179, 2009.

[150] William Q. Meeker, Luis A. Escobar, and C. Joseph Lu. Accelerated Degradation Tests: Modeling and Analysis. *Technometrics*, 40(2):89–99, 1998.

[151] Milton A. Miner. Cumulative Damage in Fatigue. *Journal of Applied Mechanics*, 12(3):A159–A164, 03 1945.

[152] Davoud Esmaeil Moghadam, Christoph Herold, and Rolf Zbinden. Effects of Resins on Partial Discharge Activity and Lifetime of Insulation Systems Used in eDrive Motors and Automotive Industries. *2020 IEEE Electrical Insulation Conference, EIC 2020*, pages 221–224, 2020.

[153] Max D. Morris. Three "Technometrics" Experimental Design Classics. *Technometrics*, 42(1):26, 2000.

[154] Praveen Kumar N., Vinothraj C., and Isha T.B. Effect of wear and tear bearing fault in induction motor drives using fem. In *2018 IEEE International Conference on Power Electronics, Drives and Energy Systems (PEDES)*, pages 1–6, 2018.

[155] Takuya Nakamura, Oga Kataoka, Hidenori Yoshimura, Hideyuki Hirata, Shuxiang Guo, and Kazunari Fujiyama. Modelling of creep property of base material for life assessment of mod.9cr-1mo steel welded joint. In *2019 IEEE International Conference on Mechatronics and Automation (ICMA)*, pages 2100–2104, 2019.

[156] Nishant Narayan, Thekla Papakosta, Victor Vega-Garita, Zian Qin, Jelena Popovic-Gerber, Pavol Bauer, and Miroslav Zeman. Estimating battery lifetimes in Solar Home System design using a practical modelling methodology. *Applied Energy*, 228:1629–1639, 2018.

[157] Bechara Nehme, Nacer K M'Sirdi, Tilda Akiki, and Barbar Zeghondy. Assessing the effect of temperature on degradation modes of pv panels. In *2020 5th International Conference on Renewable Energies for Developing Countries (REDEC)*, pages 1–4, 2020.

[158] Wayne Nelson. Accelerated life testing - step-stress models and data analyses. *IEEE Transactions on Reliability*, R-29(2):103–108, 1980.

[159] Wayne Nelson. Analysis of Performance-Degradation Data from Accelerated Tests. *IEEE Transactions on Reliability*, R-30(2):149–155, 1981.

[160] Wayne B. Nelson. *Accelerated Testing: Statistical Models, Test Plans, and Data Analysis*, volume 41. Wiley-Interscience, 1990.

[161] Thomy H. Nilsson. Photometric specification of images. *Journal of Modern Optics*, 56(13):1523–1535, 2009.

[162] Stefan Nowy, Wei Ren, Andreas Elschner, Wilfried Lövenich, and Wolfgang Brütting. Impedance spectroscopy as a probe for the degradation of organic light-emitting diodes. *Journal of Applied Physics*, 107(5), 2010.

[163] Michael Orey. *Emerging Perspectives on Learning, Teaching, and Technology*. 2010.

[164] John W Osenbach. Corrosion-induced degradation of microelectronic devices. 11(2):155–162, feb 1996.

[165] Rémy Ouaida, Maxime Berthou, Javier León, Xavier Perpiñà, Sebastien Oge, Pierre Brosselard, and Charles Joubert. Gate oxide degradation of sic mosfet in switching conditions. *IEEE Electron Device Letters*, 35(12):1284–1286, 2014.

[166] Huiqing Pang, Lech Michalski, Michael S Weaver, Ruiqing Ma, and Julie J Brown. Thermal behavior and indirect life test of large-area OLED lighting panels. *Journal of Solid State Lighting*, 1(1):7, 2014.

[167] N. C. Park, W. W. Oh, and D. H. Kim. Effect of temperature and humidity on the degradation rate of multicrystalline silicon photovoltaic module. *International Journal of Photoenergy*, 2013:925280, Dec 2013.

[168] M.R. Parker, S. Venkataram, and D. DeSmet. Magnetic and magneto-photoellipsometric evaluation of corrosion in metal-particle media. *IEEE Transactions on Magnetics*, 28(5):2368–2370, 1992.

[169] Devyani Patra, Ahmed Kamal Reza, Mehdi Katoozi, Ethan H. Cannon, Kaushik Roy, and Yu Cao. Accelerated bti degradation under stochastic tddb effect. In *2018 IEEE International Reliability Physics Symposium (IRPS)*, pages 5C.5–1–5C.5–4, 2018.

[170] Kreczanik Paul, Martin Christian, Venet Pascal, Clerc Guy, Rojat Gerard, and Zitouni Younes. Constant power cycling for accelerated ageing of supercapacitors. *Power*, (2009):1–10, 2009.

[171] D. Stewart Peck. Comprehensive model for humidity testing correlation. In *24th International Reliability Physics Symposium*, pages 44–50, 1986.

[172] M. Petelin and A. Fix. Comparison of metals in their steadiness to pulse-periodic microwave heating fatigue. In *2009 IEEE International Vacuum Electronics Conference*, pages 163–164, 2009.

[173] G Peyrache. article sur la fiabilité. *Encyclopaedia Universalis*, 6:1059, 1968.

[174] A. Pinato, M. Meneghini, A. Cester, N. Wrachien, A. Tazzoli, E. Zanoni, G. Meneghesso, B. D'Andrade, J. Esler, S. Xia, and J. Brown. Improved reliability of organic light-emitting diodes with indium-zinc-oxide anode contact. *IEEE International Reliability Physics Symposium Proceedings*, pages 105–108, 2009.

[175] E. Pinotti, A. Sassella, A. Borghesi, and R. Paolesse. Characterization of organic semiconductors by a large-signal capacitance-voltage method at high and low frequencies. *Synthetic Metals*, 138(1-2):15–19, 2003.

[176] Plackett R. L. and Burman J . P. THE DESIGN OF OPTIMUM MULTIFACTORIAL EXPERIMENTS. *Biometrika*, 33(4):305–325, 1946.

[177] Yuning Qian, Ruqiang Yan, and Shijie Hu. Bearing degradation evaluation using recurrence quantification analysis and kalman filter. *IEEE Transactions on Instrumentation and Measurement*, 63(11):2599–2610, 2014.

[178] K. Sudheendra Rao and Y.N. Mohapatra. Disentangling degradation and auto-recovery of luminescence in alq3 based organic light emitting diodes. *Journal of Luminescence*, 145:793–796, 2014.

[179] Marvin Rausand and Arnljot Hoyland. *System reliability theory: Models, Statistical Methods, and Applications*. 1996.

[180] Martin Riera-Guasp, Manés Fernández Cabanas, Jose A. Antonino-Daviu, Manuel Pineda-Sánchez, and Carlos H. Rojas García. Influence of nonconsecutive bar breakages in motor current signature analysis for the diagnosis of rotor faults in induction motors. *IEEE Transactions on Energy Conversion*, 25(1):80–89, 2010.

[181] S. C. Roberts and J. Peter. Discussion on: Review of motor insulations with special reference to breakdowns by discharges encountered in the mining industry. *Transactions of the South African Institute of Electrical Engineers*, 52(12):322–325, 1961.

[182] Farah Salameh. *Méthodes de modélisation statistique de la durée de vie des composants en génie électrique*. PhD thesis, 2016.

[183] Farah Salameh, Andrea Al Haddad, Antoine Picot, Laurent Canale, Georges Zissis, Marie Chabert, and Pascal Maussion. Modeling the luminance degradation of oleds using design of experiments. *IEEE Transactions on Industry Applications*, 55(6):6548–6558, 2019.

[184] Farah Salameh, Antoine Picot, Laurent Canale, Georges Zissis, Marie Chabert, and Pascal Maussion. Parametric lifespan models for OLEDs using Design of Experiments (DoE). *2018 IEEE Industry Applications Society Annual Meeting, IAS 2018*, (September 2013):1–11, 2018.

[185] P K Samanta, W E Vesley, F Hsu, and M Subudhi. Degradation Modeling with Application-to Aging and Maintenance Effectiveness Evaluations. In *18. water reactor safety information meeting*, 1991.

[186] S. Savin, S. Ait-Amar, D. Roger, and G. Vélu. Aging effects on the AC motor windings: A correlation between the variation of turn-to-turn capacitance and the PDIV. *Annual Report - Conference on Electrical Insulation and Dielectric Phenomena, CEIDP*, pages 64–67, 2011.

[187] Philipp Schwamb, Thilo C.G. Reusch, and Christoph J. Brabec. Passive cooling of large-area organic light-emitting diodes. *Organic Electronics*, 2013.

[188] Gideon Schwarz. Estimating the Dimension of a Model. *The Annals of Statistics*, 6(2):461 – 464, 1978.

[189] George A. F. Seber and Alan J.Lee. *Linear Regression Analysis*. John Wiley Sons, Inc., 2003.

[190] F. I. Sempurna, Sirliyani, Y. P. Handoko, I. M. Nurdin, and H. Devianto. Effect of start-stop cycles and hydrogen temperature on the performance of proton exchange membrane fuel cell (pemfc). In *2014 International Conference on Electrical Engineering and Computer Science (ICEECS)*, pages 27–29, 2014.

[191] Lijuan Shen, Yudong Wang, Qingqing Zhai, and Yincai Tang. Degradation modeling using stochastic processes with random initial degradation. *IEEE Transactions on Reliability*, 68(4):1320–1329, 2019.

[192] Tseng Sheng-Tsaing and Yu Hong-Fwu. A termination rule for degradation experiments. *IEEE Transactions on Reliability*, 46(1):130–133, 1997.

[193] H. J. Shin, M. C. Jung, J. Chung, K. Kim, J. C. Lee, and S. P. Lee. Degradation mechanism of organic light-emitting device investigated by scanning photoelectron microscopy coupled with peel-off technique. *Applied Physics Letters*, 89(6):87–90, 2006.

[194] Sergei Shipilov. *Catastrophic Failures due to Environment-Assisted Cracking of Metals: Case Histories*, pages 225–241. 08 1999.

[195] D.M Shprekher, G. I. Babokin, and E. B Kolesnikov. Application of neural networks for prediction of insulation condition in networks with isolated neutral. In *2019 International Russian Automation Conference (RusAutoCon)*, pages 1–6, 2019.

[196] Xiao Sheng Si, Wenbin Wang, Chang Hua Hu, Dong Hua Zhou, and Michael G. Pecht. Remaining useful life estimation based on a nonlinear diffusion degradation process. *IEEE Transactions on Reliability*, 61(1):50–67, 2012.

[197] Vishwanath A. Sindagi and Sumit Srivastava. Oled panel defect detection using local inlier-outlier ratios and modified lbp. In *2015 14th IAPR International Conference on Machine Vision Applications (MVA)*, pages 214–217, 2015.

[198] Sakshi Singh, M. M. Mohsin, and Aejaz Masood. Prediction of breakdown strength of non-cellulosic insulating materials using artificial neural networks. In *2017 14th IEEE India Council International Conference (INDICON)*, pages 1–4, 2017.

[199] Archana Sinha, Hamsini Gopalakrishna, Arun Bala Subramaniyan, Deepak Jain, Jaewon Oh, Dirk Jordan, and GovindaSamy TamizhMani. Prediction of climate-specific degradation rate for photovoltaic encapsulant discoloration. *IEEE Journal of Photovoltaics*, 10(4):1093–1101, 2020.

[200] Kandler Smith, Ying Shi, and Shriram Santhanagopalan. Degradation mechanisms and lifetime prediction for lithium-ion batteries — a control perspective. In *2015 American Control Conference (ACC)*, pages 728–730, 2015.

[201] Grigorii L. Soloveichik. Regenerative fuel cells for energy storage. *Proceedings of the IEEE*, 102(6):964–975, 2014.

[202] T. D. Stanley and Stephen B. Jarrell. Meta-regression analysis: A quantitative method of literature surveys. *Journal of Economic Surveys*, 19(3):299–308, 2005.

[203] M. A. Stephens. Edf statistics for goodness of fit and some comparisons. *Journal of the American Statistical Association*, 69(347):730–737, 1974.

[204] M Stolka. *"Organic Light Emitting Diodes (OLEDs) for General Illumination Update 2002"*. 2002.

[205] G. C. Stone, M. Sasic, D. Dunn, and I. Culbert. Recent problems experienced with motor and generator windings. *2009 Record of Conference Papers - Industry Applications Society 56th Annual Petroleum and Chemical Industry Conference, PCIC 2009*, pages 1–9, 2009.

[206] Greg C. Stone, Ian Culbert, Edward A. Boulter, and Hussein Dhirani. *Electrical Insulation for Rotating Machines*. 2014.

[207] Malgorzata Sumislawska, Konstantinos N. Gyftakis, Darren F. Kavanagh, Malcolm D. McCulloch, Keith J. Burnham, and David A. Howey. The Impact of Thermal Degradation on Properties of Electrical Machine Winding Insulation Material. *IEEE Transactions on Industry Applications*, 52(4):2951–2960, 2016.

[208] Chuang Sun, Zhousuo Zhang, and Zhengjia He. Research on bearing life prediction based on support vector machine and its application. *Journal of Physics: Conference Series*, 305:012028, jul 2011.

[209] Fuqiang Sun, Xiao-Yang Li, and Tongmin Jiang. Statistical analysis of constant-stress accelerated degradation testing with multiple performance parameters. *Transactions- Canadian Society for Mechanical Engineering*, 40:631–644, 12 2016.

[210] Mateusz Szczepanski. *Development of methods allowing the test and the comparison of low-voltage motors insulation systems running under partial discharges (fed by inverter)*. PhD thesis, Univ. Paul Sabatier - Toulouse III, 2019.

[211] Hideo Tanaka, Satoru Uejima, and Kiyoji Asai. Linear regression analysis with fuzzy model. *IEEE Transactions on Systems, Man, and Cybernetics*, 12(6):903–907, 1982.

[212] C. W. Tang and S. A. Vanslyke. Organic electroluminescent diodes. *Applied Physics Letters*, 51(12):913–915, 1987.

[213] L. C. Thomas. A survey of maintenance and replacement models for maintainability and reliability of multi-item systems. *Reliability Engineering*, 16(4):297–309, 1986.

[214] Dimitri Torregrossa and Mario Paolone. Novel experimental investigation of supercapacitor ageing during combined life-endurance and power-cycling tests. *IECON Proceedings (Industrial Electronics Conference)*, pages 1779–1785, 2013.

[215] Giulio Torrente. *Investigation of degradation mechanisms and related performance concerns in 40nm NOR Flash memories*. PhD thesis, Université Grenoble Alpes, 2017.

[216] Oliver Triebl. *Reliability Issues in High-Voltage Semiconductor Devices*. PhD thesis, 2012.

[217] US Department of Energy. Solid-State Lighting Technology Fact Sheet. Technical report, 2016.

[218] Vladimir N. Vapnik. *Statistics for Engineering and Information Science*. second edi edition, 2000.

[219] W E Vesely and P K Samanta. Applications of reliability degradation analysis. *Other Information: PBD: Feb 1996*, page Medium: ED; Size: 43 p., 1996.

[220] Felipe A.C. Viana. A Tutorial on Latin Hypercube Design of Experiments. *Quality and Reliability Engineering International*, 32(5):1975–1985, 2016.

[221] Scott I. Vrieze. Model selection and psychological theory: A discussion of the differences between the akaike information criterion (aic) and the bayesian information criterion (bic). *Psychological Methods vol. 17 iss. 2*, 17, 2012.

[222] Xing Wan. The effect of regularization coefficient on polynomial regression. *Journal of Physics: Conference Series*, 1213(4), 2019.

[223] Peng Wang, Robert X. Gao, and Wojbor A. Woyczynski. Lévy process-based stochastic modeling for machine performance degradation prognosis. *IEEE Transactions on Industrial Electronics*, 68(12):12760–12770, 2021.

[224] Zezhong Wang, Chengrong Li, Pai Peng, Lijian Ding, Yimei Jia, Wei Wang, and Jingchun Wang. Partial discharge recognition of stator winding insulation based on artificial neural network. In *Conference Record of the 2000 IEEE International Symposium on Electrical Insulation (Cat. No.00CH37075)*, pages 9–12, 2000.

[225] Philipp Wellmann, Michael Hofmann, Olaf Zeika, Ansgar Werner, Jan Birnstock, Rico Meerheim, Gufeng He, Karsten Walzer, Martin Pfeiffer, and Karl Leo. High-efficiency p-i-n organic light-emitting diodes with long lifetime. *Journal of the Society for Information Display*, 2005.

[226] Xiao Ming Xu, Wen Qing Zhu, Qiang Wang, Zhi Lin Zhang, and Xue Yin Jiang. Study on the degradation of sealed organic light-emitting diodes under constant current. *2009 International Conference on Electronic Packaging Technology and High Density Packaging, ICEPT-HDP 2009*, 3:778–781, 2009.

[227] R. Y. Yang and X. A. Cao. Thermal and nonthermal factors affecting the lifetime of blue phosphorescent organic light-emitting diodes. *IEEE Transactions on Electron Devices*, 2018.

[228] Hua Ye, Cemal Basaran, and Douglas C. Hopkins. Mechanical degradation of microelectronics solder joints under current stressing. *International Journal of Solids and Structures*, 40(26):7269–7284, 2003.

[229] Zhi Sheng Ye, Nan Chen, and Yan Shen. A new class of Wiener process models for degradation analysis. *Reliability Engineering and System Safety*, 139:58–67, 2015.

[230] Zhi Sheng Ye, Loon Ching Tang, and Hai Yan Xu. A distribution-based systems reliability model under extreme shocks and natural degradation. *IEEE Transactions on Reliability*, 60(1):246–256, 2011.

[231] Hang You, Jun Fu, and Xi Li. Research on ecsa degradation model for pem fuel cell under vehicle conditions. In *2020 4th CAA International Conference on Vehicular Control and Intelligence (CVCI)*, pages 573–577, 2020.

[232] Hong F. Yu and Sheng Tsaing Tseng. Designing a degradation experiment. *Naval Research Logistics*, 46(6):689–706, 1999.

[233] Jianping Zhang, Wenbin Li, Guoliang Cheng, Xiao Chen, Helen Wu, and M. H. Herman Shen. Life prediction of OLED for constant-stress accelerated degradation tests using luminance decaying model. *Journal of Luminescence*, 154:491–495, 2014.

[234] Jianping Zhang, Tingjun Zhou, Helen Wu, Yu Wu, Wenli Wu, and Jianxing Ren. Constant-step-stress accelerated life test of white OLED under weibull distribution case. *IEEE Transactions on Electron Devices*, 59(3):715–720, 2012.

[235] Qin Zhang, Jian Zhang, Youtong Fang, Xiaoyan Huang, Jinhao Shen, and Ziang Li. Research on thermo-electric degradation tests based on polyimide degradation data. In *2021 IEEE 12th Energy Conversion Congress Exposition - Asia (ECCE-Asia)*, pages 2432–2437, 2021.

[236] Xinghui Zhang, Lei Xiao, and Jianshe Kang. Degradation prediction model based on a neural network with dynamic windows. *Sensors (Switzerland)*, 15(3):6996–7015, 2015.

[237] Zhengxin Zhang, Changhua Hu, Xiaosheng Si, Jianxun Zhang, and Jianfei Zheng. Stochastic degradation process modeling and remaining useful life estimation with flexible random-effects. *Journal of the Franklin Institute*, 354(6):2477–2499, 2017. Special issue on recent advances on control and diagnosis via process measurements.

[238] Zhengxin Zhang, Xiaosheng Si, Changhua Hu, and Xiangyu Kong. Degradation modeling–based remaining useful life estimation: A review on approaches for systems with heterogeneity. *Proceedings of the Institution of Mechanical Engineers, Part O: Journal of Risk and Reliability*, 229(4):343–355, 2015.

[239] Yipeng Zhu, Tingdi Zhao, Jian Jiao, and Zhiwei Chen. The lifetime prediction of epoxy resin adhesive based on small-sample data. *Engineering Failure Analysis*, 102(October 2018):111–122, 2019.